Structural and Biochemical studies of a small Ras-like GTPase MglA and its activator MglB involved in *Myxococcus xanthus* motility

A thesis
Submitted in partial fulfilment of the requirement
of the degree of

Doctor of Philosophy

By

Jyoti Baranwal
20123174

INDIAN INSTITUTE OF SCIENCE EDUCATION AND RESEARCH PUNE

IISER PUNE

Indian Institute of Science Education and Research Pune

Dr. Homi Bhabha Road, Pashan, Pune 411 008.

Dr. Gayathri Pananghat
Assistant Professor

Certificate

Certified that the work incorporated in the thesis entitled "**Structural and Biochemical studies of a small Ras-like GTPase MglA and its activator MglB involved in *Myxococcus xanthus* motility**", submitted by **Ms. Jyoti Baranwal**, was carried out by the candidate under my supervision. The work presented here or any part of it has not been included in any other thesis submitted previously for the award of any degree or diploma from any other University or institution.

Gayathri

Gayathri Pananghat

Date: 15 January 2019

Tel.: +91 020 2590 8128; Fax: +91 020 2586 5315 Web: www.iiserpune.ac.in/~gayathri

Declaration

I declare that this written submission represents my ideas in my own words and where others' ideas have been included; I have adequately cited and referenced the original sources. I also declare that I have adhered to all principles of academic honesty and integrity and have not misrepresented or fabricated or falsified any idea/data/fact/source in my submission. I understand that violation of the above will be cause for disciplinary action by the Institute and can also evoke penal action from the sources that have not been properly cited or from whom proper permission has not been taken when needed.

Jyoti Baranwal

20123174

Date: 15th January, 2019

Acknowledgements

I would really like to thank my guide, Dr. Gayathri Pananghat for her generous support and guidance throughout my PhD. She has kept me motivated throughout this journey. Each and every day has been a new learning for me and I'm thankful to her for sharing this knowledge with me. She has contributed immensely towards my overall growth as a person too. I can't thank her enough for being with me all the time and taking care of me professionally and personally while keeping me focussed towards my research. I must admit I have been extremely fortunate to get an opportunity to work with her.

I would specially like to thank Prof. L. S. Shashidhara for his kind support throughout my PhD. He was my biggest motivation to work throughout these years. I'm thankful for his trust and faith on me.

I want to thank my Research Advisory Committee (RAC) members Dr. Nagaraj Balasubramanian, Prof. C.G. Suresh and Prof. L. S. Shashidhara for their advice during the yearly meetings and discussions by providing me insights into the research and motivating me to carry on with my work.

I would like to thank Dr. Sai Krishnan Kayarat for his advice on research and the discussions we had in our lab meetings. More specifically I'm thankful to him for making me strong in terms of facing the audience confidently.

I'm thankful to Sébastien Lhospice and Dr. Tâm Mignot, CNRS Aix-Marseille University, Marseille, France for validating my findings in vivo.

I'm thankful to Dr. Sudha Rajamani for allowing me to use her HPLC facility along with her lab members specially Chaitanya Mungi for his help with the instrument.

I would like to thank Prof. Arvind Sahu and Hina Ojha for allowing me to use their facility for ITC experiments at NCCS. I'm also thankful to IISER Mass Spectrometry facility.

I'm thankful to Mohan and Swati for all their help with mass-spectrometry.

I would like to thank CSIR for providing fellowship to complete my PhD.

I would like to thank Tushar, Nayna, Shabnam, Kalpesh, Piyush, Mrinalini, Deepali and whole admin staff of IISER for making our work easier.

There are many good friends I have in IISER Sonashree, Nishtha, Kunalika, Tanushree, Aman, Himani, Ravi, Niraja, Sudeshna, Piyanka, and Gunjan. I must say I have amazing friends in the whole world. I'll remember the laughter and fun we had together, thank you all. Special thanks to Chetan, Shrikant, Kunalika and Nishtha for their care and love. Tanushree in the person whom I can connect emotionally and I'm thankful to her for being very supportive throuout. I can't thank you all enough for being with me at some or the other point of my life and making this whole journey of PhD easier. I'm thankful to Ravi for helping me in all technical issues related to phone and laptop.

I would like to thank all my friends Shishir, Kunal, Sneha, Sanku, Babar, Bag, Harshini, Nandi Reza, Reman, Yashwant, Shalini, Parth, Anushree, Sikha, Susovan, Panja and Triparthi for being with me. I would also like to thank Palak and Deepali from NCCS, for being part of my life. The games we all played together i.e. badminton, carrom, table tennis, monopoly and the activities i.e. swimming, dancing, painting, cooking we have done together kept me energetic and motivated towards my work.

I would like to thank all my M.Sc. friends specially Priyansha, Parul, Keshav, Balgovind, Divyank, Jaya di, Deepshikha, Manasi and Suneeta. I would like to thank my school friends Ambrish, Vibha, Shailesh, Yogesh and Meenu. I would specially like to thanks my school friend Vandita for being my strength since we met till date and I hope this bond will stay forever. I want to say thanks to my B. Sc. friends Jyoti, Sneha, Heena and Deepali.

Lab members Neha, Manasi, Sujata, Ishtiyaq, Mahesh, Vishal, Pratima, Joyeeta, Vani, Mrinmayee, Vinayak, Sutirtha, Suman and Basila. I'll take this opportunity to thank Sukanya, Shrikant, Sukriti, Birjeet, Jasleena, Smarth and Sonal for helping me to accomplish this project. Special thanks to Priyanka and Manil for being around and helping me. I'm thankful to you all for making my life easier in the lab and will definitely going to miss the scientific, non-scientific chats and dinner we had.

Uncle, aunty and their whole family in Pune, for making me feel that I'm part of their family and I have a home away from home. I would like to thank Sarita di, Karunesh bhaiya, Deepika

Bhabhi and Palaksha. I'm also thankful to my friend Suman, Sandhya, Rakesh, Pratap, Garima and the little cutie Rachit in Pune for all the fun we had together.

The biggest support system I have, is my family and specially my brother for being with me and trusting me when no one did.

Dedicated to

my parents, brother and my guide.

Thank you all for being part of my journey.

Abstract

Myxococcus xanthus is a gram-negative, soil bacterium that reverses its direction of movement by frequently switching the leading and lagging poles. *Myxococcus xanthus* motility has many similarities with the eukaryotic cell crawling machinery, i.e. small Ras-like GTPases, focal adhesion-like complexes and an actin-like protein, MreB are involved in the process. A small Ras-like GTPase, MglA and a cognate GAP (GTPase Activating Protein), MglB play significant roles in the regulation of polarity determination and motility. MglA and MglB are present at leading and lagging poles of the bacterium, respectively, and re-localize at the time of polarity reversal, i.e. they oscillate between the poles.

With the goal of understanding the molecular mechanism of polarity oscillations driven by MglA and MglB, structural and biochemical aspects of these two proteins were studied. Crystal structures of various conformational states of MglA and complexes of MglA bound to MglB have been obtained. Structure of the MglAB complex has revealed a novel allosteric interaction of C-terminal helix of one of the MglB monomers with MglA. Biochemical and mutational studies have revealed a role for the C-terminal helix in stimulating GTPase activity and in nucleotide exchange. *In vivo* studies in *M. xanthus* demonstrate severe abnormalities in motility and a bipolar localization of MglA and MglB upon deletion of the C-terminal helix from MglB, highlighting the relevance of the interaction.

A comparison of structures of the complexes of GAP and GEF (Guanine nucleotide Exchange Factor) proteins with eukaryotic small Ras-like GTPases available in the Protein Data Bank suggests that the MglAB complex structure reveals a unique mechanism of allosteric regulation of small Ras-like GTPases. Instead of interacting directly at the nucleotide binding site and exerting GAP or GEF activity as observed in majority of the structures, the C-terminal helix of MglB interacts at a binding site distal from the nucleotide binding pocket of MglA. This allosteric regulation is important for localization of proteins and polarity oscillations in *M. xanthus*.

Table of Contents

Synopsis

Structural and Biochemical studies of a small Ras-like GTPase MglA and its activator MglB involved in *Myxococcus xanthus* motility

Name: Jyoti Baranwal
Roll Number: 20123174
Name of Supervisor: Dr. Gayathri Pananghat
Department: Biology
Date of registration: August, 2012

Polarity is essential for many cellular functions such as cell division, growth, motility and migration in eukaryotes. Prokaryotes are also known to achieve polarity to perform many functions i.e. cell division and motility (Mauriello, 2010). *Myxococcus xanthus* is a gram-negative, rod-shaped bacterium, which undergoes reversals i.e. change in polarity during motility that helps in deciding the direction of movement (Mauriello and Zusman, 2007). MglA, a small Ras-like GTPase, and its activator protein MglB play a major role in polarity determination, by positioning various motility complexes at the leading and lagging poles (Zhang *et al.*, 2010; Zhang *et al.*, 2012). These proteins also assist the bacterium in polarity reversals in response to environmental signals (Bulyha *et al.*, 2011; Kaimer *et al.*, 2012; Keilberg *et al.*, 2012). My PhD research involved the biochemical and structural characterization of MglA and MglB, with the aim of understanding their mechanism of action, and how they regulate the positioning of the motility complexes.

Small Ras-like GTPases are proteins which can hydrolyse GTP to GDP and inorganic phosphate (Vetter and Wittinghofer, 2001). They are regulated by different proteins such as GTPase activating proteins (GAP) and guanine nucleotide exchange factors (GEF) (Bos *et al.*, 2007; Cherfils, 2014). These GTPases are involved in many cellular functions i.e. cell crawling, migration and maintaining polarity of eukaryotic cells (Bourne *et al.*, 1990; Wittinghofer and Vetter, 2011; Song *et al.*, 2018). MglA is an example of a prokaryotic small Ras-like GTPase involved in motility. MglA acts as a molecular switch and regulates the localization of motility complexes between the poles with the help of a GTPase Activating Protein (GAP), MglB (Miertzschke *et al.*, 2011). These two proteins, MglA and MglB, oscillate in the bacterial cell

from one pole to another, and localize at the leading and lagging poles, respectively (Leonardy *et al.*, 2010).

Towards understanding the biochemical oscillations driven by MglA and MglB, we characterized the GTPase activity and interaction between the proteins using various tools of biochemistry, biophysics and structural biology. Crystal structures of MglA and MglB and their complex in the presence of GTP analogues were determined. The structure of the MglAB complex led to the discovery of the C-terminal helix of MglB bound to a novel allosteric binding pocket on the small Ras-like GTPase. Further biochemical assays and binding studies proved the significance of this binding in facilitating nucleotide exchange of MglA. Thus, MglB was discovered to possess bifunctional activities of both GAP and a GEF. A detailed structural analysis of complexes of all small Ras-like GTPases available in the PDB provided insights into mechanisms of action of interactors of small Ras-like GTPases, especially GAPs and GEFs, and allowed for a comparison with the mechanism of action of MglB.

A chapter wise summary of the thesis is given below:

Chapter 1 gives an introduction to *Myxococcus xanthus* motility machinery and localization of the components. The role of MglA and MglB in polarity oscillations and the rationale behind deciding the objectives of PhD are described.

Chapter 2 mainly discusses about the structure of MglA, MglB and MglAB complex. We observed a novel allosteric interaction of the C-terminal helix of MglB (one out of two protomers of MglB bound to MglA) to MglA (interaction is opposite to the nucleotide binding site).

To characterize this interaction and its importance for the activity of MglA, biochemical assays i.e. GTP hydrolysis assays and binding assays were performed. These are discussed in **Chapter 3**. Our results showed that MglB, a proposed cognate GAP, binds to GTPase in GDP-bound state of MglA too, in addition to the GTP-bound state. So, we looked for the possibility of involvement of the C-terminal helix in exchange of the nucleotide (GDP) bound to MglA. Biochemical studies and GEF assays (Guanine nucleotide exchange assays), with wild type protein and mutant constructs revealed the role of the allosteric interaction of C-terminal helix of MglB with MglA in nucleotide exchange.

Further, to understand the mechanism of action of GAP and GEF in other GTPases, the available structures in the PDB of other GTPase, GAP, and GEF complexes were studied.

Chapter 4 describes all the extensive analysis done with the structures and the mechanism of action of GTPases and their interacting partners. This study suggested that all these proteins interacts mostly at the nucleotide binding pocket of GTPase. But there are a few exceptions where instead of directly interacting through nucleotide binding site, GEF interacts at the side opposite to nucleotide binding site similar to the MglAB complex.

Significance of allosteric interaction of MglB C-terminal helix with MglA was explored by performing *in vivo* studies in *Myxococcus xanthus*, in collaboration with Dr. Tâm Mignot, CNRS Aix-Marseille University, Marseille, France. Motility and reversal phenotypes were severely affected upon deletion of the Ct-helix of MglB in *M. xanthus.* Mechanistic insights and relevance of the proposed regulation of MglA and MglB in *M. xanthus*, and future prospects are discussed in **Chapter 5**.

The overall results from structural and biochemical information of *Mx*MglAB, *in vivo* experiments and comprehensive structural analysis of small Ras-like GTPases highlight the discovery of a unique mechanism of allosteric regulation of a prokaryotic small Ras-like GTPase by MglB. This regulation is important for polarity determination, localization of proteins and polarity oscillations in *Myxococcus xanthus*. Based on our study we hypothesize that the chemosensory pathway transmits its signal through the cross-talk between Frz-signaling pathway to C-terminal helix of MglB for polarity reversal in *M. xanthus*.

List of publications (Under preparation)

1. Allosteric regulation of a prokaryotic small Ras-like GTPase contributes to polarity oscillations in bacterial motility. (Manuscript communicated)
Authors: **Jyoti Baranwal**, Sebastian L'Hospice, Manil Kanade, Priyanka Gade, Shrikant Harne, Tâm Mignot, Pananghat Gayathri
Structures of MglAB complex and MglA-GDP, and supporting biochemical and *in vivo* data showing that the C-terminal helix of MglB is essential for GTPase activity and driving polarity oscillations are described. The study reports the first demonstration of a dual role of an activator of a small Ras-like GTPase both as a GAP and a GEF.

2. Mechanism of GTPase activation of a small Ras-like GTPase MglA by an asymmetric dimer of MglB.

Authors: Sukanya Chakraborty, **Jyoti Baranwal**, Pananghat Gayathri

The study carried out for dissecting the role of each C-terminal helix of the dimeric MglB is described. The design of an asymmetric construct and their relevant mutants, their crystal structures, and role of the C-terminal helix of each MglB protomer in GAP and GEF activities are included.

3. Analysis of dimeric interface in crystal structures of *Myxococcus xanthus* MglB.

Authors: **Jyoti Baranwal**, Priyanka Gade, Pananghat Gayathri

This consists of a report of full length and truncated crystal structures and analysis of the relative orientations of the MglB monomers in 12 different dimers present in asymmetric units of all crystal structures including MglAB.

4. A unifying mechanism of action of GAPs and GEFs of small Ras-like GTPases.

Authors: **Jyoti Baranwal** and Pananghat Gayathri

A comprehensive analysis of all structures of small Ras-like GTPases was carried out. This points out that the allosteric activation mechanism in MglA is unique, since most reported GEFs and GAPs are regulated through a direct interaction with Switch I or Switch II near the nucleotide binding pocket.

References

- Bos, J.L., Rehmann, H., and Wittinghofer, A. (2007). GEFs and GAPs: Critical Elements in the Control of Small G Proteins. Cell *129*, 865-877.
- Bourne, H.R., Sanders, D.A., and McCormick, F. (1990). The GTPase superfamily: a conserved switch for diverse cell functions. Nature *348*, 125.
- Bulyha, I., Hot, E., Huntley, S., and Søgaard-Andersen, L. (2011). GTPases in bacterial cell polarity and signalling. Current Opinion in Microbiology *14*, 726-733.
- Cherfils, J. (2014). GEFs and GAPs: Mechanisms and Structures. In Ras Superfamily Small G Proteins: Biology and Mechanisms 1: General Features, Signaling, A. Wittinghofer, ed. (Vienna: Springer Vienna), pp. 51-63.

- Kaimer, C., Berleman, J.E., and Zusman, D.R. (2012). Chemosensory signaling controls motility and subcellular polarity in Myxococcus xanthus. Current Opinion in Microbiology *15*, 751-757.

- Keilberg, D., Wuichet, K., Drescher, F., and Søgaard-Andersen, L. (2012). A Response Regulator Interfaces between the Frz Chemosensory System and the MglA/MglB GTPase/GAP Module to Regulate Polarity in Myxococcus xanthus. PLOS Genetics *8*, e1002951.

- Leonardy, S., Miertzschke, M., Bulyha, I., Sperling, E., Wittinghofer, A., and Søgaard-Andersen, L. (2010). Regulation of dynamic polarity switching in bacteria by a Ras-like G-protein and its cognate GAP. The EMBO journal *29*, 2276-2289.

- Mauriello, E.M.F. (2010). Cell polarity/motility in bacteria: closer to eukaryotes than expected? The EMBO Journal *29*, 2258.

- Mauriello, E.M.F., and Zusman, D.R. (2007). Polarity of motility systems in Myxococcus xanthus. Current Opinion in Microbiology *10*, 624-629.

- Miertzschke, M., Koerner, C., Vetter, I.R., Keilberg, D., Hot, E., Leonardy, S., Søgaard-Andersen, L., and Wittinghofer, A. (2011). Structural analysis of the Ras-like G protein MglA and its cognate GAP MglB and implications for bacterial polarity. The EMBO journal *30*, 4185-4197.

- Song, S., Cong, W., Zhou, S., Shi, Y., Dai, W., Zhang, H., Wang, X., He, B., and Zhang, Q. (2018). Small GTPases: Structure, biological function and its interaction with nanoparticles. Asian Journal of Pharmaceutical Sciences.

- Vetter, I.R., and Wittinghofer, A. (2001). The Guanine Nucleotide-Binding Switch in Three Dimensions. Science *294*, 1299.

- Wittinghofer, A., and Vetter, I.R. (2011). Structure-Function Relationships of the G Domain, a Canonical Switch Motif. Annual Review of Biochemistry *80*, 943-971.

- Zhang, Y., Franco, M., Ducret, A., and Mignot, T. (2010). A Bacterial Ras-Like Small GTP-Binding Protein and Its Cognate GAP Establish a Dynamic Spatial Polarity Axis to Control Directed Motility. PLOS Biology *8*, e1000430.

- Zhang, Y., Guzzo, M., Ducret, A., Li, Y.-Z., and Mignot, T. (2012). A Dynamic Response Regulator Protein Modulates G-Protein–Dependent Polarity in the Bacterium Myxococcus xanthus. PLOS Genetics *8*, e1002872.

List of figures

List of tables

Abbreviations

A-motility	Adventurous gliding motility
ATP	Adenosine triphosphate
Ct-helix	C-terminal helix
E. coli	*Escherichia coli*
EDTA	Ethylenediaminetetraacetic acid
FAC	Focal adhesion complex
FAS	Focal adhesion site
GAP	GTPase Activating protein
GDF	GDI displacement factor
GDI	Guanine nucleotide dissociation inhibitor
GDP	Guanosine diphosphate
GEF	Guanine nucleotide exchange
GPCR-	G-Protein coupled receptor
GppCp (GMPPCP)	Guanosine-5'-[(β,γ)-methyleno]triphosphate
GppNHp (GMPPNP)	Guanosine 5′-[(β,γ)-imido]triphosphate
GTP	Guanosine triphosphate
GTPase	GTP hydrolysing enzyme
HPLC	High Pressure Liquid Chromatography
M. xanthus	*Myxococcus xanthus*
MglA	Mutual gliding protein A
MglB	Mutual gliding protein B
$MglB^{Ct}$	MglB C-terminal helix deleted construct
*Mx*MglA	*Myxococcus xanthus* MglA
*Mx*MglB	*Myxococcus xanthus* MglB
*Tt*MglA	*Thermus thermophilus* MglA
*Tt*MglB	*Thermus thermophilus* MglB
OM	Outer membrane
PCR	Polymerase Chain Reaction
Pi	Inorganic phosphate
PMF	Proton motive force
RMSD	Root Mean Square Deviation
SDS	Sodium dodecyl sulphate
S-motility	Social gliding motility
SRP	Signal Recognition protein
T. thermophilus	*Thermus thermophilus*
T4P (TFP)	Type IV Pili

Chapter 1

Introduction

1.1 Background

Motility is a very important aspect from cells to multicellular organism and higher order animals, especially for the survival of many organisms. For predatory animals, speed of the prey and predator are important. In case of drought, whole herd of animals move from one place to another (Lennox *et al.*, 2016; Åkesson *et al.*, 2017; Alerstam and Bäckman, 2018). At a cellular level in eukaryotes, cell migration and cell crawling play essential physiological roles i.e., diapedesis of white blood cells due to immune response, networking of nerve cells at the time of development, sperm motility and they also exhibit pathological effects, for example, in metastasis of cancer cells (Ridley *et al.*, 2003; Bockhorn *et al.*, 2007; Bershadsky and Kozlov, 2011; Vicente-Manzanares and Horwitz, 2011; Fife *et al.*, 2014). For lower organisms like bacteria, chemotaxis is one of the aspects to which they respond. Motility in bacteria is important for biofilm formation, sporulation and for host pathogen interaction (Mitchell and Kogure, 2006). *Myxococcus xanthus* (*M. xanthus*) is an example of a bacterium where motility has an overall effect on its life cycle i.e. effects on predation, fruiting body formation, sporulation, etc. (Spormann, 1999). It exhibits social behaviour, as it organises into swarms (a co-ordinated movement in groups) and undergoes differentiation from vegetative form to mature spores (Wolgemuth *et al.*, 2003; Berleman *et al.*, 2008; Mignot and Kirby, 2008; Kaiser and Warrick, 2014).

1.2 *Myxococcus xanthus* as a model organism to study motility

In bacteria, different types of motility have been observed i.e. twitching, swarming, gliding, etc. Many bacteria use appendages such as flagella and pili for their motility (McBride, 2001; Jarrell and McBride, 2008). There are many other bacteria - e.g. *P. aeruginosa, N. gonorrhoeae,* where pili play an important role in motility (Henrichsen, 1983; Whitchurch *et al.*, 1991), similar to *Myxococcus xanthus*. Type IV pili is mainly used for movement in groups. *Myxococcus* is an example of a bacterium that uses pili for movement, and also exhibits movements that do not require the presence of pili. In *Myxococcus*, proteins that perform functions similar to focal adhesion complexes of eukaryotic systems are responsible for gliding motility. Also, the bacterium has polarity which is recognised by the presence of pili. The pole where pili is present is called the leading pole while the other is called the lagging pole. It also has a property that it reverses its polarity, thus deciding the direction of movement.

M. xanthus is a predatory, rod-shaped, gram-negative, soil-dwelling deltaproteobacterium, with a very large genome size of 9.454 Mb (Chen *et al.*, 1990). It has one of the largest bacterial genomes and have more complex signalling pathways than *E. coli*. There are approximately 8000 genes encoded by the genome. It was always a curiosity for many groups to study because of its complexity and unique life cycle compared to other bacteria (Figure 1.1) (Shimkets, 1990; Ward and Zusman, 1997). Hence, it is a model to study intercellular signalling and signal transduction, ecology and social behaviour, mechanism of gliding motility, etc. (Kroos, 2007).

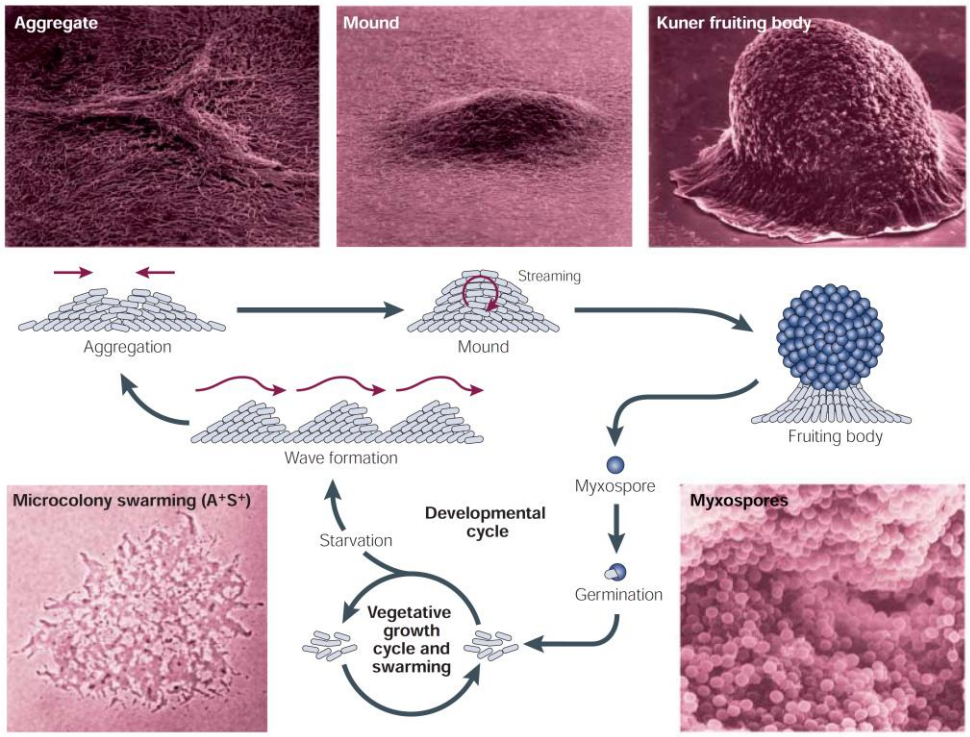

Figure 1.1 Life cycle of *Myxococcus xanthus*
The images of different stages of life cycle of bacteria with the schematic just below the images showing aggregation, mound and fruiting body formation at the time of starvation. When favourable condition arrives, spores germinate to get into the vegetative life cycle**.** (Reproduced from Kaiser, 2003)

Its life cycle undergoes complex developmental processes, which include aggregation and sporulation, depending upon the availability of nutrients (Kaiser, 2003). When nutrients are sufficient, all of them move together as swarms while in scarcity of nutrients, many bacteria aggregate together to form dome-shaped fruiting bodies and further endospores. These endospores have a property to regenerate in favourable conditions (Ward and Zusman, 1997). The life cycle of the bacterium has many similarities with the amoeba, *Dictiostelium discoidum*. Both of them go through stages of vegetative life cycle and formation of fruiting bodies

(Claessen *et al.*, 2014). Also, *D. discoidum* and *M. xanthus* share many similarities in cellular organisation, social behaviour and signalling (Jelsbak and Søgaard-Andersen, 1999).

1.3 Motility mechanism in *Myxococcus xanthus*

To assist the bacterium in its complex life cycle, there are two types of motility - (i) Social motility (S-motility) assisted by Type IV pili (T4P) and (ii) Adventurous gliding motility (A-motility) assisted by focal adhesion complexes (Mauriello *et al.*, 2010a). The purpose of motility in *Myxococcus xanthus* is to feed on soil detritus, predation, swarming, leading to fruiting body formation and sporulation. The life cycle and motility of bacterium is dependent on external stimulus. The bacterium moves at a speed of 2-4 µm/min, which is 1000 times slower than flagellated bacteria. These bacteria move on the surface by S-motility and A-motility (Shimkets, 1990; Ward and Zusman, 1997).

1.3.1 Social motility (S-motility)

As the name suggests, social motility is the movement of bacteria in a group. Even though bacteria move individually too in adventurous motility, still they tend to co-ordinate beautifully at the time of social movement. This is a very good example to understand cell-cell interaction and organization taking place in biological systems. The bacterium uses the type IV pili for S-motility and hence, it is also called twitching motility (Wall and Kaiser, 1999). Genetic studies and behavioural studies have confirmed the role of pili in the S-motility of *M. xanthus*.

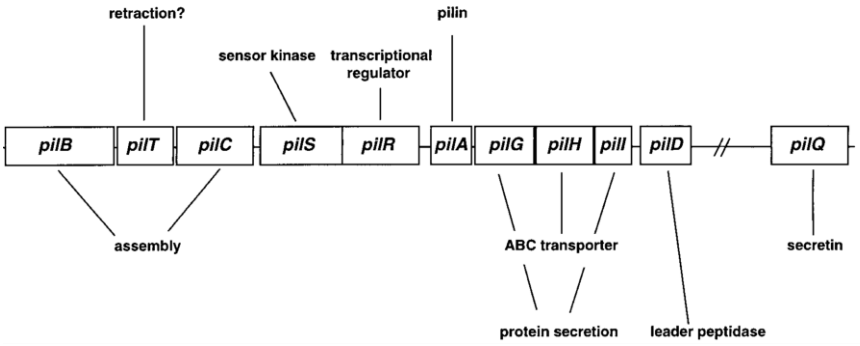

Figure 1.2 Genes involved in S-motility
Schematic representation of the role of proteins encoded by the genes in the S-motility (Reproduced from Sporman, 1999)

Pili-based motility is slow in comparison to other motility appendages i.e. flagella of *E. coli*. To move forward, three basic actions of pili have been observed - i) extension ii) attachment iii) retraction. All these processes help bacteria to move forward as a group. Pili of bacteria help in adhesion with other bacteria, while the bacteria at the edges of the cluster adhere their pili to the substratum. Hence social motility is correlated and dependent on pili-based motility.

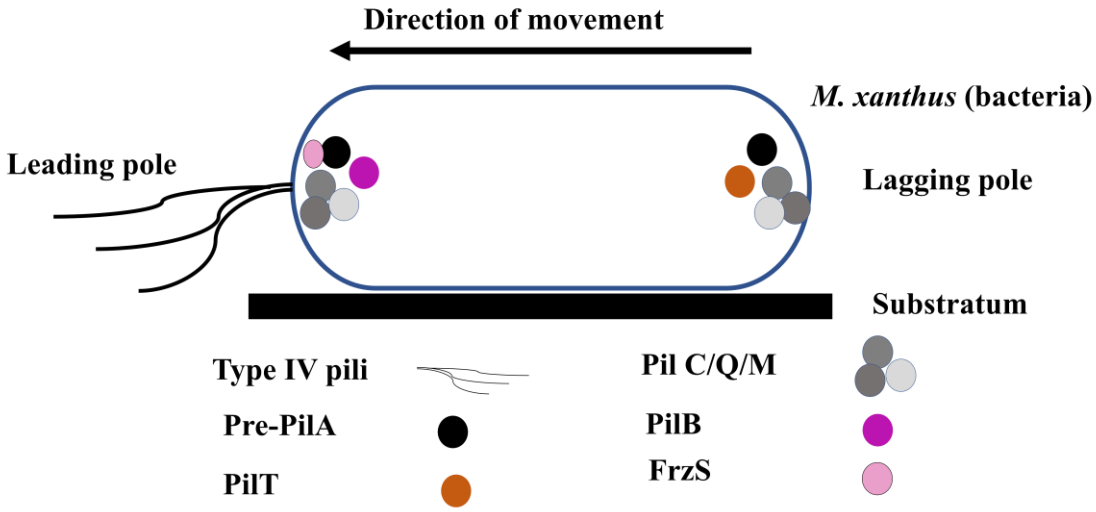

Figure 1.3 Schematic representation of proteins involved in S-motility.
Rod-shaped structure is a bacterium with pili at one end and circles represents proteins. The colour key of the representative proteins are shown below the schematic (Adapted from Bulyha *et al.*, 2011).

There are many genes involved in pili formation (Figure 1.2). Some pili proteins are involved in biogenesis of pili at the poles, for example, PilA, PilN, PilC, PilQ (Figure 1.3) (Nudleman *et al.*, 2006), while some other pili proteins such as PilT, PilB are ATPases assist in extension and retraction of the pili. PilA is the major component of the pili protein. There are proteins which regulate the PilA transcription i.e. PilR and hence regulate the polymerization of pili (Wall and Kaiser, 1999). Pilus assembly and polymerization is carried out by PilB with PilC. They are one of the inner membrane components of pili (Bischof *et al.*, 2016). At the time of reversals, some of the proteins relocalize from one pole to the other while others remain stationary. The proteins present at both the poles are PilC, PilQ, PilM and pre-PilA while there are proteins which are specifically present at one pole only i.e. PilB at the leading pole and PilT at the lagging pole (Bulyha *et al.*, 2009). This organisation of proteins allows pili to disassemble at one and regenerate at the other pole during reversal.

The polymerization and depolymerization of PilA cause displacement of the bacterium. For depolymerization, it is proposed that PilT, an ATPase, is important. It catalyses or hydrolyses ATP that releases the energy for depolymerization and hence, pilus retraction takes place. The retraction of pilus leads to the movement of bacteria along the cell axis (Jakovljevic *et al.*, 2008). The overall pili extension-retraction and displacement leads to S-motility in *M. xanthus* as explained in the review by Spormann (1999).

1.3.2 Adventurous gliding motility (A-motility)

Although these bacteria can stay and move in groups, they have individual movements, especially observed at the edge of colonies, and is known as adventurous motility. Adventurous motility includes movement of isolated cells on the solid surface i.e. soil. Focal adhesion-like complexes are involved in this type of motility, and function by periodically attaching and detaching from the surface, thus facilitating gliding (Sliusarenko *et al.*, 2007). This kind of gliding movement was observed on hard and relatively dry surfaces compared to that of S-motility. Bacteria move by exerting force on the substratum through these focal adhesion-like complexes (Nan *et al.*, 2010). These complexes are formed at the cytoplasmic side of the bacterial cells and extend across the inner and outer cell membranes. These complexes push the bacterium against the surface and hence help the cell to move forward. The machinery involved in A-motility is different from S-motility. Instead of ATP, proton motive force (PMF) provides the energy for the propulsion (Nan *et al.*, 2011). There are motor proteins like flagellar motor protein i.e. MotA and MotB. They are responsible for providing energy for gliding (Nan *et al.*, 2013).

There are few models which describe A-motility in *M. xanthus* (Nan and Zusman, 2011). These are:

i) Slime secretion model (Burchard, 1981)

ii) Focal adhesion complex-based model (Mignot, 2007; Mignot *et al.*, 2007; Nan *et al.*, 2010)

iii) Helical rotor model (Nan *et al.*, 2011)

According to these models, motor proteins are a part of the focal adhesion complexes and they move along a helical cytoskeletal track (Mignot *et al.*, 2007). This create force which further generate waves on the substrate and distort the cell surface that push the bacterial cell forward. All of them together explains the localization and movement of the motility complexes. They also give mechanistic insights into motility complexes that move in a helical path formed by

MreB (Mauriello *et al.*, 2010). Energy for movement is provided by the proton motive force generated by using AglQRS complex (Sliusarenko *et al.*, 2007; Nan *et al.*, 2010; Nan *et al.*, 2011). These complexes generate friction, when they come in contact with the substratum. Periodic arrangement of the focal adhesion complex was explained by the MreB helix or short filaments that are believed to span over the membrane of the bacteria (Figure 1.4) (van Teeffelen *et al.*, 2011; Treuner-Lange *et al.*, 2015; Faure *et al.*, 2016).

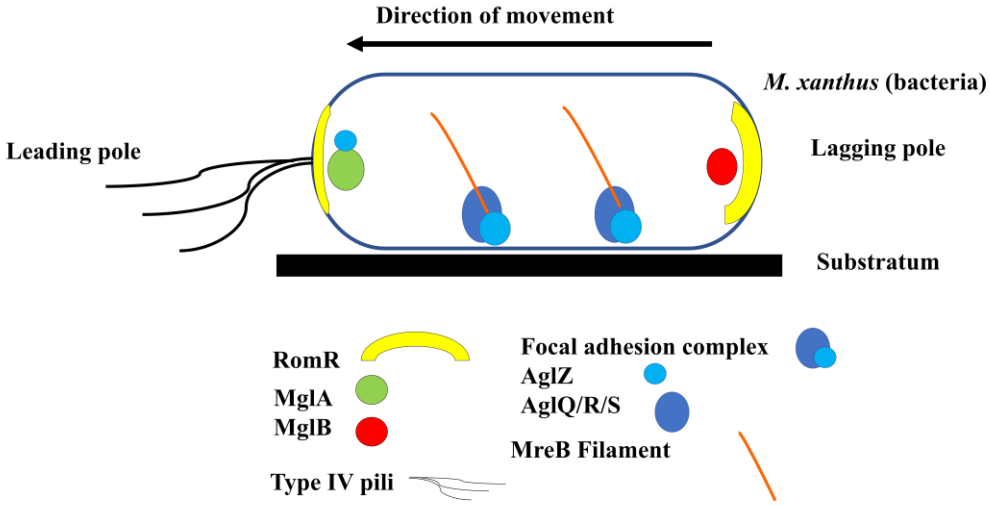

Figure 1.4 Schematic representation of proteins involved in A-motiltiy
Different proteins involved in A-motility are shown by circles of different colours, depicted in figure. RomR has asymmetric localization at the poles and hence it has been represented by thin and thick curved shapes (Adapted from Bulyha *et al.*, 2011).

According to recent studies, there are cytoplasmic, inner membrane, periplasmic and outer membrane components of proteins, which exert pressure on the substratum and help in moving forward. There are different sets of genes involved in production of proteins in the complex formation. They are named as *glt* genes or *gl*iding *t*ransducer genes. Out of these 40 motility proteins encoding genes, 11 genes were found to be the *glt* genes and are clustered in the G1, G2 as shown in figure 1.5B (Islam and Mignot, 2015). It was found out that GltA, GltB, GltC, GltH and GltK are present on the outer membrane of the bacteria. Based on the interaction studies amongst the proteins, it was hypothesized that AglR from the AglQRS interacts with the inner membrane Glt proteins (Wartel *et al.*, 2013), and transmits the force through the periplasmic proteins to outer membrane proteins (Mignot and Nöllmann, 2017).

Figure 1.5A shows protein complexes interacting with each other while figure 1.5B shows genetic arrangement of these proteins. AglZ is present at the lagging pole and in the focal adhesion complex too (Yang *et al.*, 2004; Mignot, 2007). MreB is another protein that interacts

with the focal adhesion complexes at the cytoplasmic side. MglA has also been observed along with MreB at the focal adhesion sites (Faure *et al.*, 2016).

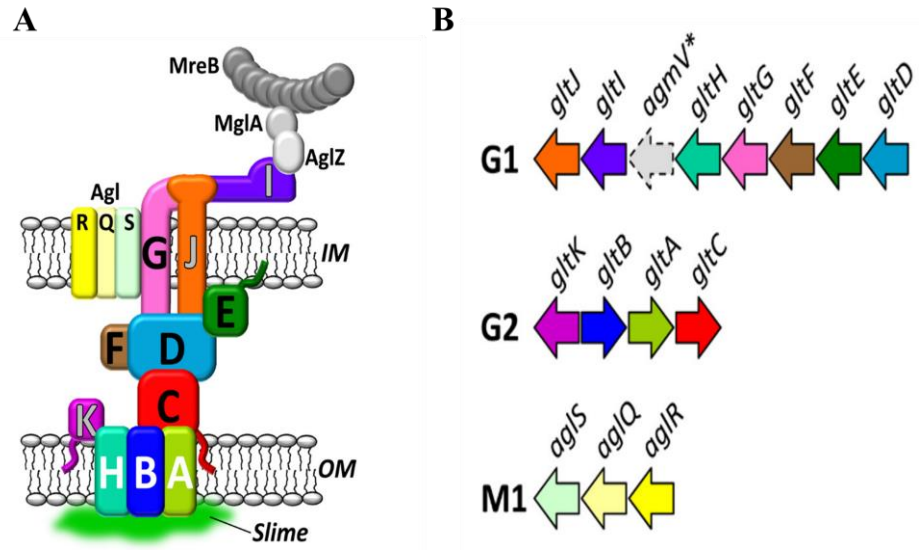

Figure 1.5 Focal adhesion complex of A-motility
A. Proteins involved in the formation of the focal adhesion sites in the cytoplasm, outer membrane and the inner membrane complexes **B.** Schematic of genetic arrangement of proteins in A-motility of the bacteria shown by the G1, G2 and M1 (Reproduced from Islam and Mignot, 2015)

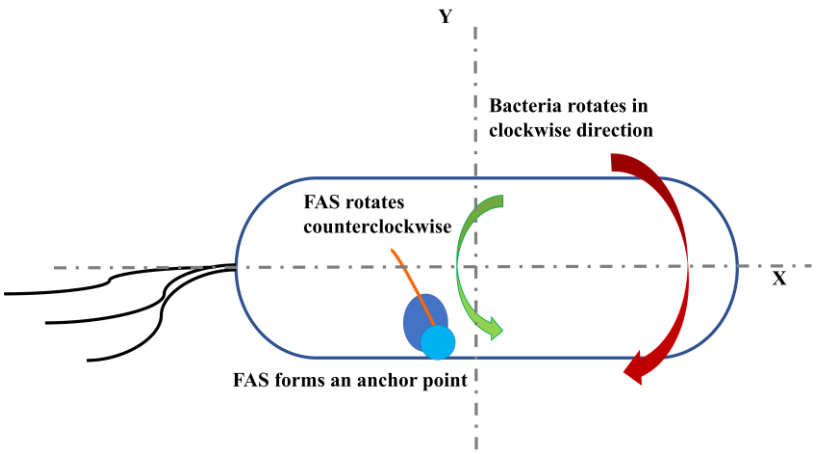

Figure 1.6 Propulsion in A-motility
Schematic representation of bacterial movement on its axis in clockwise direction in A- motility is shown, while focal adhesion sites move counter-clock wise. The FAS provide the force to move on the surface. Green arrow depicts the direction of movement of FAS while red arrow represents bacterial rotation on its axis. Blue circles represent the focal adhesion complex, and orange line represents MreB. Axes of rotation are shown by grey lines (Adapted from Faure *et al.*, 2010).

Propulsion mechanism: According to Faure *et al.*, 2016, focal adhesion complexes generate force on the surface and drive propulsion of bacteria. It was shown that there is a strong interaction at these focal adhesion sites with surface and that generates force on the substratum,

to move forward (Faure *et al.*, 2016). According to study, FAS moves across the poles along the helical path and in counter-clockwise direction to generate force while on the other hand bacterium moves in a clockwise direction. It seems that propulsion of bacteria in forward direction is linked to the anticlockwise movement of the FAS and this generates propulsion to move on surface (Figure 1.6). This is accompanied by release of slime trails which comprises extracellular matrix to smoothen the surface for bacterial movement. Regulatory proteins i.e. MglA and cytoskeletal protein, MreB in the cytoplasm also interact to these FAS, to perform their function in response to signalling by the cytoplasmic chemosensory proteins of the Frizzy pathway (Guzzo *et al.*, 2015).

1.3.3 Localization of the motility complexes in polarity reversals

An active mechanism for localization of proteins in bacteria is an emerging concept, which has come up recently. Bacteria do not have organelles, but they regulate many processes inside the cell by managing the localization and amount of proteins. However, how these proteins are localized still needs to be understood. Because of its frequent polarity reversals, *M. xanthus* serves as a model organism to understand active localization of proteins in bacteria.

Spatial positioning of proteins has been observed in many bacteria. Examples are i) MinCD oscillations at the time of cytokinesis in *E. coli* for positioning of FtsZ ring at mid-cell (Pichoff and Lutkenhaus, 2001) ii) clustering of chemosensory proteins in *E. coli*, (Ward and Zusman, 1997) iii) asymmetric localization of proteins at the septum in *B*. *subtilis,* at the time of spore formation (Lybarger and Maddock, 2001; Shapiro *et al.*, 2002; Kroos, 2007). Polarity is a special case of spatial positioning where asymmetric localization of proteins occurs at the poles. Motility complexes in *M. xanthus* have also been found to be asymmetrically localized at the poles and some other proteins have been found to be periodically arranged along the body of the cell, as observed in A-motility complexes (Treuner-Lange and Sogaard-Andersen, 2014). Leading and lagging poles in *M. xanthus* are decided by the presence of pili. The pole which has pili is considered as the leading pole while the other one is the lagging pole as explained earlier. Different sets of proteins are localized at these poles and hence provide polarity to bacteria. Figure 1.7 shows a schematic representation of the protein localization at the poles. The polarity in this bacterium is maintained by a small Ras-like GTPase, MglA. Small Ras-like GTPases in eukaryotes are well-known determinants of cell polarity.

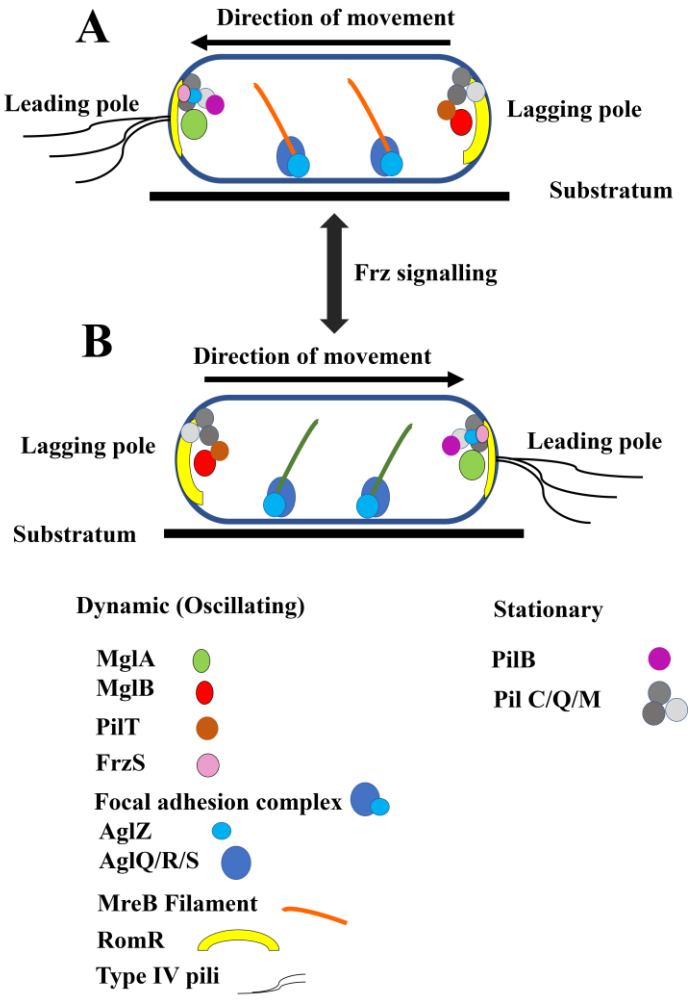

Figure 1.7 Polarity reversal in *M. xanthus*
Schematic depiction of the proteins that relocalize across the poles at the time of reversals. Proteins are categorised into stationary and dynamic based on the position i.e. they remain at the same pole or relocalize during polarity reversal in A-motility and S-motility. The size of RomR at the two poles depicts the asymmetric distribution while others are only a representation of the localization of the proteins (Adapted from Treuner-Lange and Sogaard-Andersen, 2014; Bulyha *et al.*, 2011)).

Reversal can be explained as a change in polarity of the bacterial cell, achieved by switching the localization of proteins at the poles (Figure 1.7) (Bulyha *et al.*, 2011). Physiologically it is very relevant to the bacterium for choosing the direction of movement towards nutrients. Reversal, polarity and motility of *Myxococcus* (Mauriello and Zusman, 2007) are correlated with each other and regulated by a combination of two pathways i) signalling from bacterial chemosensory Che-like Frz pathway, and ii) a small Ras-like GTPase MglA dependent pathway (Mauriello *et al.*, 2010b; Keilberg *et al.*, 2012). Localization of motility proteins in *M. xanthus* during reversals were studied by phenotypic characterization of fluorescently tagged constructs in various genetic backgrounds (Table 1.1).

Table 1.1 Localization of proteins in *M. xanthus*

Protein	Localization	References
MglA	Leading pole	Zhang et al. 2012, Miertzschke et al. 2011, Keilberg et al. 2012
MglB	Lagging pole	Zhang et al. 2012, Miertzschke et al. 2011, Keilberg et al. 2012
MglA in the absence of MglB	Bipolar, reversal is there	Zhang et al. 2010, Zhang et al. 2012, Keilberg et al. 2012
MglA GDP bound state	Diffusely localised	Leonardy et al. 2010
MglA in the absence of RomR	Mostly diffused and minor unipolar	Zhang et al. 2012
MglB in absence of MglA	Bipolar, no reversal	Zhang et al. 2010, Zhang et al. 2012
AglZ	Leading pole and in fixed clusters	Zhang et al. 2012, Leonardy et al. 2010
AglZ localisation in absence of RomR	Diffused	Zhang et al. 2012
RomR	Bipolar, asymmetric (more at lagging pole)	Leonardy et al. 2010, Zhang et al. 2012, Keilberg et al. 2012
RomR in the presence of GDP-bound state of the MglA	Lagging pole	Leonardy et al. 2010
MglB in the absence of RomR	Unipolar but reversal affected	Zhang et al. 2012
Sof G	Subpolar region	Bulyha et al. 2013
RomR in absence of MglA	Unipolar	
MglB in absence of MglA and RomR	Mostly unipolar	Zhang et al. 2012
RomR in absence of MglA and MglB	Bipolar symmetrical	Zhang et al. 2012
AglZ in absence of MglB	Bipolar and in the internal cluster	Zhang et al. 2012,
MglA GTP bound state	Bipolar	Miertzschke et al. 2011, Leonardy et al. 2010
PilB	Unipolar, leading pole	Bulyha et al, 2009
PilT	Unipolar, lagging pole	Bulyha et al, 2009
FrzS	Unipolar, lagging pole	Bulyha et al, 2009
FrzX	Unipolar, lagging pole	Guzzo et al. 2017

Proteins which oscillate across the poles during a polarity reversal are termed as dynamic, while those which are present at the poles only and do not relocalize as the result of reversals are termed as stationary. Here, only few proteins have been represented but there are a lot of proteins which relocalize as a result of reversal. This reversal is governed by environmental signals i.e. chemotaxis response. The signal is recognised by the chemosensory pathway of *M. xanthus* called the Frz signalling pathway. This is equivalent to the chemosensory pathway of *E. coli* and are encoded by "*frizzy*" genes (McBride *et al.*, 1989).

1.4 Frz, a chemosensory pathway for reversal of polarity in *M. xanthus*

Frz pathway regulates reversals in both social and adventurous motilities (Leonardy *et al.*, 2008). Multiple proteins need to be synchronized together in space and time to give the output

of motility in *M. xanthus* (Bustamante *et al.*, 2004). Proteins which have been discussed above have their localization either at the poles or at the FASs. Interestingly, the relocalization and oscillations at the time of reversal is strategic and decisive for choosing the direction of movement. All these processes are regulated by the signal sensor domain which further transfers the signal to other associated proteins.

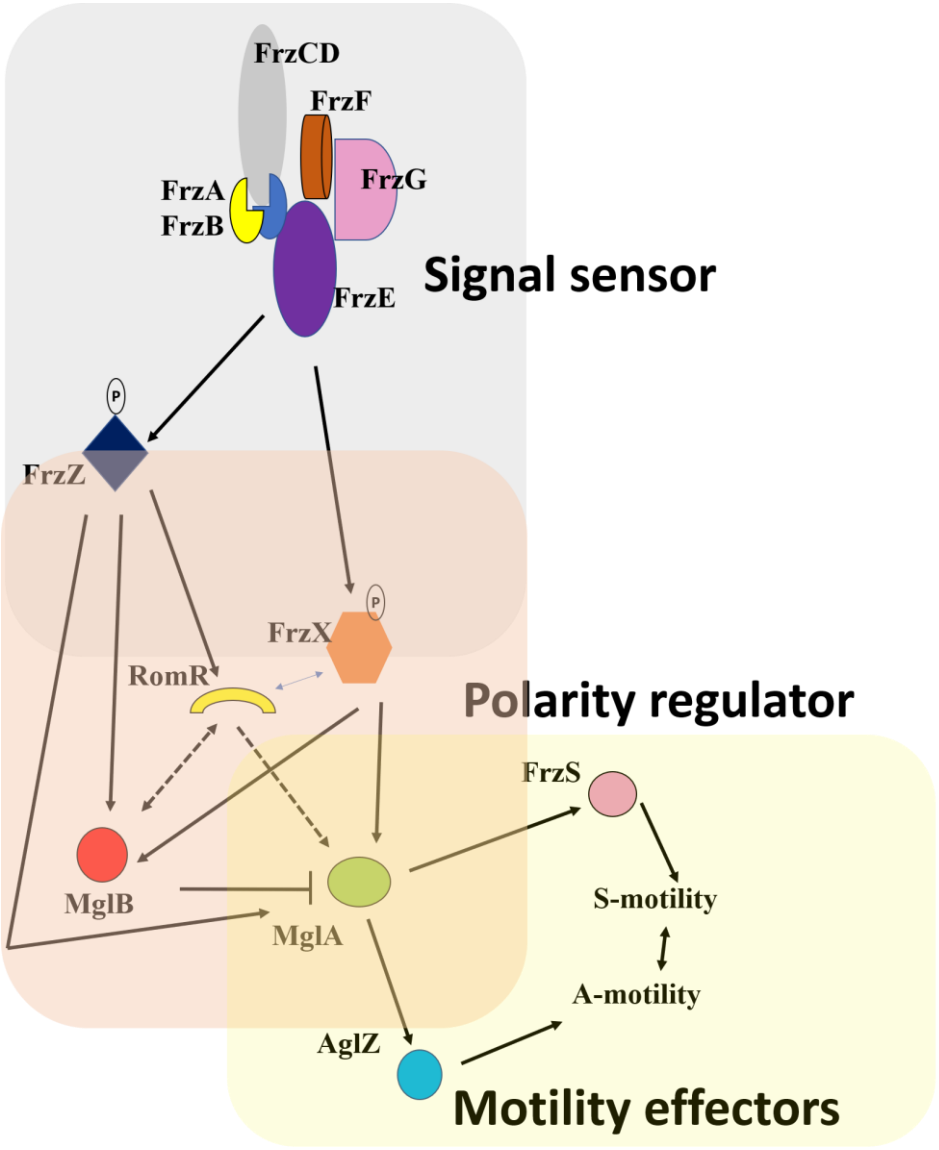

Figure 1.8 Signalling pathway of the *M. xanthus* from signal sensing to motility
The signal is sensed by the chemosensor i.e. proteins in the *frizzy* pathway and transferred to the polarity regulators i.e. MglA and MglB (Adapted from Zhang *et al.*, 2012; Mercier and Mignot, 2016).

FrzCD is a chemosensory component of this pathway, unlike other homologous receptor molecule (chemosensory system) it is present in the cytoplasm of bacteria, because of lack of transmembrane domain (McBride *et al.*, 1992). Bacteria with deletion mutants of FrzCD never

reverse while constitutively expressed FrzCD (frz^{on}) mutant of *M. xanthus* shows hyper-reversal (Blackhart and Zusman, 1985). Other components of this chemosensory pathway are FrzA, FrzB, FrzE, FrzF and FrzG; where FrzE acts as a kinase, while FrzF and FrzG act as methyltransferase and methyl esterase, respectively (Zusman, 1982; Blackhart and Zusman, 1986; McBride *et al.*, 1989). FrzA and FrzB are coupling proteins (Figure 1.8). FrzZ is a response regulator, necessary for reversal (Blackhart and Zusman, 1986; Spormann and Kaiser, 1999; Mauriello *et al.*, 2009).

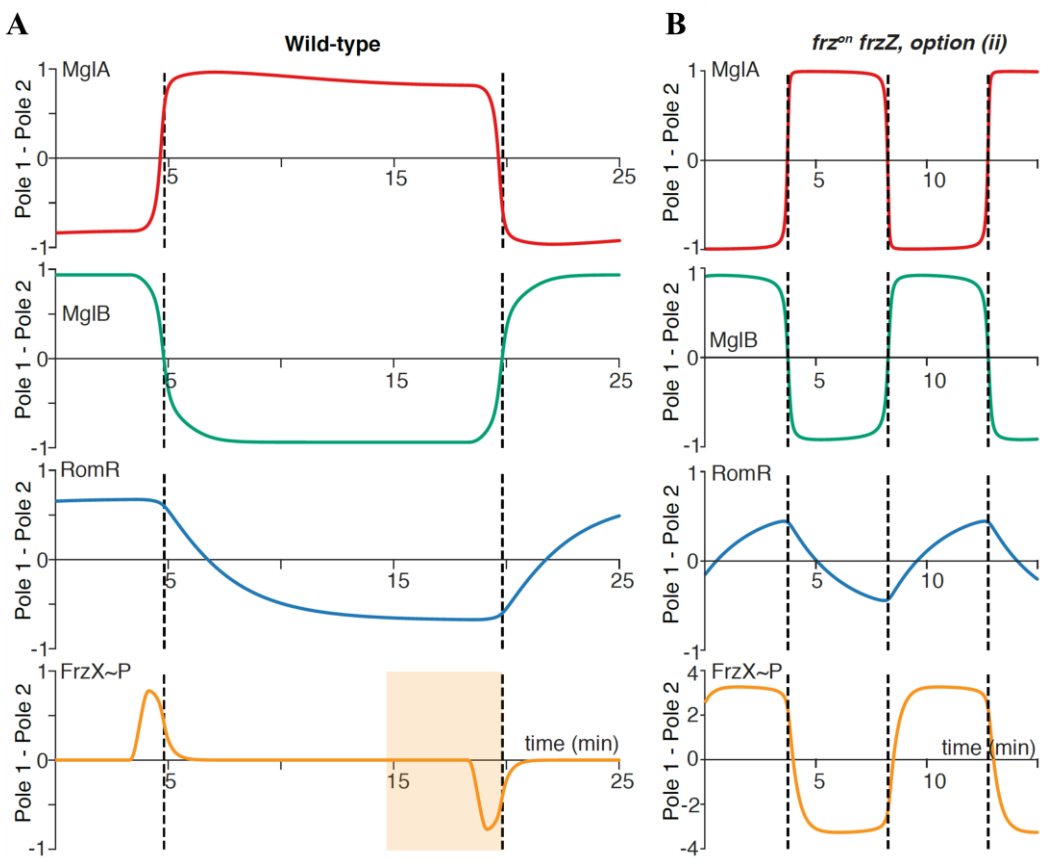

Figure 1.9 The oscillator-gated regulation of polarity reversal by RomR and FrzX
Localisation of MglA, MglB, RomR and FrzX are represented by the red, green, blue and orange solid lines, respectively. Y-axis represents intensity differences of protein localization between pole 1 and pole 2. MglA and MglB switch poles while RomR starts accumulating at the pole where MglB has already reached, shown as a refractory period (shaded) in the figure. However, when RomR accumulates to a certain level, FrzX starts accumulating which has been shown as primed period and as soon as FrzX is phosphorylated, reversal of polarity sets in. Panel **A** show reversal in wild type cell while panel **B** represent the continuous reversal when frz pathway is constitutively on (Reproduced from Guzzo *et al.*, 2018).

There is a very complex network of regulation where many proteins act together to make the process of reversal to happen (Eckhert *et al.*, 2014). The kinase, FrzE gets activated in response to the cues by the Frz-signalling proteins shown in figure 1.8 (McCleary and Zusman, 1990; Mercier and Mignot, 2016). It phosphorylates the downstream proteins e.g. FrzZ and FrzX.

These two proteins are mediators between sensory module and the polarity control module. FrzZ acts upstream of MglA, MglB and RomR (Leonardy *et al.*, 2010). Along with FrzZ and RomR, FrzX has an effect on polarity regulators. In fact, FrzX, RomR, MglA and MglB work together to regulate the whole process of polarity reversal (Kaimer *et al.*, 2012). According to a recent study, FrzE phosphorylates FrzZ and FrzX. FrzX and RomR act together to initiate the polarity reversal (Figure 1.8 and 1.9). When the concentration of RomR reaches to a certain level at the lagging pole, it recruits FrzX at the lagging pole. Accumulation of FrzX triggers the polarity reversal. The reversal cycle and accumulation of RomR and phosphorylation status of FrzX at lagging pole seems to be working together to regulate the polarity of *M. xanthus* as a relaxed gated regulator in a MglA-MglB dependent manner as shown in figure 1.9 (Zhang *et al.*, 2012; Guzzo *et al.*, 2018).

1.5 MglA and MglB: a molecular switch for polarity regulation in *M. xanthus*

Between 1970-1999, genetics of *Myxococcus xanthus* development and motility have been extensively studied. In that time period (Hodgkin and Kaiser (1977); Hodgkin and Kaiser (1979)) found out that there are two genes involved in motility. Mutation in these genes caused defects in sporulation and affected both types of motility (A-motility and S-motility) of *M. xanthus*. Since the locus affected both types of motility, it was named as *mgl*, which stands for *m*utual *gl*iding motility and it contains two genes; *mglA* and *mglB* (Hartzell and Kaiser, 1991c). In non-motile bacteria, gene that was found mutated was named *mglA* (Hartzell and Kaiser, 1991a). Mutation of *mglB* has also affected the motility, with similar phenotype as *mglA* mutation. Kroos *et al.* (1988) showed that *mglA* gene encodes for a 22 kDa protein. The *mglB* gene produced a protein of 17 kDa.

MglA - a small Ras-like GTPase and MglB, its cognate GAP:

It was suggested that MglB might be an effector of MglA based on its position in the operon and also from a bioinformatics study (Zhang *et al.*, 2010; Miertzschke *et al.*, 2011; Keilberg and Søgaard-Andersen, 2014). Later, it was proved that MglA is a small Ras-like GTPase while MglB is a cognate GTPase Activating Protein (GAP) for MglA and helps MglA in the hydrolysis of GTP (Figure 1.10) (Leonardy *et al.*, 2010; Zhang *et al.*, 2010; Zhang *et al.*, 2012). *Mx*MglA (*Myxococcus xanthus* MglA) is closest to the Arf subfamily of small Ras-like GTPase

(Miertzschke *et al.*, 2011) while *Mx*MglB (*Myxococcus xanthus* MglB) possesses a Roadblock domain like structure (Levine *et al.*, 2013), similar to the longin domain in eukaryotes (Miertzschke *et al.*, 2011).

Small Ras-like GTPases are proteins that can hydrolyse GTP to GDP and inorganic phosphate. These proteins were first discovered in eukaryotic cells and were categorised under oncogenic proteins because mutation in these proteins led to cancer. Later such hydrolases have been found to involved in many essential cellular processes i.e. cell division, growth, metabolism and migration etc. They have been classified based on their structure and function. These GTPases switch between active to inactive state, where the active state is GTP bound state while inactive state is GDP bound state. There are proteins which regulate the two nucleotide bound states of GTPases i.e. GTPase Activating Protein (GAP) and Guanine nucleotide exchange factor (GEF). GAPs are responsible for bringing GTPase to inactive state by helping in GTP hydrolysis. GAPs provide the catalytic residue for GTP hydrolysis and also, help in positioning the catalytic residue present in GTPase near the gamma phosphate for water mediated catalysis. There are many exceptions to GAPs providing catalytic residues and this has been discussed extensively in chapter 4. GEFs are mainly involved in bringing back the GTPase into active form by replacing the GDP with GTP. There are many other regulators for small Ras-like GTPases. Mechanism of action for all different regulators is further discussed in Chapter 4.

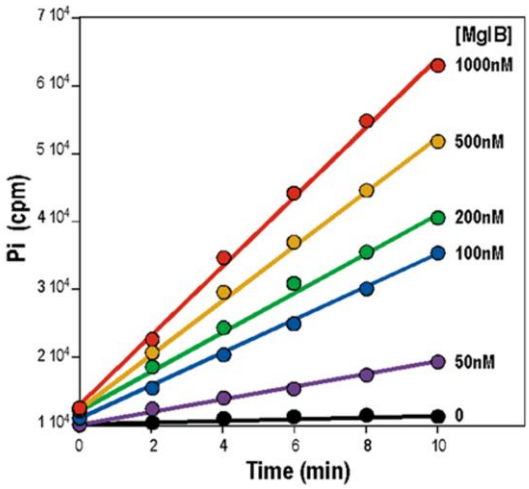

Figure 1.10 MglB, a cognate GAP for MglA
Radioactivity based GTP-hydrolysis assay (Y-axis represents the inorganic phosphate released) for MglA in presence of different concentrations of MglB (Reproduced from Zhang *et al.,* 2010)

MglA-GTP tends to remain at the leading pole while MglB stays at the lagging pole (Figure 1.11A). This has been shown using *in vivo* experiments in *M. xanthus* using fluorescently-tagged MglA and MglB, and GTP hydrolysis mutants of MglA (Zhang *et al.*, 2010; Zhang *et al.*, 2012; Keilberg and Søgaard-Andersen, 2014). They invert their location at the time of reversals i.e. MglA moves to the new leading pole and MglB (Hartzell and Kaiser, 1991b) to the new lagging pole.

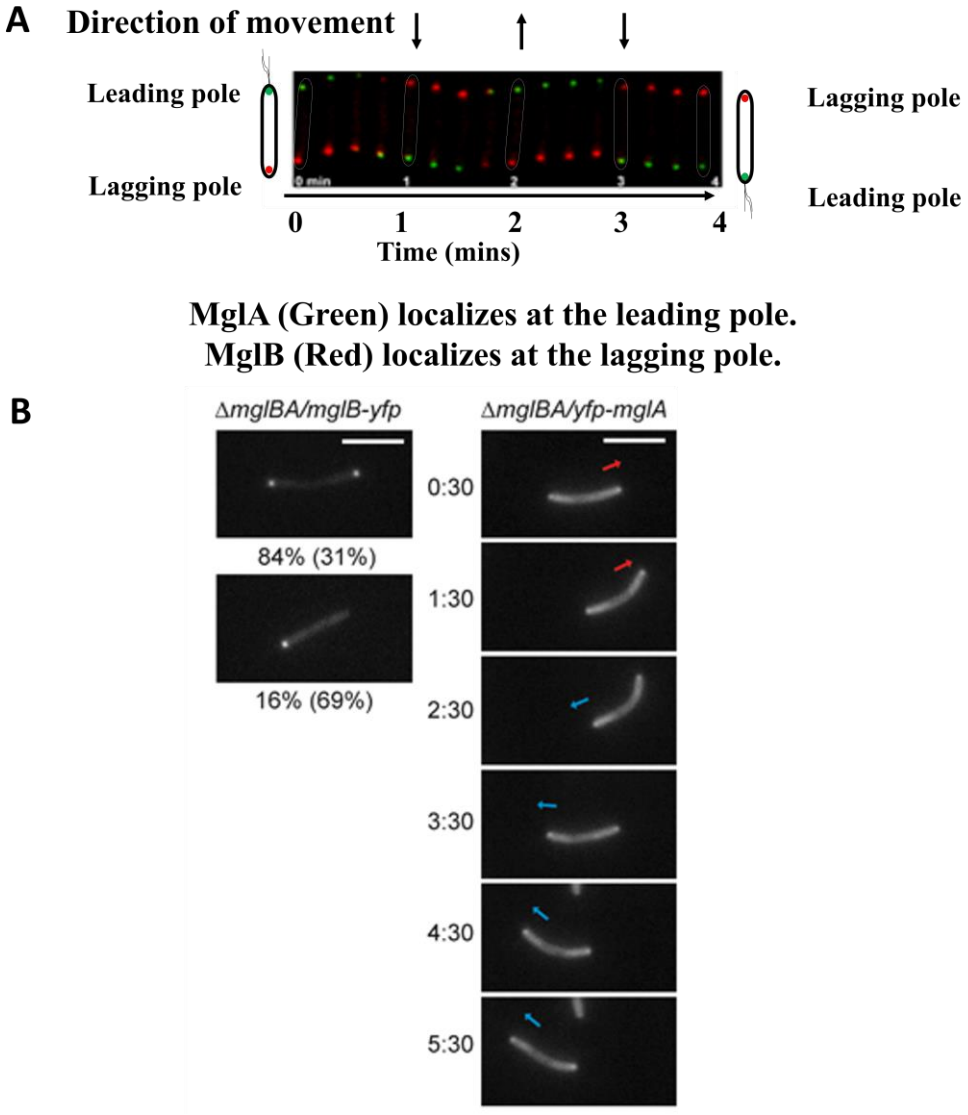

Figure 1.11 Localization of MglA and MglB.
A. Oscillation of MglA and MglB at the time of reversal is shown in this figure. Single bacterium is shown by a solid outline, arrow represents the reversal of polarity while red and green spots at the poles represent MglB and MglA at the lagging and the leading poles, respectively (Adapted from Zhang et al., 2010). **B.** Red and blue arrows represent the direction of motility; MglB becomes bipolar and non-motile in the absence of MglA while MglA also becomes bipolar and loses its direction of motility and polarity. (Reproduced from Leonardy *et al.*, 2010).

MglA-GDP bound form remains uniformly distributed in the cytoplasm. MglB, which helps MglA in hydrolysing GTP, displaces MglA from the poles when GTP is hydrolysed (Fremgen *et al.*, 2010). This results in relocation of MglA to the opposite pole, leading to reversal in cell polarity. This process repeats when MglB reaches the new pole, and this results in oscillations (Figure 1.11A).

Experiments with deletion mutants of either MglA or MglB (Figure 1.11B) (Zhang *et al.*, 2010) shown that the localization pattern is affected and polarity is lost in both the cases (Leonardy *et al.*, 2010). MglA deletion mutants resulted in non-motile cells with bipolar localization of MglB. But in case of MglB deletion, cells were motile but their reversal period decreased. So, they started hyper-reversing and lost their directionality. Hence, net movement was lost. Also, MglA exhibited bipolar localization (Figure 1.11B (Leonardy *et al.*, 2010; Zhang *et al.*, 2010)). Structures of MglA and MglB from *Thermus thermophilus (T. thermophilus)* have been determined. *T. thermophilus* proteins share 64% and 29% sequence identity with the *M. xanthus* MglA (Figure 1.12) and MglB, respectively.

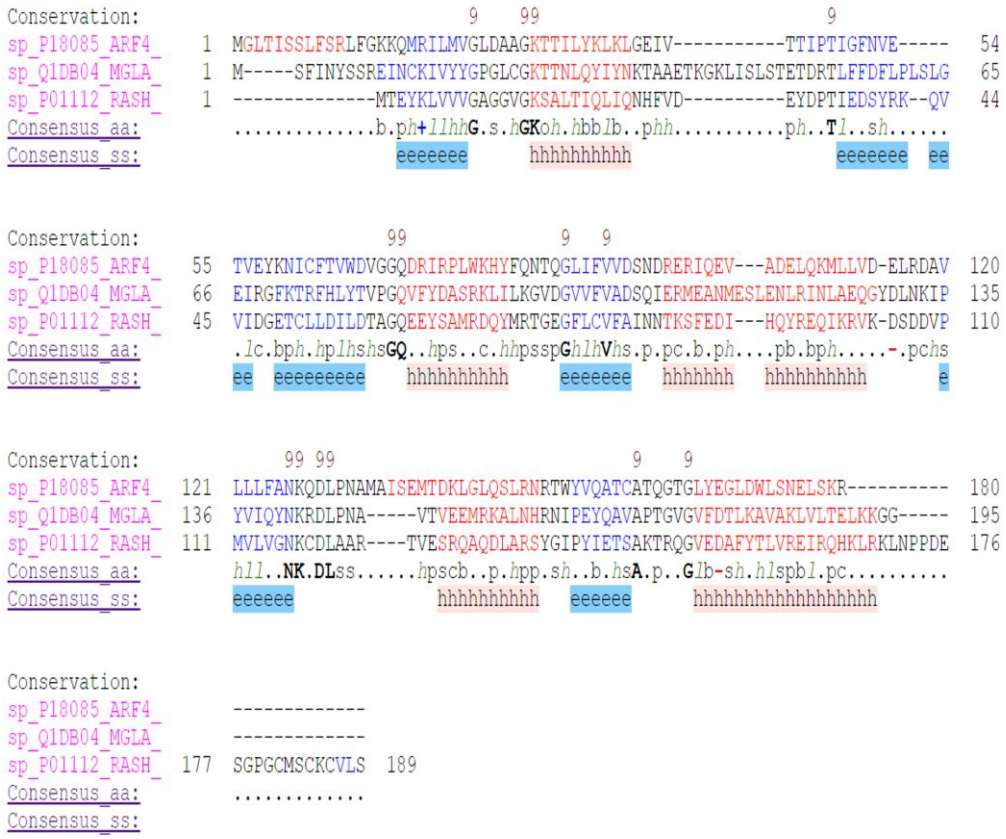

Figure 1.12 Sequence alignment of MglA with Arf and Ras
The alignment was generated using ProMALS3D (Pei *et al.*, 2008). "e" denotes residues in beta-strands, while "h" denotes residues that form helices.

Also, it was confirmed from biochemical studies that MglB acts as a GAP for MglA in *T. thermophilus*. But the functional role of these proteins is unknown in this bacterium and also not much information is available on *T. thermophilus* life cycle and motility, etc. They solved the structure of *T. Thermophilus* MglA (*Tt*MglA) and *T. thermophilus* (*Tt*MglB) in complex with GTP-bound state using X-ray-crystallography. MglA is bound to two protomers of MglB (Figure 1.13; (Miertzschke *et al.*, 2011)).

Another small Ras-like GTPase involved in *M. xanthus* motility is SofG. SofG is a paralog of MglA in *M. xanthus* involved in S-motility and helps in sorting the motility proteins to two different poles i.e. polar localization of PilB and PilT, important for Type-IV pili formation. SofG is another GTPase (Bulyha *et al.*, 2013), with 45 % identity with MglA. But it is larger in size than MglA. MglA is a 23 kDa protein while SofG is 35 kDa protein. Apart from core GTPase domain, SofG has extra N-terminal and C-terminal extension. Corresponding GAP for SofG has not been discovered yet. Schematic diagram for switch cycle of MglA and MglB is shown in figure 1.14.

Figure 1.13 MglA and MglB complex structure from *Thermus thermophilus* (3T1Q)
MglA is shown in green with bound GTP-γ-S and Mg^{2+} in the nucleotide bound pocket. MglB protomer in cyan and magenta.

In the case of *M. xanthus* motility, MglA-GTP bound form is the active form and present at the leading pole while MglB stays at the lagging pole. MglB binds to MglA in the GTP bound state and causes conformational changes that leads to hydrolysis of GTP. GDP bound to MglA needs to be replaced by GTP in order to bring MglA into the active form such that it can bind at the other pole.

Generally, the process of nucleotide exchange is mediated by Guanosine nucleotide exchange factor (GEF) to make the exchange of GDP with GTP faster (Bos *et al.*, 2007), but for *Mx*MglA, the GEF is not known.

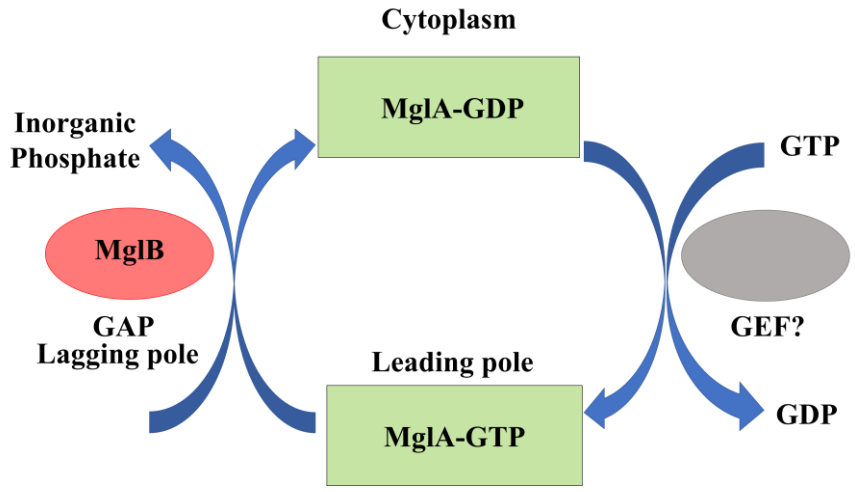

Figure 1.14 Schematic of the GTPase cycle of MglA
MglA GTP-bound state is converted to GDP-bound state after hydrolysis of GTP with the help of MglB. The resultant GDP-bound form of MglA falls off from the poles into the cytoplasm while the GTP bound state of MglA is capable of binding at the leading pole. MglB stays at the lagging pole. Both MglA and MglB are exclusively present at opposite poles. For MglA to regenerate into the GTP-bound form GEFs are required which is unknown in this case (Adapted from Leonardy *et al.*, 2010; Bulyha *et al.*,2011).

1.6 *Myxococcus* motility – Similarities to eukaryotic system

Motility of *Myxococcus* has many similarities with the eukaryotic system (Figure 1.15) (Cogan and Guy, 2010; Mauriello, 2010). Involvement of small Ras-like GTPases and switch cycle of small Ras-like protein, interaction of the protein to cytoskeletal proteins, signalling pathways, formation of focal adhesion complex and force generation by the focal adhesion complex; all these processes in bacteria looks interesting to study and explore. Compared to the eukaryotic system, this system is simple to understand because of the reduced number of components. It is relatively easy to decipher the role of proteins in a minimal system.

There are many questions that are still unanswered in the field of *M. xanthus* motility i.e. how this bacteria senses cues from the environment; how signal is being transferred to regulatory proteins and how these signals affect motility and other cellular responses such as swarming, motility, aggregation, colony formation, fruiting body formation, predation and cell division etc.

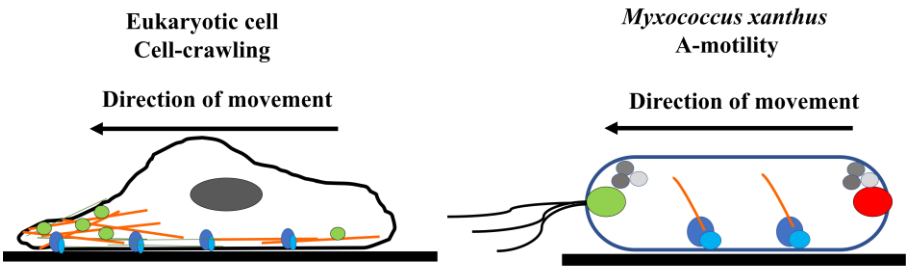

Components	Eukaryotic cell	*M. xanthus*
Ras-like GTPase	Rho, Rac, Cdc42	MglA
Cytoskeleton	Actin	MreB
Signalling	GPCR	Frz
Focal adhesion complex	Present	Present

Figure 1.15 Eukaryotic counterparts in *M. xanthus* motility
Comparison between eukaryotic and prokaryotic motility systems and the respective components involved in cell crawling of eukaryotic cell and A-motility of *M. xanthus* (Adapted from Cogan & Guy, 2010; Bulyha *et al.*, 2010).

There are many proteins which are involved in the motility, and their mechanism of action is unknown. How do SofG and MglA work together? What drives them? What is the possible mode of action of MglB and MglA in regulation of polarity? How do MglA and MglB regulate the localization of other motility proteins?

1.7 Rationale behind the study

Diffusion and capture is one of the mechanisms of spatial transitions of molecules in the cell (Laloux and Jacobs-Wagner, 2014). In this mechanism, proteins or molecules diffuse in the cell but then are captured by other molecules i.e. lipid, landmark proteins, polymer proteins, etc. (Ebersbach and Jacobs-Wagner, 2007; Treuner-Lange and Søgaard-Andersen, 2014). There are many cytoskeleton proteins involved in the spatial localization of proteins and hence, in turn control the function in that particular space of the protein. In *Myxococcus*, some of examples are actin-like cytoskeleton protein, MreB; bactofilin (BacP); and AglZ, a coiled coil protein (Yang *et al.*, 2004). While BacP and AglZ form nucleotide-independent polymers, MreB polymerizes in the presence of actin.

Localization of protein by P-loop ATPases or small GTPases is another mechanism of protein localization within prokaryotes (Ebersbach and Jacobs-Wagner, 2007). In case of *M. xanthus*, MglA and SofG are the GTPases found in regulating the localization of other motility proteins.

However, the GAP, GTPase activating proteins are involved in regulation of the switch cycle of the GTPase. MglB, a GAP is another regulator of motility in the *M. xanthus* of the motility and polarity by detaching MglA from the lagging pole as shown in the figure 1.16.

The idea of this part of work is to characterize the biochemical oscillator MglA and MglB. How does MglB act as a GAP for MglA? What could be the possible mechanism of action of MglA and MglB? For the recycling of MglA to GTP bound form, what is the possible nucleotide exchange factor in *M. xanthus*? To answer all these questions, structural and biochemical studies were carried out. Also, a comprehensive analysis of the small Ras-like GTPase family and their regulator proteins were performed, for a comparison with the mechanism of action of *Mx*MglAB.

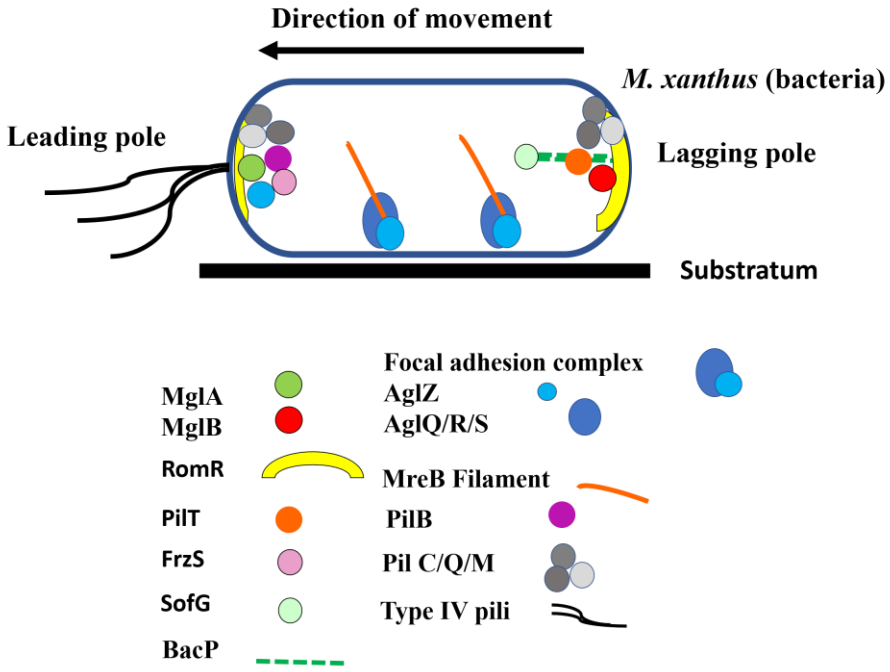

Figure 1.16 Proteins involved in the motility of *M. xanthus*
Schematic of localization of proteins in motility (Adapted from Zhang *et al.*, 2012; Leonardy *et al.*, 2010)

In the following chapters, work done on *Myxococcus xanthus* MglA and MglB are discussed. Chapter 2 describes the structure determination of MglA, MglB and the MglAB complex using X-ray crystallography. This led to the characterization of the interaction between MglA and MglB. To estimate the activity of the protein, biochemical assays have been performed. Also, mutants have been generated to confirm the binding affinity and activity of both the proteins. All the biochemical studies are described in chapter 3. From the biochemical and structural analyses, a mechanism of action of MglB and MglA was proposed. Further, to understand how

other GTPases and their interacting proteins i.e. GAP and GEF, function together, structural analysis of all the GTPases and the complexes have been explored and discussed in chapter 4. This allowed for a comparison of MglAB interaction with all characterized GTPases and activator complexes. Chapter 5 summarises the findings of the thesis and future prospects.

Chapter 2

Structure determination of *M. xanthus* MglA and MglB

2.1 Background

From structural and biochemical studies on *Thermus thermophilus* MglA and MglB (Miertzschke *et al.*, 2011), we know that *Myxococcus xanthus* MglA (*Mx*MglA), is a small Ras-like GTPase while *Mx*MglB is a protein with the Roadblock domain which helps in GTP hydrolysis. Since our aim was to understand the whole motility mechanism of *M. xanthus*, we started with characterization of MglA and MglB, that has been found to drive the polarity oscillations. Both of them are mediators between the sensory control module, an example of chemotaxis which senses the environmental signal, and the motility regulator of *M. xanthus* (Bulyha et al., 2011).

For the structural insights into the protein-protein interaction, X-ray crystallography was carried out. Using which atomic details of interactions among proteins can be studied. Nucleotide bound states of MglA and the complex of MglA-MglB can help in providing insights into the mechanism of action of MglA as a GTPase and also to understand the role of MglB in activating the GTP hydrolysis by MglA. This chapter discusses the structural aspects of MglA, MglB and structure of the complex between them.

2.2 Introduction to X-ray crystallography

The major techniques available today to deduce the structure of protein molecules are NMR, X-ray crystallography and cryo-electron microscopy. Every technique has its own advantages and limitations i.e. for NMR and Cryo-EM protein size should be smaller than 20 kDa and 100 kDa, respectively. X-ray crystallography would be best approach to get structural information in this case. One of the requirements in X-ray crystallography is that we need a protein sample of very high quality (homogeneous) and in good quantity. Crystal should be of good quality to diffract and give high resolution data (Dessau and Modis, 2011).

Structure determination using recombinant proteins consists of several steps – cloning of the desired gene, its overexpression, purification of the protein, crystallization, collection of diffraction data from the crystals and finally phase determination, and cycles of model building and refinement (Hui and Edwards, 2003). The whole process is shown by the flow chart below (Figure 2.1).

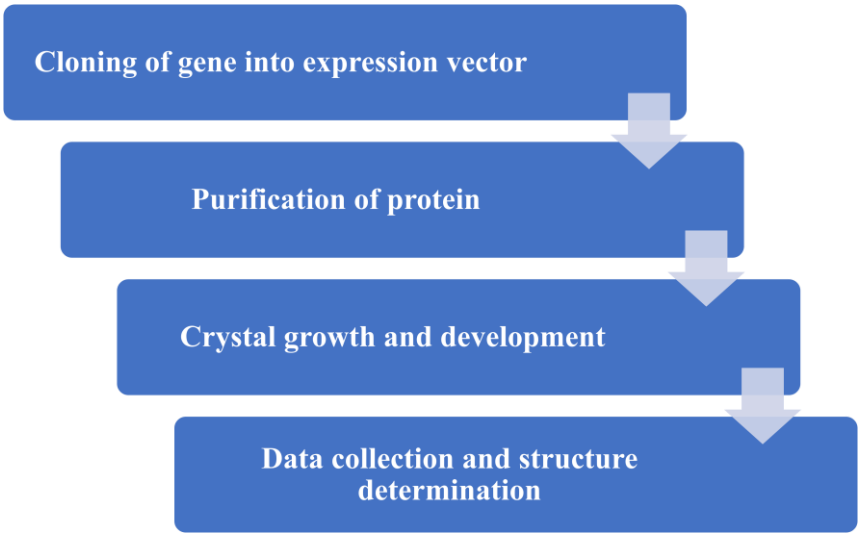

Figure 2.1 Steps in protein crystallography.
Flow chart represents schematically the steps involved in the X-ray crystallography of recombinant proteins.

2.2.1 Cloning and protein purification

For crystallographic studies, protein of interest is required in large quantities and in purified form. To obtain high quantities, these proteins are cloned into a suitable expression vector, which is compatible with the expression system. Sometimes different tags are attached to the proteins to facilitate purification. There are different ways to get the purified protein. Protein purification steps include passing the cell lysate through multiple purification columns i.e. affinity chromatography, ion-exchange chromatography, size-exclusion chromatography, etc. Purified protein will be allowed to crystallize at different conditions.

2.2.2 Instrument

Crystals are the periodic array of unit cells and it consists of an arrangement of protein molecules. The diffractometer is the instrument used to obtain the diffraction data from the crystals. X-ray generated at the cathode is allowed to pass through the crystal and rays diffracted by the crystal give unique diffraction pattern. Integral parts of the diffractometer are (Rupp, 2010):

1. A **source** of strong X-ray
2. Suitable optics to get the **monochromatic beam** of X-rays
3. **Goniostat**, to orient the crystals in the path of X-rays
4. A good quality **detector** to capture the diffracted X-rays

Other than these, there are a few more components of the system, namely a cryocooler, to reduce radiation damage of the crystals; a microscope to align the crystal in the path of X-ray beam; and instrument to handle data collection software.

2.2.3 Crystallization

To do X-ray crystallography, the basic requirement is a crystal of that particular protein. The method or process through which protein crystals are formed is called protein crystallization.

What are crystals?

Crystals are repeated arrays of unit cells in three-dimensional space to form a lattice. The whole crystal can be generated by the arrangement of asymmetric units (smallest component of unit cell with no symmetry) through symmetry operations. Different unit cells are characterized by the parameters i.e. lengths of the three sides and the angles between them. Crystal systems defined based on dimensions and angles of unit cell are triclinic, monoclinic, trigonal, orthorhombic, tetragonal, hexagonal and cubic. There are only 14 unique crystal lattices and are called Bravais lattices. 32-point groups and 230 different space groups exist. The dimension of the unit cell can be obtained from the diffracting pattern of the crystal.

A. Principle of crystallization

The basic idea of crystallization is to separate out the protein molecules from solution, which can be achieved by adding molecules or compounds that assist in the precipitation or segregation of the protein molecules out of the solvent. There are many parameters which affect the crystallization process i.e. pH, buffers, salts, temperature etc.

Gibbs-Helmholtz equation is valid for protein crystallization where free energy is directly associated with enthalpy. The change in the Gibbs-free energy, ΔG at constant temperature is dependent on entropy, ΔS and enthalpy, ΔH (shown below equation 1). For the crystallization of protein, ΔG should be negative, to favour the process of nucleation.

The crystallization constant is associated with the Gibbs-free energy at equilibrium as shown in the equation 2, where R is the gas constant and T is the absolute temperature.

$$\Delta G^{\circ}_{cryst} = \Delta H^{\circ}_{cryst} - T\Delta S^{\circ}_{cryst} \quad \ldots\ldots\ldots\ldots\ldots\ldots\ldots\ldots 1$$

$$K_{cryst} = \exp\left(-\Delta G^{\circ}_{cryst} / RT\right) \quad \ldots\ldots\ldots\ldots\ldots\ldots\ldots\ldots 2$$

The protein crystallization is very sensitive because ΔG is less and can be easily shifted to positive values and this makes the process very difficult. So, it is sensitive to any slight change in the temperature or solvent constituents including pH and salt concentrations. Also, ΔH in the protein crystallization is less or insignificant because of lack of strong intermolecular bond during crystallization. Hence protein crystallization is an entropy-driven process (DeLucas *et al.*, 2003).

The process of crystallization is the arrangement of protein molecules in a unit cell which is against the entropy. The process of crystallization becomes favourable when entropy increases. This is possible only by the water molecules trapped inside the protein and also the water molecules which surround these proteins. These water molecules remain in equilibrium with the bulk water molecules to make the process of crystallization favourable. Based on that the equation for the crystallization is modified as below in equation 3 (Derewenda, 2004).

$$\Delta H^{\circ}_{cryst} = \Delta H^{\circ}_{cryst} - T\,(\Delta S^{\circ}_{Protein} + \Delta S^{\circ}_{solvent})_{cryst} \quad \ldots\ldots\ldots\ldots\ldots\ldots 3$$

There are three different paths which a protein can choose during crystallization setup i.e. precipitation, metastable zone and nucleation. The crystals are formed in supersaturated state as shown in the Oswald-Miers diagram (Manuel García-Ruiz, 2003) (Figure 2.2). Nucleation is defined as the process when the protein reaches to the state of supersaturation and starts coming out of solution as a crystal (Nanev, 2013).

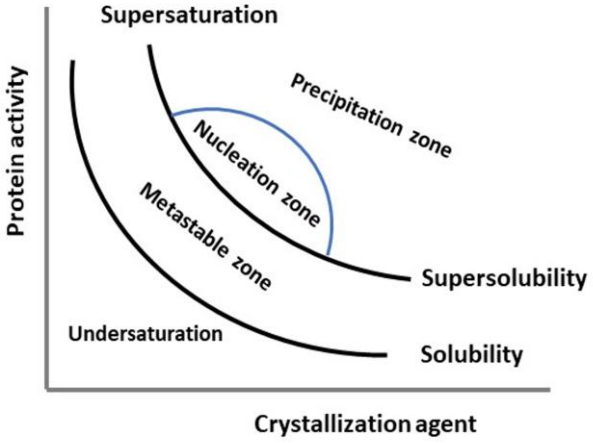

Figure 2.2 Oswald-Miers phase diagram.
Proteins starts crystallizing in the supersaturation state (Adapted from Nanev, 2013).

Nucleation can be controlled by seeding i.e. micro-seeding and macro-seeding. In micro-seeding, some amount of liquid from the drop is transferred to the new crystallization drop

while in the case of macro-seeding, the small crystals are transferred to the new fresh drop to drive the crystallization process. The quality of crystals decides the resolution of diffraction.

B. Crystallization techniques

There are many methods to crystallize proteins - a few of them are vapour diffusion, batch crystallization, dialysis and free-interface diffusion (Salemme, 1972), etc. Vapour diffusion methods are the most common among all the crystallization techniques (DeLucas *et al.*, 2003). In vapour diffusion, the droplet contains the protein mixed with the crystallization condition. This droplet is allowed to exchange with a large reservoir of the same crystallization condition containing buffers, salts and precipitants. This method of crystallization is appropriate for both hanging and sitting drop methods of crystallization. In the hanging drop method, a mix of drop, containing the protein and the condition is placed on an inverted coverslip and placed onto the reservoir of the crystallization condition and vaccum sealed. This mimics a small closed chamber. Because the droplet contains the mix of protein and the condition, it has a lower concentration of salts and precipitant. But with time, vapour diffusion takes place between the droplet and the reservoir, which continues till the system reaches equilibrium. This results in crystals if the condition is appropriate for the proteins. The gradual changes in concentration of the protein and the precipitant leads to supersaturation, thereby resulting in nucleation and then growth of the crystal (Hui and Edwards, 2003; Dessau and Modis, 2011; McPherson, 2017).

On the other hand, in micro-batch the mix of protein and condition is immersed in the oil. In micro-dialysis, there is a membrane which allows the small molecules and salt to pass but not the protein and polymer and this way it reaches towards a state of supersaturation where proteins start crystallizing. Free-interface diffusion is another strategy that allows the protein and condition to mix through diffusion and not by prior mixing as used in the other methods explained above (Dessau and Modis, 2011).

C. Crystallization strategies

The buffer conditions or the temperature at which the protein will crystallize is unknown for any new protein. Hence, different combinations of buffers (pH), salts and precipitating agents require to be tried. This can only be achieved by multiple trials and different possible combinations of the components of the conditions because the prediction of the condition in which the protein will crystallize is not possible. Nowadays there are companies which provide

the innumerable combinations of crystallization conditions or kits for the initial trials. The parameters to be taken care for the crystallization of proteins are mentioned below:

a. Protein constructs and affinity tags (Derewenda, 2004)
b. Purity, freshness, conformational state, batch variation and contaminants (Dessau and Modis, 2011)
c. Purity and exact composition of the buffer, salts, and additives in crystallization condition.

2.2.4 Structure determination and refinement

There are many processes and experiments after getting the crystal. Figure 2.3 shows the steps to obtain structure from the crystal. During, crystal diffraction by X-ray, data is recorded as intensities that yield an estimate of structure factor amplitudes with unique h, k and l values (F_{hkl}). All the electrons in the molecules of a crystal structure are denoted by an electron density function and it is related to the amplitude and phase of diffracted wave through a mathematical calculation called Fourier transform. Using inverse fourier transform, the structure of protein is derived in real space from reciprocal lattice as shown in figure 2.4.

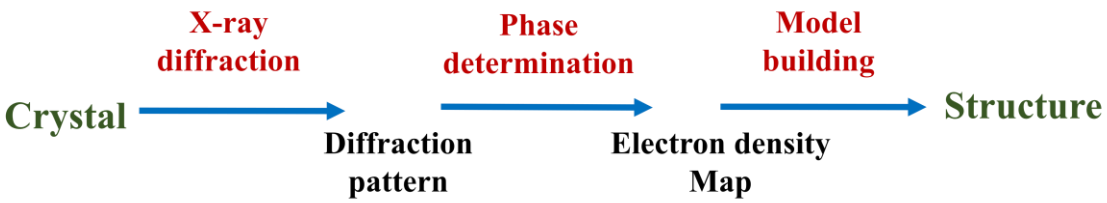

Figure 2.3 From crystal to structure
First step to study proteins by crystallography is to get crystals. Then it should be diffracted by X-ray. The diffraction pattern obtained is used to finally determine the structure of protein.

Both amplitude and phase of the structure factors are required for the calculation of the electron density maps. Amplitude can be obtained from the intensities but to get the phase information, there are methods available in X-ray crystallography (Rupp, 2010). Some of them are mentioned below:

1. Single isomorphous replacement / Multiple isomorphous replacement (SIR/MIR): Data from two sets is required i.e. native data and data from crystals soaked with heavy atom solution are required.

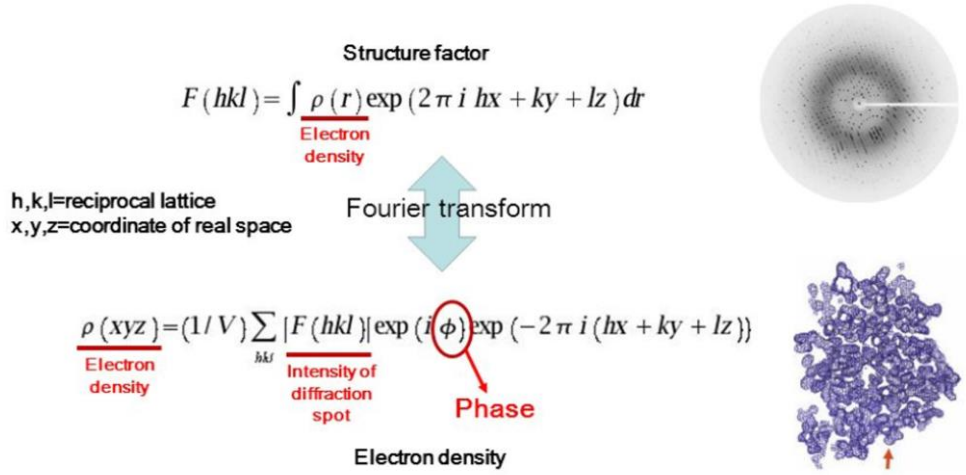

Figure 2.4 Fourier transform and the phase problem in crystallography
(Reproduced from Rupp, 2010).

2. Single wavelength anomalous diffraction/Multi-wavelength anomalous diffraction (SAD/MAD): Data from native crystal and from anomalous (with selenomethionine) crystal of same protein collected to solve the structure. This can be collected at single or multiple wavelength to get the phase information.

3. **Molecular replacement:** Structure of similar protein can be used to solve the structure.

From these methods, phase problem can be solved and the electron density map can be calculated. The electron density map is derived from the phase information by the above-mentioned methods and the amplitude by the native crystal, using inverse Fourier transform. The interpretation of electron density map during the process of model building and refinement determines the coordinates of the atoms in the protein.

There are many parameters to be taken care at the time of data collection i.e. R_{meas}, R_{pim}, $CC_{1/2}$, mean I/σI, while refinement statistics which need to be taken care for the good quality data are R_{work}, R_{free}, B-factor, Ramachandran outliers and RMSD of all bond length and angles (Karplus and Diederichs, 2015).

2.3 Materials and methods

2.3.1 Cloning and overexpression

Genes corresponding to *mglA* and *mglB* were amplified from *Myxococcus xanthus* genomic DNA (obtained from DSMZ, Germany, catalogue number 16526) using suitable primers and cloned into *pHis17* vector (Addgene plasmid #78201) between the restriction enzyme sites

NdeI and BamHI using a PCR based method for restriction free cloning (RF-cloning). Deletion constructs of MglB, MglB^{Ct} were created using a site-directed mutatgenesis strategy utilizing PCR based methods followed by DpnI digestion, transformation and screening of positive clones as shown in figure 2.5. All clones were confirmed by sequencing. The list of clones and the primers used to generate them are summarized in Appendix.

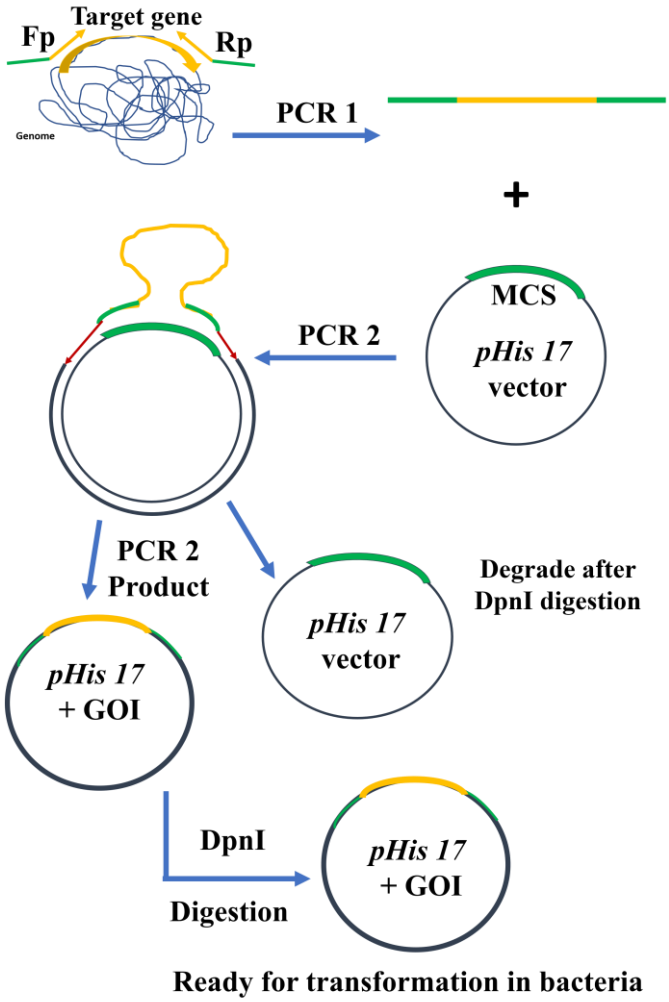

Figure 2.5 Restriction free cloning
Gene of interest (GOI) shown in yellow, multiple cloning site in green, and the rest of *pHis 17* vector in black, the red line shows region of initiation of amplification of the vector.

Plasmid containing the gene of interest was transformed into suitable *E. coli* strains and culture was grown at 37 °C and at 30 °C post induction. *E. coli* strain BL21-DE3 was used for expressing *Mx*MglA wild type and mutants. The cultures were grown in LB media containing 50 µg/ml of ampicillin, and induced with 0.5 mM IPTG at OD_{600} value of 0.8, while *Mx*MglB and its mutants were expressed in the strain BL21-AI and induced with 0.02 % L-arabinose at

OD_{600} value of 0.6. The presence of protein in the culture or overexpression was checked on SDS-PAGE gel.

The gene of interest was transformed into *E. coli* and plated on agar plate containing LB media with ampicillin as an antibiotic. From this plate next day, the colonies were inoculated in 5 or 10 ml LB broth containing ampicillin and culture was grown at 37˚C. When the $O.D._{600}$ reached at optimum expression level, (0.6 for the MglB and 0.8 for the MglA) the bacterial cultures were induced by 0.02% of L-arabinose or 0.5 µM IPTG for BL21AI or BL21DE3, respectively and temperature was shifted to 30˚C of the shaker-incubator. 5 ml bacterial culture was centrifuged at 5000 rpm for 5 minutes to pellet down the cells, then 200 µl of lysis buffer (50 mM Tris, 200 mM NaCl pH 8.0 and 10 % glycerol) added and the cells were resuspended into this buffer. After resuspension, the bacterial cells were sonicated to break open the cells. Sonication cycle was 5 sec on and 5 sec off for 1 minute. Then the samples were spun at 15,000 rpm for 10 minutes. 10 µl supernatant and pellet was mixed with 10 µl and 50 µl SDS-PAGE loading dye, respectively, then heated for 10 minutes at 99˚C then again spun at 15,000 rpm for 5 minutes and loaded on 12% or 15% SDS-PAGE gel. After loading the sample, the gel was electrophoresed at a constant voltage 230 mV for approximately 40 minutes. Then the gel was stained and de-stained by dye and picture was taken on E-gel imager (Life Technologies).

2.3.2 Purification of proteins MglA and MglB

A. Purification of $MglA_{(His6)}$

For purification, the cells were harvested, resuspended in the lysis buffer L (50 mM Tris, 200 mM NaCl pH 8.0 and 10 % glycerol) and then spun at 39000xg for 45 mins at 4 °C. Supernatant was loaded on to a 5-ml HisTrap (GE) column since the presence of hexahistidine tag at the C-terminus facilitated binding of the overexpressed protein of interest to the column. The column was equilibrated with binding buffer (Buffer A: 50 mM Tris pH 8.0, 200 mM NaCl) prior to loading the supernatant and the bound protein was washed and eluted with a step gradient of 2%, 5%, 10%, 20%, 50% and 100% of Buffer B (Buffer A containing 500 mM imidazole). The presence of protein at each step was confirmed by the UV peak on the FPLC system and fractions corresponding to that were run on the gel to confirm the presence of pure protein. Mostly, MglA elutes into the fractions of 20% and 50% Buffer B. The fractions containing the protein were pooled, concentrated and loaded onto the Superdex75, 10/300 (GE Lifesciences). The protein was eluted into 50 mM Tris pH 8.0, 50 mM NaCl, fractions containing the protein

were pooled, concentrated using centricon, flash frozen and stored at -80 °C. Concentration of the protein was estimated by measuring absorbance at 280 nm using Nanodrop 2000 (Thermo). Concentration was also confirmed by Bradford assay (protein estimation method)g (Bradford, 1976).

B. Purification of MglB

$MglB_{(His6)}$ and $MglB^{Ct}_{(His6)}$ were purified using the same protocol as described for $MglA_{(His6)}$. Following affinity chromatography, MglB was either purified further by gel filtration or ion exchange chromatography using MonoQ (GE Lifesciences). After Ni-NTA purification, the eluted fractions of MglB were pooled and concentrated, to do gel-filtration chromatography (Size-exclusion chromatography, SEC). But to get more purer MglB MonoQ was performed instead of SEC, MglB fractions eluted from Ni-NTA were dialysed into Buffer A25 (50 mM Tris pH 8.0, 25 mM NaCl) again spun at 39000 g at 4 °C and filtered before loading on the MonoQ 10/100 (GE Lifesciences). Buffers used for binding and elution are Buffer A (50 mM Tris pH 8.0, 50 mM NaCl), along with a linear gradient of mix with Buffer B (50 mM Tris pH 8.0, 1 M NaCl) respectively, ranging from 0 % to 50 % B over 20 column volumes. Before loading the proteins, the column was equilibrated with Buffer A. Fractions from the MonoQ run were checked on SDS-PAGE and fractions with protein of interest were concentrated, flash frozen and stored at -80 °C.

After trying the gel filtration and MonoQ, after the Ni-NTA affinity purification, MonoQ was found to give purer protein than gel filtration, so later all the purifications were done with MonoQ after Ni-NTA. The protein quality was checked at every step. MglB elutes at the conductivity of 28 mS/cm during MonoQ run. MglB concentration was estimated using Bradford method of protein estimation. In case of both MglA and MglB, the proteins do not have tryptophan and hence the concentration could not be reliably estimated using absorbance at 280 nm.

C. Concentration estimation of proteins

Bradford Protein assay: This has been performed with Bradford reagent (Bio-Rad). Different concentrations of BSA ranging from 0.2 – 2 mg/ml were used to obtain the standard curve (Appendix). 250 µl of the Bradford reagent was added in the 96 well plate and 5 µl of the protein containing either the BSA standard concentrations or the protein sample was added. The absorbance measurements were taken at a wavelength of 595 nm (Bradford, 1976).

D. Oligomerization studies by SEC-MALS

Size exclusion chromatography (SEC) separates the molecules according to their hydrodynamic radius. Elution of proteins are dependent upon the molecular size not on the molecular weight i.e. molecules of bigger size elute first than smaller molecules. Sometimes it becomes difficult to get the correct size of protein from SEC only because it doesn't consider shape of protein. On the other hand, in SEC-MALS light scattering enables to get the molecular size correctly because this technique measures the intensity of scattering and calculates the molar mass and rms radius in solution along with the elution volume (Folta-Stogniew and Williams, 1999). Superdex 200, 10/300 (GE Lifesciences) column used for SEC-MALS connected to an Agilent HPLC (18-angle light scattering detector, Wyatt Dawn HELIOS II) and a refractive index detector (Wyatt Optilab Tr-Ex). ASTRA software (Zimm model implemented) was used for curve fitting and estimation of molecular weight. BSA 2 mg/ml was used for calibration. 100 ul of 2 mg/ml MglB was injected onto the column to confirm the oligomerization status of MglB.

2.3.3 Crystallization

A. Crystallization of MglA

About 500 conditions of commercially available screens (Molecular dimensions, Hampton Research) were screened using Mosquito® crystallization robotic system, using drop sizes consisting of 100 nl of protein at a concentration of 10 mg/ml and 100 nl of crystallization cocktail, in 96-well sitting drop plates (MRC plate, SWISS-SCI). Initial hits were obtained in many of the conditions and, further it was optimized and reproduced to get well-diffracting crystals. For crystallization of MglA, protein was diluted to a final concentration of 10 mg/ml in A50 buffer (50 mM Tris pH 8.0, 50 mM NaCl). Many drop ratios of the protein and condition were tried. As per the ratio of protein and condition, different ratios of 0.5 µl + 0.5 µl, 0.5 µl + 0.8 µl, 0.5 µl + 1.0 µl and 1.0 µl + 1.0 µl were tried in the crystal optimization process. All these drop ratios were tried in all other protein crystals too. For MglA, 0.5 µl + 0.5 µl gave good quality crystals.

Diffraction quality crystals were obtained using the following conditions in a drop ratio of 1:1 volume: i) 0.1 M sodium cacodylate pH 6.5, 40 % v/v 2,4-methyl pentane diol, and 5 % PEG 8000 ii) 0.1 M imidazole pH 8.0, 30 w/v % 2,4-methyl pentane diol, and 10 % w/v PEG 4000

iii) 0.1 M sodium citrate pH 5.6 and 35% w/v tertiary-butanol. 20 % ethylene glycol was included as cryoprotectant in the parent condition during crystal freezing.

B. Crystallization of MglB

For MglB crystallization more than 960 different conditions were tried using Mosquito® crystallization robotic system, which can aliquot crystallization drops as low as 100 nl. Extensive screening was done for MglB at different conditions. All the crystallization drops which gave some initial hits were optimised further for good quality crystals. There were a few conditions in which MglB formed crystals. But only a few gave diffracting crystals. The conditions in which the crystals diffracted the best were: i) 1M Succinic acid pH 7.0, 0.1M HEPES pH 7.0, PEG2K (2%) ii) 1M Succinic acid pH 7.0, 0.1M HEPES pH 7.0, PEG 3350K (2%). Crystallization conditions for $MglB^{Ct}$ were i) 50% v/v Pentaerythritol propoxylate (5/4 PO/OH) ii) 0.2M Sodium chloride, 20% w/v PEG 3350, pH 6.9. Condition containing 20 % PEG 400 was used as cryoprotectant.

C. Crystallization of MglAB Complex

To acquire the MglAB complex, screening for crystallization hits yielded a few conditions that were further optimized to get desirable crystals. MglAB complex was crystallized in the presence of different nucleotides i.e. GMPPNP, GDP.AlF_x, GTP-γ-S; where GDP.AlF_x is the transition state analog of GTP while GMPPNP and GTP-γ-S are the non-hydrolysable analogs of GTP. GDP.AlF_x was obtained by mixing 20 mM NaF and 2 mM $AlCl_3$ with GDP in a ratio of 10:1:1, respectively. GDP used in the reaction was 2 mM. All the components were mixed to form a reaction mix for crystallization. Also, MglA and MglB were mixed in different ratios i.e. 1:1, 1:2, 1:4 in µM, for the crystallization trials. MglA and MglB were mixed in different ratios, i.e., 1:1, 1:2, 1:4 in A50 buffer containing 5 mM $MgCl_2$ and 2 mM GTP-γ-S (Sigma), but the ratios which gave crystals of the MglAB complex were 1:1 and 1:2. MglA was used at a concentration of 4 mg/ml in the mix. The crystals were obtained in two different conditions namely i) PEG 4000 (8 %) and ammonium sulphate (200 mM); and ii) PEG 3350 (12 %) and ammonium sulphate (200 mM). Different cryoprotectants were tried and checked i.e. crystallization conditions containing 20 % ethylene glycol, 20 % glycerol or 20 % PEG 400. But finally, crystallization conditions containing 20 % PEG 400 were used as cryoprotectant during freezing of crystals because that gave the best results.

2.3.4 Structure determination

Diffraction data from the crystals were collected at home source using Rigaku MicroMax-007 HI X-ray generator, and higher resolution data and anomalous data were collected at the synchrotron sources at Diamond Light Source, Harwell, UK and ESRF, Grenoble. Data reduction was performed using iMOSFLM (Battye *et al.*, 2011) or XDS (Kabsch, 2010b, a), and scaling using AIMLESS (Evans and Murshudov, 2013) in CCP4 package (Murshudov *et al.*, 1997; Winn *et al.*, 2011; Potterton *et al.*, 2018). Molecular replacement was performed using PHASER (Bunkóczi *et al.*, 2013) available in CCP4 package. Refinement was carried out using PHENIX package (Echols *et al.*, 2012) and model building using *Coot* (Emsley et al., 2010) MglA and MglB structures were solved by molecular replacement using the *Tt*MglAB structure (PDB ID: 3T12).

In order to confirm the registry of the amino acids belonging to the C-terminal helix of MglB, selenomethionine-labelled protein for mutant constructs of MglB where I^{148} and L^{156}, respectively were mutated to methionines, were purified and selenomethionine-labelled MglB was used to obtain *Mx*MglAB crystals in the same crystallization conditions. The anomalous data from the crystals were collected and the correct amino acids could be modelled into the electron density.

2.3.5 Methionine mutants of MglB to confirm registry of the C-terminal helix

A. Cloning and expression

$MglB^{L156M}$ and $MglB^{I148M}$ mutants was expressed and the culture was grown by the feedback inhibition method to incorporate selenomethionine instead of methionines. Expression check was done similarly as mentioned in the section 1.2.1 for MglB.

B. Purification and crystallization

For MglB constructs without histidine tag, i.e. MglB and selenomethionine-labelled $MglB^{L156M}$ and $MglB^{I148M}$, ion exchange chromatography was used to purify the proteins. First, the cells were resuspended in the lysis buffer (50 mM Tris pH 8.0, 200 mM NaCl, 10% glycerol), and then spun at 39000 g for 45 mins at 4 °C. An ion exchange column, QHP (GE Lifesciences) was used to purify the protein. Buffers used for binding and elution are Buffer A (50 mM Tris pH 8.0, 50 mM NaCl), along with a linear gradient of mix with Buffer B (50 mM Tris pH 8.0,

1 M NaCl) respectively, ranging from 0 % to 50 % B over 20 column volumes. 20% of Buffer B fractions containing the protein of interest were pooled. This protein was dialysed into Buffer A25 (50 mM Tris pH 8.0, 25 mM NaCl) again spun at 39000g at 4 °C, filtered and loaded on the next column i.e. MonoQ 10/100 (GE Lifesciences) to remove minor impurities present. Binding and elution buffers were the same as earlier. Fractions from the MonoQ run were checked on SDS-PAGE and those containing protein of interest were concentrated, and stored at -80 °C.

The crystallization of these MglB mutants, $MglB^{L156M}$ and $MglB^{I148M}$ with MglA was performed in the same conditions as MglA-MglB complex, discussed above in the section 2.3.3C.

2.3.6 HPLC to determine the presence of bound nucleotide in MglA

Purified MglA was diluted to 2-3 mg/ml concentration in buffer A50 and then heated at 65 °C. The heated protein sample was spun at 21,000 g for 10 mins at 4 °C. Then the supernatant was filtered with 0.22 μm cellulose acetate filter (Corning) and the sample was loaded on a DNAPac 200 ion-exchange analytical column 4*250nm (Dionex, Cat No. 63000). Buffers used for binding and elution are Buffer A (2 mM Tris pH 8.0), along with a linear gradient of mix with Buffer B (2 mM Tris pH 8.0, 1.25 M NaCl) respectively, ranging from 0 % to 50 % B over 20 column volumes. The runs were performed at a flow rate of 0.8 ml/min, with steps of 0 % buffer B for 3 minutes, followed by linear gradients of 0 to 30 % B for 10 minutes, and 30 to 100 % B for 12 minutes. The peak profile obtained was compared for runs of 18 μM of MglA and 50 μM GDP solutions, respectively, with 35 μl of sample injection volume for both. The absorbance at 260 nm, indicative of the presence of GDP was plotted against retention time.

2.4 Results

2.4.1 Protein purification

*Mx*MglA and *Mx*MglB was cloned in *pHis17* vector and overexpressed in BL21DE3 and BL21AI, respectively. Before starting the protein purification, the protein was checked for its presence in 1 ml culture as mentioned in the Materials and Methods section 2.3.1.

Purified MglB was 95 % pure while *Mx*MglA appears to be a single band of protein based on the SDS-PAGE gel as shown in the figure 2.6. The size-exclusion chromatography showed that *Mx*MglA is a monomer and *Mx*MglB eluted at a volume higher than a dimer (Figure 2.7A).

The dimeric state of *Mx*MglB was confirmed by the SEC-MALS, (shown in figure 2.7B). All the proteins were characterized by mass spectrometry to confirm the exact molecular weight and detect for any proteolytic degradation of the purified protein (Appendix).

3L of *E. coli* culture was grown to extract the protein of interest. After all the steps of purification, final amount of protein obtained was around 8 mg and 18 mg per litre of *Mx*MglA and MglB culture, respectively. Different batches of culture gave almost similar amount of proteins. Approximately 50 batches of *Mx*MglA and 23 batches of *Mx*MglB were purified for our study. The yields for *Mx*MglB$^{sel\text{-}met}$, *Mx*MglB^{Ct}, *Mx*MglB^{L156M} and *Mx*MglB^{I148M} were the same as *Mx*MglB.

*Mx*MglA tends to precipitate while *Mx*MglB is comparatively more stable than *Mx*MglA. It has been observed that while concentrating the protein, *Mx*MglA tends to precipitate but *Mx*MglB becomes viscous.

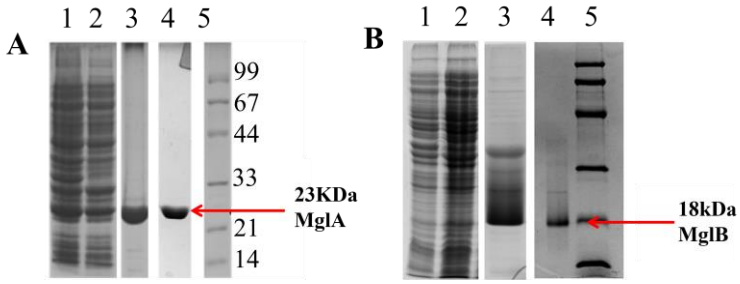

Figure 2.6 SDS-PAGE profiles of MglA and MglB purification
A. Purification profile of *Mx*MglA **B.** Purification profile of *Mx*MglB. For both the panels, lane 1: total cell extract; lane 2: soluble fraction of the cell extract (cell lysate); lane 3: fraction from Ni-NTA affinity column; lane 4: elute from gel-filtration chromatography; lane 5: protein marker.

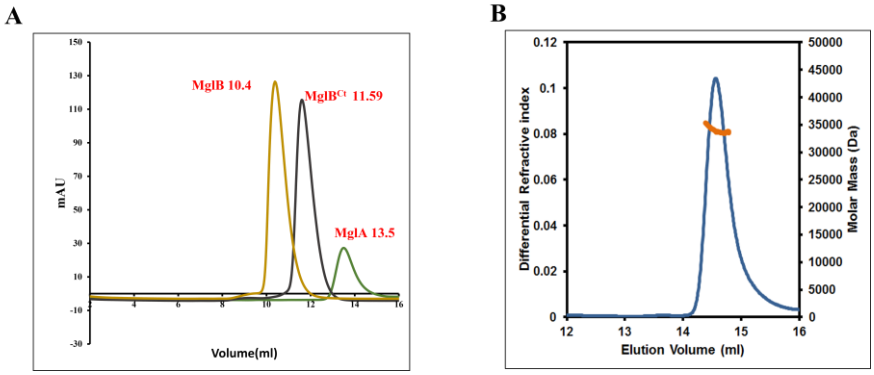

Figure 2.7 Characterization of MglA and MglB
A Size-exclusion chromatography (column -Superdex 75) of *Mx*MglA, *Mx*MglB and *Mx*MglB^{Ct} (*Mx*MglB with truncated C-terminal helix) **B** SEC-MALS profile for *Mx*MglB

2.4.2 Crystal structure of *M. xanthus* MglA

Two different kinds of crystals were obtained in the same condition (Figure 2.8). The structure of *Mx*MglA was solved by molecular replacement using PHASER using the *T. thermophilus* structure of *Mx*MglA as model because sequence identity is 62%. The structure of *Mx*MglA obtained was of 1.35 Å resolution.

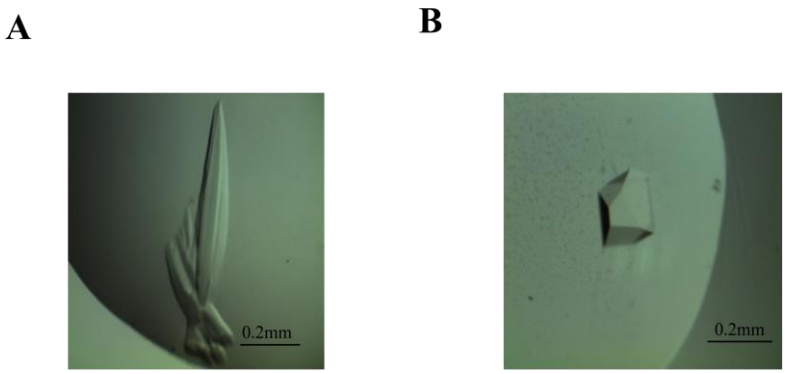

Figure 2.8 Crystals of MglA
A *Mx*MglA crystal 1 **B** *Mx*MglA crystal 2

Even though nucleotide was not added at any step of purification or crystallization, the protein crystallized has GDP in it, as observed by the clear electron density (Figure 2.9A). The 260/280 value show high ratio, which is a kind of quick check that tells whether protein is bound with nucleotide or not. This has been confirmed by HPLC analysis of the protein extract. HPLC confirmed the presence of GDP in the purified protein. Hence, the electron densities and HPLC data both suggested that MglA is bound to GDP.

The affinity of MglA to the nucleotide also matters and it is discussed in great detail in the coming chapter (Chapter 3). In that regard it has been found that MglA have higher affinity towards GDP than GTP, that could be one of the reasons why we have got the protein i.e. MglA with the GDP.

MglA crystallized in two different cell parameters in the space group $P2_12_12_1$ (as listed in table 2.1). There are two MglA-GDP bound molecules in the asymmetric unit. The two proteins are interacting through switch II loop of each other in the $P2_12_12_1$ space group. *Mx*MglA is homologous to Ras superfamily and is almost similar to *Tt*MglA (3T1T) in many ways i.e. they have 6 β-sheets and 5 α-helices just like other GTPase with typical G-domain. Just like MglA from *T. thermophilus*, *M. xanthus* MglA has two extra β-strands i.e. β_0 and β_2^*. β_0 is present at

the N-terminal end of the MglA while β_2^* is present in between α_1 and β_2. More specifically, it is present in between switch I and loop connecting α_1 to β_2^*.

MglA is a 23 kDa protein belonging to the small Ras-like GTPase fold. It contains the conserved motifs and residues of small Ras-like GTPases from G_1-G_5 motif and the GTPase characterizing loops i.e. the P-loop, switch I, switch II and interswitch regions. P-loop, switch I and switch II are conserved motifs G_1, G2 and G3, respectively that binds to the nucleotide. Switch I and switch II undergoes conformational change upon GTP binding and after GTP-hydrolysis. While G4 mainly contribute towards guanine specificity and G5 is less conserved motif, which interact with guanine base (Wittinghofer and Vetter, 2011; Wuichet and Søgaard-Andersen, 2014).

Table 2.1 Data collection and refinement statistics of MglA

	MglA-GDP 1 (5YMX)	MglA-GDP 2
Data Collection statistics		
Space Group	$P2_12_12_1$	$P2_12_12_1$
a, b, c (Å)	67.2, 68.6, 89.5	52.06, 88.14, 119.73
α, β, γ (°)	90, 90, 90	90, 90, 90
Resolution (Å)	32.0 - 1.35 (1.42 – 1.35)	29.58-2.16
Number of unique reflections	91269 (13188)	32741
R_{merge} (%)*	5.5 (73.4)	4.2 (48.2)
R_{pim} (%)*	2.2 (29.4)	2.1 (23.9)
CC_{half}*	0.999 (0.784)	0.999
Mean I/σI	8.0 (2.6)	20.2 (2.5)
Completeness (%)*	99.7 (100)	99.3 (99.8)
Redundancy*	7.2 (7.2)	4.5
Refinement statistics		
Resolution (Å)	28.92 – 1.35	70.98-2.1
Number of unique reflections	910151	30828
R_{work} / R_{free} (%)	15.0/17.8	27.5/25.6
Average B-factor (Å^2)		
Wilson B-factor (Å^2)	15.2	50.23
RMS deviations		
Bond lengths (Å)	0.005	0.019
Bond angles (°)	0.878	1.996
Ramachandran map		
Favoured (%)	99	
Allowed (%)	1	
Outliers (%)	0	

* Values in parentheses denote the last resolution shell

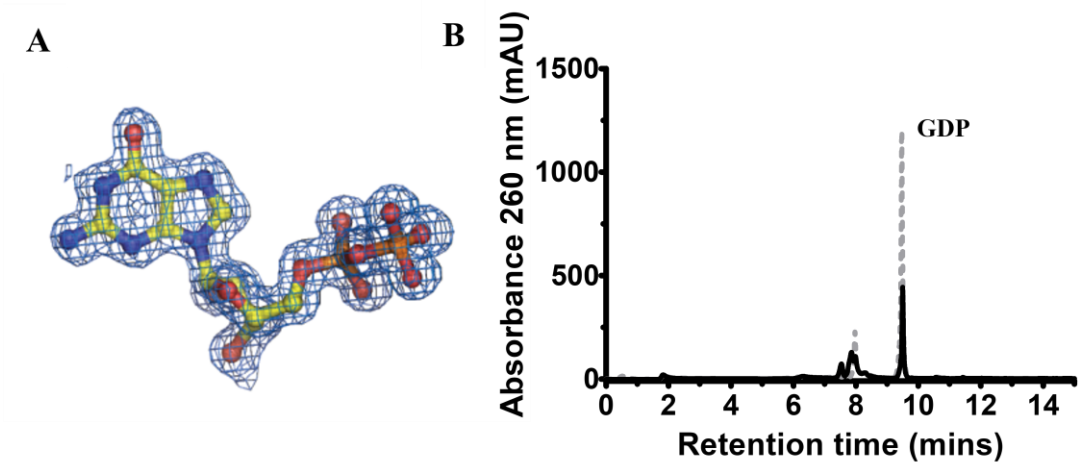

Figure 2.9 MglA in GDP bound state
A Electron density of GDP in the structure of MglA **B** HPLC run to confirm the presence of GDP with the MglA

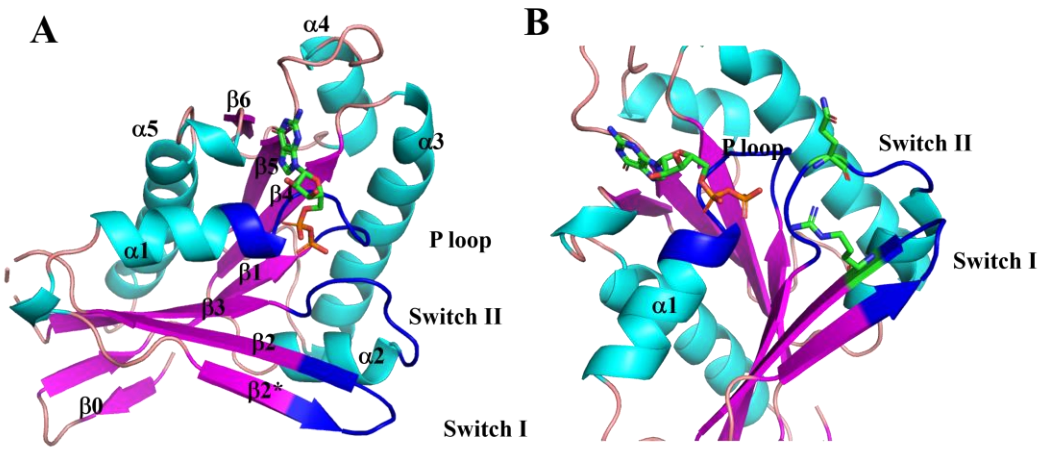

Figure 2.10 Structure of MglA in GDP-bound state
α-helices are shown in cyan; β-sheets are in pink; P-loop, switch I and switch II are in blue colour while other loops are shown in wheat colour. Right side is a view of the P-loop, switch I and switch II with nucleotide in the vicinity of R^{53} and Q^{82} catalytic residues.

The MglA structure obtained from X-ray crystallography has GDP bound in the nucleotide binding pocket, even though no nucleotide was added at any step of purification and crystallization of MglA (as shown in figure 2.9 and 2.10). P-loop of *Mx*MglA consists of conserved sequence G^{19}PGLSGKT^{26}. Catalytic residues of *Mx*MglA consist of an arginine (R^{53} in switch I) and glutamine (Q^{82} in switch II). GTPases require at least two residues to perform the GTP hydrolysis. Usually, arginine comes from the GTPase activating protein (GAP) while glutamine from the GTPase. There are a few exceptions where it is vice-versa (refer Chapter 4 for further discussion) but in the case of MglA both the residues are present in the GTPase itself.

There are many other residues from MglA that interact with the nucleotide. T^{54} in switch I and DXXGQ/H/T in switch II is conserved in *M. xanthus*. The only difference is that in place of negatively charged amino acid, aspartic acid, the uncharged threonine is present in MglA i.e. $T^{78}VPGQ^{82}$ where $G^{81}Q^{82}$ is conserved. In G_4, NKXD motif is present in MglA and the G_5 motif (S/CAK/L/T) is absent. In *M. xanthus*, $N^{141}KRD^{144}$ is present as a G_4 motif while G_5 is represented by the $V^{169}AP^{171}$ is present (according to sequence alignment of chapter 1 in figure 1.12). In *T. thermophilus*, NKRD is there but VAT is the G_5 motif instead of $V^{169}AP^{171}$.

2.4.3 Crystal structure of *M. xanthus* MglB

MglB was crystallized in different conditions, but the crystals formed stacked clusters and did not diffract to high resolution (Figure 2.11). The highest resolution obtained was of ~ 5 Å (Table 2.2).

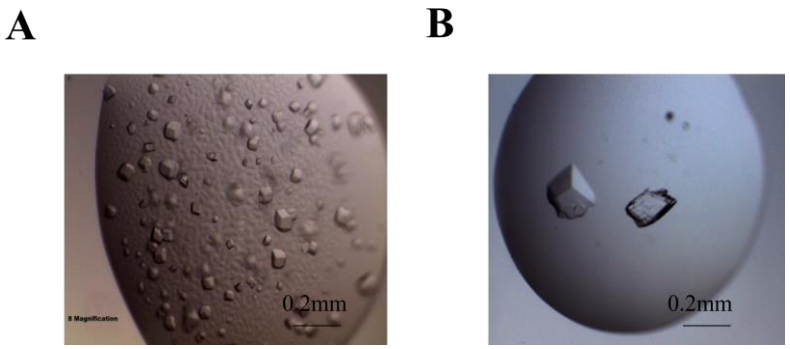

Figure 2.11 Crystals of MglB

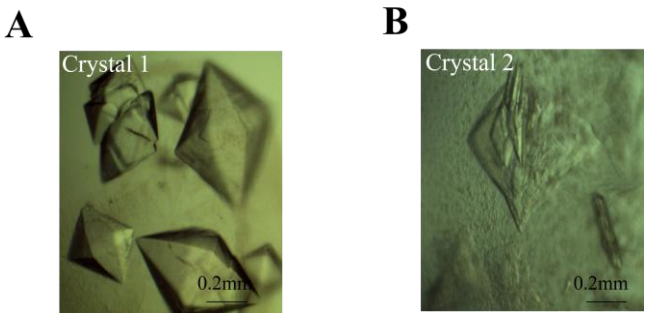

Figure 2.12 Crystals of $MglB^{Ct}$
Two crystal forms Crystal 1 and Crystal 2 are shown in panels A and B, crystal form in panel B gave the high-resolution data.

The structure could not be solved because there were 28 molecules in the asymmetric unit, and the low-resolution data was not sufficient for molecular replacement trials to be successful. But

MglB^{Ct}, the C-terminal truncated construct of MglB, where last 20 amino acids were deleted, produced well diffracting crystals (Figure 2.12 and table 2.2).

Table 2.2 Data collection and refinement statistics for MglB and MglB^{Ct}

	MglB 1	MglB 2	MglB^{Ct} 1	MglB^{Ct} 2
Data Collection statistics				
Space Group	**P222**	**P1**	**$C222_1$**	**$I4_1$**
a, b, c (Å)	**75.26, 84.89, 93.15**	**102.6, 160.15, 163.68**	**66.13, 105.9, 72.75**	**126.01,126.01, 105.29**
α, β, γ (˚)	**90, 90, 90**	**115.07, 101.7, 100.7**	**90, 90, 90**	**90, 90, 90**
Resolution (Å)	**46.57-3.4**	**50-4**	**56.09- 2.21**	**49.68-3.2**
Number of unique reflections	**_**	**_**		
R_{merge} (%)*	**16 (44.9)**	**7.9 (47.8)**	**9.6 (41)**	**10.7 (49.2)**
R_{pim} (%)*	**7.9 (22)**	**_**	**6.7 (30.2)**	
CC_{half}*	**0.990 (0.904)**	**_**	**0.995 (0.814)**	
Mean I/σI	**10.3 (4)**	**6.3 (1.4)**	**6.7 (2.1)**	
Completeness (%)*	**99.2 (99)**	**99.3 (99)**	**77.3 (65.8)**	**100 (100)**
Redundancy*	**2.7**	**2**	**1.5 (1.4)**	**3.4 (3.3)**
Refinement statistics				
Resolution (Å)			**56.092- 2.229**	
Number of unique reflections			**11629**	
R_{work} / R_{free} (%)			**21/27**	
Average B-factor (Å²)				
Wilson B-factor (Å²)			**27.7**	
RMS deviations				
Bond lengths (Å)			**0.007**	
Bond angles (˚)			**0.962**	
Ramachandran map				
Favoured (%)			**96.3**	
Allowed (%)			**3.7**	
Outliers (%)			**0**	

* Values in parentheses denote the last resolution shell

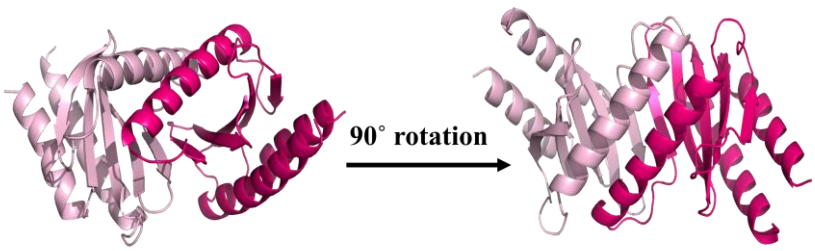

Figure 2.13 Structure of MglB^{Ct}
Dimer of MglB^{Ct} is shown with the protomers in light pink and dark pink.

The structure has been solved at a resolution of 2.2 Å by molecular replacement. MglB is a protein, belong to the group of Roadblock/LC7 domain fold (Figure 2.13).

Longin domain in eukaryotes are similar to roadblock domain of prokaryotes where five β-stands and three α-helix arrange to form a β-meander i.e. ββαββββαα and αββαββββα in longing domain and roadblock domain, respectively (Levine *et al.*, 2013). Rag GTPases are the best example where Longin domain of protein is performing the function of GEF, it has been discussed in detail in forth chapter. In the case of *Tt*MglB, it was found that it acts as a GAP. MP1 and P14 (PDB ID: 1VEU) also possess Roadblock domain fold and regulate Rho GTPases (Lunin et al., 2004; Pullikuth et al., 2005).

2.4.4 Crystal structure of *M. xanthus* MglAB complex

The structure of MglA and MglB complex in presence of different nucleotide states were captured (crystals shown in figure 2.14 and structure in figure 2.15). Crystals were obtained in two different space groups $P6_522$ (Figure 2.14) and $P3_121$. The data collection statistics and refinement statistics is shown in tables 2.3 and 2.4. In the structure of MglA and MglB complex, two molecules of MglB interacts with one molecule of MglA. The structure and conformation of MglA and MglB are similar in the different nucleotide states i.e. transition state analog and non-hydrolysable analog of GTP.

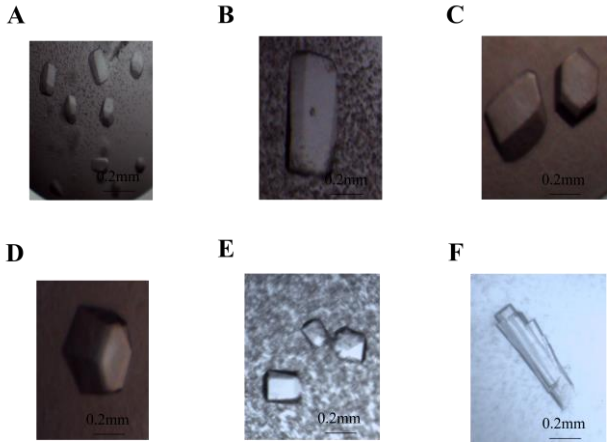

Figure 2.14 Crystal images of MglAB complex in $P6_522$ space group

Since the best resolution of 2.3 Å was obtained for the GTP-γ-S bound complex, further refinement and structure analysis were done using the MglAB-GTP-γ-S complex. MglB interacting at the opposite side of the nucleotide binding pocket is called as $MglB_1$ while MglB

interacting towards the nucleotide binding pocket of MglA is designated as $MglB_2$ (Figure 2.15A and 2.16A).

The structures of MglA-GDP and MglA-GppNHp-MglB show that the P-loop does not change its conformation during the GTP-hydrolysis while switch I and switch II does which is similar to the other small Ras-like GTPases. It appears that Mg^{2+} is important for the binding and hydrolysis of GTP. Main chain amide group of the $S^{23}GKT^{26}$ from the P-loop forms hydrogen bond with the phosphoryl oxygen of GTP. T^{26} side chain hydroxyl interacts with the β-phosphate of GTP and Mg^{2+}. K^{25} interacts with both β- and γ- phosphate oxygens. R^{53} and Q^{82} in switch I and switch II of MglA, respectively, come closer to the nucleotide after binding to MglB (as shown in figure 2.16B). Generally, arginine finger is provided by the GAP, but in this case arginine residue is present in MglA only. MglB helps in positioning the catalytic residues R^{53} and Q^{82} near the γ-phosphate of the GTPase.

P-loop formed by Y^{18}-K^{25} remains the same in either of the case whether MglA is bound to MglB or not, which means there is no change in conformation of the P-loop upon MglB binding. β_2^* is the strand which extends from I^{45}- T^{49} and I^{45}- L^{46}, in the two conformational states respectively. This allows the switch I loop to adopt a conformation for interacting with

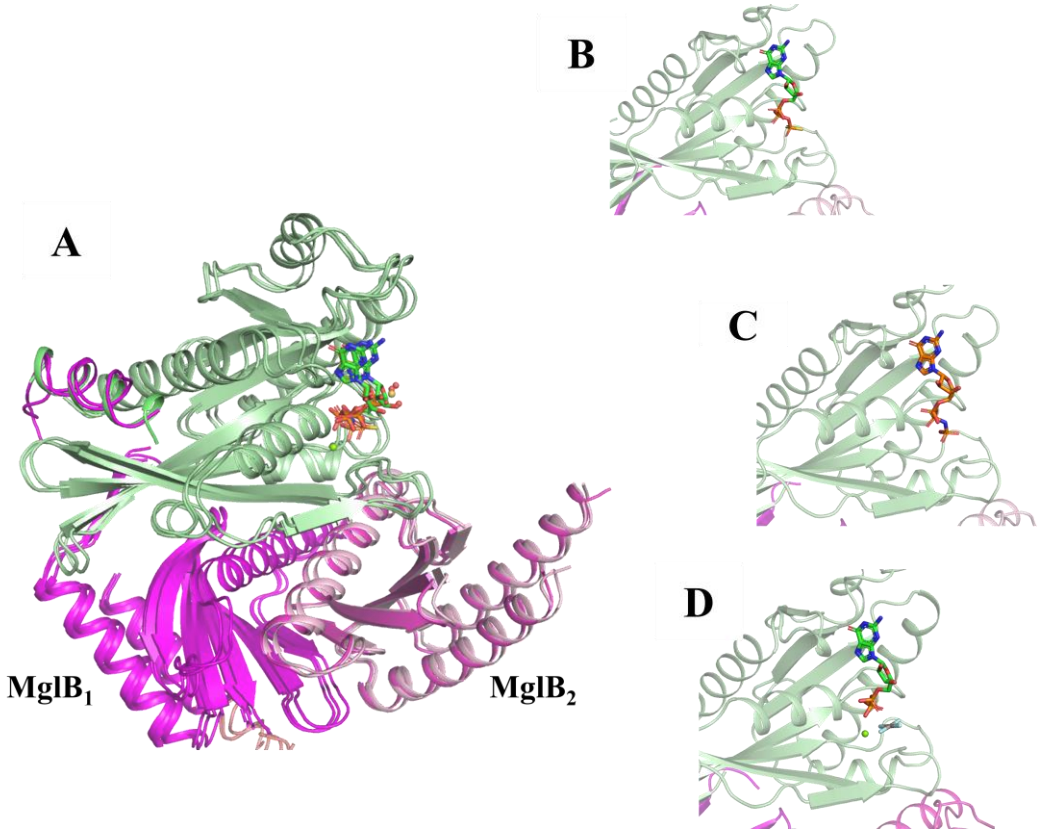

Figure 2.15 Structure of MglA and MglB complex with different GTP analogues
A. Superposed structures of the three MglAB complex structures with GTP-γ-S, GppNHp and GDP.AlF_x bound to the MglA. MglA is shown in green, while MglB dimer is in shades of pink. **B, C and D** panels show the active site geometry with GTP-γ-S, GppNHp and GDP.AlF_x in the nucleotide bound pocket, respectively.

the GTP in the presence of MglB. Switch II also changes its conformation in the presence of MglB and GTP-γ-S.

The two protomers of MglB interact asymmetrically with MglA. In the two MglB protomers, the structure includes full length of MglB in the $MglB_1$ (except for a disordered segment from residues 139 – 147) while in the case of $MglB_2$, electron density for C-terminal residues is not available. This is because flexible regions will not show a clear electron density in crystal structures. C-terminal helix (Ct-helix) of one of the monomers of MglB (labelled $MglB_1$) bound to a pocket distal from the nucleotide-binding pocket of MglA (Figure 2.15A and 2.16A). Most of the interactions with the MglB helix comprised hydrophobic residues on the MglA interface (Figure 2.16A and 2.16C, table in appendix). Residues from the C-terminal helix, β_2 strand, and loop connecting β_2 - β_3 strands of MglA formed the binding pocket. β_2, β_3 strands and the loop connecting them comprise the interswitch region, connecting switch I and switch II loops in small Ras-like GTPases (Vetter, 2001). The corresponding loop was disordered in the *Tt*MglAB structure.

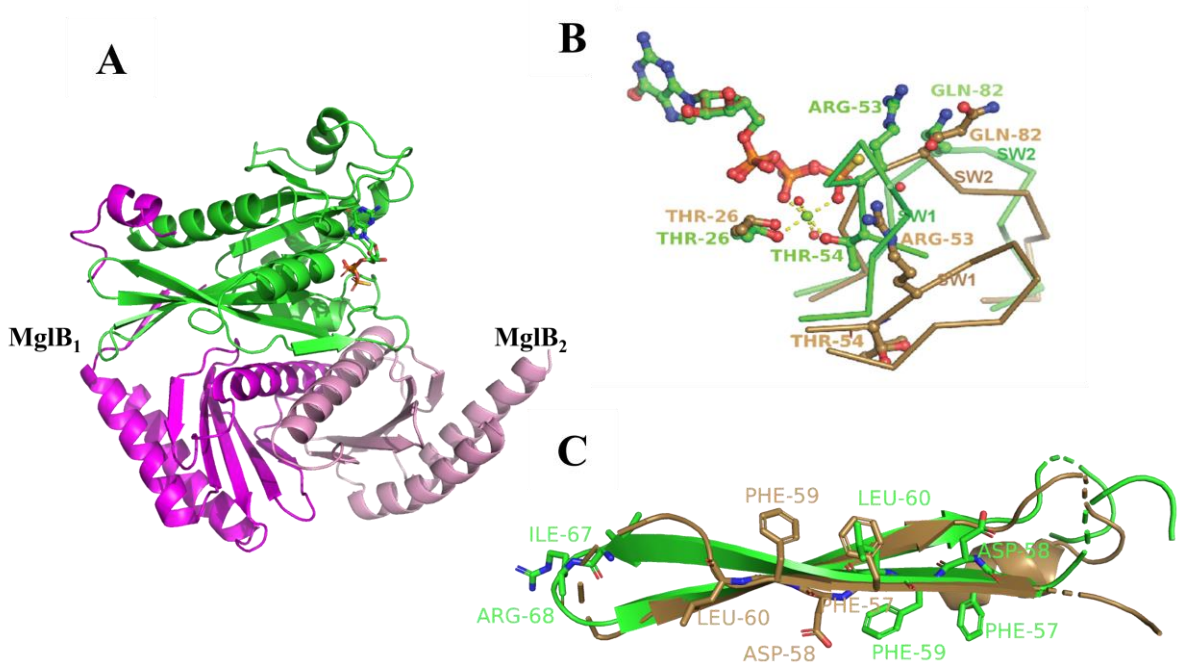

Figure 2.16 MglAB complex structure

A. Structure of MglAB complex (MglA is shown in green, $MglB_1$ in dark pink while $MglB_2$ in light pink.) **B.** Superposed structures of MglA (brown) from MglA-GDP structure and MglA (green) from MglAB complex, with the active site residue conformations highlighted. **C.** β-screw movement and the flipping of phenylalanine side chains during the conformational change upon MglB binding.

Residues 147 to 157 of the helix of $MglB_1$ monomer were modelled into the electron density, following a disordered segment from residues 131 till 146 for which no density was observed.

In order to unambiguously determine the registry of amino acids in the electron density, we generated selenomethionine-labelled MglB for two mutant constructs, $MglB^{I148M}$ and $MglB^{L156M}$. The anomalous signal from the methionines in these two mutants, respectively, confirmed the registry of the amino acids of the MglB Ct-helix (Figure 2.17; table 2.3 and 2.4). The chain was ordered with clear electron density only till residue 130 in the other monomer ($MglB_2$) of MglB dimer. The asymmetry between the two monomers of MglB was also reflected in the N-terminal residues. The N-terminal amino acids (2 – 7) of $MglB_1$ comprised a β-strand that formed hydrogen bonds with the β_0 strand of MglA, thus continuing the central β-sheet in the MglA fold (Figure 2.16C). Residues 1 – 7 were disordered in $MglB_2$. Following this, residues from Glu^{11} in $MglB_1$ formed the first helix of the Roadblock domain fold whereas residues from Tyr^8 formed the corresponding helix in $MglB_2$.

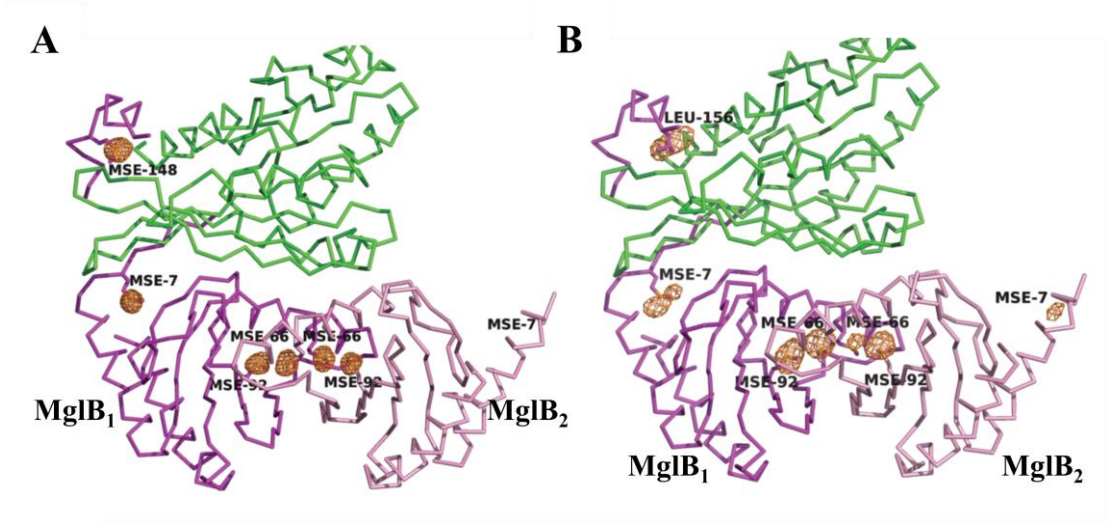

Figure 2.17 Confirmation of registry shift of C-terminal helix residue
Two different mutants of MglB were generated $MglB^{I148M}$ and $MglB^{L156M}$, and anomalous data collected from crystals of MglAB complex, produced using selenomethionine labelled MglB. Anomalous map (orange mesh) has been depicted at 5σ and 4σ around the methionines in MglB. **A.** anomalous map and crystal structure of $MglB^{I148M}$ mutant **B.** anomalous map calculated for $MglB^{L156M,}$ shown on superposed crystal structure of $MglB^{I148M}$ mutant.

Table 2.3 Data collection and refinement statistics of MglAB complex in different nucleotide states

	MglAB GTP-γ-S ($MglB^{I148M}$) (6IZW)	MglAB GppNHp	MglAB GDP.AlF_x
Data Collection statistics			
Space Group	$P3_121$	$P6_522$	$P6_522$
a, b, c (Å)	88.5, 88.5, 131.3	113.47, 113.47, 291.64	114.59, 114.59, 288.75
α, β, γ (˚)	90,90,120	90, 90, 120	90, 90, 120
Resolution (Å)	44.2-2.4 (2.49-2.4)	52.7-2.78	49.9-3.2
Number of unique reflections	23862		
R_{merge} (%)*	9.0 (73.0)	13.0 (164)	19.2 (131)
R_{pim} (%)*	4.4 (35.8)	6.5 (75.9)	8.4 (57)
CC_{half}*	0.998 (0.792)	0.954 (31.7)	0.993 (0.585)
Mean I/σI	16.5 (3.5)	6.2 (1.0)	7.6 (2.4)
Completeness (%)*	100 (100)	98.4 (99)	99.9 (100)
Redundancy*	9.8 (9.9)	5.3 (5.4)	6.2 (6.3)
Refinement statistics			
Resolution (Å)	44.24-2.4	52.87-3.0	49.91-3.2
Number of unique reflections	23825	22594	19262
R_{work} / R_{free} (%)	20.0/24.3	22.46/26.72	25.5/28.7
Average B-factor (Å²)	56		
Wilson B-factor (Å²)	44.7	78.38	73.91
RMS deviations			
Bond lengths (Å)	0.008	0.003	0.002
Bond angles (˚)	1.016	0.626	0.510
Ramachandran map			
Favoured (%)	96.0	94.0	94.04
Allowed (%)	3.69	5.67	5.96
Outliers (%)	0	0.33	0

* Values in parentheses denote the last resolution shell

Table 2.4 Data collection and refinement statistics of MglAB complex

	MglAB GTP-γ-S (MglB sel met)	MglAB GTP-γ-S	MglAB GTP-γ-S ($MglB^{I156M}$)
Data Collection statistics			
Space Group	$P6_122$	$P6_522$	P622
a, b, c (Å)	114.68, 114.68, 291.45	113.14, 113.14, 289.23	118.63, 118.63, 285.88
α, β, γ (°)	90, 90, 120	90, 90, 120	90, 90, 120
Resolution (Å)	50.2-2.8 (2.95-2.8)	46.4-2.6 (2.72- 2.6)	48.34-3.3 (3.56-3.3)
Number of unique reflections		39358	18419
R_{merge} (%)*	41.5	11.5	9.7 (58.1)
R_{pim} (%)*	44.4	4.5 (51.7)	2.9 (17.2)
CC_{half}*	0.920 (0.273)	0.995 (0.673)	0.99 (0.935)
Mean I/σI	5.5 (1.3)	11 (1.8)	19.9 (4.8)
Completeness (%)*	93.9 (87.9)	99 (98.9)	99 (99.5)
Redundancy*	8.2	7.2 (7.5)	11.7 (12)
Refinement statistics			
Resolution (Å)		46.4-2.6	
Number of unique reflections		34091	
R_{work} / R_{free} (%)		23.59/28.38	
Average B-factor (Å²)			
Wilson B-factor (Å²)		57.16	
RMS deviations			
Bond lengths (Å)		0.022	
Bond angles (°)		0.884	
Ramachandran map		0.57	
Favoured (%)		94.51	
Allowed (%)		4.91	
Outliers (%)		0	

* Values in parentheses denote the last resolution shell

2.5 MglA MglB interface

The interaction of the MglB C-terminal helix and the N-terminal strand with MglA is not present in the *Thermus thermophilus* structure. But there are similarities, among *Thermus thermophilus* and *Myxococcus xanthus* structures. β-screw movement of MglA was observed in both the structures upon MglB binding where one beta strand (β_2) undergoes a twist movement, resulting in exposure of hydrophobic residues to the MglB binding interface (Figure 2.16C). A comparison between the interacting residues at the interface of MglA and MglB between *T. thermophilus* and *M. xanthus* are tabulated in Appendix.

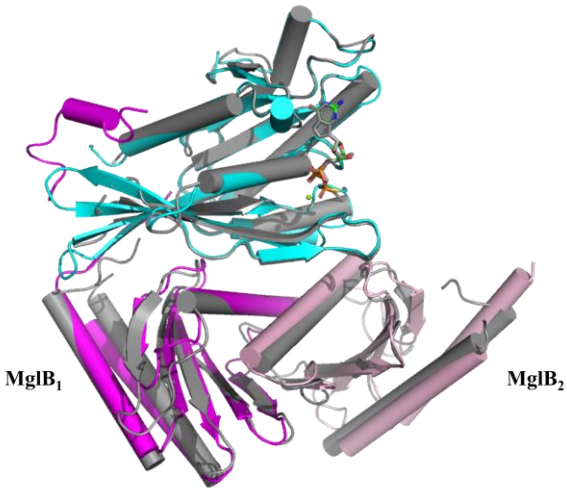

Figure 2.18 Superposed structures of MglA-MglB complex from *T. Thermophilus* and *M. xanthus.*
M. xanthus MglA is shown in cyan colour while the two protomers of MglB are in two different shades of pink. *T. thermophilus* structure is shown in grey (3T1Q). The green sphere is Mg^{+2}.

β2 of MglA undergoes movement after binding to MglB and this is called β-screw movement because the residues flip from one side to the other, and the strand shifts two amino acids. But the truncated protein of MglB with the C-terminal amino acids deleted can also interact with MglA as observed in the *Thermus thermophilus* structure (Figure 2.18 and 2.19).

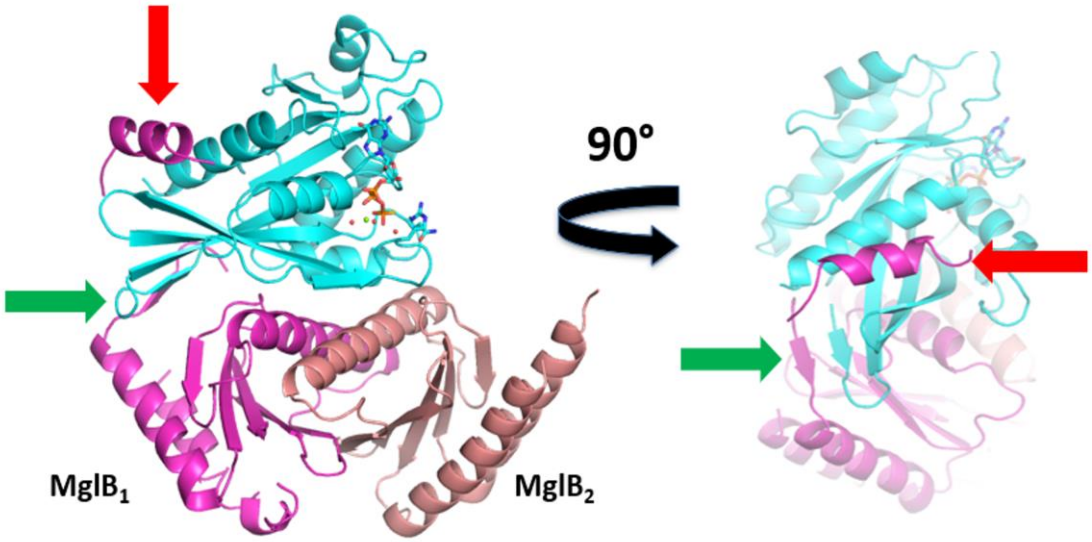

Figure 2.19 Structure of *Myxococcus xanthus* MglAB complex
MglA is in cyan. $MglB_1$ (one protomer of MglB) is in pink while $MglB_2$ is in wheat colour. The interactions which are different from *Thermus thermophilus* is highlighted with the arrow. Green arrow highlights the N-terminal interaction of MglB with MglA while red arrow represents the C-terminal helix interaction with MglA); on the right-hand side of the figure the same complex is shown at 90˚orientation.

Based on the observations from the crystal structure, especially the interaction of the C-terminal helix of MglB with MglA, we proceeded to confirm if the helix binding has any role to play in activating the GTP hydrolysis by MglA. To determine the role of the C-terminal helix of *Mx*MglB, mutants of *Mx*MglB (a deletion construct and point mutations of interacting residues) were created. Also, the mutants were created in *Mx*MglA, the amino-acid residues of MglA interacting with the C-terminal helix of *Mx*MglB were mutated. Further biochemical assays and interaction studies were carried out with these mutant constructs, as described in the next chapter (Chapter 3).

Chapter 3

Mechanism of activation of MglA by MglB

3.1 Role of C-terminal helix of MglB in activation of MglA

To further substantiate our conclusions based on the crystal structures, we proceeded to characterize the action of MglA and MglB through biochemical assays. Since, MglA is a GTPase, we measured the activity of protein and carried out binding assays between MglA and MglB. As I have mentioned in Chapter 1, studies on *T. thermophilus* MglA and MglB suggested that MglB helps MglA in the hydrolysis of GTP. To get the activity and effect of *Mx*MglB on *Mx*MglA as a GTPase activating protein, GTP hydrolysis assays were performed. The GTPase activity of MglA was monitored in the presence and absence of MglB. Also, the activity assays were carried out with different mutants. Since both the catalytic residues are present in MglA only (Figure 2.16B), MglA catalytic site mutants $MglA^{R53A}$ and $MglA^{Q82L}$ were created to verify their role in GTP-hydrolysis.

Based on the structural studies (Chapter 2), we discovered a novel interaction of C-terminal helix of *Mx*$MglB_1$ with β_2-strand, loop connecting β_2 and β_3 and α_5-helix of *Mx*MglA in the crystal structure of *Mx*MglAB complex (Figure 3.1). To characterize the functional relevance of this interaction, several mutants were created in *Mx*MglA and *Mx*MglB. In the construct $MglB^{Ct}$, the whole MglB C-terminal helix from residues 139 – 159 was deleted, to validate the functional role of C-terminal helix binding.

To confirm the role of the residues in the binding pocket in *Mx*MglA, mutant constructs namely, double mutant of K^{181} and K^{185} to Ala (referred to as $MglA^{K}$), double mutant of I^{64} and L^{67} to A (referred to as $MglA^{L}$) were prepared to perform activity assays and binding study. K^{181} and K^{185} are on the C-terminal helix of MglA. K^{181} interacted with F^{157} of the MglB helix while K^{185} formed water-mediated hydrogen bonds with D^{154} (Figure 3.1). I^{64} and L^{67} were on the loop connecting β_2 and β_3 strands, and made contacts with the hydrophobic residues on MglB helix. Comparison between *Mx*MglA-GDP bound structure and *Mx*MglAB complex showed that the loop underwent a change in conformation during the β-screw transition by β_2-strand (Miertzschke *et al.* (2011); observed in this study also). The residues on this loop might contribute to the allosteric communication between the helix-binding site and the nucleotide-binding site of *Mx*MglA.

For characterization of these mutants, first GTP hydrolysis activity was checked. Then binding of these MglA mutants to nucleotide and also with MglB were studied and compared with the wild type proteins, to find out any kind of anomalies in binding.

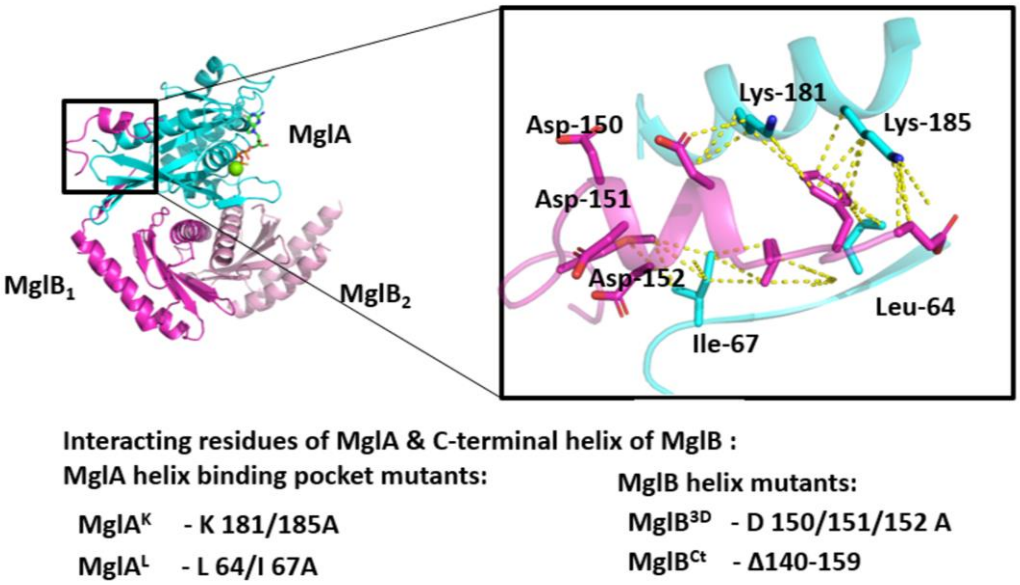

Figure 3.1 Helix binding Mutants of MglA MglB
MglA is shown in cyan colour and MglB protomers in different shades of pink**.** *Mx*MglA and *Mx*MglB mutants are shown in inset.

This chapter discusses about the hydrolysis activity and binding studies which were carried out. Binding affinities between *Mx*MglA and *Mx*MglB in presence of different nucleotides i.e. GDP and GTP, led us to uncover a novel mode of action of MglB, where *Mx*MglB could potentially function as a nucleotide exchange factor of MglA, along with its GAP activity. To characterize the GEF activity, assays were performed, and are discussed in the later sections of this chapter.

3.2 Material and methods

3.2.1 Protein expression and purification for *Mx*MglA and *Mx*MglB mutant constructs

The mutations were created in the gene by site directed mutagenesis using restriction free cloning method. $MglA^{L}$ and $MglA^{K}$ are double mutants where $MglA^{L}$ have mutations at L^{64} and I^{67} while $MglA^{K}$ have mutations at K^{181} and K^{185}. In the case of

MglB, two mutants were made $MglB^{Ct}$ and $MglB^{3D}$. Primer and clone details are given in Appendix.

3.2.2 GTP hydrolysis assays

Various methods were used for measurement of GTP hydrolysis by MglA. The principle for every method is described in each section.

A. HPLC (High Pressure Liquid Chromatography)

Chromatography is a technique used to separate components from a mixture. First, it was performed using paper as the matrix for separation and this was named as paper chromatography (Coskun, 2016). After that chromatography technique have evolved and expanded, and took different forms for better efficiency. One of its versions is column chromatography. HPLC is an advanced version of chromatography where high pressure is applied by the instrument on the bead packed column for quick and efficient separation of components.

1. Principle

For monitoring GTP hydrolysis by HPLC, the amounts of substrate (GTP) or product (GDP) present in a reaction mixture were calculated by comparing the retention times and peak heights (Eberth and Ahmadian, 2009; Mungi and Rajamani, 2015). Because of the difference of one phosphate, GDP and GTP have different retention times on an ion exchange column. DNAPac column (Dionex) was the ion exchange column used in our experiments. Approach to analyse GTP hydrolysis was through separation of GDP and GTP on column, and to estimate the concentrations based on the area estimates of individual peaks and comparison with a standard curve obtained using known concentrations.

2. Experimental details

Purified *Mx*MglA was diluted to 2-3 mg/ml concentration in buffer A50 and then heated at 65°C. The heated protein sample was spun at 21,000 g for 10 mins at 4 °C. The supernatant was filtered with 0.22 μm cellulose acetate filter (Corning) and the sample was loaded on to DNAPac Analytical 2000 ion-exchange column (Dionex). Buffers used for binding and elution are Buffer A (2 mM Tris pH 8.0), along with a linear gradient of mix with Buffer B (2 mM Tris pH 8.0, 1.25 M NaCl) respectively, ranging

from 0 % to 50 % B over 20 column volumes. The runs were performed at a flow rate of 0.8 ml/min, with steps of 0 % buffer B for 3 minutes, followed by linear gradients of 0 to 30 % B for 10 minutes, and 30 to 100 % B for 12 minutes. The peak profile obtained was compared for various reaction mixtures with 35 µl of sample injection volume. The absorbance at 260 nm, indicative of the presence of GDP was plotted against retention time.

B. Malachite green assay

It is a colorimetric assay where the reaction of the phosphate with the components of malachite green reaction mixture results in a green colour, dependent on the concentration of the phosphate released (Baykov *et al.*, 1988).

1. Principle

The inorganic phosphate released after GTP hydrolysis interacts with the ammonium molybdate in presence of H_2SO_4 to give a yellow colour complex (Baykov *et al.*, 1988; Geladopoulos *et al.*, 1991). Then it further interacts with malachite green to give the green coloured complex as shown in figure 3.2. This green colour intensity varies with the amount of inorganic phosphate. The intensity of green colour can be monitored at a range 630-650 nm (Monroy *et al.*, 2013). The amount of Pi released is calculated by comparing with the standard consisting of known concentrations of phosphate ion (Appendix).

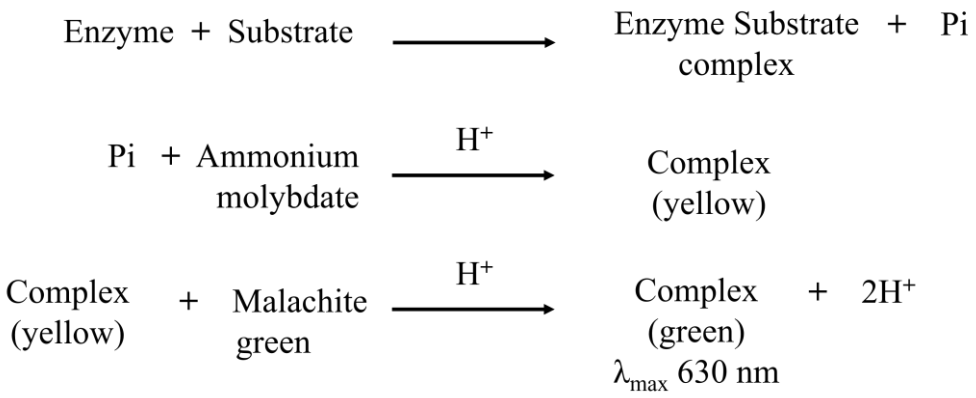

Figure 3.2 Chemical reaction in malachite green assay for phosphate estimation
(Adapted from Monroy et al., 2013)

2. Experimental details

This assay was done using *Mx*MglA (or *Mx*MglA mutants) at a concentration of 10 μM, while *Mx*MglB and its constructs were used in two different molar ratios 1:2 and 1:10 (20 μM and 100 μM) with 1 mM GTP in the buffer A50 (50 mM Tris, 50 mM NaCl, pH 8.0) containing $MgCl_2$ 5 mM. All the enzyme activity assays were performed at 30 ˚C. Readings were taken at different time points i.e. 0, 15, 30, 45, 60, 75, 90, 105, 120 minutes. Various methods were tested to stop the reaction. These included addition of EDTA (to chelate the Mg^{2+} ion), H_2SO_4 or HCl (the acidic pH denatures the enzyme) and SDS treatment (to denature the enzyme) but heating at 65 ˚C worked the best for our assay. So, to stop the reaction the sample was heated at 65 °C and then malachite green solution was added and measurement was taken at 630 nm using a plate reader (Varioskan, Thermo Scientific). To quantify the inorganic phosphates released by the hydrolysis of GTP by MglA, the standard curve was obtained by mixing a set of known concentrations of NaH_2PO_4 with malachite green solution and the absorbance recorded after 20 minutes (Appendix). The experiments were repeated multiple times and the results were compiled, averaged and SEM (Standard Error Mean) calculated with GraphPad Prism.

C. NADH-GTPase Coupling assay

It is a technique developed to monitor the amount of GDP/ADP released by the GTPase/ATPase after hydrolysis (Ingerman and Nunnari, 2005). In this system, the regeneration of GTP/ATP is coupled with hydrolysis by GTPase. It has many advantages over the malachite green assay. One of the advantages is that it enables a continuous monitoring of the hydrolysis reaction. Hence, there is less chance of manual error than a malachite green assay. It monitors the reaction at short intervals in seconds and also it can continuously regenerate the triphosphate form of the nucleotide. This also removes the requirement of stopping the reaction before estimating the amount of product formed in a specified incubation time.

1. Principle

GTPase activity measurements were made using a coupled enzyme based assay where the conversion of NADH to NAD^+ is coupled to the utilization of GDP produced (Kiianitsa *et al.*, 2003). The GTPase or ATPase hydrolyses the nucleotide while pyruvate kinase (PK) uses GDP/ADP and phosphoenol pyruvate to regenerate

GTP/ATP and produce pyruvate. Lactate dehydrogenase (LDH) utilizes NADH and pyruvate to produce NAD^+ and lactate. Since the utilization of NADH is equivalent to the GDP produced by the GTPase reaction, the actual read out is a decrease in absorbance of NADH, which in turn gives information about the GDP produced by the GTPase (Figure 3.3).

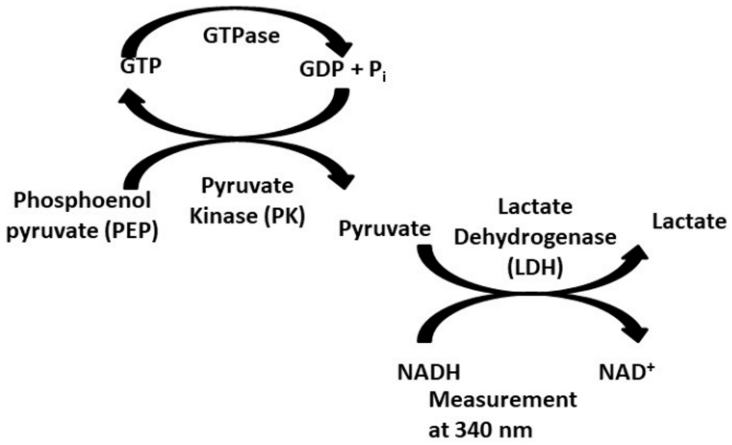

Figure 3.3 Schematic representation of the NADH-GTPase Coupling assay
(Adapted from Ingerman & Nunnari, 2005)

2. Experimental details

The amount of NADH utilized in the reaction was measured by monitoring the NADH absorbance at 340 nm using a multiplate reader, Varioskan Flash (Thermo Scientific). A master mix was prepared in Buffer A50 containing PEP (1 mM; Sigma), GTP (1mM; Jena Bioscience), NADH (600 nm; Sigma), PK/LDH mix (~ 25 U/ml; Sigma), added in the same order. All the components of NADH reaction were mixed in a total reaction volume of 200 µl and added in a 96-well plate (Ingerman and Nunnari, 2005). The reaction was initiated by addition of *Mx*MglA or *Mx*MglAB mix and their relevant mutant constructs. *Mx*MglA or *Mx*MglA mutants of 10 µM and *Mx*MglB or its mutants were used at the concentrations 20 µM and 200 µM, in a molar ratio of 1:2 and 1:10.
Readings were recorded at intervals of 20 secs for 2 hours. The concentration of GDP released was calculated based on the absorbance readings, by using a conversion factor calculated from the standard graph obtained by plotting the readings for known concentrations of NADH. The k_{cat} was calculated and plotted using GraphPad Prism. Readings from 0 – 8000 seconds was fitted to a line using linear regression, and the slope of the fitted line was calculated to obtain the amount of GDP released (in µM)

per unit time. k_{cat} was calculated as the amount of GDP released per unit time per unit enzyme concentration. This value was used further to compare the enzyme activity among all the mutants. The significance was calculated on GraphPad Prism, using one-way ANOVA with Tukey test of 95% confidence interval and significance was marked on the scatter plot.

3.2.3 Binding assays

There are many methods available to measure the interaction between two molecules. Analytical size exclusion chromatography and isothermal titration calorimetry are a couple of methods utilized in this study. Due to the ease of the experiment and requirement for less quantities of samples, fluorescence anisotropy was used extensively for multiple experiments involving many mutants. In fluorescence anisotropy, we can directly monitor the binding of *Mx*MglA to the nucleotide because the nucleotide is fluorescently labelled and we can observe an increase in fluorescence anisotropy after binding of proteins to these labelled nucleotide (Moerke, 2009).

A. Analytical Size exclusion chromatography

1. Principle

It is based upon the principle of size-exclusion chromatography/gel-filtration chromatography where large molecules or complexes, elute faster than small molecules through the column. The elution is dependent on the size of the beads and also on the type of molecules to be analysed or separated.

2. Experimental details

4 mg/ml *Mx*MglA was mixed with *Mx*MglB/ $MglB^{Ct}$ in the molar ratio 1:2.5 or 1:3 in the buffer A50 containing of 5 mM of Mg^{2+} and different nucleotides 0.1 mM of GTP, GDP, GMPPNP (non-hydrolysable GTP analogue), respectively. The reaction was injected onto Superdex75 (GE Healthcare) equilibrated with buffers containing respective nucleotides and eluted. The samples were run on SDS-PAGE gel. The marker proteins were run on Superdex75 for calibration of molecular weight (Appendix).

B. ITC (Isothermal titration calorimetry)

This is one of the most widely used techniques to understand and quantify protein-ligand, protein-protein, DNA-protein or protein-small molecule interaction (Saponaro, 2018).

1. Principle

ITC measures the change in heat between molecules when they interact and determines the energy absorbed or released as a result of binding. It has a reference cell which is attached to the sample cell. When any heat change occurs in sample cell after mixing the interacting molecules, the temperature in the sample cell is maintained same as that of the reference cell electrically. In this process, the energy provided or taken away from the reference cell to maintain the temperature is recorded by the instrument. This gives information about enthalpy (ΔH), entropy (ΔS) and stoichiometry (n) of the molecules which are interacting (Figure 3.4).

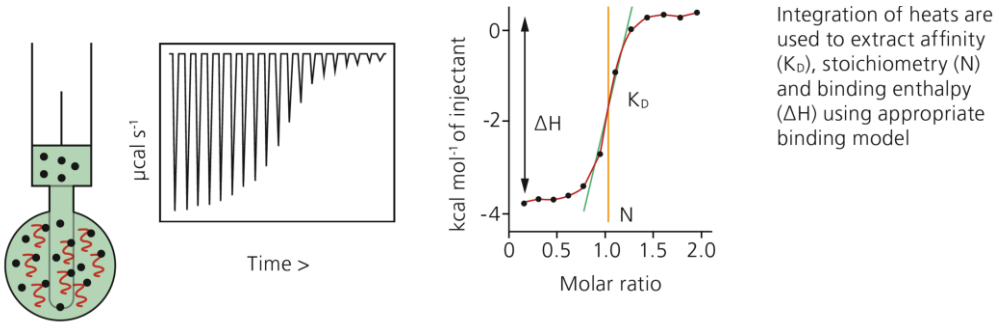

Figure 3.4 Principle of Isothermal Titration Calorimetry
(Reproduced from Malvern brochure for ITC)

2. Experimental details

ITC experiments were performed using MicroCal ITC200 system. *Mx*MglA was added in the cell while the other interacting partner protein, *Mx*MglB/MglB^{Ct} was added in the syringe of the instrument. All the proteins were dialyzed in buffer containing 50 mM Tris, 50 mM NaCl, 2 mM $MgCl_2$, at pH 8.0, prior to the experiment. The binding was studied in the presence of different nucleotides i.e. GDP (Sigma), GppNHp (Jena Bioscience) at a concentration of 2 mM, which was included in both cell and syringe solutions. For the runs, the concentration of MglA used were in between 20 - 35 µM while for MglB/ MglB^{Ct} concentrations were in the range of 200 - 500 µM. The run was done at 25 °C with 20 injections of 2 µl each with a mixing time of 60 seconds.

The data was analysed using Origin 8.0. K_d values reported are averages of at least three independent ITC runs, from different purification batches of proteins.

C. Fluorescence anisotropy

It is an event where if fluorescent molecules are exposed to polarised excitation light, the emitted fluorescence is depolarised due to rapid rotation of the fluorescent molecule. The difference in fluorescence intensity in two directions parallel and perpendicular to source are measured, to obtain the fluorescence anisotropy.

1. Principle

The difference in intensity at parallel and perpendicular directions is dependent on the tumbling speed as shown in the figure below (Figure 4.5). When a large molecule binds to the fluorescently labelled molecule, the tumbling speed of the fluorescently labelled molecule slows down (Maziarz and Garcia-Marcos, 2017). The reduction in tumbling speed results in an increase in the fluorescence anisotropy. This helps in estimating the fraction of bound and unbound molecules. When fluorescent molecules are exposed to polarised light, small molecules can move freely. As a result, the emitted light is depolarised while when this fluorescent molecule is bound to larger complex, it will not be able to move freely and hence, the light emitted will be polarised as shown in figure 3.5. This difference is measured and the increase in fluorescence anisotropy upon complex formation is used to estimate the binding affinity (Samokhvalov *et al.*, 2017).

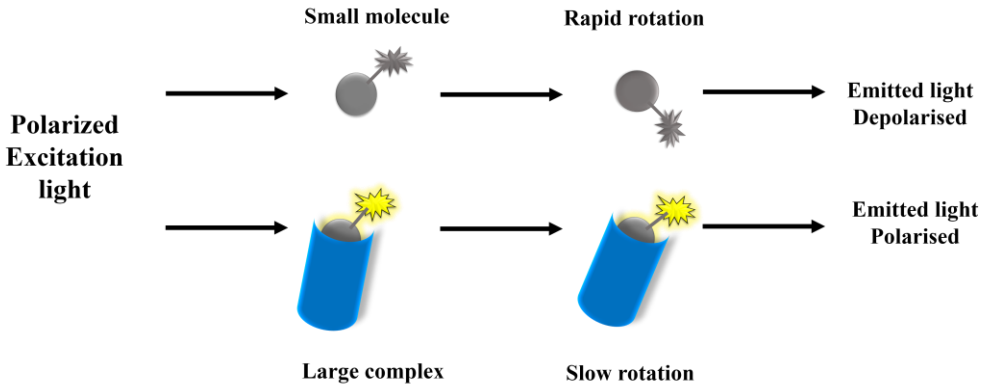

Figure 3.5 Principle of fluorescence anisotropy
(Adapted from Samokhvalov, 2017)

2. Experimental details

For the proteins *Mx*MglA and *Mx*MglB, two kinds of experiments were performed i) binding between the nucleotide and *Mx*MglA ii) binding of *Mx*MglB to the nucleotide

bound MglA. The concept behind this is when MglA binds to the fluorescently labelled nucleotide, the anisotropy should increase (Maziarz and Garcia-Marcos, 2017). Binding of MglB to the fluorescent nucleotide bound MglA causes further increase in anisotropy (Figure 3.6).

Binding of fluorescently-labelled nucleotides, *mant*-GDP (*m*-GDP) or *mant*-GppNHp (*m*-GppNHp) (Jena Bioscience) with the proteins were monitored by measuring the change in anisotropy. The excitation and emission wavelengths used for monitoring the *mant*-labelled nucleotide fluorescence were 360 nm and 440 nm respectively. The experiments were performed on Fluoromax-4 (Horiba), with a sample volume of 200 µl in a cuvette, and excitation and emission slit widths of 5 nm.

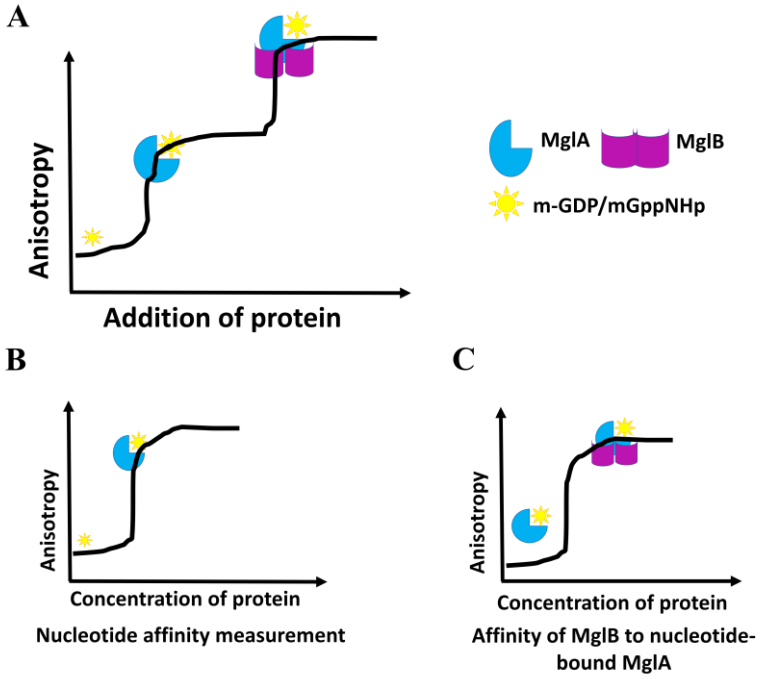

Figure 3.6 Experimental design for binding affinity estimation using fluorescence anisotropy

A. Increase in fluorescence anisotropy upon binding of MglA to nucleotide and then nucleotide bound MglA to MglB **B.** Titration for estimation of nucleotide binding affinity of MglA **C.** Titration for estimation of binding affinity of MglB with the nucleotide-bound MglA

We observed nucleotide binding of *Mx*MglA and its mutants by measuring the change in fluorescence anisotropy of the *mant*-nucleotide upon titration with increasing concentrations of the protein (Brownbridge *et al.*, 1993). Protein samples (*Mx*MglA or its mutants) were titrated against a fixed concentration of *mant*-labelled nucleotide (100 nM). The initial value of anisotropy of the *mant*-labelled nucleotide was subtracted from all the values. The fluorescence anisotropy values were plotted to obtain a binding

curve. Similarly, anisotropy measurements for increasing amounts of *Mx*MglB/MglB^{Ct} with nucleotide-bound *Mx*MglA provided information about the binding affinity of *Mx*MglB to nucleotide-bound *Mx*MglA. A mix of 400 nM of *mant*-labelled nucleotide with 2 μM of *Mx*MglA was titrated with increasing concentrations of *Mx*MglB/MglB^{Ct}. The initial value of *mant*-nucleotide bound *Mx*MglA was subtracted from all the values. Each reading corresponds to 10 averaged single point anisotropy values. GraphPad Prism was used to plot the values against the concentration of protein, and to fit the data to the binding equation for estimation of K_d. Since it is known that *Mx*MglA has a single binding site for nucleotides and also for a dimer of *Mx*MglB, equation for one site-specific binding from the GraphPad Prism was used to fit the data points. Each data point is an average of at least three independent measurements, and the standard error is shown where each data represents 3 to 5 repeats. Error bar represents standard error.

3.2.4 Nucleotide exchange assays

The nucleotide exchange was also measured based on fluorescence anisotropy explained in the previous section.

A. Kinetics of nucleotide exchange

This assay utilises the same instrument and concept of fluorescence anisotropy but in this case, the change in fluorescence intensity upon binding is monitored against time, at particular concentrations of protein and ligand. This provides us information on the kinetics of nucleotide exchange (Eberth and Ahmadian, 2009).

1 Experimental detail

Intensity of mant-GDP (Jena Bioscience) at 440 nm was monitored after excitation at 360 nm. *mant*-GDP (Jena Bioscience) was added with Buffer A50 (50 mM Tris, 50 mM NaCl, $MgCl_2$ 5mM, pH 8.0) in the cuvette 10*2 mm path length and the fluorescence monitored for 600 seconds. Fluoromax 4 (Horiba) was used to monitor all the kinetic studies for MglA, MglB and their mutants. The protein i.e. *Mx*MglA or the mix of *Mx*MglAB (in a molar ratio of 1:2) was added to the cuvette containing *mant*-nucleotide at 600 seconds. This was monitored for another 1200 seconds at 25 ˚C. For plotting the relative intensities from the measurements, each value was divided by the average of

first 300 readings (600 seconds). A running average of 50 data points was plotted to obtain the curves using GraphPad Prism. Every run was performed at least thrice.

B. Quantitation of nucleotide exchange by binding affinity measurements

In this, the fluorescence anisotropy measurements were carried out with the mix of MglA, MglB in a ratio of 1:2.5 and added to *mant*-GDP (400 nm) and readings were taken at different concentrations (Figure 3.6C). Graph was plotted on GraphPad Prism and K_d was calculated.

3.3 Results

3.3.1 GTP hydrolysis assays: Comparison between different methods

We have confirmed GTP hydrolysis activity of *Mx*MglA by HPLC, colorimetric assay for phosphate release estimation (malachite green assay) and NADH assay. Using HPLC, we measured the formation of GDP while in the malachite green assay the inorganic phosphate release was measured. In case of NADH assay, the amount of GDP produced is calculated. All the methods gave similar results.

HPLC results showed that in the presence of MglB the peak of GTP decreased and the peak of GDP increased in height, indicating that GTP hydrolysis occurred. In the graph, area occupied by the peak for GTP was more in case of the *Mx*MglA (Figure 3.7A) compared to the reaction mixture containing *Mx*MglA-MglB (Figure 3.7B). This verified that the GTP hydrolysis by *Mx*MglA is enhanced in presence of MglB. Hence, we concluded that *Mx*MglB acts as a GAP for *Mx*MglA. Further quantification of the peak area was not carried out, as quantitative assays were done using malachite green and NADH coupled assays. Malachite green estimation was an easier process than the HPLC assay, and it estimates the P_i (inorganic phosphate) release in the reaction rather than GDP.

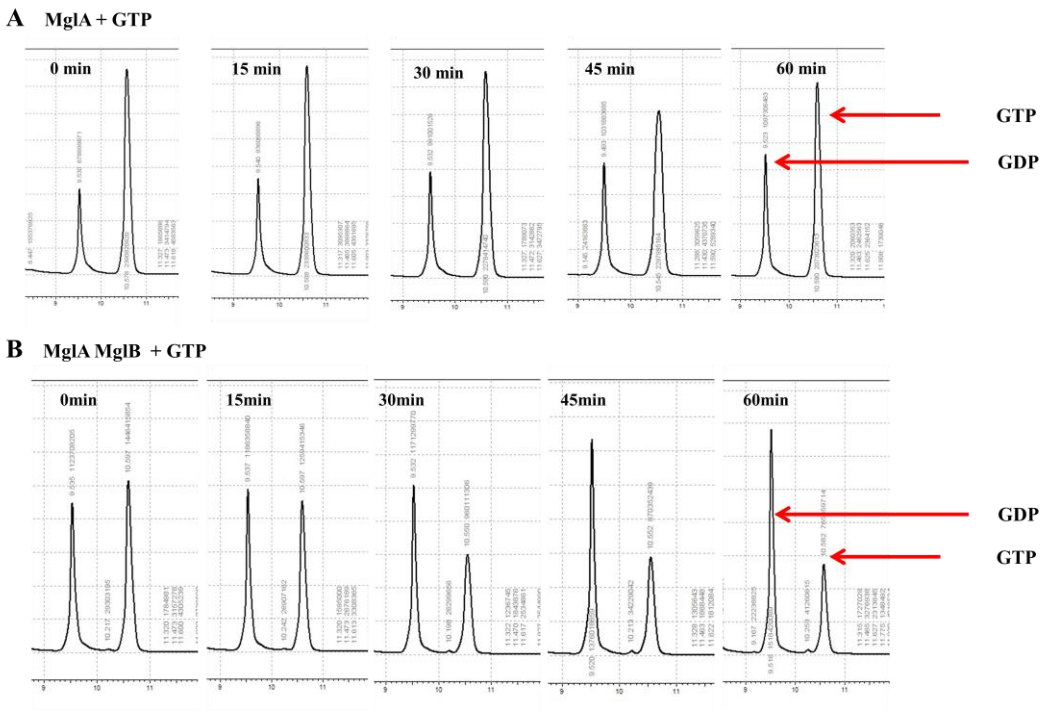

Figure 3.7 GTP hydrolysis measurement by HPLC
A. MglA only **B.** MglA with MglB GTP and GDP peak are shown by red arrow. X-axes denotes the retention time in minutes, while Y-axes represents the absorbance at 280 nm. The time of incubation for each reaction is highlighted on individual graphs.

Malachite green assay was performed with the *Mx*MglA catalytic mutants (Figure 3.8A and 3.8B) and *Mx*MglA helix binding mutants (Figure 3.9B) and with the MglB helix mutants (Figure 3.9A). But the malachite green method had a drawback here that the zero time point of the assays showed significant activity. Usually EDTA is used to stop the reaction of GTP hydrolysis. In the case of *Mx*MglA, we were not able to stop the reaction by addition of EDTA. So, we tried many other ways to stop the reaction and found that heating the reaction mixture, causes denaturation of protein, and hence stopp the reaction. So, for all the malachite green assay trials, heating at 65 ˚C for 10 minutes stopped the reaction. But it takes time to reach the temperature and denature the protein, resulting in measurement of considerable activity at zero time points (Figure 3.8A, B). Hence, we shifted to a continuous enzyme assay, instead of a time point based assay system.

Further experiments for GTPase activity were carried out using NADH coupled assays, where the hydrolysis of GTP within the same reaction volume was monitored continuously with time, thereby reducing the chances of manual error too.

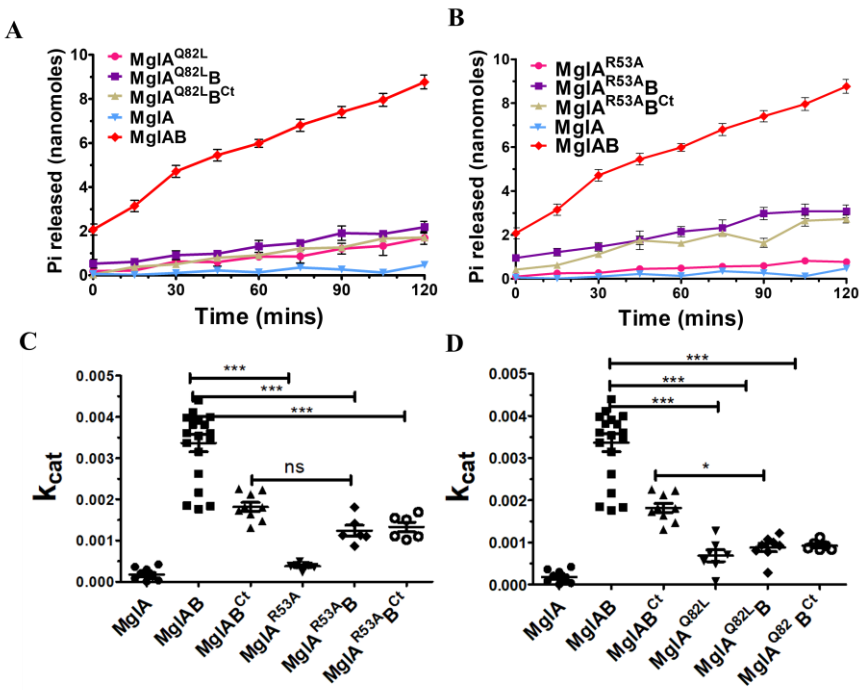

Figure 3.8 GTP hydrolysis measurement by malachite green assay

A GTP hydrolysis monitored by phosphate release using malachite green assay. The curves correspond to MglA (blue), MglA with MglB in 1:2 ratio (red), MglAR53A (hot pink), MglAR53A with MglB in 1:2 ratio (purple), MglAR53A with MglBCt in 1:2 ratio (yellow). **B.** GTP hydrolysis monitored by phosphate release using malachite green assay. The curves correspond to MglA (blue), MglA with MglB in 1:2 ratio (red), MglAQ82L (hot pink), MglAQ82L with MglB in 1:2 ratio (purple), MglAQ82L with MglBCt in 1:2 ratio (yellow). **C, D.** k_{cat} (s-1) obtained from the graphs of malachite green assay from panels A & B with p values < 0.05 (95% Confidence interval)

NADH coupled assay gave same results as malachite green where MglA GTP hydrolysis activity increased in the presence of MglB. Mutants of MglB C-terminal helix (Figure 3.9 C) and MglA helix binding mutants (Figure 3.9D) also supported the above stated fact. GTP hydrolysis rates for various reactions described above were repeated with NADH assay, and results confirmed the fact that *Mx*MglB is a GAP for *Mx*MglA. Also, our results suggested that interaction of C-terminal helix of *Mx*MglB to *Mx*MglA is important for the GTP-hydrolysis activity of the *Mx*MglA. k_{cat} was calculated for each reaction and 95 % confidence interval was calculated for conclusive comparison of the activities of different mutant constructs with the wild type (3.8C, D and 3.9E, F)

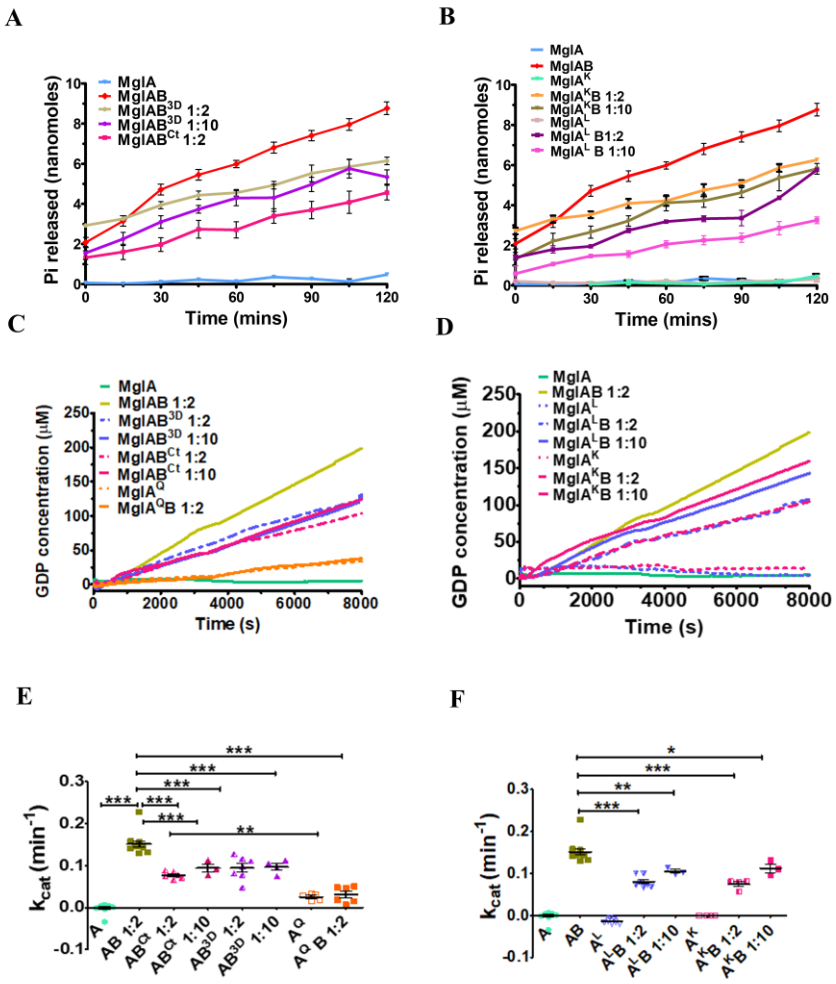

Figure 3.9 GTP hydrolysis assay of MglA helix binding mutants and MglB C-terminal helix mutants

A B C GTPase activities of wild type *Mx*MglA alone (blue), and with MglB (dark yellow), MglB^{Ct} (dark pink), and MglB^{3D} (blue). Ratio variations of 1:2 and 1:10 for MglB^{Ct} and MglB^{3D} are shown in dotted and solid lines, respectively. **D.** GTPase activities of MglA helix-pocket mutants MglA^{L} (purple) and MglA^{K} (pink) compared to WT MglA (green) and MglA with MglB (dark yellow; 1:2 ratio). Ratio variations of 1:2 and 1:10 for the mutants are shown in dotted and solid lines, respectively. **E.** 95% confidence intervals (CI) comparing the values of k_{cat} for MglA, MglAB, MglB^{Ct}, MglB^{3D} and MglA^{Q}B. **F.** 95% confidence intervals (CI) comparing the values of k_{cat} for MglA, MglA^{K} and MglA^{L} in the presence of MglB.

3.3.2 MglB acts as a GTPase activating protein (GAP) of MglA

Compared to the *Mx*MglA-GDP bound structure, conformational changes in switch I and switch II were observed upon MglB binding in the presence of GppNHp (Figure 2.16B). These conformational changes in switch I and switch II positioned the side chains of the active side residues of *Mx*MglA, R^{53} and Q^{82}, in a suitable conformation for carrying out GTP hydrolysis as shown by GTP hydrolysis assay (Figure 3.8A, B).

" –OH" of Thr-54 contributed towards Mg^{2+} ion coordination in the MglB bound state, while it was facing away from the nucleotide binding pocket in the GDP state. These structural observations are consistent with MglB functioning as a GAP, and similar features were observed in the *Thermus thermophilus* structure (Miertschke, et al, 2010). Estimation of the GDP released showed that the GTPase activity of MglA on its own was negligibly low, while the activity increased in the presence of *Mx*MglB in a 1:2 ratio (Figure 3.9C). This confirmed the role of *Mx*MglB as a GAP (GTPase activating protein), consistent with earlier published results (Leonardy, et al, 2010, Miertschke, et al, 2010, Zhang, et al, 2010). GTPase activity measurements of *Mx*$MglA^{R53A}$ and *Mx*$MglA^{Q82L}$ mutants confirmed loss of activity upon mutation of the active site residues (Figure 3.8A, B and 3.9C), similar to earlier studies (Leonardy, et al, 2010, Miertschke, et al, 2011, Zhang, et al, 2010).

3.3.3 Role of the C-terminal helix of MglB in MglA binding and GTPase activity

In order to validate the role of C-terminal helix, we compared the GTPase activities of *Mx*MglA in the presence of *Mx*MglB and *Mx*$MglB^{Ct}$, respectively (Figure 3.9 A and C). The hydrolysis rate of GTP by *Mx*MglA in the presence of *Mx*$MglB^{Ct}$ was less compared to that of wild type *Mx*MglB. If the reduced activity for *Mx*$MglB^{Ct}$ were due to decreased binding affinity with MglA, higher amounts of *Mx*$MglB^{Ct}$ compared to the ratio of 1:2 used for wild type *Mx*MglB should result in an increase in activity. However, the GTPase activity did not catch up to the levels of *Mx*MglB despite using *Mx*$MglB^{Ct}$ in 1:10 ratio (Figure 3.9 A and C).

Similar, assays were carried out with a mutant of *Mx*MglB, in which 3 aspartates (D^{150}, D^{151} and D^{152}) of the C-terminal helix (*Mx*$MglB^{3D}$), which formed water-mediated interactions with MglA in the helix-binding pocket, were mutated to alanines. The mutant $MglB^{3D}$ also showed differences in GTPase activity compared to that of wild type *Mx*MglB (Figure 3.9A, C).

The GTPase activity in the presence of 1:2 ratio of MglB was found to be less than that of the wild type for both the mutants. A higher ratio of 1:10 for $MglA^K$:MglB and $MglA^L$:MglB resulted in increased GTPase activity (Figure 3.9D). The data from these two mutants showed that the residues in the helix-binding pocket contribute towards nucleotide hydrolysis, though they are away from the nucleotide binding pocket or the active site residues.

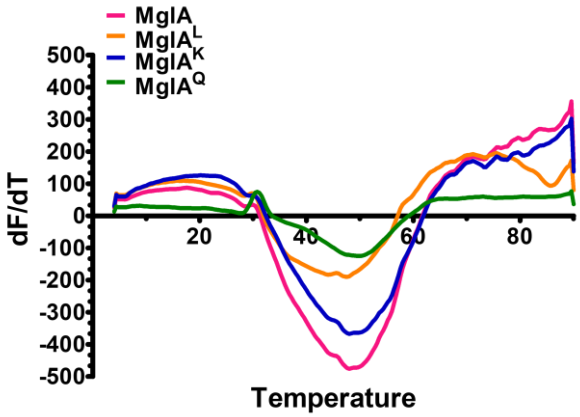

Figure 3.10 Thermal stability assay for MglA and its mutants
Thermal shift assay for MglA (pink) , $MglA^K$ (purple) , $MglA^L$ (orange) and $MglA^Q$ (green) demonstrating that the T_m for unfolding remains similar.

$MglA^Q$, $MglA^L$ and $MglA^K$ mutants were well folded as the wild type *Mx*MglA, as observed from thermal stability assays (Figure 3.10). Also, the mutations did not affect nucleotide binding for $MglA^K$ and $MglA^L$ (Figure 3.11). K_d values for all MglA mutants for different nucleotides are given in the table 3.1. This suggests that the decrease in the activity of the GTP hydrolysis was not because of mutations affecting the protein fold or due to a decrease in the binding affinity of the nucleotide to the MglA mutants. GTP hydrolysis assays, suggested that MglB activates GTP hydrolysis of MglA and the interaction of C-terminal helix of MglB to MglA is important for the GTP hydrolysis of MglA. However, the decrease in GTP hydrolysis activity might be because of the decrease in affinity between MglA and MglB. To, address this, binding studies between these two proteins and their mutants were carried out, as explained in the next section.

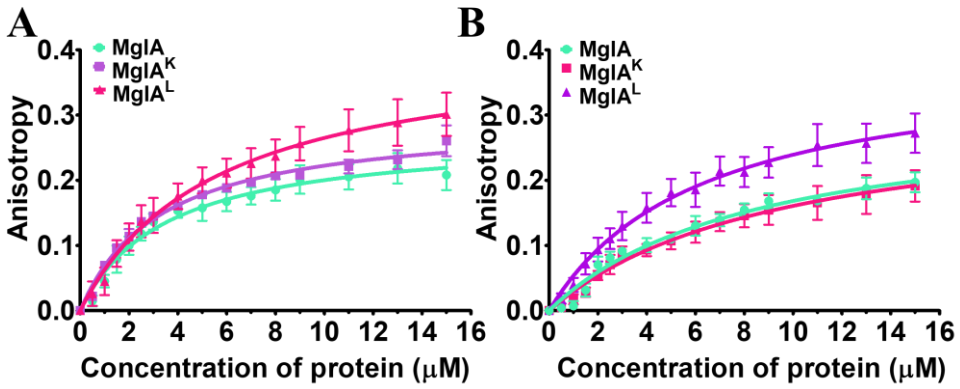

Figure 3.11 Nucleotide binding of MglA and its mutants

A Fluorescence anisotropy measurement for MglA (circle, blue), $MglA^K$ (square, purple), $MglA^L$ (triangle, pink) titrated against mGDP, demonstrating that the binding affinity for GDP remains similar. **B** Fluorescence anisotropy measurements for MglA (circle, blue), $MglA^K$ (square, purple), $MglA^L$ (triangle, pink) titrated against mGppNHp, demonstrating that the binding affinity for GTP remains similar.

Table 3.1 Binding affinity of MglA and its mutants with nucleotide

Protein	m-GDP (K_d in μM)	m-GppNHp (K_d in μM)
MglA	3.2 ± 1	8.5 ± 1.4
$MglA^K$	3.8 ± 0.3	9.5 ± 2.4
$MglA^L$	5.5 ± 0.03	6.2 ± 1.3

3.3.4 Interaction studies between MglA and MglB

Binding of MglA to MglB was checked by three different methods i.e. size-exclusion chromatography, isothermal titration calorimetry and fluorescence anisotropy.

According to size exclusion chromatography (SEC), single proteins i.e. MglA or MglB elute at different elution volumes compared to the MglAB complex, because the complexes are larger in the size compared to individual MglA or MglB. In these experiments, MglA and MglB complexes were prepared in different nucleotide states i.e. without addition of any nucleotide, or in the presence of GDP, GTP and GMPPNP (non-hydrolysable analog of GTP), as explained in the experimental methods. It was observed that MglB bound with MglA in both the nucleotide states i.e. either in GDP or GTP-bound states. However, the C-terminal truncated version of MglB, $MglB^{Ct}$ did not bind to MglA in presence of the GDP, but bound only in the presence of GTP analogues (Figure 3.12).

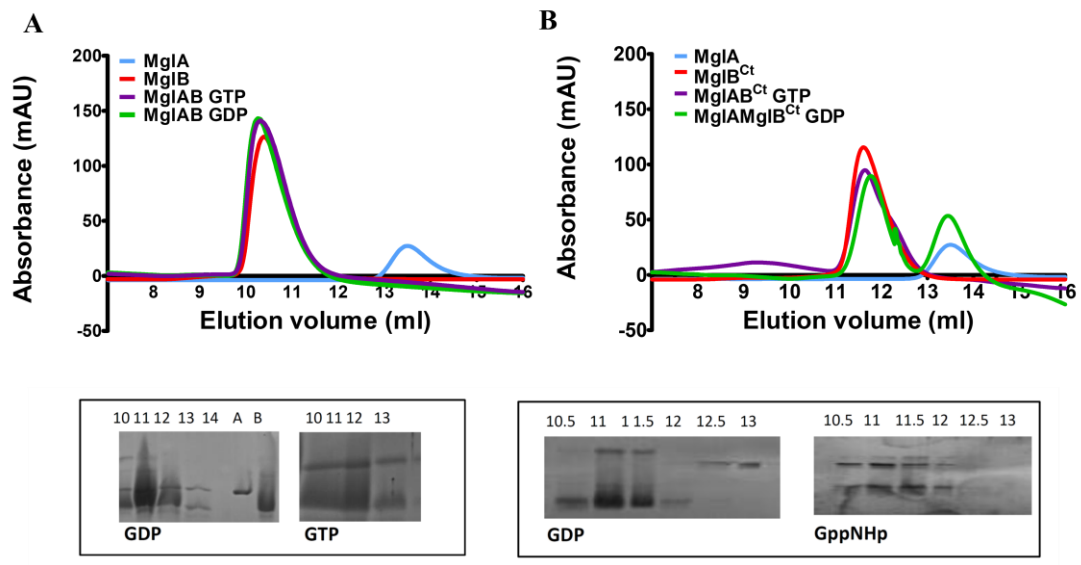

Figure 3.12 Characterization of MglAB binding by Size-exclusion Chromatography

A Gel filtration profile of MglAB complex. MglA (blue), MglB (red) MglAB complex with GDP (green) and MglAB complex with GTP (purple) (SDS-PAGE gels shown below in inset with the fractions depicted**). B** Gel filtration profile of MglAB^{Ct} complex with GDP (green), MglAB^{Ct} complex with GTP (purple), MglA (blue), MglB^{Ct} (red) (SDS-PAGE gel with details of fractions given in inset). In the SDS-PAGE gel in presence of GDP there is no band of MglA and the band mentioned in the comment is oligomer of MglB^{Ct} itself. The MglA band is observed in the fraction 13 itself, where MglA elutes and not along with MglB^{Ct}.

Our studies with size exclusion chromatography showed that *Mx*MglA interacts with *Mx*MglB in presence of either GDP or GTP-analogs (GMPNP, GTP-gamma-S). Shift in appearance of MglA containing fractions from an elution volume of 13.2 to 10.4 qualitatively showed that MglA interacted with MglB, both in GDP and GTP states (Figure 3.12 A and B). Presence of both the proteins in the fractions were observed on SDS-PAGE analysis. Interestingly, MglB alone and MglAB complex elutes at approximately the same volume. This is because MglB elutes anomalously in size exclusion chromatography and the elution volume does not correspond to the mass according to a calibration graph valid for globular proteins. A SEC-MALS measurement for MglB confirmed this observation (Figure 2.7B). Interestingly, MglB^{Ct} also co-eluted with MglA only in the presence of GTP or its analogs (Figure 3.12).

Size exclusion chromatography is a qualitative method for studying protein-protein interaction, and it does not give information on the binding affinities between the two proteins. Hence, we carried out ITC to find out the binding affinities between MglA and MglB in the various nucleotide states. MglAB exhibited binding both in presence of GDP and GppNHp respectively (Figure 3.13), with K_d corresponding to 0.67 ± 0.8 μM for both, while MglB^{Ct} interacted with MglA only in the GTP equivalent state, i.e.

either in presence of GTP, GppNHp or GTP-γ-S, confirming the SEC results (Figure 3.12).

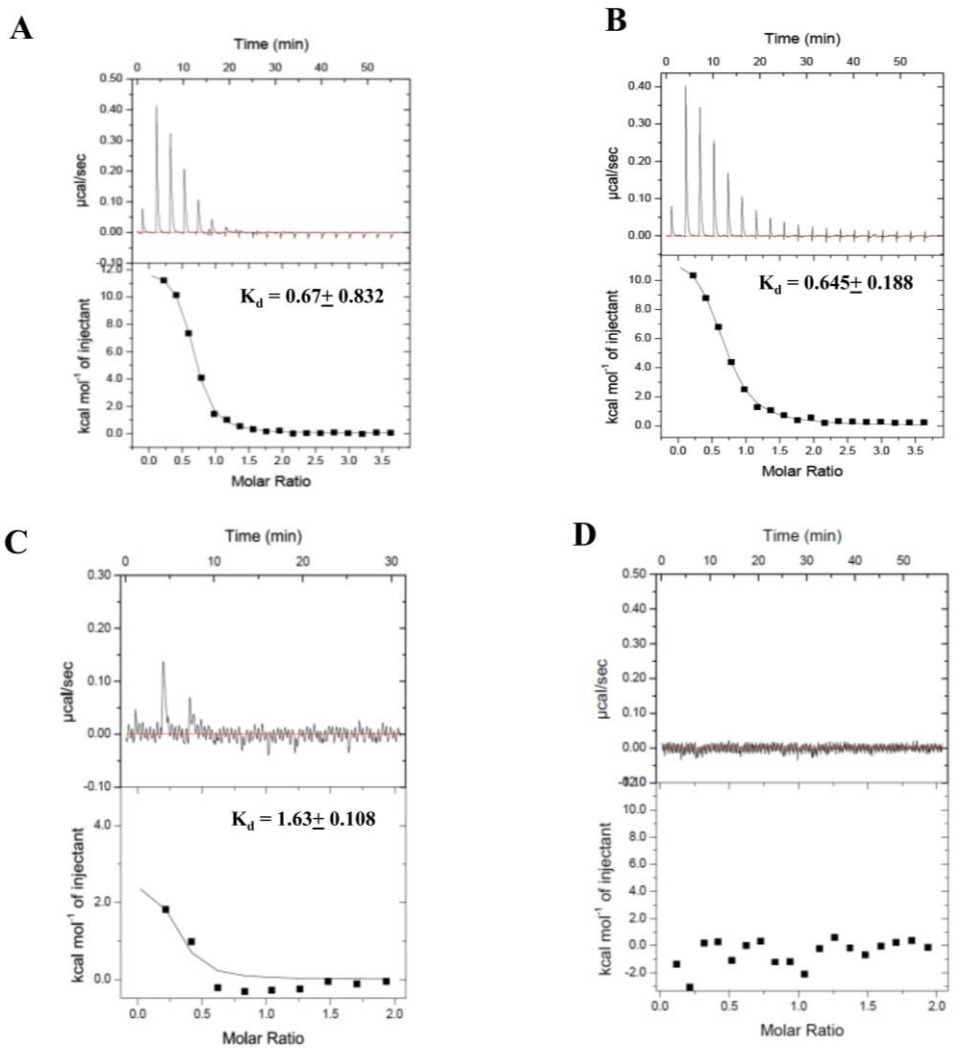

Figure 3.13 Characterization of MglAB binding by ITC
A, B. ITC profile for MglAB interaction in the presence of GMPPNP and GDP, respectively. **C, D.** ITC profile for $MglAB^{Ct}$ in the presence of GMPPNP and GDP, respectively.

Although ITC can quantify the binding affinities among the two proteins, this method required large amounts of protein for multiple repeats. Since the purified MglA was bound to GDP, it was not possible to distinguish whether the binding affinities obtained in the presence of GMPPNP were indeed for MglA that was bound to GMPPNP. This is especially reflected in the quality of the results obtained for $MglB^{Ct}$ titrated against MglA-GMPPNP (Figure 3.13). The poor binding profiles of MglA with $MglB^{Ct}$ in ITC may be due to predominant presence of GDP in the mixture from the purified MglA.

In order to rule out misinterpretation of results due to the presence of GDP, we proceeded with characterizing the binding affinities based on fluorescence anisotropy measurements of *mant*-labelled nucleotides. This approach confirmed that the binding affinity estimated is based only on the MglA molecules that had exchanged the relevant *mant*-labelled nucleotide that was being monitored, i.e. either GDP or GMPPNP, and not on the intrinsic nucleotide present in the protein. These experiments indeed confirmed the results obtained from the SEC and ITC experiments.

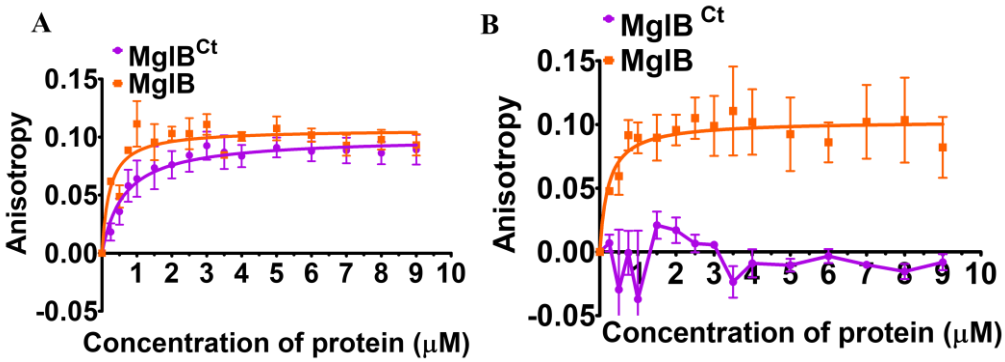

Figure 3.14 Binding affinity of MglB to nucleotide bound MglA
A Fluorescence anisotropy measurement for MglB (orange) and MglB^{Ct} (violet) titrated against mGppNHp bound MglA. **B** Fluorescence anisotropy measurements for MglB (orange) and MglB^{Ct} (violet) titrated against mGDP bound MglA.

Table 3.2 Binding affinities for *m*GDP and *m*GppNHp bound to MglA with MglB, MglB^{Ct}

Protein	m-GDP (K_d in μM)	m-GNP (K_d in μM)
MglB	0.22 ± 0.13	0.21 ± 0.08
MglB^{Ct}	No binding	0.63 ± 0.18

MglA interacted with MglB in presence of either *m*-GDP or *m*-GppNHp (Figure 3.14A). However, MglB^{Ct} bound to MglA only in the presence of *m*-GppNHp but not in the presence of *m*-GDP (Figure 3.14B). The binding affinities (reported as K_d values) between MglB and *m*-GppNHp - and *m*-GDP-bound MglA (0.21 ± 0.08 μM and 0.22 ± 0.13 μM, respectively) were comparable to the binding affinity of 0.63 ± 0.18 μM between MglB^{Ct} and *m*-GppNHp-bound MglA (Table 3.2). K_d between MglB^{Ct} and *m*-GDP-bound MglA could not be estimated, as the binding was insignificant (Figure 3.14).

Next, we proceeded to estimate the binding affinities of MglB to the mutants $MglA^K$ and $MglA^L$ (Figure 3.14). Though the binding affinities of MglB to $MglA^K$ and $MglA^L$ were not affected, GTPase activity of the mutants with MglB was found to be less than that of the wild type (Figure 3.15 and Table 3.3). The GTPase activity remained lower despite increasing the concentration of MglB 5-fold. The above data demonstrated that mutation of residues in the helix-binding pocket affected nucleotide hydrolysis, even though they were located away from the GTPase active site. This implied an allosteric role for the MglB Ct-helix in regulating the GTPase.

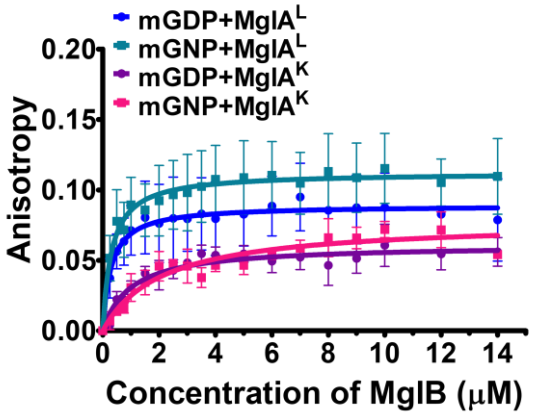

Figure 3.15 Binding of MglA mutants with MglB
Fluorescence anisotropy measurements for $MglA^L$ & $MglA^K$ bound to mGDP and mGppNHp, respectively, titrated with MglB demonstrating that the binding affinities to MglB for the mutants are not affected. The data shown correspond to mGDP (circle) and mGppNHp (square) bound to $MglA^L$ (pink) and $MglA^K$ (purple), respectively.

Table 3.3 Binding affinities of MglA mutants with MglB

Protein	m-GDP (K_d μM)	m-GppNHp (K_d μM)
MglA	0.22 ± 0.13	0.21 ± 0.08
$MglA^K$	0.99 ± 0.27	2.1 ± 0.5
$MglA^L$	0.29 ± 0.17	0.31 ± 0.15
$MglA^Q$	0.20 ± 0.05	0.29 ± 0.05

One very important aspect that has come out from the binding studies between MglA and MglB is that MglB binds to MglA in both nucleotide states i.e. GDP and GTP. Generally, for small Ras-like GTPases, GTPase activating proteins (GAPs) bind to the GTPase in GTP bound state only to help in GTP hydrolysis (Mishra and Lambright, 2016) not in the GDP bound state. Guanine nucleotide exchange factors (GEFs)

typically bind to the GTPase in GDP bound state to facilitate exchange (Cherfils and Zeghouf, 2013).

3.3.5 C-terminal helix of MglB contributes towards GDP exchange

The Ct-helix could allosterically affect the GTPase activity either by activation of catalysis or by stimulating exchange of the product (GDP) with the substrate (GTP). Since the cognate GEF for MglA remains unidentified, we investigated if the Ct-helix has a role in nucleotide exchange.

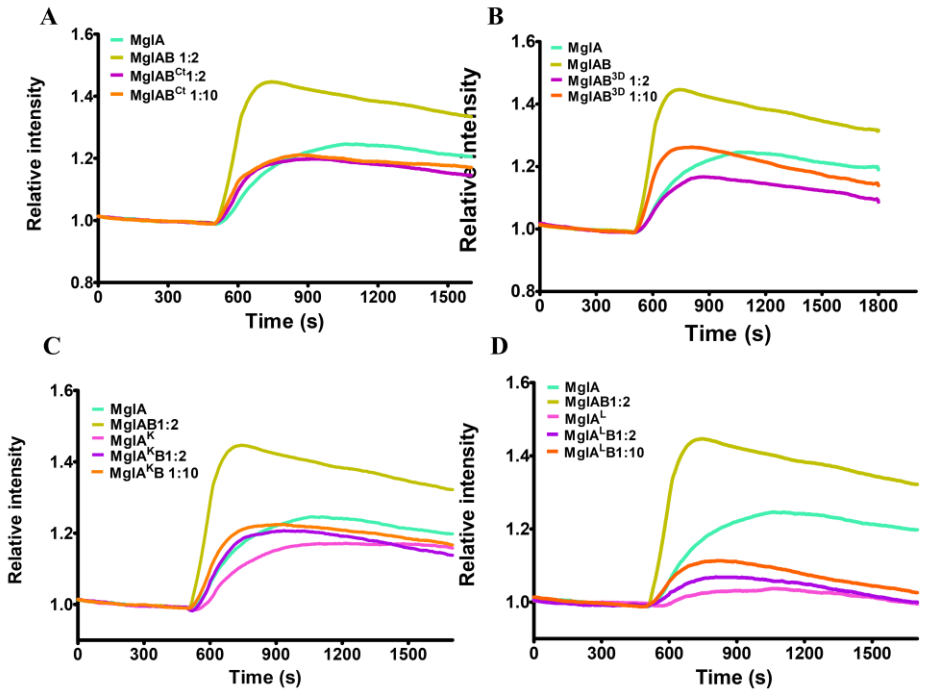

Figure 3.16 Nucleotide exchange kinetics
A, B MglB helix mutants: GDP exchange for MglA (green), MglA + MglB 1:2 (dark yellow), MglA + MglB^{Ct} /MglB^{3D} 1:2 (magenta), MglA + MglB^{Ct} /MglB^{3D} 1:10 (orange). **C, D** GDP exchange for MglA^{K} / MglA^{L}(pink), MglA^{K} / MglA^{L} + MglB 1:2 (purple), MglA^{K} + MglB 1:10 (orange).

As mentioned earlier, the purified MglA had GDP bound to the active site pocket. To measure the exchange between pre-bound GDP and *mant*-labelled GDP (*m*-GDP) in solution, fluorescence intensity of *m*-GDP was monitored upon addition of MglA only, and a mix of MglA and MglB. It was observed that the relative fluorescence intensity was higher with MglB than without (Fig. 3.16). This implied that addition of MglB to MglA increased the replacement of GDP by *m*-GDP substantially.

However, addition of MglB^{Ct} instead of MglB gave a fluorescence rise that was comparable to that observed in presence of MglA alone (Fig. 3.16A), suggesting that the C-terminal deletion failed to stimulate GDP exchange.

Next, we proceeded to quantify the affinities of MglA for *m*-GDP in the presence of MglB or MglB^{Ct}. The apparent binding affinities (denoted by K_d^{app}) for *m*-GDP to MglA, MglA+MglB or MglA+MglB^{Ct} were 3.2 ± 1.0 μM, 0.87 ± 0.07 μM, and 2.7 ± 0.36 μM, respectively (Figure 3.17, table 3.4). This demonstrated that the apparent affinity for *m*-GDP increased in the presence of MglB, but not in the presence of MglB^{Ct}. The approximately equal *m*-GDP binding affinities of MglA and MglA+MglB^{Ct} are consistent with our conclusion that MglA does not interact with MglB^{Ct} in the presence of GDP (see above).

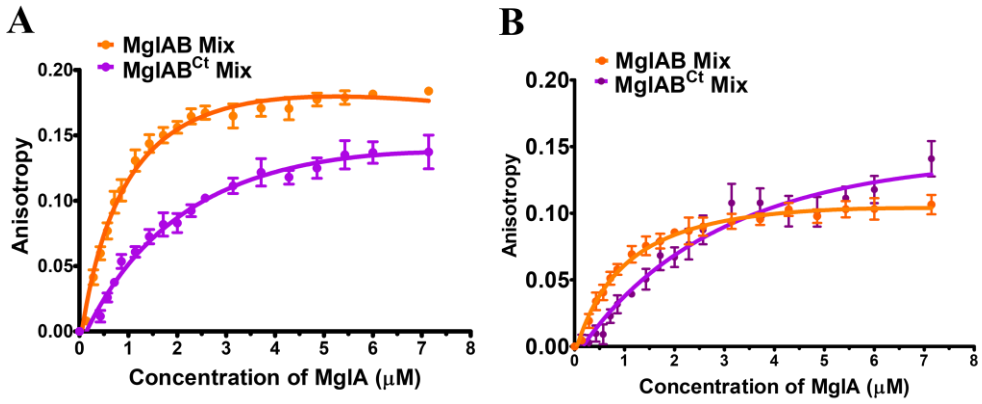

Figure 3.17 Estimation of binding affinities of nucleotides to a mixture of MglA and MglB/B^{Ct}

A. Fluorescence anisotropy measurements for MglA and MglB mixed in ratio 1:2.5 (orange) and MglA and MglB^{Ct} in ratio 1:2.5 (violet) titrated against mGppNHp **B.** Fluorescence anisotropy measurements for MglA and MglB mixed in ratio 1:2.5 (orange) and MglA and MglB^{Ct} in ratio 1:2.5 (violet) titrated against mGDP,

Table 3.4 Apparent binding nucleotide binding affinities of MglA in the presence of MglB/B^{Ct}

Protein	m-GDP (K_d in μM)	m-GppNHp (K_d in μM)
MglA	3.2 ± 1	8.5 ± 1.4
MglAB Mix (ratio A:B::1:2.5)	0.87 ± 0.07	1.08 ± 0.26
MglAB^{Ct} Mix (ratio A:B^{Ct}::1:2.5)	2.7 ± 0.36	4.1 ± 1

The same experiment was repeated with *m*-GppNHp instead of *m*-GDP to quantify the exchange of bound GDP with *m*-GppNHp, a relevant replacement occurring in a reaction catalysed by a GEF.

The corresponding values of affinities for *m*-GppNHp were 8.5 ± 1.4 μM, 1.1 ± 0.26 μM and 4.1 ± 1 μM (Figure 3.17, table 3.4). The ~8-fold increase in apparent affinity of MglA for *m*-GppNHp in presence of MglB strongly suggested that MglB could function as a GEF. However, the increase in affinity of MglA for *m*-GppNHp was only ~2-fold in the presence of $MglB^{Ct}$. This clearly implied that the Ct-helix played a role in nucleotide exchange. Consequently, we concluded that MglB activates MglA GTPase not only by appropriately orienting the catalytic residues, but also by exerting an allosteric effect via the Ct-helix to facilitate nucleotide exchange. This effect increases the overall GTPase activity over several enzyme cycles as observed in our enzyme-coupled assay, which are multiple-turnover rather than single turnover enzymatic reactions.

In summary, *Myxococcus xanthus* MglB regulates the activity of MglA *in vitro* in two ways: by helping in GTP hydrolysis and by involvement of the C-terminal helix in the exchange of the nucleotide. To our knowledge, this is the first demonstration where a single protein performs both the functions. Small Ras-like GTPases that have been characterized till date in eukaryotes or prokaryotes have separate proteins which function as GAP or GEF. To understand the functioning of different regulators of small Ras-like GTPases and the structural basis of their action, an analysis of all small Ras-like GTPases and their protein complexes available in PDB was carried out (Chapter 4).

Chapter 4

Structural analysis of small Ras-like GTPases

4.1 Background

Based on our structural and biochemical data of MglA, MglB and their mutants, we obtained insights into the mechanism of how MglB stimulates hydrolysis of GTP by MglA. Our experimental data suggests that MglB is an activator, which regulates MglA in two possible ways i.e. either by helping in the hydrolysis of GTP or by providing exchange of nucleotide as discussed in chapter 3.

We showed that two molecules of MglB interact with one molecule of MglA; MglB dimer interacts asymmetrically with MglA. According to the crystal structure of MglAB complex, the C-terminal helix of one of the MglB protomers ($MglB_1$) interacts with MglA at a site away from the nucleotide binding site and facilitates nucleotide exchange by maintaining a conformation that favours GTP binding. GTP hydrolysis stimulation is caused by conformational changes in switch I and switch II regions of MglA, by bringing the catalytic residues towards nucleotide bound in the catalytic pocket of MglA. This has also been confirmed by other *in vitro* experiments. This is a unique case where the same protein (MglB) performs both the functions of GAP and GEF, by interaction at an allosteric pocket.

Discovery of the allosteric action of MglB C-terminal helix prompted us to analyze the available structures of interacting complexes of small Ras-like GTPases and their mechanism of GAP and GEF action. Such a comparative analysis will help us to bring out unifying features in the action of GAP and GEF and also other effectors that interact with small Ras-like GTPases. This will also highlight unique features of MglA activation by MglB. The analysis also helped to compare the structural features of other proteins of the Roadblock domain (Rbl; fold of MglB) that interact with the small Ras-like GTPase fold, and also partners that interact through the helix-binding pocket.

4.2 Introduction to small Ras-like GTPases

Small Ras-like GTPases (Figure 4.1A) are a large family of hydrolase enzymes that can bind and hydrolyse GTP to GDP and inorganic phosphate (Figure 4.1B). They consist of more than 100 proteins, with a common core G-domain (Figure 4.1C), and act as molecular switches (Vetter and Wittinghofer, 2001). They are key regulators of diverse cellular and development events, including cell division, vesicle transport, nuclear assembly etc. in eukaryotes (Bourne *et al.*, 1990, 1991). *Mx*MglA is the first

prokaryotic small Ras-like GTPase to be characterized (Hartzell and Kaiser, 1991a; Wuichet and Søgaard-Andersen, 2015). The G-domain is approximately 20 kDa, it carries out the function of nucleotide binding and hydrolysis. G-domain consists of 6 β-strands and 5 α-helices with 4-5 conserved sequence elements as shown in figure 4.1A and 4.1C (Bourne *et al.*, 1990; Vetter and Wittinghofer, 2001; Wittinghofer and Vetter, 2011).

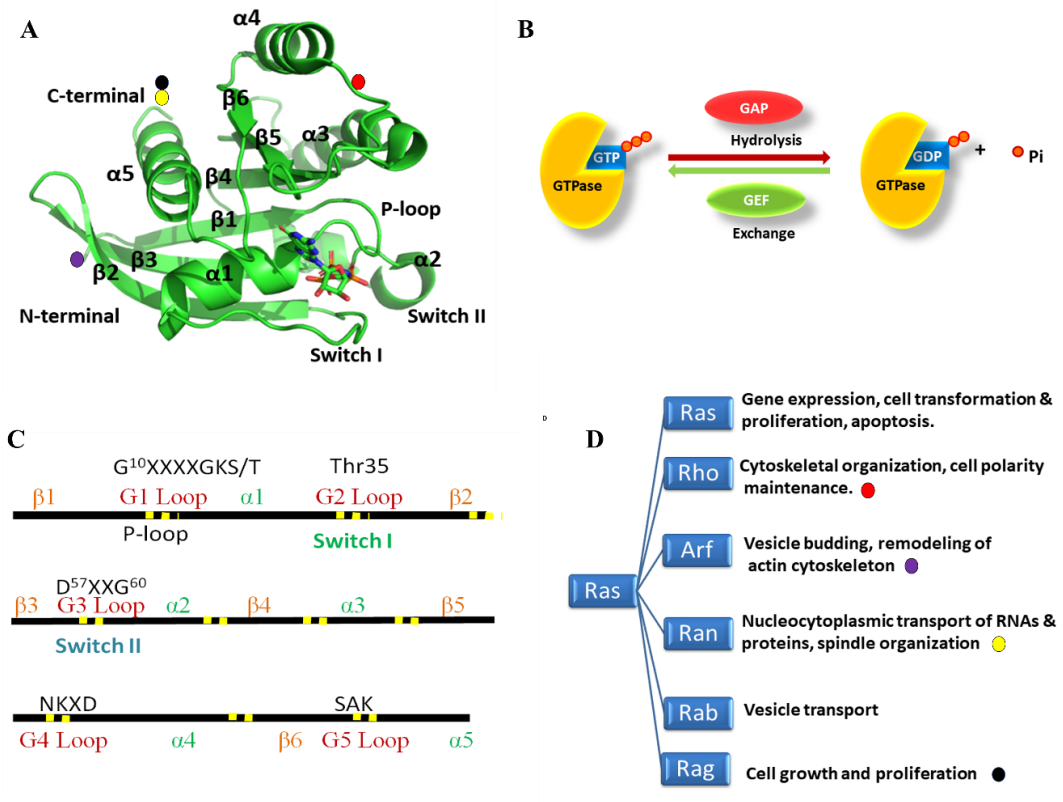

Figure 4.1 Structure and function of small Ras-like GTPases

A. A small Ras like GTPase (PDB ID 3RSO) **B.** GTPase undergoes a switch cycle of GDP and GTP bound states. GTPase is shown in yellow with two different nucleotides bound to it , nucleobase is shown by blue rectangle while phosphate by orange circle and the main players to regulate the two states - GAP in red, and GEF in green. **C.** Conserved motifs and loops in G-domain, yellow dots represent loops, conserved motifs are written in red. Switch I and switch II are conserved loops which undergo conformational change between the two different nucleotide states **D.** Structural and functional classification of small Ras-like GTPases; Insertions to the common small Ras-like GTPase fold are highlighted by coloured spheres in panel A and also highlighted in the corresponding families in panel D. (Adapted from Vetter and Wittinghofer, 2001)

Small Ras-like GTPases have been classified based on structure and function into six different groups i.e. Arf, Ras, Rab, Rho, Ran and Rag as listed in figure 4.1D (Vetter and Wittinghofer, 2001; Wennerberg *et al.*, 2005; Vetter, 2014; Song *et al.*, 2018). In addition to the function-based classification, all the subfamilies of small Ras-like GTPases have specific insertions to the basic G-domain, as shown in figure 4.4D. Rag

is a family of small Ras-like GTPases that consists of heterodimer of RagA or RagB with RagC or RagD of sizes 36, 40, 55 and 57 kDa (Sekiguchi *et al.*, 2001). The Rag GTPases consists of two parts N-terminal which is a GTPase and the C-terminal domain of Roadblock domain fold. They have considerably higher molecular weight than other small Ras-like GTPases.

G1 to G5 loops are characteristic functional features of the small Ras-like GTPase fold. P-loop/G1-loop interacts with β, γ phosphates by the conserved motif, GXXXXGKS/T (Wittinghofer and Vetter, 2011). G2 loop contains the highly conserved "Threonine" residue, which is important for binding and hydrolysis of GTP. Hydroxyl group of threonine interacts with Mg^{2+} and makes hydrogen bond with a γ-phosphate oxygen of GTP. Glycine from DXXG (G3 loop) interacts with γ-phosphate oxygen of GTP. A conserved Asp interacts with Mg^{2+} through a water molecule. N/TKXD, considered as G4 loop, interacts with guanine ring, thus providing the specificity to guanine base over adenine. The G5 loop is not well-conserved, and it interacts with the G4 loop and guanine (Figure 4.1C).

G2 and G3 loops are called as switch I and switch II regions since they undergo conformational changes in the GTPase cycle. Switch I and switch II regions are connected to γ-phosphate of GTP (Sprang, 1997). Upon GTP hydrolysis, release of γ-phosphate causes breaking of hydrogen bonds that hold the two switch regions, and this leads to relaxation of Switch I and switch II regions as seen in GDP-bound state (Wittinghofer and Vetter, 2011). The CAAX motif is required for membrane binding (Figure 4.1C).

4.3 Regulators of small Ras-like GTPases

Many proteins interact with small Ras-like GTPases and regulate their activity and control the pathways associated with these GTPases i.e. GAPs (GTPase Activating Proteins), GEFs (Guanine Nucleotide Exchange Factors), GDIs (Guanine Dissociation Inhibitors), GDFs (GDI Dissociation Factors) and effectors, as shown in figure 4.2. GTPase activating proteins (GAP) are proteins which help GTPases in the hydrolysis of GTP while GEFs, guanine nucleotide exchange factors, are proteins which exchange the GDP bound to the GTPase with GTP (Figure 4.1D) (Bos *et al.*, 2007; Carvalho *et al.*, 2015). GEFs are essential for most small Ras-like GTPases because their affinity to the product GDP is much higher than the affinity to the substrate GTP. The GTP-bound

form of GTPase is generally considered as the active form of GTPase while GDP-bound form is the inactive form. GAP proteins bind to the GTPase in the GTP bound form while GEFs bind to the GDP-bound conformation of the GTPase. Activities of GEFs and GAPs are also governed by another stimulus. There are proteins which regulate the activity of GEF i.e. guanine nucleotide exchange inhibitors or GDI. GDIs bind to the GTPase in the GDP-bound state and prevents binding of the GEF to the GTPase. Hence, GEFs will not be able to exchange the nucleotide of the GTPase and the GTPase remains in the inactive form (Cherfils and Zeghouf, 2013). The GTPase is released from the GDI only when a type of protein named GDF, guanine nucleotide dissociation factor binds to the GDI. When GDI binds to the GDF, GTPases are free to bind to the GEF. Effectors are the proteins which bind to the active state of GTPases and further activates many signalling pathways and thus, the GTPase will be able to control many important cellular processes i.e. cell motility, cellular growth, development and differentiation etc, with the help of suitable effector proteins (Bourne *et al.*, 1991).

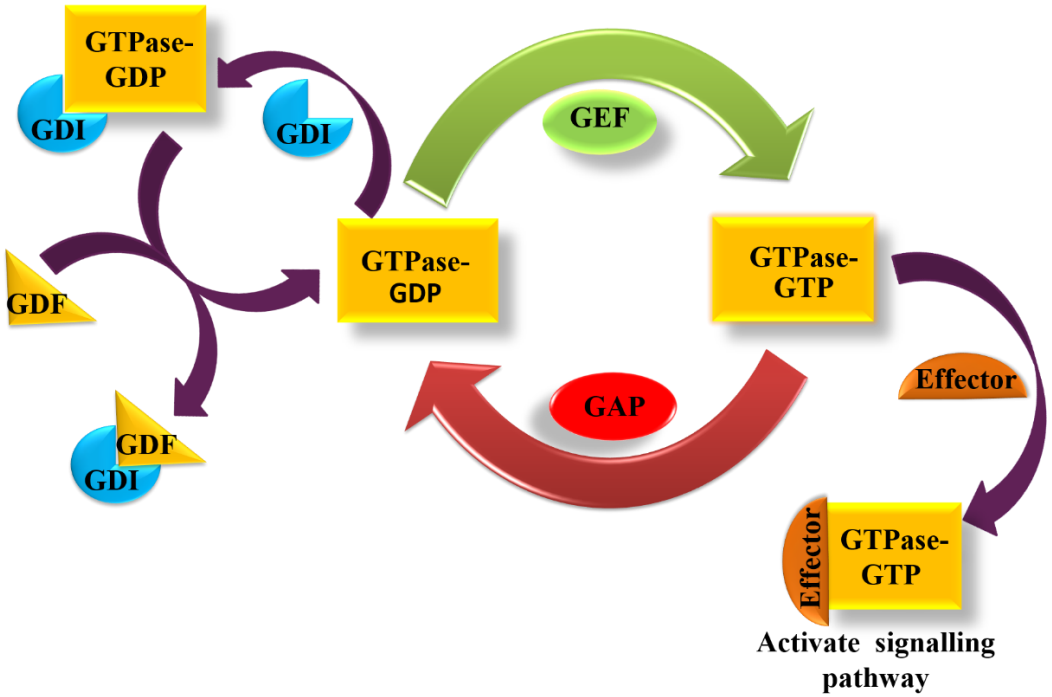

Figure 4.2 GTPase regulating proteins
GTPases are shown by yellow rectangles, GEFs (green) and GAPs (red) are part of the switch cycle of GTPase, while there are proteins i.e. GDI (blue), GDF (yellow triangle) that indirectly regulate the activity of GTPase and hence exert their action on downstream effectors (brown semi-circle).

4.4 Structure analysis of small Ras-like GTPase complexes

To understand how GTPases and their regulators interact to perform their functions, we carried out a structural analysis of all small Ras-like GTPases and their interacting proteins, and looked for the similarities and differences between these interactions amongst the same or different group of proteins/ interactors. The main objective was to compare the mechanism of activation of MglA by MglB with other small Ras-like GTPase activators (especially GAPs and GEFs). Some of the questions addressed by this analysis are: i) What are the different mechanisms of action of GAP and GEF in other GTPases? ii) Are there any functionally important residues which are conserved among them? iii) Are there conserved faces for interaction that are suggestive of a common mechanism? This analysis will also help to understand the mechanism of action of GAPs, GEFs, GDIs, and effectors, and to explore if mechanisms analogous to the allosteric activation observed in MglAB exist, especially among eukaryotic GTPases.

Crystal structures of complexes of small Ras-like GTPases with their interacting partners are available in the PDB. Analysis of these structures will provide insights on the mechanism of action of these proteins. Though some reviews that summarise these results are available in literature (Corbett and Alber, 2001; Cherfils and Zeghouf, 2013) (Vetter Ingrid, 2017), none of these provided us with the information on allosteric action similar to that of the newly discovered MglAB mechanism. Also, the missing part in these reviews, was a clear list of various interactors that function through a pocket similar to the helix binding pocket that we observed in our results.

4.5 Methods

To extract structures of all small Ras-like GTPases and their complexes from PDB (as of November 2018), structure of MglA from *Mx*MglAB was used as query in DALI server to find out similar structures and their complexes. We removed the redundancy from the total GTPases and complexes obtained from DALI server in terms of duplication of chains of the same molecule from the PDB and selected 864 unique structures for our analysis. These structures include proteins with 100 % identical sequence also, if the interacting ligand or protein partner is different or if it is present in a different crystal packing.

All the structures obtained from DALI were classified according to the GTPase family. Further, complexes were categorized into GAP, GEF, GDI and effectors, on the basis of their function mentioned in the literature (van Dam *et al.*, 2011; Cherfils and Zeghouf, 2013; Mishra and Lambright, 2016; Müller and Goody, 2018). In every case, the presence of ligand (nucleotide or inhibitor) bound to the nucleotide binding pocket of the GTPase was also recorded. In addition to the list of proteins obtained using MglA as query, the database was searched using one member from each superfamily of Ras-like GTPases (3QBT, 4JVS, 3LVR, 3MSX, 1RRP, 1XD2) as queries and the output was compared to ensure a comprehensive list. All interaction analysis of the structures was done using PyMol (L DeLano, 2002). To characterize the interacting distances between the GTPase and their interacting partners, inter-residue distances less than 4 Å were considered in PyMol and the secondary structure of the GTPases and the interaction interfaces of proteins were examined. For confirming the fold details of the interactors, Superfamily (Andreeva *et al.*, 2008) and SMART (Letunic *et al.*, 2015; Letunic and Bork, 2018) servers available online were used. Superfamily and SMART give details of the fold and domain.

4.6 Distribution of structures of small Ras-like GTPases

The unique PDB IDs which consist of only GTPase as protein chains are 433 in number while the rest of 431 structures include all the structures with different regulators. The distribution of GTPases with their complexes are shown in the graph below (Figure 4.3A and B). The structures of GTPases belong to all the 6 different classes, as given in Table 4.1. The details of the complexes have been discussed in each section below.

The variation of the nucleotide bound states of these GTPases are classified according to the subgroups (Figure 4.4A). It shows that most of the structures belong to the nucleotide bound state, either GDP or GTP analogs. The GTP bound state consists of GTP and analogs of GTP with a tetrahedral gamma phosphate moiety such as GppNHp, GppCp, GTP-γ-S, GDP with BeF_3 and GDP with VO_3, etc. Most of the GTP bound structures of GTPases are catalytic residue mutants. All the structures were further classified according to the sub-family of small Ras-like GTPases (Figure 4.4B, C).

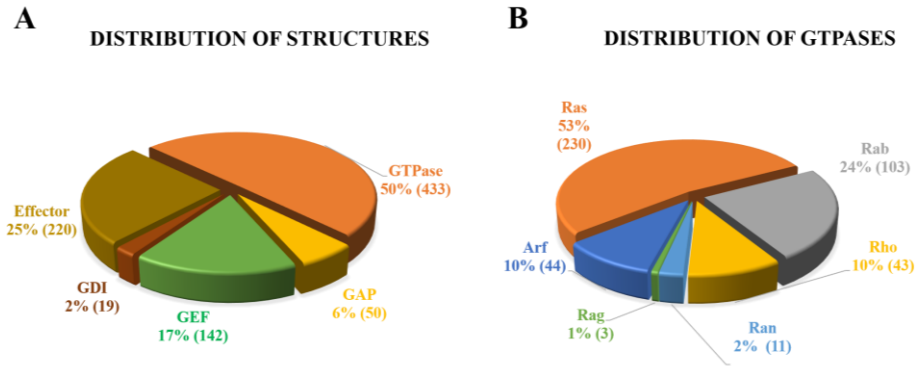

Figure 4.3 Distribution of structural information on small Ras-like GTPases
A. Distribution of structures according to bound interactors - GTPases without any protein partner (orange), and GTPases in complex with GAPs (yellow), GEFs (green), GDIs (dark brown), effectors (brown), respectively **B.** Distribution of GTPases without any protein partners, divided into various classes of small Ras-like GTPases - Ras (orange), Rab (grey), Rho (yellow), Ran (cyan) and Arf (dark blue).

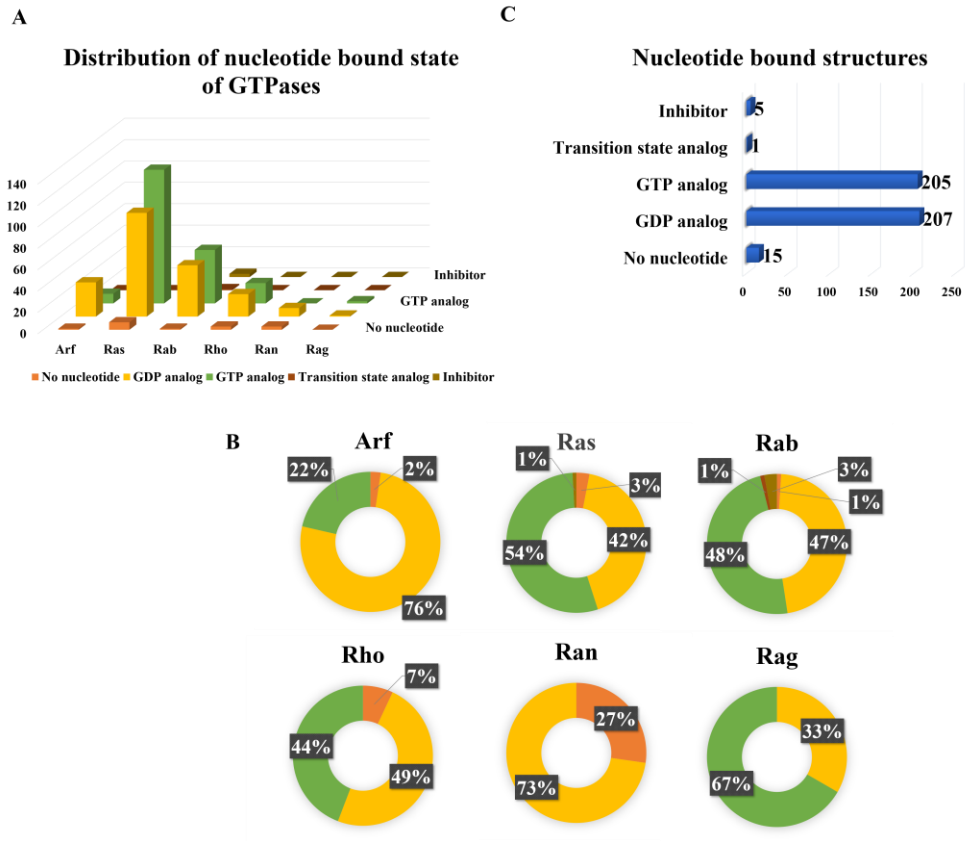

Figure 4.4 Structural information on small Ras-like GTPases without any protein partners
A. Family-wise distribution based on the ligand in the nucleotide-binding pocket of small Ras-like GTPases.**B.** Percentages of nucleotide bound in each sub family are shown (same colour key as in panel A). **C.** Overall distribution of nucleotide bound GTPase structures.

Table 4.1 Details of sub-family of GTPase structures available in the PDB. Structures without any protein partners are listed.

Arf	Ras	Rab	Rho	Ran	Rag
Arl	M-Ras	Rab3a	Cdc42	Ran	Gtr1p-GTr2p
Arl1	N-Ras	Rab4a	Rac1,1b		
Arl2	di-Ras	Rab5a, 5b, 5c	Rac2		
Arl3	R-Ras	Rab9,9a	Rac3		
Arl6	K-Ras	Rab1a	Rho1		
Arl8a	H-Ras	Ara	RhoA		
Arl10b	Rem	Rab8	RhoB		
Arl13b	Gem	Rab21	RhoC		
Arf1	Rheb	Rab22	RhoD		
Arf2	Ral	Rab25	RhoE/Rnd1,Rnd3		
Arf4	Rit	Rab14	RhoI		
Arf5	Rap	Rab3b	RhoUa		
Arf6		Rab6,6a,6b	Rop5		
Arf10b		Rab7	Rop9		
Arf13		Rab11a	TC10		
Sar1,1a,1b		Rab27a,27b			
		Rab28,28a			
		Rab31			
		Rab33			
		Rab43			
		Sec2			
		Sec4p			
		Ypt 1p			
		Ypt7			
		Ypt51			

Interestingly, there is only one structure existing in the transition state in the small Ras-like GTPases (unbound to any other interacting protein), which highlights that it is difficult to capture most small Ras-like GTPases in the transition state without a binding partner such as GAP. The number of nucleotide free states is also very less (15) in comparison to nucleotide bound GTPase structures (412), which could be because most small Ras-like GTPases are unstable in the absence of a bound nucleotide.

The complexes of small Ras-like GTPases were classified into those bound with GAP, GEF, GDI and effector. The number of complexes in each category are listed in the pie chart (Figure 4.3A). The maximum number of structures available were of small Ras-like GTPases bound to effectors, followed by those bound to GEFs, GAPs and GDIs.

All the complexes were classified into various sub-families (Figure 4.5A). Maximum structures available in the GEF family belong to the Ras subfamily while for GAPs, maximum complexes available belong to Rho and Rab families (17 and 10, respectively). For GTPase-effector complexes, most of the structures belong to the family of Rab, Ran and Ras. On the other hand, for complexes with GDI, most of the structures are available from Rho and Rab (7 and 9, respectively).

Nucleotide state of GTPases in the complexes were examined, to understand the dependence of the nucleotide bound state of GTPase for forming the complex with the interacting partner. GTPases bound to most of the effectors and GAPs were found in GTP-bound state (Figure 4.5C), majority of GEFs were found in the nucleotide free state (Cherfils, 2014), while GDIs in the GDP-bound state (Cherfils and Zeghouf, 2013). Among the GEF-bound structures, there are many Ras-SOS complexes crystallized in the presence of different small molecule inhibitors, which are not bound in the GTP binding pocket, but affects the GEF activity.

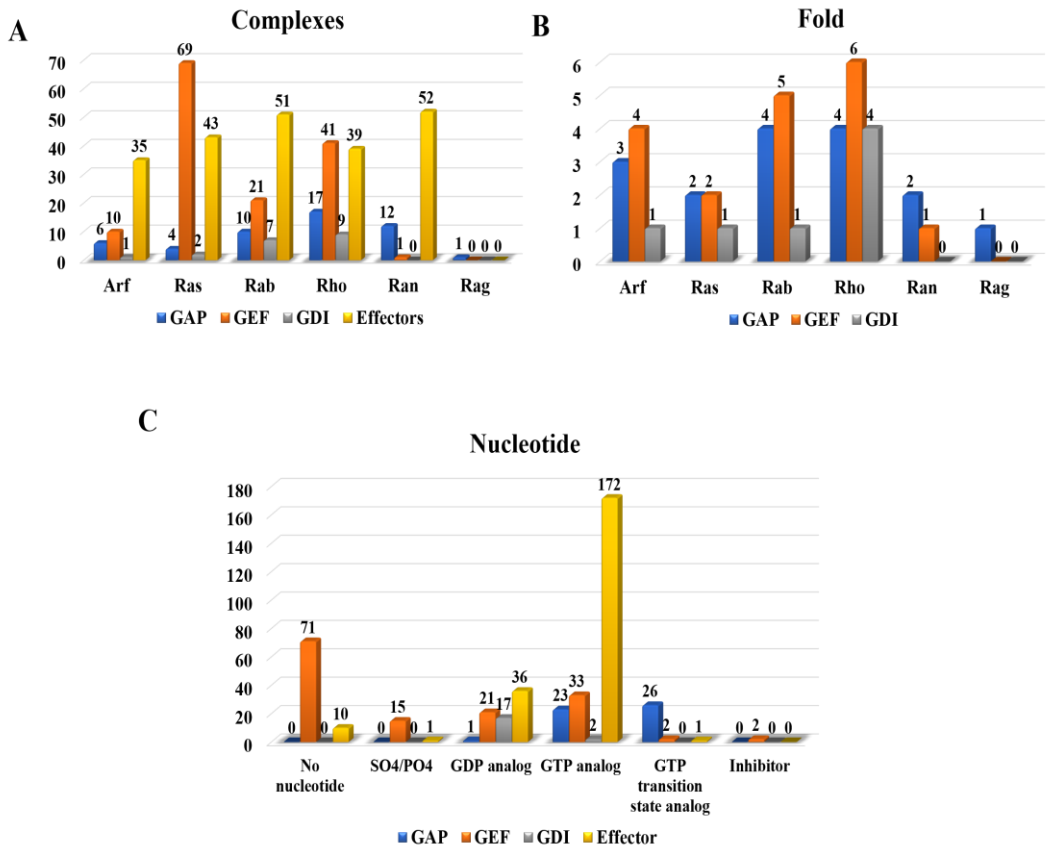

Figure 4.5 Distribution of structures of protein complexes of GTPases
A. Distribution according to complexes and their GTPase subfamilies **B**. Distribution according to fold C. Distribution according to bound nucleotide.

GTPase regulators possess different folds. The variety of these folds of GTPase regulators are summarised in Figure 4.5B. Here, GAPs and GEFs share almost the same number of folds among the available structures i.e. 17 and 18 respectively; while GDI have 8 folds found based on the structures in the PDB. Maximum number of GAP folds were observed in the Rab, Rho and Arf bound structures i.e. 4, while for GEFs, a variety of folds were observed among the complexes with Rho and Rab. GDIs have most folds in the Rho subfamily complexes. The details of the relevance of the fold variation and mechanism of action associated with each fold is discussed below in the corresponding section for each regulator.

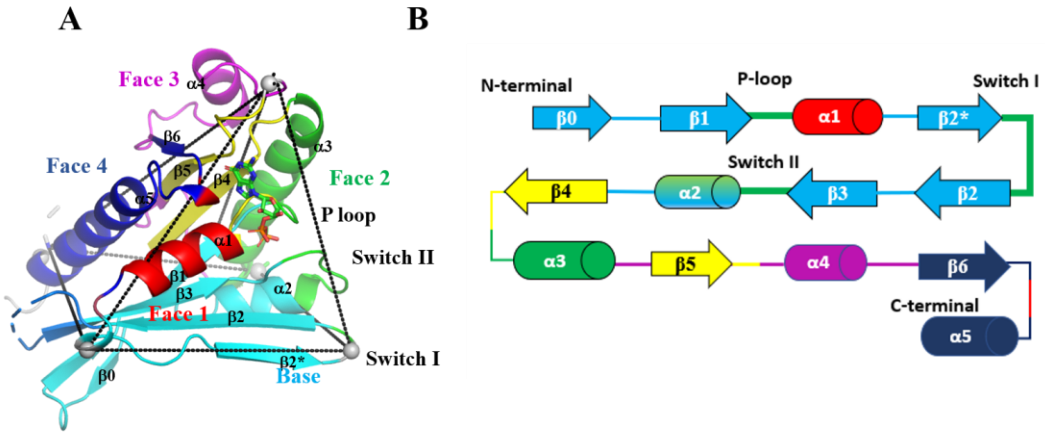

Figure 4.6 Assigning faces to GTPase
Representation of faces of approach for complex formation of small Ras-like GTPases
A. Taking *Mx*MglA as a reference, the GTPase fold is divided into 5 faces and coloured accordingly i.e. face 1, face 2, face 3, face 4, base and inner core (buried inside) is coloured with red, green, magenta, blue, cyan and yellow, respectively. **B.** Secondary structure arrangement is shown with their respective positions in tertiary structure by the same colour code.

The interaction of these regulator proteins with the GTPase and interacting surfaces on the GTPase in GTPase-regulator complexes were studied to highlight the unifying features of mechanism of action among the various GTPase interactors. For GTPases bound to their interacting partners, a detailed analysis was carried out where the complexes were classified according to the face of approach to the GTPase. For this study, the GTPase fold was classified into 5 different faces as shown in Figure 4.6, named as face 1, face 2, face 3, face 4 and base. MglA structure was used as a reference for assigning the different faces for the small Ras-like GTPase fold, with different secondary structures comprising each face (figure 4.6 A, B shows a face-wise colour highlighted on MglA structure and secondary structure representation of the fold). The interactions to multiple faces were conveniently represented by a Venn diagram. We

also looked for the secondary structures on the GTPase fold (Figure 4.6B) with which they interact, to arrive at unique and diverse features of the mechanism of action of these regulatory proteins.

4.7 GTPase Activating Proteins (GAPs)

The typical nature of a GAP is that it binds to the GTPase in the GTP bound state and helps in assisting GTP hydrolysis (Mishra and Lambright, 2016). This section describes the analyses carried out for complexes of GAPs with small Ras-like GTPases.

4.7.1 Nucleotide specificity of GTPases bound to GAPs

In correlation to its function in GTP hydrolysis, GAPs do not generally interact with the GDP-bound state of the Ras-like GTPase. Consistently, when the nucleotide state of the GTPase-GAP complexes were checked, out of 50 GTPase-GAP complexes, only one structure is GDP bound (PDB 3O47) while all other structures are in the GTP-bound state.

They are either GTP analogs or transition state analogs (Figure 4.7 A and B), which possess the γ-phosphate equivalent to either the tetrahedral geometry or in the planar bipyramidal geometry. Also, as mentioned earlier, GAPs appear to stabilise the transition state of small Ras-like GTPases, as these conformations were not captured in the absence of GAPs (section 4.6).

4.7.2 Folds of GAPs

Structures of GAP proteins for all the small Ras-like GTPases were classified in terms of family and fold of the proteins (Figure 4.8). Details of the fold and PDB IDs of their representative structures are given in table 4.2. These include only the GAPs that have been crystallized with GTPases and is not a comprehensive list of all existing GAPs. GAPs bound to the Arf GTPase family have 4 different folds categorised based on the available structures (as shown in figure 4.8 and table 4.2). RP2 (PDB IDs 3BH6 and 3BH7) is a GAP that has two domains - an N-terminal nucleoside phosphate kinase domain and a C-terminal domain of adenyl-cyclase associated protein. The N-terminal domain interacts with the GTPase and contains the catalytic residues.

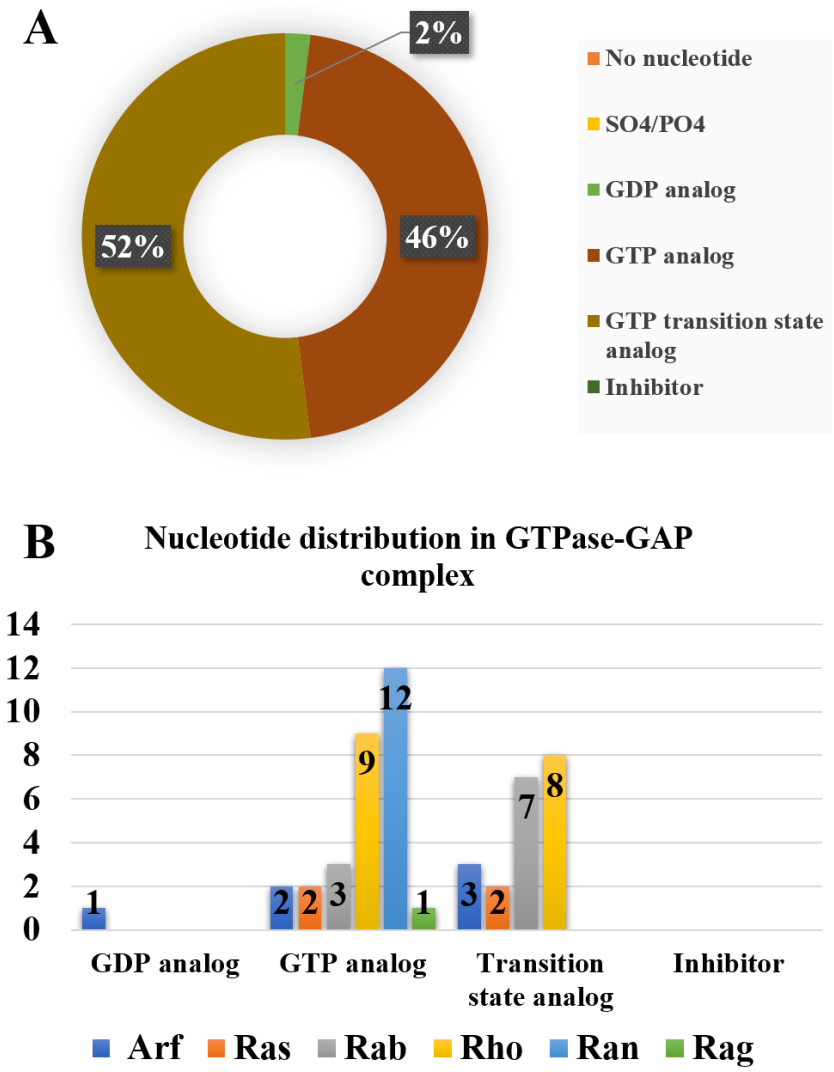

Figure 4.7 Nucleotide distribution of GTPase-GAP complex structures
A. Percentage representation of bound nucleotide observed in all structures of the GTPase-GAP complexes. **B** Family-wise nucleotide distribution in GTPase-GAP complex structures.

3LVQ and 3LVR are two GAP complexes in different nucleotide analogs of GTP which belong to the ArfGAP fold, while 3O47 belongs to the same fold. All the three structures were captured as a fusion with the Arf GTPase and have different interactions of the GAP with the GTPase. The active form appears to be the conformation in 3LVR (3LVQ) (Ismail *et al*, 2010). This might be one of the reasons that 3O47 could be captured in the GDP-bound state, which is rare for a GTPase-GAP complex. 2J59 belongs to ArfBD (Arf-GAP21) with a Pleckstrin-Homology domain (PH domain), but in this case the GAP acts as an effector for Arf while it acts as a GAP for Rho.

Ras GAPs in the PDB possess two unique folds identified in the complexes represented by the PDB IDs 4M8N and 3BRW (Figure 4.8). The GAP protein in 3BRW belong to the Rap-GAP fold, while 4M8N and 1WQ1 are representatives of the p120 GAP domain-like fold.

Rab family of GTPases have 10 GAP-bound structures in the PDB, which were classified into 4 different folds (Figure 4.8). A TBC (Tre2-Bub2 and Cdc16)-like domain is present in the Rab GAPs 4HLQ (representative fold) and 2G77. Many GAPs from pathogenic bacteria that hijack the host machinery GTPase signalling cascade bind to Rab GTPases, but belong to novel GAP folds, not observed among eukaryotic GAPs. Two such folds are represented by 4FME and 4JVS, which are structures of EspG/VirA and LepB respectively. 1M2O is another representative fold of this family.

Unique folds of Rho GAPs identified from the structures available are four in number, represented by the structures 1AM4, 5CJP, 3RYT and 1HE1 (Figure 4.8). The GAP domains represented by 1AM4 belong to the BCR-Homology (BH) domain, and includes the maximum number of GTPase-GAP structures (13, including 1AM4). 5CJP belongs to the class of IQGAPs, and the GAP does not provide a catalytic residue similar to arginine, and hence does not possess a strong catalytic activity (LeCour *et al.*, 2016). GAP proteins in 3RYT and 3SU8 are plexin A1 and B1 respectively, which act as GAPs for Rap, but requires activation by Rho GTPases (Bell *et al.*, 2011). Hence, the active site residue equivalent to the arginine appears to be missing in these complexes. The GAP in 1HE1 is ExoS which is a toxin protein from *Pseudomonas* that activates Rho GTPases. It possesses a novel fold not found in any other eukaryotic GAPs, and is one of the smallest GAPs with only 130 amino acids (Würtele *et al.*, 2001). 5CJP has a GAP of p120 domain like fold similar to the IQGAP fold (as shown in figure 4.8E and I).

Out of the 12 structures of Ran-GAP complexes of interest to GAP activity, RanGAP and RanBP1 of 1K5D and 5DIF were considered as representative folds (Figure 4.8). There are many structures available for Ran RanBP1 and exportin but they are different only in terms of binding of exportin to the small molecule or peptide. So, only the structures which are relevant to our face interaction analysis were considered. RanGAP in 1K5D requires the PH domain of RanBP1 also for GAP activity (Seewald *et al*, 2002).

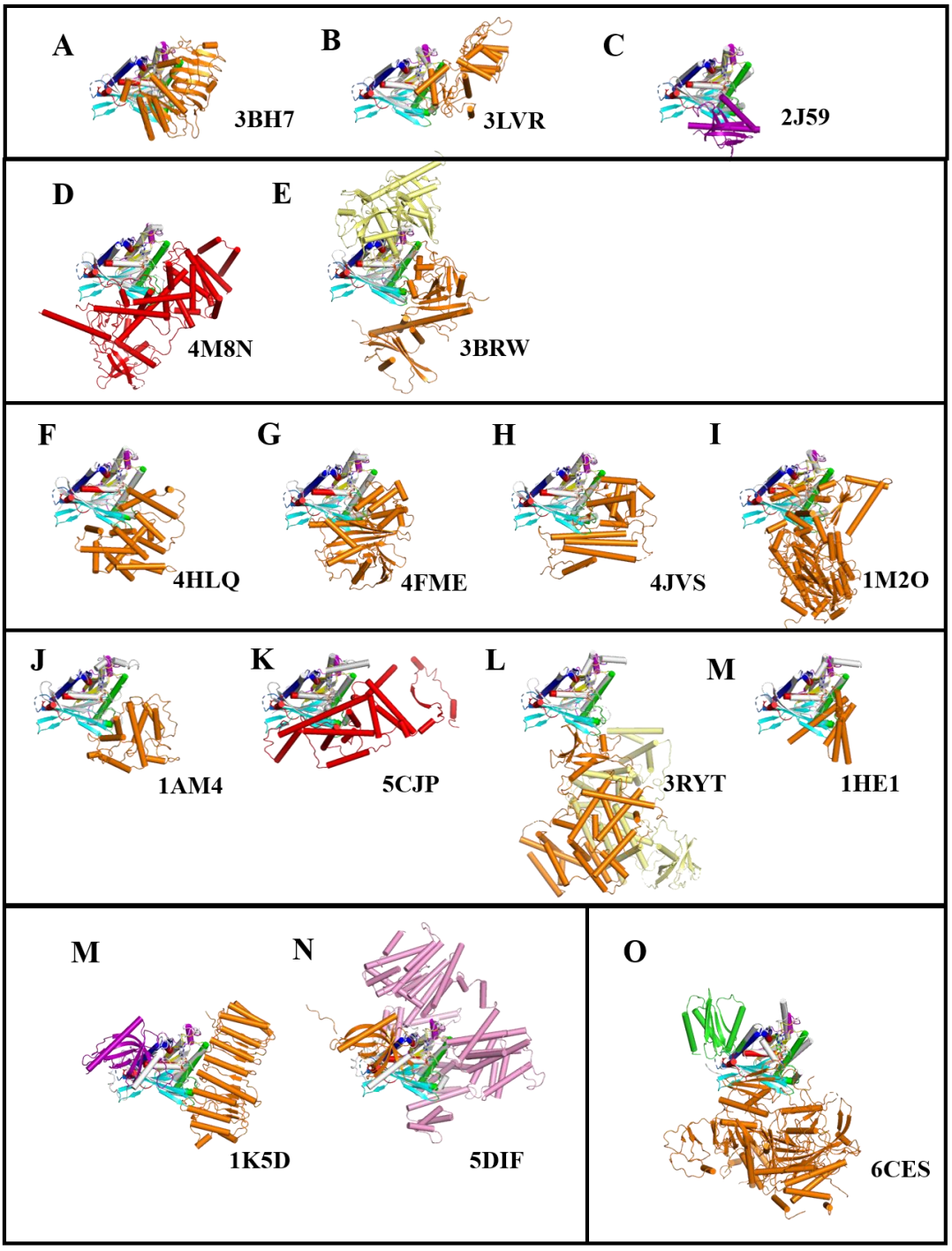

Figure 4.8 Different GAP folds available in the PDB
The GTPase is shown in grey, while the superposed MglA is shown according to the face colour described in section 4.6. GAPs are represented in shades of orange. The exportin subunit in 5DIF is shown in pink. GAPs that possess PH domains (5JCP and 1KSD) are shown in purple to highlight the common fold, but different orientations of interaction with the GTPase. 4M8N and 5JCP, with the GAPs coloured in red, also share the same fold, and interact with different Ras subfamilies.

Hence, both these were considered as two independent GAP domains bound to Ran family. 5DIF also contains a RanBP1 bound to it, which is of PH domain. Interestingly,

PH domain was also found as a complex with Arf GTPases (2J59) as discussed earlier. A GAP complex of Rag GTPases include the Gator1 complex (6CES). The mechanism of activation by the GAP complex is through the interaction with the C-terminal Rbl fold domains and not directly through the GTPase (Shen *et al.*, 2018).

Table 4.2 Fold and catalytic residues of GAP.

Ras families	GAPs complexes	Folds	PDB ID	Catalytic residues	
				GTPase	GAP
Ras	4	2	4M8N	Q-63	R-711
			3BRW	Y-32	N-290
Arf	6	3	3LVR	Q-67	R-469
			2J59*	Q-71	---
			3BH7*	Q-71	R-118
Rab	10	4	4JVS	Q-70	R-447
			4FME	Q-293	R-208
			4HLQ*	---	Q-144, R-105
			1M2O	H-77	R-722
Rho	17	4	3RYT*	Q-61	
			1HE1	Q-61	R-146
			5CJP*	Q-62	---
			1AM4*	Y-64	R-85
Ran	12	2	1K5D	Q-69, Y-39	---
			5DIF	Q-69, Y-39	---
Rag	1	1	6CES	Q- 66	---

Refer text for further explanation on PDB IDs marked with a ''*

4.7.3 Mechanism of action of GAPs

For the hydrolysis of GTP, two basic requirements are important (Cherfils, 2014) stabilization of phosphate negative charge that develops at the time of GTP hydrolysis especially required at the transition state.

a) stabilization of phosphate negative charge that develops at the time of GTP hydrolysis especially required at the transition state.
b) Activation of water molecule for nucleophilic attack.

The two residues that serve as catalytic residues in most GTP hydrolysis reactions are glutamine (Q), serves as the residue orienting the catalytic water molecule for nucleophilic attack, and arginine (R), functions for stabilization of charge. Some of the exceptions include the presence of tyrosine or asparagine instead of arginine, and glutamic acid or histidine instead of glutamine (Figure 4.9 and Table 4.2).

The two catalytic residues require to be optimally positioned for catalysis to occur. In majority of the small Ras-like GTPase families, both catalytic residues may not be present in the enzyme, but one of the catalytic residues is normally contributed by the GAP (Mishra & Lambright, 2016; Bos *et al*, 2007). Hence, the rate of hydrolysis in the absence of the GAP is negligibly slow (Mishra & Lambright, 2016). Another mechanism of action of GAPs is through the optimal positioning of the active site residues which may be present on the GTPase itself. MglA, Ran (Seewald *et al.*, 2002) and also the heterotrimeric GTPases (Sprang, 1997) fall under this class, where the GAP helps in orienting the catalytic residues.

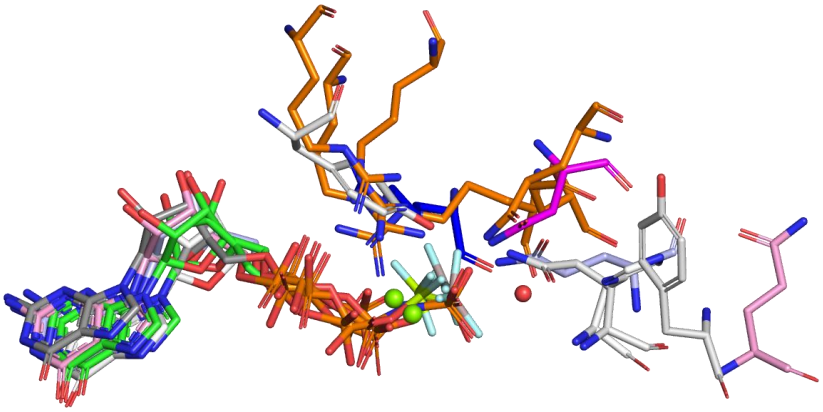

Figure 4.9 Catalytic residues in GTPase-GAP complex
GTPase-GAP complexes from Rab GAP structures of three different folds are shown. 1K5D (Q and Y in pale green from GTPase), 4M8N (Q in light blue from GTPase, R in dark blue from GAP), 4HLQ (Q and R in dark red from GAP), 3BRW (Y from GTPase in pink and N290 from GAP in magenta), 1M2O (H in light orange from GTPase and R from GAP in dark orange), 1AM4 (Y in wheat colour from GTPase and R from GAP), and 4JVS (Q from GTPase and R from GAP) where catalytic groups are oriented similarly with respect to the nucleotide when the GTPases are superposed, despite the variation in folds and irrespective of whether the residue belongs to the GTPase or the GAP. Mg^{2+} and the catalytic water are shown as green and red spheres, respectively. Water molecule and Mg^{2+} is in red and green, respectively.

Catalytic residues involved in increasing the activity of hydrolysis in the different classes and folds of GAPs are included in Table 4.2. This table provides details of the fold in each subfamily of Ras and whether the contribution of catalytic residues are from the GTPase or the GAP. Instead of the commonly observed glutamine or arginine, other amino acids might function as an active site residue, as observed from the table, where tyrosine, glutamate or a histidine can replace a glutamine. Similarly, an asparagine or a tyrosine can be present instead of arginine as a catalytic residue. An

interesting feature to note is that the chemical groups of the amino acid side chains that contribute to catalysis is always oriented at the optimal geometry, irrespective of the amino acid, or the fold of the protein (Figure 4.9).

Though 2J59 is included in the GAP family among Arf-GAPs structure in the current analysis, there is no active site residue contributed by the GAP. Hence in this case, it functions more like an effector, but is known to act as a GAP to Cdc42 of the Rho family of GTPases. The PH domain fold observed in 2J59 is also part of other GTPase binding proteins such as RanBP1s (represented by 5DIF and 1K5G). RanBP1 functions along with other proteins to increase the GAP activity, but does not provide an active site residue. Consistently, they are bound far off from the nucleotide.

In 4HLQ, both the catalytic residues appear to be provided in *trans* by the GAP, which possesses a glutamine and arginine as catalytic residues. Catalytic residues involved in increasing the activity of hydrolysis in the different classes and folds of GAPs are included in Table 4.2. This table provide details of the fold in each subfamily of Ras and the residues for that particular PDB ID involved in GTP hydrolysis mechanism.

In some of the cases, mutant enzymes have been used to capture the substrate bound conformation within the crystal (e.g. the representative structures marked by a star in Table 4.2). The PDBs 2J59, 3BH7, 3RYT and 5CJP have the catalytic glutamine mutated in the GTPase structures. Arf21, GAP present in 2J59 perform GAP activity for Rho GTPases. In 1AM4, the catalytic Q^{61} is not properly oriented in the crystal structure. So, instead of Q^{61}, Y^{64} plays the catalytic role. In 1K5D, Ran GAP mediates GTP-hydrolysis by a conformational change of the GTPase, as both the catalytic residues are present in GTPase. Instead of an arginine, a tyrosine functions as the catalytic residue. Though Rab1 in 4HLQ possesses a glutamine that could be possibly act as a catalytic residue, but upon interaction with the GAP, a trans glutamine from the GAP functions as the catalytic residue. In the case of Arf-Arf GAP complex with PDB ID 3O47, Arf GAP does not provide the catalytic residue, instead this is provided by the coatomer proteins present in the tripartite complex (Goldberg, 1999).

An interesting feature is that despite being from a variety of folds, the relevant chemical groups of the active site residue and their orientation converge to a similar manner in all the GTPase and GAP families.

4.7.4 Interaction interfaces of GAPs with GTPases

Based on the face of approaches described in the previous section, GAPs interact with GTPase predominantly at the base and face 2 (19 structures) or only face 2 (13 structures) as given in Figure 4.10. There are a few examples where interaction is not through the face 2 i.e. face 1 only, face 3 and face 4 or base and face1. There are also structures where face 4 interacts along with base and face 1 or with face 3.

,

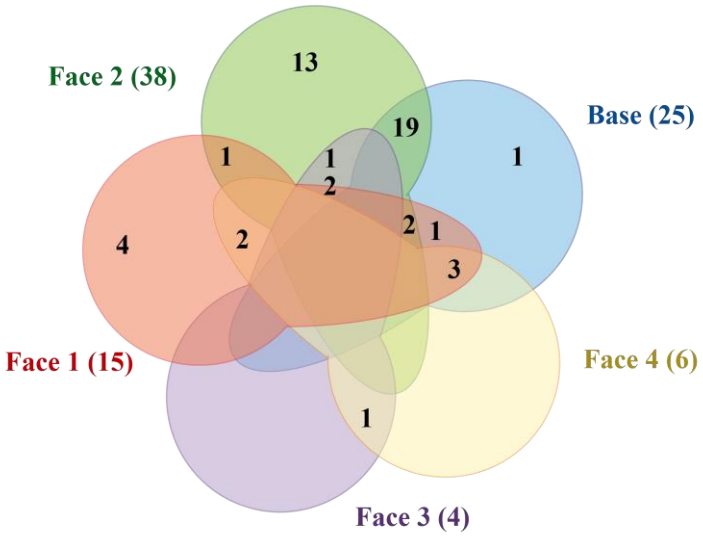

Figure 4.10 Distribution of interacting faces of GTPases with GAPs
Face 1, face 2, face 3, face 4, base is represented by red, green, magenta, yellow, and cyan, respectively. Cumulative number of structures interacting at each face is written in brackets while cases of interactions with multiple faces are given inside in the relevant overlapping regions of the five-part Venn diagram.

Face 2 is the side of GTPase where switch I and switch II is present. Conformation of Switch I and Switch II loops and the orientation of the active site residues are important for catalysis driven by GAPs. When the catalytic residue belongs to the GTPase and the other catalytic residue is contributed from the GAP, it becomes essential that there is a direct interaction between the GAP and the GTPase at the face containing the nucleotide binding pocket, i. e, face 2. Thus, the mechanism of action in all of these cases where a direct interaction is involved requires the approach of the GAP essentially through face 2 of the GTPase. In addition to the face 2, depending on the interaction interfaces, any of the other neighbouring faces are part of the interaction.

In the few cases where face 2 is not involved in the GTPase-GAP interaction, the GAP activation is through conformational changes in the GTPase which contains both the

catalytic residues (e.g. RanBP1). PDB ID 3BRW has two interacting proteins whose combined action serves to activate the GTPase. A face 3 and face 4 interaction is observed in one of the interactors while face 2 is seen in other. 3O47 is example where the interaction is at the base but in this case as discussed earlier, the GAP is linked to GTPase and not free to move and so interaction cannot be really considered as a bonafide GAP interaction (Goldberg, 1999).

4.8 Guanine Nucleotide Exchange Factor (GEF)

GEFs are the group of proteins which regulate the activity of the GTPase by bringing the GTPase to the active form after replacement of GTP in the place of GDP. A total of 142 complexes of GTPase-GEFs were identified from the whole list of complex structures of Ras-like GTPases. Out of these, 22 structures belong to Ras-SOS complexes where two Ras GTPase molecules are bound. Each Ras was considered as an independent GTPase chain when two molecules of Ras are bound, and hence these contribute for 44 of the structures.

4.8.1 Nucleotide specificity of GTPases to bound GEFs

The structures available in the PDB for the GTPase-GEF complexes include various nucleotide states of the GTPase (Figure 4.11). Majority of them are in the nucleotide free state. These also include structures with inhibitors bound to the GEF. Analysis of conformation of all the bound nucleotides show that GEFs do not distort the nucleotide conformation, instead it acts by interacting with the residues of the GTPase to either change the affinity towards nucleotide or by opening up or unfolding the nucleotide binding pocket, mainly switch I and switch II.

Because many of the structures are nucleotide free, it suggests that GEFs have a preference for interaction with the nucleotide-free state of GTPase, or that the GEF pushes out the GDP once it binds to the Ras-like GTPase. Many Ras-like GTPases have a tendency to unfold in the absence of a bound nucleotide. The lagre number of structures of small Ras-like GTPase without bound nucleotide also supports this observation. Binding of GEFs to a GTPase functions to stabilise the Ras-like GTPase in the nucleotide-free state till GTP is available for occupying the pocket.

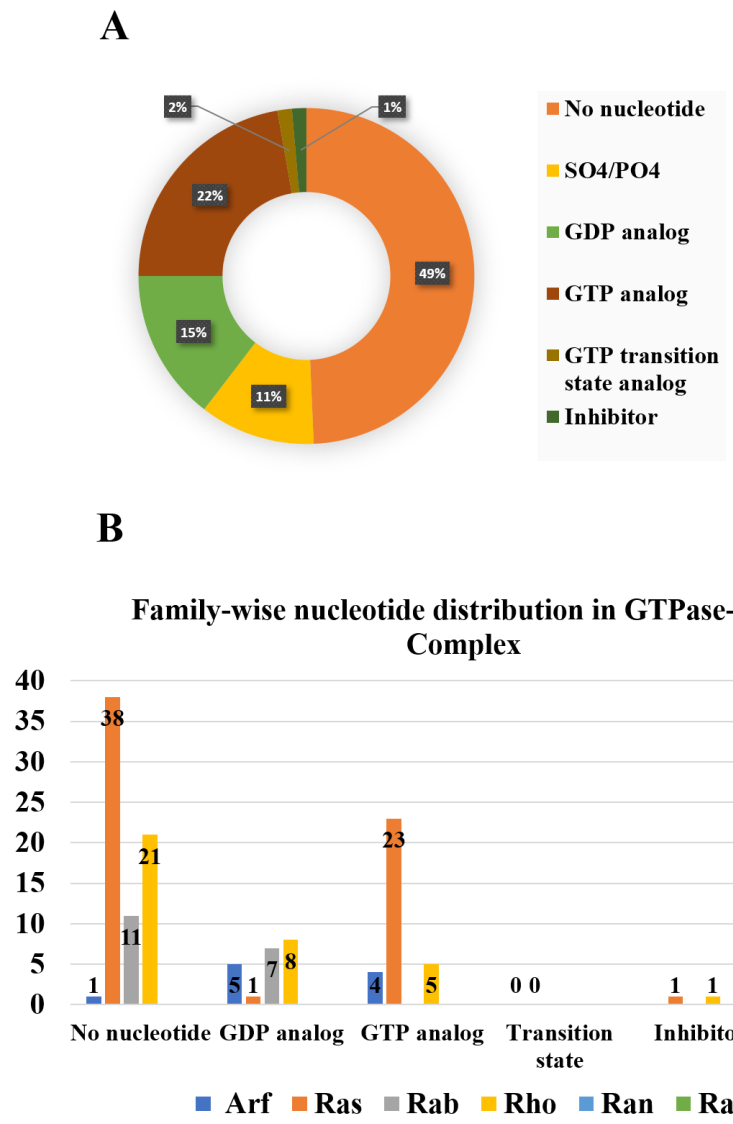

Figure 4.11 Nucleotide distribution of GTPase-GEF complex structures.
A. Percentage representation of bound nucleotide for all structures of the GTPase-GEF complexes. **B** Family- wise nucleotide distribution in GTPase-GEF complex structures.

Out of all the regulators, GTPase-GEF structures are the only complexes found with the phosphate and sulphate in the nucleotide binding pocket. Out of 69 structures of GEF, 15 of GTPase binding pockets are filled with the PO_4/SO_4. This is an interesting observation because out of all the 864 structures there are 16 structures with phosphate and sulphate in the nucleotide bound pocket without any nucleotide in it and 15 belong to GEF complexes. This could imply that a stabilised nucleotide binding pocket including the phosphate binding site exists only in the presence of GEFs (Copley and Barton, 1994).

There are 23 instances of GTP-bound complexes of Ras interacting with GEFs. However, these are examples of Ras family GTPases that bind to a GEF in the GTP bound state, and the GEF does not exert an exchange activity on these GTPases. The GTP-bound Ras exerts an allosteric effect on stimulating the GEF activity on another GTPase bound to the GEF. The examples of these complexes of GEFs bound to two GTPases are also included among the GTPase-GEF structures. In addition to the 22 Ras-SOS complexes, these also include two structures of Ral-RalGDS (PDB ID: 1LFD) and Ral-Grb14 complex (PDB ID: 4K81). In addition, there are a few structures of Rab complexes with GEF in the GTP bound state, which are probably in the conformational states of GTPase-GEF complexes captured after the exchange activity has occurred.

4.8.2 Folds of GEFs

The distribution of complexes into different Ras-like GTPase superfamilies and the corresponding GEF folds are shown in figure 4.12 and table 4.3. An analysis of the number of folds of GEFs corresponding to each Ras-like GTPase superfamily showed that the GEF folds are different in different Ras-like GTPases families (Figure 4.12). Also, within a Ras-like GTPase superfamily, there are multiple folds for the GEFs. According to structures determined till date, total number of folds determined were 18 in number, while the number of folds in Rho is the maximum (6 different folds out of 41 structures), the number of folds in Arf and Rab are also high (4 and 5, respectively). Folds identified in Arf GEFs are Sec7 domain, PH domain, DCB domain and an example where a GTPase (Arl13b) itself acts as a GEF. These GEF domains are represented by the PDB IDs 4C0A, 4KAX, 5J5C and 5DI3, respectively (Figure 4.12). 4C0A (representative PDB ID mentioned in table 4.3) and 6FAE are structures with both Sec7 and PH domains present in the GEFs (BRAG1 and BRAG2), where only the Sec7 domain interacts with the Arf GTPase to perform GEF activity. There are 4 more complexes in the same category with only Sec7 domain present in the complex and function as a GEF. These are Arf1-Sec7 domain, in presence and absence of inhibitor Brefeldin A (1RE0, 1R8Q, 1R8S and 1S9D). Another example of a GEF-GTPase complex is Arf6-Grp1 (PDB ID 4KAX), where unlike in 4C0A, the PH domain functions in nucleotide exchange. The orientation of the PH domain with respect to the GTPase are different in both the cases (4KAX vs 4C0A). Another representative fold

is the DCB domain which functions as an Arl-GEF (PDB ID 5J5C and 5EE5 respectively). 5J5C contains BIG1 protein with DCB domain (ARM repeat) as the GEF.

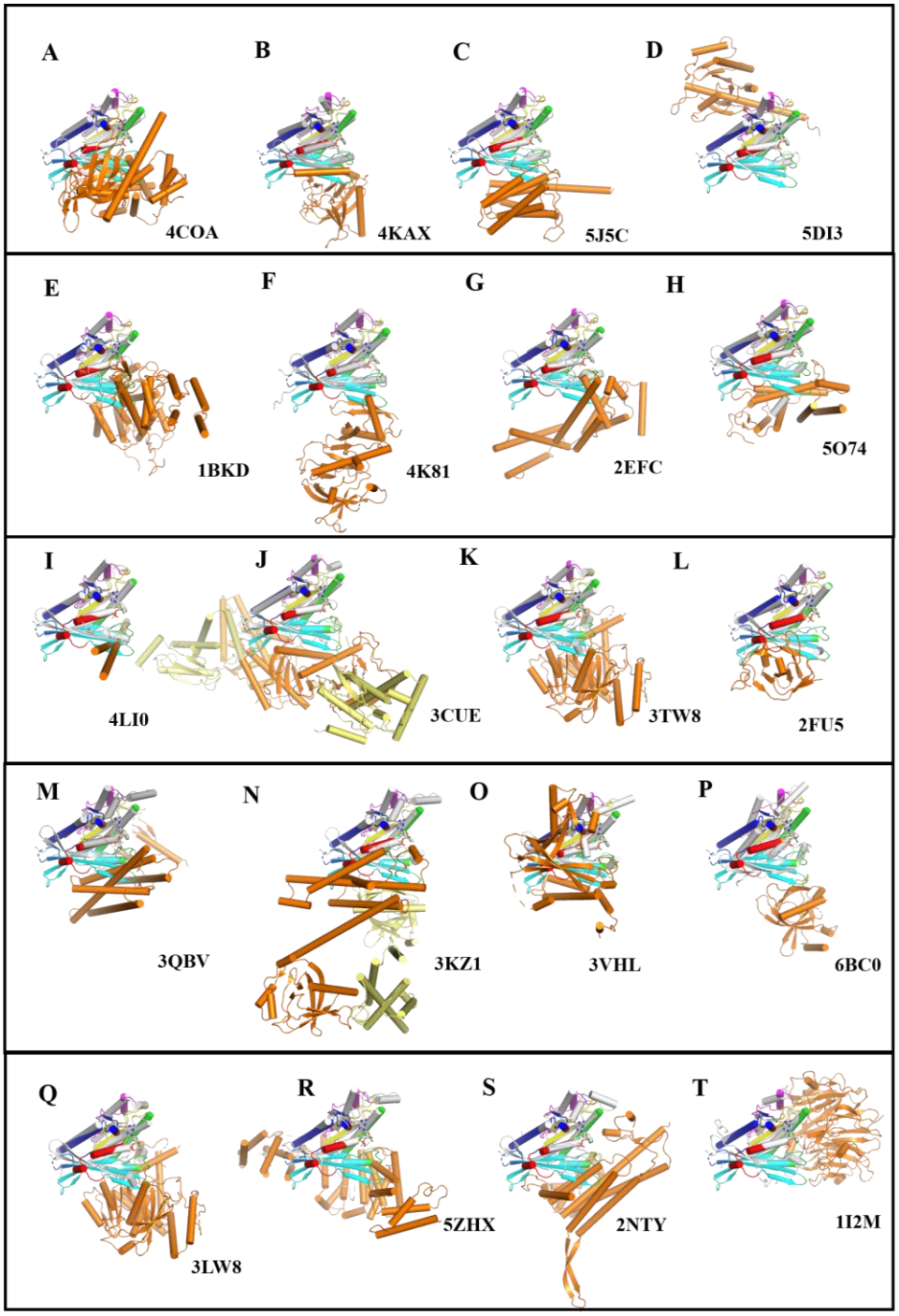

Figure 4.12 Different GEF folds available in the PDB.
The GTPase is shown in grey, while the superposed MglA is shown according to the face colour described in section 4.6. GEFs are represented in shades of orange.

In 5DI3, Arl13b, a GTPase acts as a GEF for Arl3. The C-terminal extension of Arl13b, which is not ordered in the crystal structure is expected to extend till the nucleotide binding pocket to displace the nucleotide (Gotthardt *et al.*, 2015).

The Ras subfamily has the maximum number of GEFs captured that belong to two unique folds, with 1BKD and 4K81 as the representative PDB IDs in Figure 4.12 and Table 4.3. 4K81 is the structure of Ras in complex with RalGDS, GDS is a guanosine nucleotide dissociation stimulator, a name used earlier for GEF (Huang *et al.*, 1998) . This GEF consists of two domains - a Ras Binding domain (RBD, also called RA domain) and a PH-domain. It interacts with the GTPase through the RA domain just like another GDS in the same group (PDB ID 1LFD). These structures are in the GTP-bound state as mentioned earlier. The second group consists of all other GEF complex structures with representative PDB ID 1BKD. In this category, there are two different proteins with similar fold i.e. Ras-SOS complex and Ral-Rlf complex. Rlf-GEF functions as a GEF for Ral only (5CM8). Maximum structures of GTPase-GEF complexes are the Ras-SOS-Ras complexes (27). Because there are two Ras molecules bound to SOS in each Ras-SOS complex, the GTP-bound state of Ras is involved in activating the SOS exchange activity (by feedback mechanism explained later in this chapter). So, it is important to look for the interaction of both the Ras molecules to understand the GEF activity of Ras, and they were counted separately in the analysis. There are 9 structures with a single Ras GTPase in Ras-SOS complex. In this category, there are two structures of Rap and Rap-GEF (PDB ID 3CF6, 4MGZ) and two structures of RasGrp complexes (6AXF and 6AXG).

There were 5 different folds of GEFs bound to Rab GTPases. 6 structures of GEFs of the Vps9 fold (2EFC as the representative PDB in figure 4.12 and table 4.2) are available, with the GTPase bound to different nucleotides. Another fold is the DrrA proteins represented by the PDB ID 5O74. The structures captured as complexes in this fold include GTPases in the GDP-bound form, in the presence of SO_4 ion in the nucleotide binding pocket, and another without any nucleotide. 4LI0 (Rab-Rabin8 complex) is a representative structure of a coiled-coil consisting of two alpha helices bound to the GTPase. Other members of this fold include Sec2 (2OCY, 4ZDW) and Rabin 8 (4LHX). 6DJL also contains a GEF with a coiled coil structure. Though the interaction is at the base in all the cases, the orientation of helices is perpendicular to

each other in 6DJL and 4LI0.

3CUE, a representative for the Roadblock/LC domain fold is found in TRAPP complex, and in Mon1-CcZ1 bound to Rab7 (5LDD). These occur as dimers of the Rbl/LC domain. Another example of a Rbl/LC domain includes DENND domain. Two examples from DENND domain fall under this group i.e. 3TW8 (DENND1A) and 6EKK (DENND1B). Another unique fold among Rab-GEFs is present in MSS4 (2FU5; MSS4 in complex with Rab).

Cdc42-intersectin complex (PDB ID 3QBV, representative fold with PH-DH domain) is a Rho GTPase-GEF complex, where DH-domain is involved in GEF activity (Kapp *et al.*, 2012). Including 3QBV there are 23 structures with PH-DH domain. In all the cases, DH domain acts as a GEF. But in this fold there is one complex of Rho and GAP where a dimer of Rho and GEF is present, 3KZ1. In this example, Rho interacts with GEF in GTP-bound state. The GEF dimer is oriented in such a way that both PH and DH domains with one GTPase each (dimer of GEF is in present in the structure but only one of the molecules is relevant for GEF activity). PH domain interaction acts like an effector while DH domain functions as a GEF. There are bacterial GEFs which also belong to the PH-domain like fold and bound to Rho GTPases i.e. Tiam (1FOE), and SopeE toxin (1GZS); but the orientation of interacting domains is slightly different. 6BC0 is another representative fold where only PH-domain was found to be interacting with GTPase. It is categorised into a different fold because in this case PH-domain is interacting (GEF present in this complex is p190 Rho GEF, with only PH domain included in crystallization). 3LVR represents a different fold with DOCK protein as a GEF with 6 structures (including 3LVR). 3LW8 is a representative fold with a total of four structures, two of which are IpgB2 protein (3LWN, 3LXR). 3GCG is a Cdc42 Map protein complex, where Map is an *E. coli* protein mimicking the DH -domain of Rho GEF. 5ZHX constitutes another fold of Rho GEFs. 2NTY (representative PDB ID) and 2WBL are complexes of the plant Rho-GEF PRONE with Rop (GTPase). The only GEF complex determined for Ran GTPase is with RCC1, a 7 bladed beta propeller fold (1IM2). A loop extended from the structure was found to have a role in exchange activity (Renault *et al.*, 2001).

Table 4.3 Folds of GEF and mechanism of action

Ras families	GEF Complexes	Fold	PDB IDs and mechanism
Arf	10	4	**4C0A**- Occlusion in nucleotide binding site & conformational change in switch I & switch II
			4KAX- Occlusion in nucleotide binding site & conformational change in switch I & switch II
			5J5C- Occlusion in nucleotide binding site & conformational change in switch I & switch II
			5DI3- Helix interaction (disordered) & conformational change in switch I & switch II
Ras	69	2	**4K81**- Conformational change, interacting at switch I and β_2 of GTPase
			1BKD- Conformational change in switch I & switch II (allostery in GEF domain)
Rab	21	5	**2EFC**- Occlusion in nucleotide binding site & Conformational change in switch I & switch II
			4LI0- Conformational change in switch I & switch II
			2FU5- Conformational change in switch I (Pulling switch I)
			3CUE- Occlusion in nucleotide binding site & Conformational change in switch I & switch II
			5O74- By pulling Switch I & also causing conformational change in switch I
Rho	41	6	**3VHL**- Conformational change in switch I
			3KZI- Conformational change in switch I & switch II
			3LW8- Conformational change in switch I
			5ZHX- Conformational change in switch I & switch II, also there is C-terminal prenylated GTPase which is important for causing difference in nucleotide affinity
			6BC0- Conformational change in switch I and switch II
			2NTY- Conformational change in switch I, switch II & interswitch
Ran	1	1	**1I2M**- Conformational change in switch I & switch II

4.8.3 Mechanism of action of GEFs

Table 4.3 summarises the various mechanisms of action of the representative GEF folds in the subfamilies of Ras-like GTPases. Two major categories of action that could lead to a decrease in affinity towards GDP, and thus facilitate exchange of the nucleotide were observed. A structural basis for the release of GDP could be attributed to (i) a change in conformation of Switch I and Switch II, and (ii) occluding the space so that GDP cannot occupy the binding pocket. Specific examples of folds that function in each of these cases are mentioned in Table 4.3. The GEF stabilises the GTPase in the nucleotide-free conformation till GTP fills the pocket. In most cases, binding of GTP results in a loss of affinity of the GEF for the GTPase (Vetter, 2014).

Comparing the structural complexes of GTP-bound, GDP-bound and nucleotide-free states of GTPase-GEF complexes helps us in understanding of the mechanism of action

of nucleotide exchange. A few of the examples where GTPase-GEF complexes have been determined in at least two different conformations of the same complex are Ras-SOS (1BKD, 1NVV), Cdc42-DOCK9 (2WMN, 2WMO, 2WM9), Cdc42-intersectin (1KI1, 3QBV), RhoA-Arf GEF (5JHH, 5JHG), and Rop-PRONE (PDB IDs-2NTY, 2WBL) complexes. A few of these are discussed in detail below.

The Rop-PRONE complexes 2NTY and 2WBL form GDP-bound and nucleotide free structures, respectively (as shown in Figure 4.13). The crystal structure is a complex formed by two molecules each of Rop and PRONE. One PRONE binds to the Switch I, Switch II, P-loop and α3 while the other PRONE interacts at the α1 and α4 with the β-arm, but the interaction through β-arm is not significant for GEF action. Instead the GEF action is mediated by the PRONE which interacts through Switch I and Switch II, which undergoes structural changes (Thomas *et al.*, 2009).

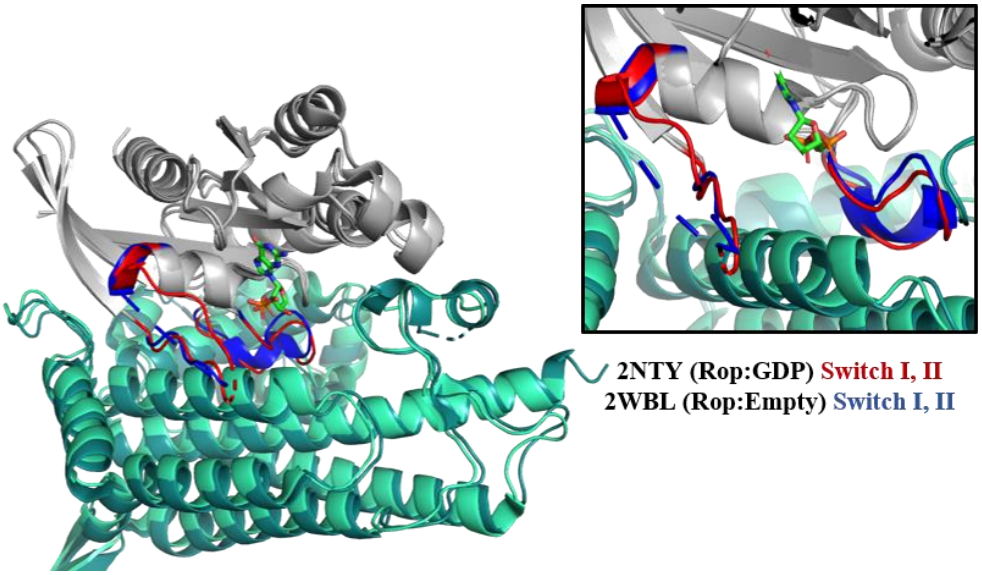

Figure 4.13 Mechanism of nucleotide exchange in Rop-PRONE complex
Rop is shown in grey and PRONE in shades of green, switch I and switch II in red and blue for GDP and nucleotide free state, respectively

After superposition of the 3QBV and 1KI1, the GDP and nucleotide-free states of Cdc42-intersectin complex, the catalytic pocket shows a clear conformational change of switch I (Figure 4.14). This is an example where the GEF facilitates nucleotide release and exchange by reorienting switch I.

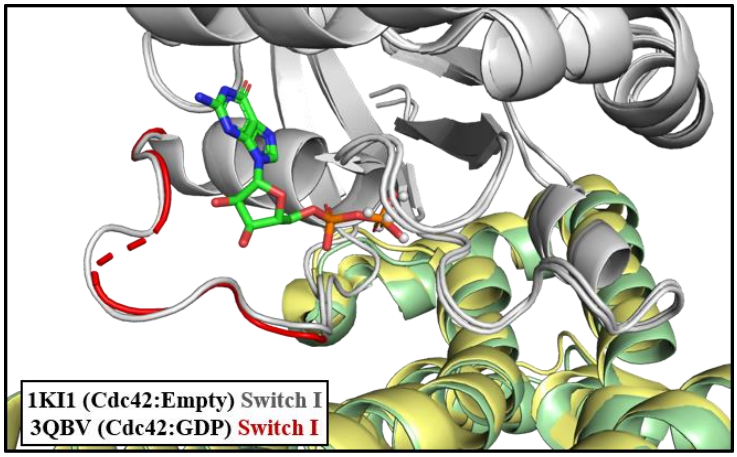

Figure 4.14. Mechanism of nucleotide exchange in Cdc42-Intersectin complex
Cdc42 is shown in grey while GEF is shown in pale yellow and pale green, switch I of GDP bound state of GTPase shown in red

DOCK is a very nice example which works by both the mechanisms (occlusion and conformational change of switch regions) (Figure 4.15). It has a GEF activity through DHR-2 domain by decreasing the affinity towards nucleotide which is a result of conformational change in Switch I region. The interaction and conformational change is majorly driven through Switch I but also contributed by Switch II, interswitch region and loop β6α5.

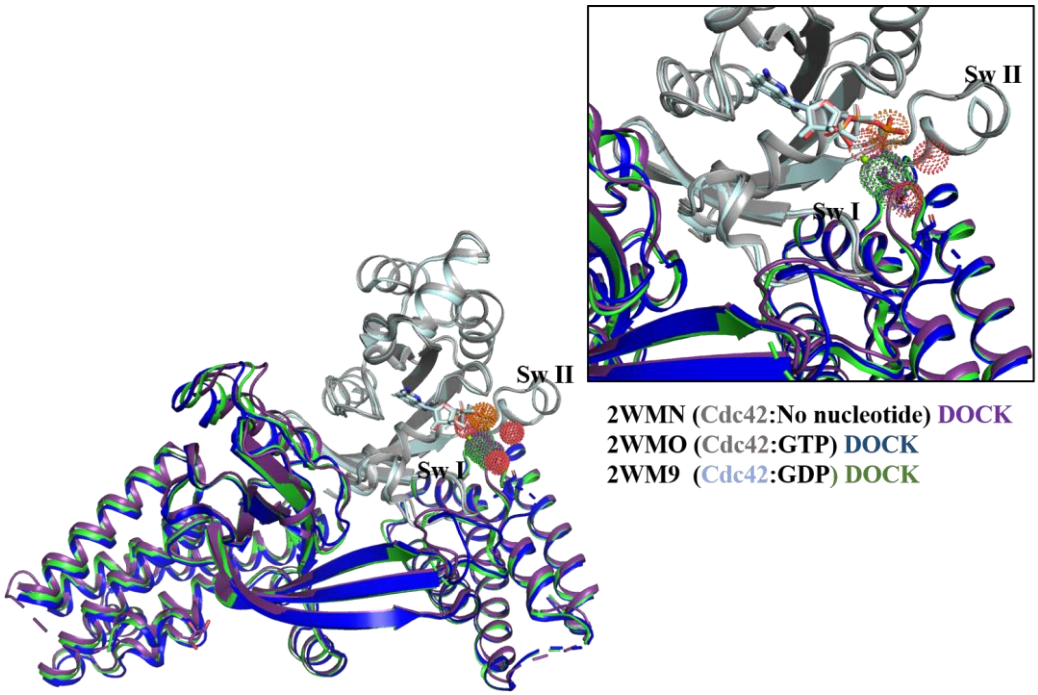

Figure 4.15 Mechanism of nucleotide exchange in Cdc42-DOCK complex
Interactions by valine are zoomed in the inset. Dots around the interacting molecules are shown to highlight the occlusion of the pocket. Switch I and Switch II are shown by Sw I and Sw II in figure. Colour code for GTPase and GEF are written below the inset, GTPase and GEF are denoted by the same colour as shown in figure.

Conformational changes in Switch II and valine residue of α10 helix from DOCK cause the occlusion of Mg^{2+} binding site, this further decreases the binding of the nucleotide. When GTP binds, conformational change involving α10 helix of DOCK removes the valine from the catalytic site of G-protein. This causes rearrangement of both the proteins i.e. GTPase (Cdc42) and GEF (DOCK) and leads to decrease in interaction between the two proteins and increase in affinity towards the GTP by enlarging the binding pocket of nucleotide (Yang *et al.*, 2009).

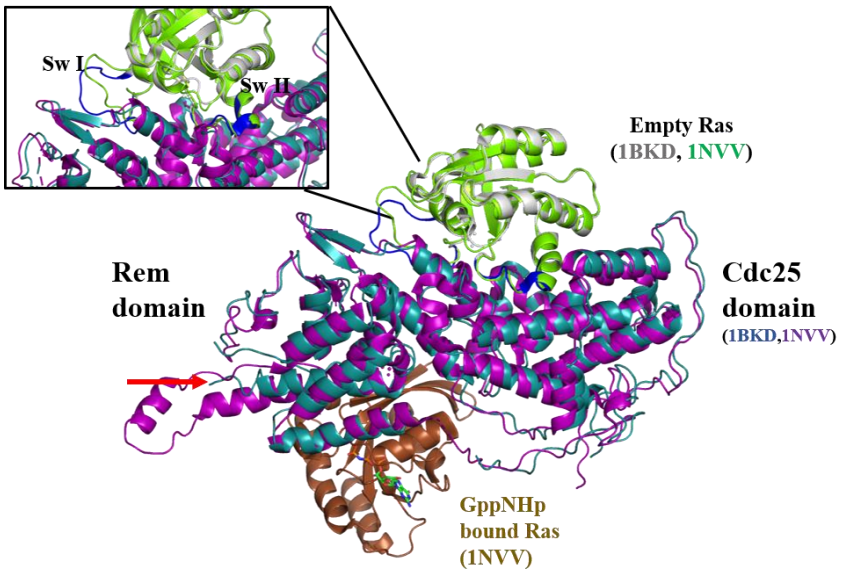

Figure 4.16 Mechanism of GEF action by SOS protein in Ras.SOS^{cat}.Ras complex

PDB ID 1BKD and 1NVV are overlapped to show conformational change in SOS and allosteric interaction after binding to Ras.GTP bound state. Colour of proteins are represented by the text in figure. Empty Ras by grey and green PDB ID 1NVV and 1BKD, respectively. GTP-bound Ras in brown, SOS by magenta and blue Ras.GTP bound and free, respectively. Red arrow represent conformational change in SOS.

In Ras (nucleotide free).SOS^{cat}.Ras(nucleotide bound) structures, nucleotide bound Ras acts as an allosteric molecule to cause the conformational change in the SOS to further catalyse the exchange of nucleotide in the other Ras. The REM of SOS^{cat} is the allosteric site on SOS that interacts with the Ras while Cdc25 domain is involved in the nucleotide exchange. The interaction of the Ras-nucleotide bound state to the REM domain allows conformational change in the Cdc25 domain of the SOS^{cat} which is responsible for exchange (Boriack-Sjodin *et al.*, 1998; Margarit *et al.*, 2003). The conformational change in Cdc25 is communicated through the loop which connects REM and Cdc25 domains of SOS (Figure 4.16).

4.8.4 Interaction interfaces of GEFs with GTPases

We proceeded to check the interaction interface between the various GEFs and small Ras-like GTPases and classify them according to the face of approach. The Venn diagram in Figure 4.17 summarises the distribution of the GEFs according to the interacting faces of the Ras-like GTPases. Majority of the GEF complexes with Ras-like GTPases (51) interact at the base and face 2 while the other major category are GEFs that interact at base, face1 and face 2 (45). Face 2 interactions involve switch I and II in all cases except for the structures of the Arf1 complexed with DCB domain of BIG-I (5EE5, 5J5C) and Rab8-MSS4 complex (PDB ID 2FU5). Since the DCB domain does not contribute towards GEF activity, the lack of interactions with both the switches may be due to the absence of the whole protein. In 2FU5, α1, Switch I and II are disordered in the crystal structure, resulting in an apparent absence of interactions with face 2. Here, MSS4 acts as a GEF by the mechanism of unfolding switch I, resulting in release of the nucleotide.

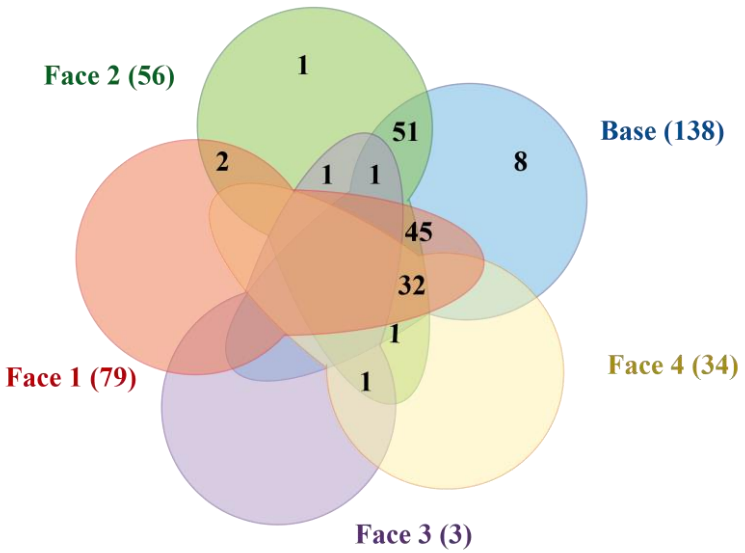

Figure 4.17 Distribution of interacting faces of GTPases with GEFs
Face 1, face 2, face 3, face 4, base is represented by red, green, magenta, yellow, and cyan, respectively. Cumulative number of structures interacting at each face is written in brackets while cases of interactions with multiple faces are given inside in the relevant overlapping regions of the five-part Venn diagram.

In addition to base and face 2, face 1 also forms part of the interacting interface in majority of the GEFs. The additional interactions in face 1 are contributed by the α1 helix (Figure 4.17). The major folds of GEF that interact through α1 helix in addition

to base and face 2 are Ras-GEFs (SopE-like fold), DOCK family of Rho GEFs, Vps9 domain of Ara7 (Rab family) and Grp1 (PH domain) of Arf6.

Face 4 also forms part of the interface in a few of the complexes in addition to base, face 2, and face 1. Face 4 interactions involve mainly the N-terminal region of α5 helix and interswitch region. The complexes in this category, 9 of the structures include nucleotide-bound GTPases of the H-Ras-SOS^{cat} complexes. In these, there are two H-Ras molecules bound to one SOS (Son of Sevenless) molecule, where one of the H-Ras is nucleotide-bound while the other is nucleotide-free (Figure 4.16). Exchange activity occurs in the nucleotide-free H-Ras molecule, while the nucleotide-bound Ras is involved in allosterically activating the exchange from the other Ras molecule (Margarit *et al.*, 2003). REM and Cdc25 domains of SOS interact with the nucleotide-bound Ras and nucleotide-free Ras respectively. Interestingly, only the interface between SOS (REM domain) and the nucleotide-bound H-Ras includes face 4 in the interaction.

The GEF folds i.e. REM domain of Ras, DOCK and PRONE folds of Rho families, mainly formed the class of proteins that interact with face 4 also in addition to base, face 2 and face 1. In the case of DOCK9 complex with the Cdc42, the loop interacts with Switch region (Figure 4.14). The loop is ordered in the nucleotide-free and GDP bound states, while in case of GTP bound state it is disordered. The loop prevents binding of the Mg^{2+} ion by occupying its position. The conformational changes between the nucleotide-bound and nucleotide-free complexes with GEF contribute towards the additional interactions at face 4.

There are two more exceptions where the interfaces are formed by face 2 and face 3; and face 2, face 3 and face 4. Currently, these are the only structures where face 3 is part of the interface, namely Ran-RCC1 complex (PDB ID 1I2M) and Arl3-A13B complex (PDB ID 5DI3). In Ran-RCC1 structure, RCC1 (7-bladed beta propeller fold) works as a GEF by increasing the dissociation rate with GDP (Renault *et al.*, 2001). A β-wedge interacts with the P-loop, Switch II and α3. Unlike other GEFs, this is an example where Switch I and other nearby residues are not involved. The interaction at the α3 and α4 causes conformational change in the guanine base recognition site (NKxD motif) in the GTPase, which leads to decrease in affinity towards GDP. 5DI3 is an interesting example of Arl3 -Arl13B complex, where both are G-proteins and Arl13B acts as a GEF for Arl3. The C-terminal helix (a part of the coiled coil domain) and

Switch regions of Arl13B are involved in the interaction interface in the crystal structure. Further experiments proved that the disordered region of Arl13B is responsible for the GEF activity (Renault *et al.*, 2001).

The mechanism of action of GEFs appear to be driven mainly through interactions with Switch I and Switch II. Hence, similar to the GAP interactions with GTPases, the major interaction interface is the face 2 of the GTPase. In addition to the direct interactions involving face 2 and base, possibilities of allosteric action through face 4 exist in the GTPase-GEF interactions. Another example of an indirect interaction through allosteric mechanism is the Rag family of GTPases, where the C-terminal domain can potentially be involved in allosteric action (Cherfils, 2017; Su *et al.*, 2017)

4.9 Guanine Nucleotide Dissociation Inhibitor (GDI)

GDI are the proteins which inhibit the exchange of nucleotide of GTPase from GDP to GTP, hence called Guanine nucleotide dissociation inhibitor. In other words, it regulates the GTPases by inhibiting the activity of GEFs.

4.9.1 Nucleotide specificity of GDIs

GDIs bind to the GTPases in GDP bound state as shown by our structural analysis, too. There are 19 GDI-GTPase complex structures found and 17 are GDP bound while 2 are GTP analog states (5MLA, 4F38). This is expected since the role of the GDIs is to inhibit the nucleotide exchange from GDP to GTP. Most of the GDI structures are from Rho and Rab family of proteins as shown in figure 4.18.

4.9.2 Folds of GDI

GTPase-GDI complexes contain GDIs of 7 different unique folds - 4 from Rho, 1 in Rab and 1 each in Ras and Arf. The GDI bound to Arf belongs to the Rho-GDI like family (IKSH), while the GDIs bound to Ras have an ankyrin repeat fold (5MLA). There are two structures present for Ras-GDI (5MLA and 5MLB) shown in figure 4.19. These proteins (DARpins) were designed as inhibitors through phage display for selective binding to Ras GTPases (Guillard *et al.*, 2017). One of them possesses high affinity to GDP-bound state, while the other binds specifically to the GTP-bound state. The 9 structures of GDIs bound to Rho belong to 4 different folds. These include complexes of Rho-GDI with Cdc42, RhoA and Rac. The four representative PDBs for

the folds are 1DOA, 4DID, 4ITR and 2H7V. The Rab representative structure, 1UKV, belongs to the NAD/FAD binding domain (Figure 4.19 and table 4.4).

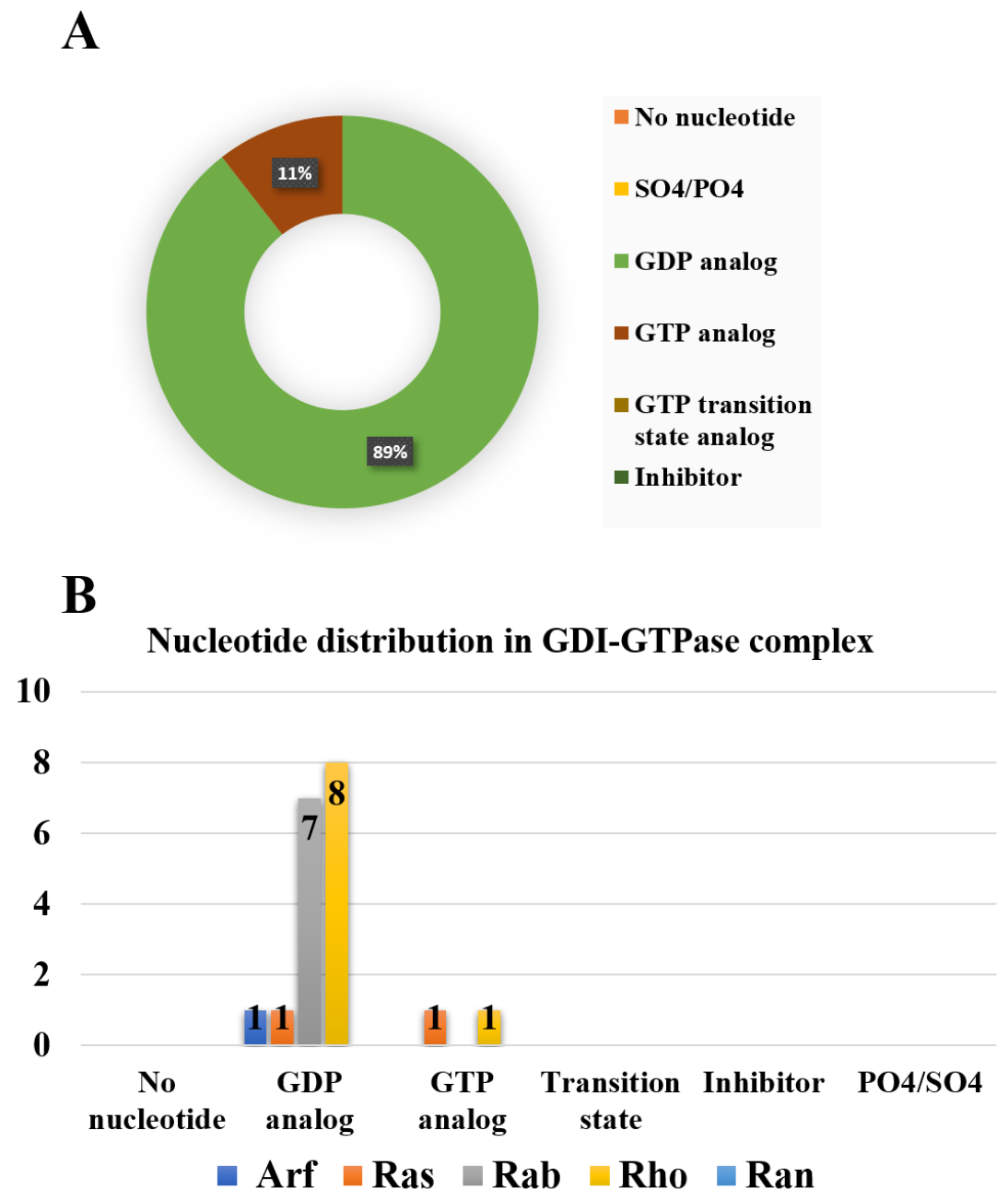

Figure 4.18 Nucleotide distribution of GTPase-GDI complex structures
A. Percentage representation of bound nucleotide for all structures of the GTPase-GDI complexes. **B** Family- wise nucleotide distribution in GTPase-GDI complex structures.

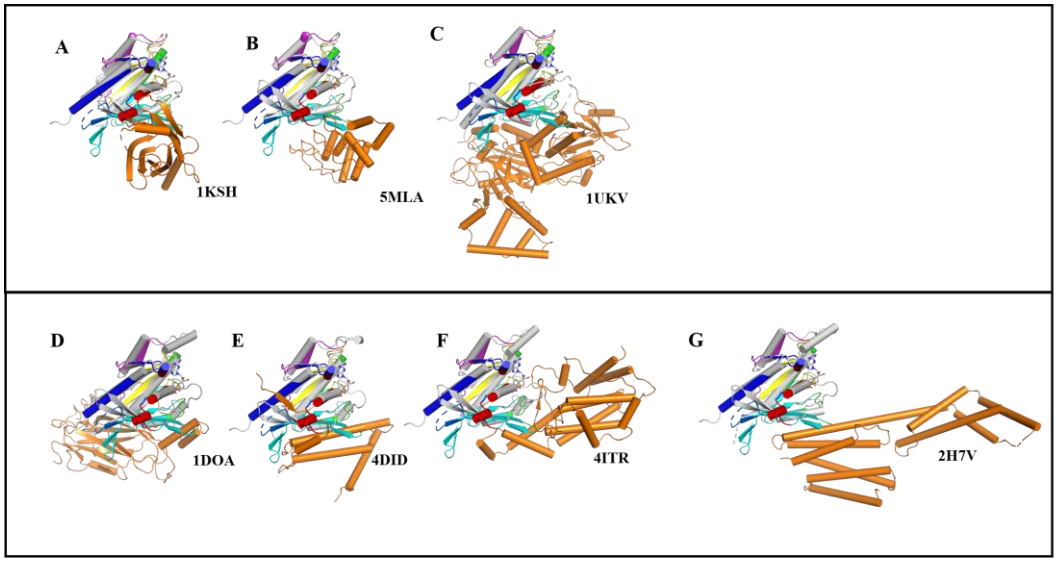

Figure 4.19 Different GDI fold available in the GDI-GTPase complex.
The GTPase is shown in grey, while the superposed MglA is shown according to the face colour described in section 4.9.2. GDIs are represented in shades of orange.

Table 4.4 Folds of GDIs and their mechanism of action

Ras families	GDI Complexes	Fold	PDB ID and Mechanism
Rab	7	1	**1UKV**- By ordering switch I and switch II, Mainly by switch II
Rho	9	4	**1DOA**- By ordering switch I
			4DID- By ordering switch II
			4ITR- BY ordering switch I and switch II, Mainly by switch II
			2H7V- By holding the switch I and switch II
Ras	2	1	**5MLA**- By holding the switch I and switch II, mainly Switch I
Arf	1	1	**1KSH**- Interacts with switch I, switch II and interswitch region

4.9.3 Mechanism of action of GDIs

Based on the interaction between GTPase and GDIs, the GDIs appear to function either 1) by stabilising the nucleotide bound conformation by interaction through Switch I and Switch II. 2) by stabilising the conformation of GTPase in the GDP-bound state by making a β-sheet interaction between the GDI and the GTPase.

Seventeen structures of GTPase-GDI complexes are available in PDB. No structures are available for Ras and Ran families while 9 structures are available for Rho GTPases. Among these structures, maximum number of folds which are available for the GDIs are 4 as shown in Figure 4.19 Some of the GDIs bound to different families of GTPases also share a common fold.

An interesting observation is that PDE delta (PDB- 1KSH), the GDI of Arf, belongs to the same fold as the Rho GDIs (i.e. PDB 5FR1) but the direction of approach of both the GDIs are different. PDE-delta interacts with the GTPase at the base and face 1. SopB the GDI of Cdc42 with PDB ID, 4DID has a β-strand which extends the central β-sheet of the GTPase by interacting with β2 of the GTPase just like PDE delta and Rho GDI. It approaches the GTPase through face 1 and continues the β-sheet with the GTPase, thus locking Arf in a GDP conformation. Since a registry shift of β2 occurs during a GTP to GDP conformational transition in the Arf family of GTPases (Burkinshaw *et al.*, 2012), an interaction leading to continuation of the β-sheet can potentially stabilise the GDP conformation. In the case of the Rho-GDIs, it interacts at the base and face 2 of the GTPase and keep the conformation of the GTPase in the GDP-bound form (Figure 4.19).

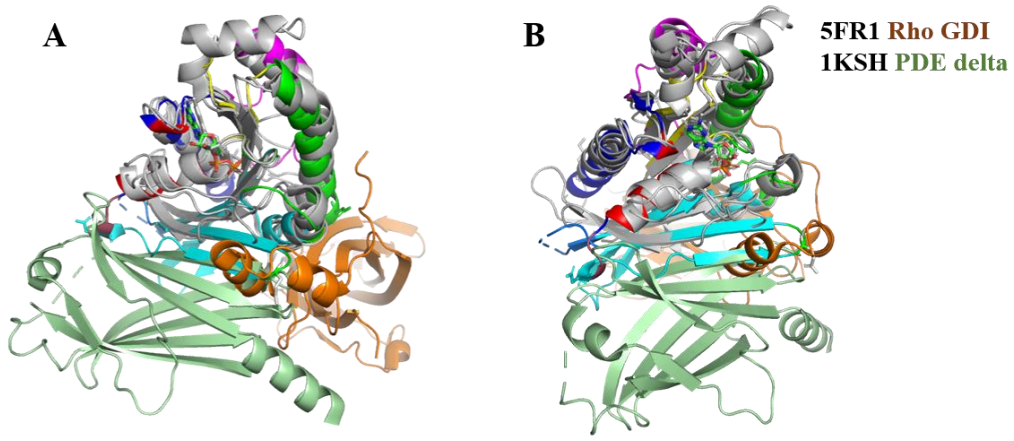

Figure 4.20 Mechanism of action for GDIs
A. 1KSH (PDE delta) and 5FR1 (Rho GDI) have the same fold but interacting faces are different **B.** PDE Delta interact with the β2 strand of GTPase to form a continuous β -sheet.

4.9.4 Interaction interfaces of GDIs with GTPases

Out of 19 structures, most of the GDIs interact with the GTPases through the base and face 2 (Figure 4.21). However, there are exceptions with respect to the face of approach. In Arl2-PDE delta (PDB ID 1KSH), GDI, the PDE delta is approaching from the side of face 1 by forming a continuous β-sheet with that of the small Ras –like GTPase. and hence, interaction is through the base and face 1. Another exception is the SopB (PDB ID- 4DID) which interacts with Cdc42 at the base, face 1, face 2 and face 4. In this case, a short β-strand forms hydrogen bonds to the interswitch region, thereby extending the sheet for a small stretch. In 2H7V, Rac1 and YpkA form a dimer, and there are two interaction interfaces between the GTPase and the GDI. Only one of these interactions, the one involving base and face 2, contribute towards GDI activity (Prehna *et al*, 2006). In 1DS6 and 1HH4, the crystal structures show interactions between Rac and Rho GDIs. the GDI is approaching from the opposite site of the nucleotide binding site but a helix moves towards the face through base. The difference in the two structures is that 1HH4 is the geranylated complex where a clear conformational change in switch I and switch II is visible. The interaction of Tyr35 (Rac) and Asp45 (GDI) is involved in inhibition of exchange of nucleotide (Grizot *et al.*, 2001).

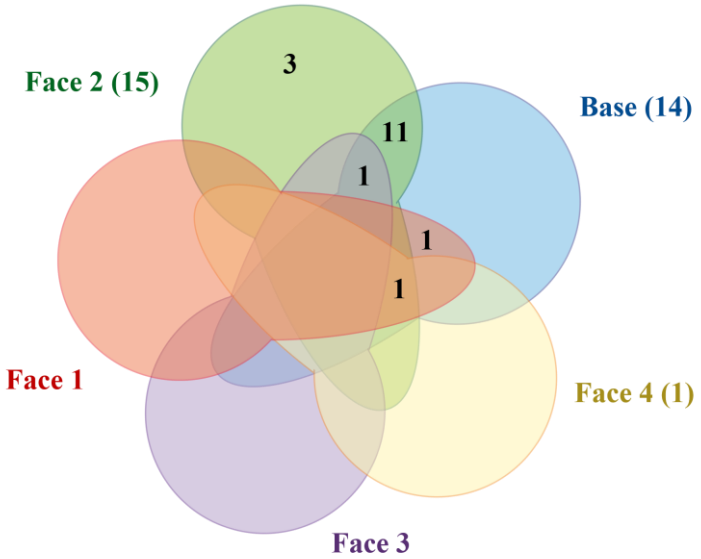

Figure 4.21 Distribution of interacting faces of GTPases with GDIs
Face 1, face 2, face 3, face 4, base is represented by red, green, magenta, yellow, and cyan, respectively. Cumulative number of structures interacting at each face is written in brackets while cases of interactions with multiple faces are given inside in the relevant overlapping regions of the five-part Venn diagram.

4.10 Effector Proteins

Effectors are proteins which are involved in the downstream signalling pathway and usually comes into action when it interacts with the active state of GTPase. Out of the 864 structures in the PDB, 433 structures are the complex of GTPases and the effectors. Most of the complexes are GTP-bound structures, only 5 are nucleotide free while one of them has PO_4 in the active site. 21 structures are GDP-bound and the rest of them are GTP-bound states as shown in figure 4.22.

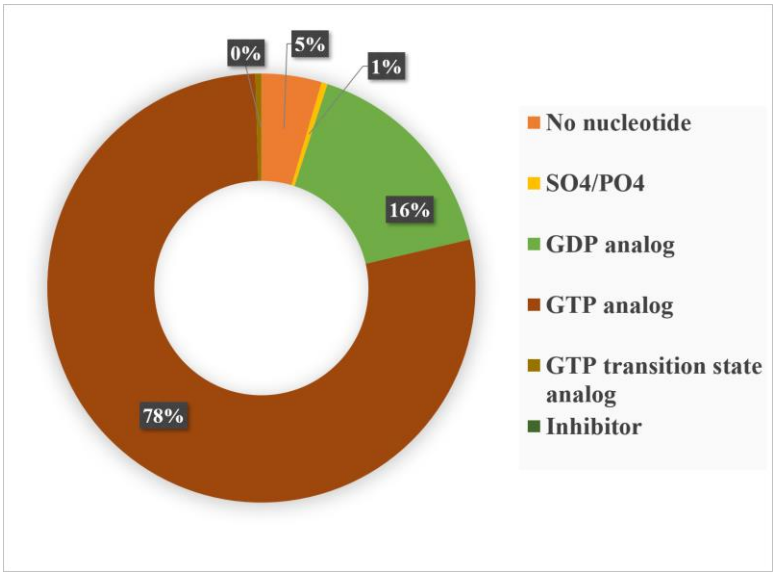

Figure 4.22 Nucleotide distribution of GTPase-Effector complex

There are many folds of proteins available in the effectors. They also interact at different faces. Face to which effectors interact are maximum at the base and base along with face 2. Almost all possible combinations of interacting faces are present (Figure 4.23). Effectors of proteins from different superfamily of GTPases perform different functions.

Most of the effectors interact at the Switch I and Switch II, but there are a lot of effectors which do not interact at face 2 and hence at Switch I and Switch II.

Ran GTPases are the group of small Ras-like GTPases, involved in the nuclear transport. So, the complex with which it is present is mostly transportin or exportin proteins (PDB ID 3A6P). The ultimate goal of these proteins is to transport proteins, and this is mediated only when Ran proteins are in active form i.e. Ran-exportin complex. In case of Rho proteins, its purpose of interaction to the effector protein is

cytoskeletal organization, cell migration etc (PDB ID 1S1C) (Wittinghofer and Vetter, 2011; Vetter, 2014; Vetter, 2017)

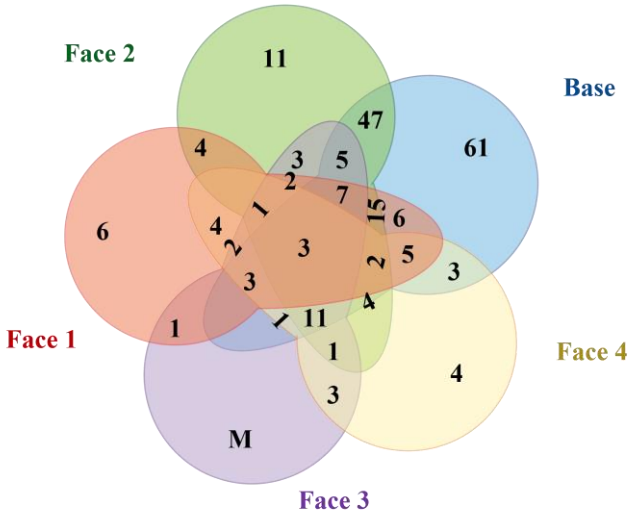

Figure 4.23 Distribution of interacting faces of GTPases with effectors
Face 1, face 2, face 3, face 4, base is represented by red, green, magenta, yellow, and cyan, respectively. Cumulative number of structures interacting at each face is written in brackets while cases of interactions with multiple faces are given inside in the relevant overlapping regions of the five-part Venn diagram.

4.11 Conclusions

After analysing the structural complexes, it looks like that in most of the cases, the GTPase interacts through its face 2 with other proteins, irrespective of the fact of type of regulatory proteins, i.e. GEFs, GAPs, GDIs, effectors. Switch I and switch II of face 2 are the major regions of interaction, as expected from their role in catalytic activity and discrimination between GDP and GTP. The cases where it does not directly interact with the switch loops, though less in number, are examples of allosteric action. The allosteric action appears to be mediated through interactions at the face 4 or with the β2 strand (as observed in the case of GDIs).

The mechanism of action of MglB acting as a GAP includes interactions with the base, and also contacts with switch I and switch II. Here, conformational changes in the GTPase drives the catalysis, since both the catalytic residues are present in the GTPase MglA itself. The GEF activity of MglA appears to be driven by an allosteric action through a side of approach through the face 4 which consists of the interswitch region and α5 helix, without a direct involvement of switch I and switch II. Here, the C-

terminal helix of $MglB_1$ (one of the two protomers of MglB dimer) plays a role in facilitating GTP binding to MglA.

A few other conclusions from the analysis with respect to comparison of MglAB interaction with eukaryotic GTPases and their interactors are discussed below:

An analogous allosteric regulation by the interswitch region has been reported in the eukaryotic ARL3 family. ARL3 GTPase attaches to the membrane with the help of an amphipathic helix at the N-terminus. In the GDP-bound conformation of ARL3, this helix is sequestered within a binding pocket comprising the α5 helix and the interswitch region (Figure 4.24B and F).

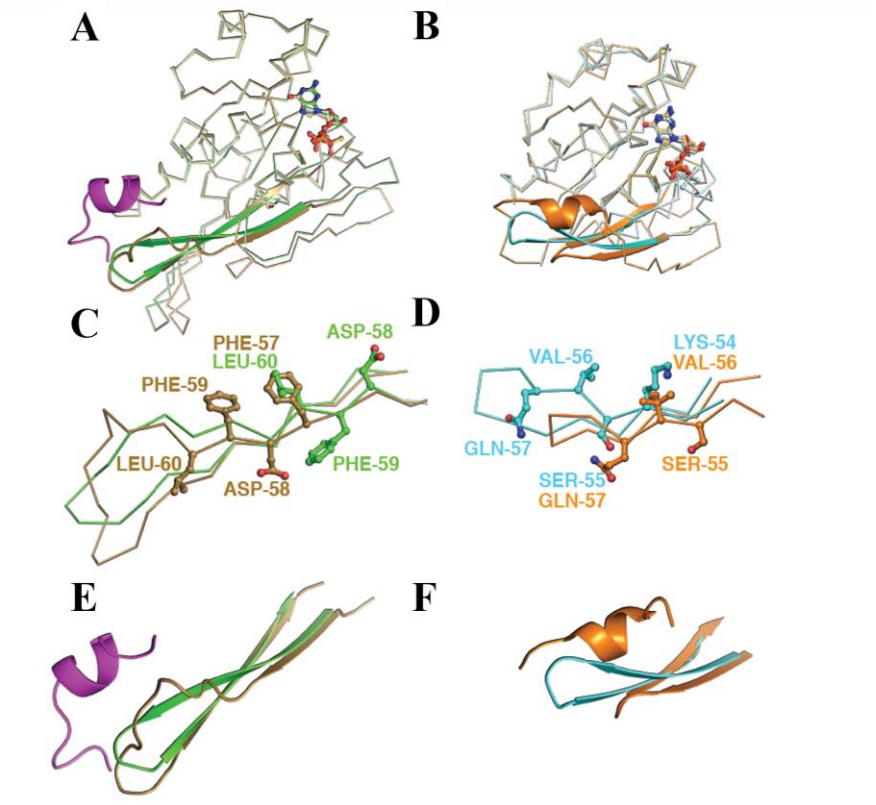

Figure 4.24 Significance of the helix-binding pocket and beta-screw movement in response to the nucleotide state and/or binding of MglB
A, B. Comparison of MglAB structures (brown: MglA-GDP, green: MglA-GMPPNP with MglB (C-terminal helix shown in magenta) with the GDP and GMPPNP-bound conformations of Arl3 GTPase (orange: Arl3-GDP, cyan: Arl3-GMPPNP).**C, D.** Registry shift observed in the MglA-GDP and Arl3 structures, resulting in an extended conformation of the loop. Registry shift is accompanied by a twist of the strand in the case of MglA. **E, F.** The extended position of the loop is incompatible with the helix position.

Sequestering the helix prevents membrane binding of GDP-bound ARL3. In the GppNHp-bound conformation, a registry shift of two amino acids extends the β_2-β_3 loop into the helix-binding pocket, thereby releasing the amphipathic helix (Figure 4.24D), a step that facilitates GTP-driven membrane binding. Just like Arl3, registry shift has also observed in Sar1. However, the conformational change is not accompanied by a twist of the β_2-strand as observed in the MglAB structure (Figure 4.24C). It is important to note that the β_2-β_3 loop extends into the helix binding pocket in the GTP-bound state of ARL3, while in MglA the β_2-β_3 loop extends into the corresponding helix-binding pocket in the GDP-bound state (Figure 4.24 A and C).

Our analysis emphasizes the significance of the pocket formed by the α5 helix and the interswitch region for regulating the GTPase. In the heterodimeric Rag GTPases RagA/B and RagC/D of mTOR signalling pathway, the Rbl/LC7 domain C-terminal to the GTPase domain forms interdomain contacts at the interswitch region (Figure 4.25C). Interestingly, a superposition of the GTPase domain with the MglAB complex shows that the C-terminal domain occupies the same region as the MglB Ct-helix (Figure 4.25). The *bona fide* GEFs of the Rag GTPases function by interacting with the Rbl/LC7 domain rather than the GTPase directly (Bar-Peled *et al.*, 2012; Levine *et al.*, 2013; Cherfils, 2017; Su *et al.*, 2017) In this context, the interaction between the GEFs and the Rbl/LC7 C-terminal domain possibly modulates the interdomain contact with the N-terminal GTPase domain. Thus, the allosteric pocket at the interswitch region presumably communicates the effect of GEF binding in Rag GTPases, thereby regulating nucleotide binding.

Blocking the movement of beta sheet and in turn the nucleotide binding pocket of GTPase by the GDIs is one of the mechanisms to keep the GTPase in GDP bound state. This might be a strategy evolved to prevent the registry shift of β2 strand. A similar interaction is also present in MglAB complex where the N-terminal strand interacts with the central β-sheet. It is currently not known if this is important for maintaining the C-terminal helix interaction of MglB.

For our small Ras-like GTPase analysis, we included Rag GTPases (even though they have long extended C-terminal domain) because the C-terminal domain has the same

fold as MglB (Roadblock/LC- domain) and, the GAP and GEF complexes of the Rag GTPase i.e. Lamtor and Gator complex, respectively interact through the C-terminal Roadblock domain. Also, just like MglA, Rag GTPase contains catalytic residues in the GTPase itself.

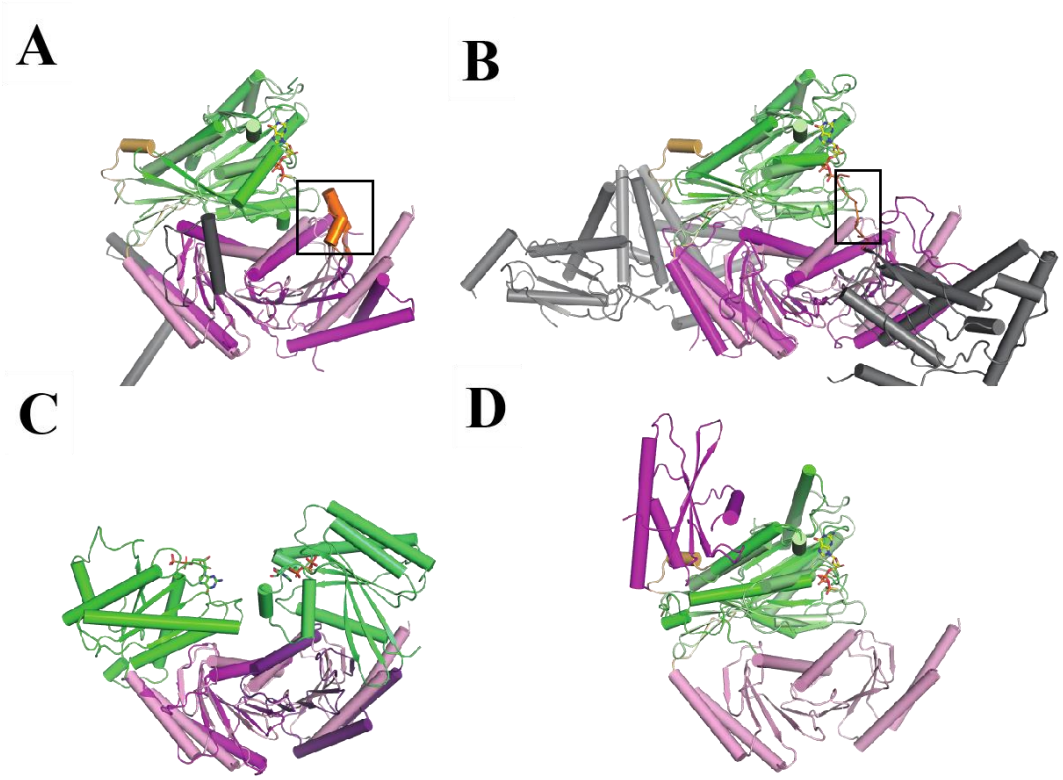

Figure 4.25 Eukaryotic GTPases associated with GEFs of Roadblock/LC7 domain.

MglAB complex superposed on

A. Rab GTPase and its GEF Mon1-Ccz1 complex (PDB ID: 5LLD). **B.** Yptp1 GTPase and TRAPP1 complex (PDB ID: 3CUE) **C.** Yeast Rag A/B (Gtr1p) and RagC/D (Gtr2p) heterodimer superposed on MglB dimer (PDB ID: 4ARZ). The two chains consist of an N-terminal GTPase domain and a C-terminal Rbl/LC7 fold domain, and form a heterodimer through dimerization of the Rbl/LC7 domains. **D.** MglA in the MglAB complex superposed on GTPase domain of Gtr1p. The C-terminal Rbl/LC7 domain overlaps with the Ct-helix binding pocket. The GTPase domains are shown in shades of green (dark green for eukaryotic GTPases, and pale green for MglA), the Rbl/LC7 domains in shades of magenta (dark shades for eukaryotic proteins and light pink for MglB), and insertions to the Rbl/LC7 fold and other associated proteins in grey. The insertions to the Rbl/LC7 fold or associated protein loops that contribute to the GEF activity are highlighted in dark orange and boxed, while the Ct-helix of MglB is in light orange.

Interestingly, like MglB, many other eukaryotic GEFs such as DENN-1B domain, TRAPP-I and Mon1-Ccz1 (Figure 4.25A and B), have the Rbl/LC7 fold (Levine *et al.*, 2013). Furthermore, we found that the inter-subunit orientation in MglAB is conserved in the GTPase-GEF complexes of Rab35 with DENN-1B domain, Rab Ypt1p with

TRAPP-I and Ypt7 with Mon1-Ccz1. However, unlike in MglAB, the mechanism of GEF action in these eukaryotic systems is based on a glutamate or aspartate residue interacting directly with switch I or switch II loops (Figure 4.25D). These residues are part of extensions from the Rbl/LC7 fold or are contributed by other interacting partners that form the GEF complex (Levine *et al.*, 2013). These comparative analyses reveal the common and distinguishing features between the prokaryotic MglA GTPase and their eukaryotic homologues.

A recent report on the structure of Armadillo repeat of SmgGDS-558 and the C-terminal farnesylated Rho suggested the role of farnesylated C-terminal end in GEF action along with the conformational change in switch I and switch II (Shimizu *et al.*, 2018). We noticed that the interaction of SmgGDS-588 with α5 and β2 of Rho is similar to MglA and MglB C-terminal helix interaction with MglA. This can be explored further to understand the mechanism of action of GEF better in both cases.

In summary, the analysis highlights the significance of the allosteric pocket and possible exploration of hitherto uncharacterised mechanisms of regulation of small Ras-like GTPases.

Chapter 5

Mechanistic insights of bi-functional properties of MglB on MglA in *Myxococcus xanthus*

Study done so far using various methods and techniques on *Myxococcus xanthus* MglA and MglB have provided us with unprecedented insights on how *Mx*MglB functions as an activator of *Mx*MglA. The major findings of this study, their implications and future directions of research are summarised in this chapter.

5.1 MglB interacts with both GDP and GTP conformations of MglA

The Ct-helix enabled *Mx*MglB to bind *Mx*MglA irrespective of whether it is bound to GTP or GDP. However, upon deletion of the helix, the complex formed only in presence of GTP but not GDP. This prompted us to ask what are the structural features that enable *Mx*MglB to bind GDP-bound *Mx*MglA.

As seen from our structure, characteristic conformational features of the *Mx*MglA-GDP structure were: i) conformation of the switch I loop proficient for GDP binding (Figure 2.10 and 2.16); ii) extension of the β_2-β_3 loop into the Ct-helix-binding pocket thus occluding it (Figure 2.16C and 2.18); iii) burial of the β_2-strand residues, which form the interface in the *Mx*MglAB structure, within the GTPase fold (unflipped state of β_2-strand, Figure 5.1). On the other hand, in the *Mx*MglAB-GTPγS structure, i) the switch I loop was oriented to interact with the γ phosphate of GTP; ii) the β-screw movement shifted the β_2-β_3 loop away from the Ct-helix binding pocket to remove the steric block (Figure 5.1); iii) the β_2-strand interface residues flipped to form the interface with MglB (flipped state of β_2-strand, Figure 5.1 and 2.16C).

An inspection of the *Mx*MglAB structure revealed that the switch I loop, and the binding pocket of the Ct-helix are at the N-and C- terminal ends of the β_2-strand, respectively (Figure 2.18). Hence, the flipped state of the β_2-strand that favors MglB binding can be achieved either by interaction of the γ-phosphate of GTP with the switch I loop, or by Ct-helix with the β_2-β_3 loop (Figure 2.16). We hypothesize that in the presence of GDP, the interactions of the Ct-helix at the allosteric site would drive the β-screw movement, thereby exposing the interface residues necessary for MglB interaction.

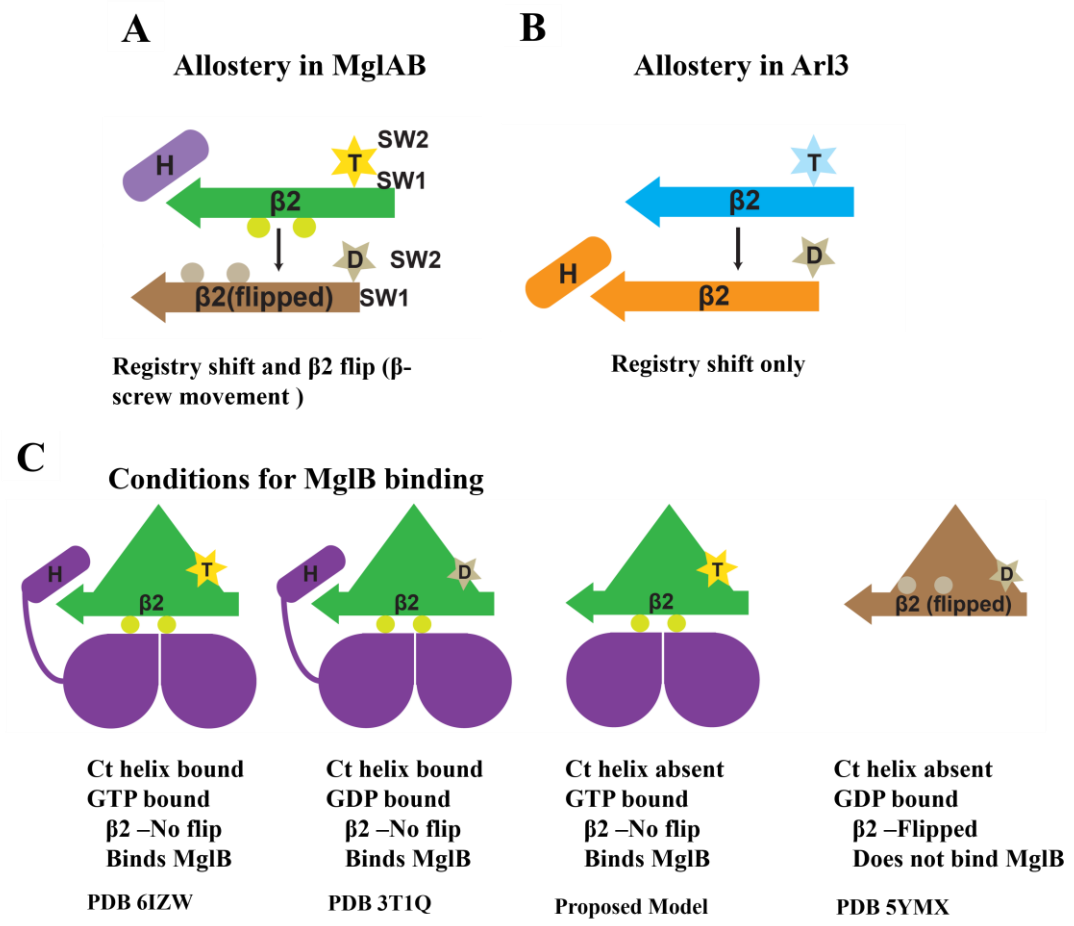

Figure 5.1 Model for MglA and MglB interaction

A, B. Schematic representation of the registry shift observed in the MglA-GDP and Arl3 structures, resulting in an extended conformation of the loop. Registry shift is accompanied by a twist of the strand in the case of MglA. Comparison of MglAB structures (light brown: MglA-GDP, green: MglA-GMPPNP with MglB (C-terminal helix shown in magenta) with the GDP and GMPPNP-bound conformations of Arl3 GTPase (orange: Arl3-GDP, cyan: Arl3-GMPPNP). **C.** Model for MglAB complex. GTP-bound MglA is shown in green, GDP-bound MglA in brown, and MglB in purple. Two small pale green circles at the interface of MglA and MglB are Phe57 and Phe59. Nucleotide in pocket of MglA GTP and GDP are in bright and pale yellow, respectively. Helix interacting at the allosteric site is shown by purple rod denoted as "H".

Similar conformational change between GDP and GTP bound states (binding of helix to the extended $\beta_2\beta_3$ strand of GTPase) is observed in Arf and Sar GTPases where helix interacts in the GDP bound state but is displaced from the binding pocket on the GTPase in the presence of GTP analogue. This helix is part of GTPase itself and is not provided by the interacting protein, unlike the case of *Mx*MglB. Also, instead of a β-screw movement, only a registry shift without any flipping of the β-sheet was observed in the Arl3 structure (Hillig *et al.*, 2000) (Figure 5.1 and 4.24) and Sar (Bi *et al.*, 2002), this makes MglA different from small Ras-like GTPase family.

5.2 MglB, a bi-functional catalyst of MglA

5.2.1 MglB binding facilitates positioning of catalytic residues

Roadblock/LC7 domain of *Mx*MglB dimer, when binds to *Mx*MglA facilitates conformational change in switch I and switch II loop of *Mx*MglA. Direction of approach of *Mx*MglB towards *Mx*MglA is from the base where α-helices of *Mx*MglB (one from each dimer) interacts with α_2, β_2 and β_2* of *Mx*MglA and also with the switch I and switch II (part of loop at the base). Interaction of *Mx*MglB α2 helix to *Mx*MglA causes flipping of β_2, shortening of β_2*, increase in length of β_2 strand (from $T^{54}F^{59}$ to $F^{56}I^{67}$) and shift of two residues in β_2 (registry shift). This leads to exposure of some residues buried inside MglA and helps in maintaining the interaction with *Mx*MglB i.e. F^{57} and F^{59}. This is termed as β-screw movement (similar to *Tt*MglAB), as shown in figure 2.16C. All these interactions and registry shift cause an increase in loop length of switch I in the GDP bound state compared to the GTP bound state. This brings R^{53} towards GTP-γ-S to perform catalytic activity. On the other hand, when MglB α-helix (from $MglB_2$) interacts with α2 and switch II, it orients the catalytic residue Q^{82} towards GTP-γ-S and catalytic water molecule (shown by structure in figure 2.16B and GTP hydrolysis activity in mutant in figure 3.9).

Mx$MglB_1$ β-strand of the N-terminal end interacts with β_0 of *Mx*MglA (Figure 2.18). This strand continues the central β-sheet of the small Ras-like GTPase fold of *Mx*MglA. The role of this interaction in optimally orienting *Mx*MglB dimer with respect to *Mx*MglA has currently not been validated experimentally. It is possible that this interaction is necessary to facilitate the interaction between the Ct-helix of *Mx*MglB and *Mx*MglA.

5.2.2 MglB Ct-helix facilitates nucleotide exchange allosterically

In the previous section (5.1), we proposed that the Ct-helix is capable of bringing *Mx*MglA to the GTP-bound conformation by interacting with the interswitch region. Conversely, presence of the Ct-helix in the pocket on *Mx*MglA will potentially prevent a relaxation to the *Mx*MglA-GDP conformation post GTP hydrolysis. Consequently, irrespective of the bound nucleotide (GDP or GTP), *Mx*MglA would maintain its conformation as seen in the *Mx*MglAB-GTPγS-bound structure as long as the Ct-helix

occupies the pocket (Figure 2.18 and 3.1). The Ct-helix could thus constrain *Mx*MglA into a pre-formed conformation that favors GTP-binding, equipping *Mx*MglB with bi-functional properties of a GAP and a GEF. Indeed, our results (Figure 3.16 and 3.17) show that *Mx*MglB accelerates GDP exchange when the Ct-helix is present.

Therefore, we propose that *Mx*MglB increases the rate of GTP hydrolysis by *Mx*MglA through two complementary ways. Firstly, *Mx*MglB stabilizes the flipped β_2-strand interface by its Rbl/LC7 domain, which orients the *Mx*MglA catalytic residues favourably. Secondly, its Ct-helix, a flexible extension from the main Rbl/LC7 fold, facilitates the flipping of the β_2-strand, resulting in a preformed GTP-binding pocket and accelerating nucleotide exchange.

The regulation of *Mx*MglA GTPase activity and *Mx*MglAB interaction by *Mx*MglB Ct-helix instigate us to explore if any analogous mechanisms exist among other prokaryotic and eukaryotic small Ras-like GTPases. In our analysis we have come across extension in the Rag GTPase with C-terminal Roadblock domain, where GAP and GEF complexes i.e. Gator and Lamtor complexes (de Araujo *et al.*, 2017) interact with the C-terminal Roadblock domain of Rag and perform GAP and GEF activities. In the Rag, GTP-hydrolysis catalytic residues are found in the Rag itself. Hence, allosteric effect mediated through the C-terminal Roadblock domain of the GTPase is sufficient to perform the activity as a GEF or GAP. Other proteins bind to the C-terminal domains and modulate the activity instead of directly interacting with the GTPase.

5.3 Implications of the results *in vivo*

To check the significance of the MglB C-terminal helix in the *Myxococcus xanthus*, motility phenotypes i.e. reversal frequency and motility phenotype was checked in presence of C-terminal truncated MglB. Also, localization of proteins *Mx*MglA and *Mx*MglB^{Ct} was observed when *Mx*MglB^{Ct} was introduced in MglB deleted background. Experiments were performed in collaboration with Dr. Tam Mignot for the motility phenotype of MglB C-terminal truncated protein in *M. xanthus*.

*Mx*MglB and the *Mx*MglB^{Ct} expressed in an *mglB* deletion mutant of *M. xanthus*. The strain *mglB*$^{+}$ complemented motility on an agar surface, while *mglB*$^{Ct+}$ led to defective motility. These defects observed at the colony scale were not due to loss of cell motility but due to aberrant cell reversals. Reversal frequency was checked to confirm this and

we observed that *Mx*MglB^{Ct+} cells did not respond to stimulator unlike *Mx*MglB (show a high-reversal frequency in response to Frz signalling) and reversed with high reversal frequencies, similar to the reversal pattern of the *mglB* deletion mutant, but different from the typical "pendulum" phenotype of the *Mx*MglA^{Q82L} mutant (Miertzschke et al., 2011). In the *mglB^{Ct}* mutant, *Mx*MglA may not be GTP-locked as in an *Mx*MglA^{Q82L} mutant, explaining why reversals are not strictly pendular. Nevertheless, the results show that the *Mx*MglB Ct-helix is strictly required for *Mx*MglB function *in vivo* (Data not shown).

5.3.1 MglA and MglB^{Ct} localizes to both the cell poles in *mglB^{Ct}*

We validated our *in vitro* results by deleting the Ct-helix from MglB *in vivo* in *Myxococcus xanthus*, and observing the motility phenotypes and localization of proteins. The *in vivo* work in Myxococcus xanthus was carried out as a collaboration with Tam Mignot's lab at Marseille, France.

To explore why MglB^{Ct} does not complement the *mglB* deletion, we analysed its localization in single cells of *M. xanthus*, by expressing C-terminal neonGreen (nG) fused to MglB and MglB^{Ct} in *mglB* deletion backgrounds. MglB-nG localized to the lagging cell pole and oscillated from pole-to-pole. In contrast, MglB^{Ct}-nG mostly localized symmetrically at both the poles. Thus, the Ct-helix is required for ensuring a unipolar localization of MglB.

To test how the expression of MglB^{Ct} might affect the localization of MglA, we further expressed *Mx*MglA-YFP in the *mglB^{Ct+}* strain. Remarkably, *Mx*MglA-YFP localization was also bi-polar (Data not shown), similar to the localization pattern observed in the *mglB* deletion mutant (Leonardy *et al.*, 2010; Zhang *et al.*, 2010). Thus, MglA and MglB^{Ct} were present at both the cell poles simultaneously in the *mglB^{Ct+}* strain. These results suggested that the Ct-helix of *Mx*MglB played a role in the polar exclusion of *Mx*MglA.

The results described above provide novel mechanistic insights into the functioning of the polarity regulator MglAB in *M. xanthus*. *In vivo*, the Ct-helix was found to be essential, as MglB^{Ct} cannot exclude MglA from the poles leading to bi-polar localization. A likely explanation for this effect is that *in vivo* the deletion of the Ct-helix leads to a net decrease in the rate of GTP hydrolysis, leaving most of the MglA

molecules to be GTP-bound and hence attached to the poles. MglB^{Ct} also remains at the poles, presumably attached to the GTP-bound form of MglA (Figure 5.2).

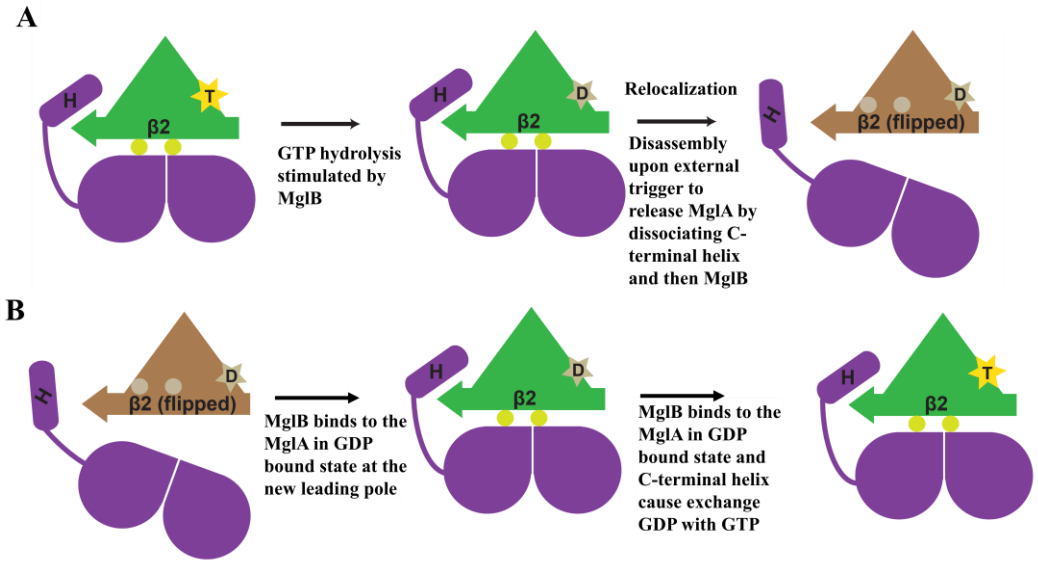

Figure 5.2 Proposed model for MglAB relocalization during polarity reversal
Model for MglAB complex formation, dissociation from each other and relocalization from one pole to other for polarity-oscillations in *M. xanthus.* MglA in complex with MglB shown in green MglB in purple MglA without nucleotide brown. Two small pale green circles at the interface of MglA and MglB are Phe^{57} and Phe^{59} (to mediate hydrophobic interaction with MglB). Nucleotide in pocket of MglA GTP and GDP are in bright and pale yellow, respectively. Helix interact at allosteric site shown by purple rod denoted as "H". **A**. MglA hydrolysis stimulation by MglB at the old leading pole and releasing MglA.GDP in cytoplasm and MglB stays at the new lagging pole. **B**. MglB C-terminal helix facilitate nucleotide exchange by binding to the MglA in GDP bound state when nucleotide exchange is required, that could be possibly at the new leading pole where MglA.GTP state stays at the pole, in response to external stimulus.

5.3.2 Regulation of the MglB Ct-helix in vivo

The bi-functional activity of MglB and the effect of Ct-helix deletion *in vivo* suggest that this protein might be subject to a number of regulations *in vivo*. A consequence of the Ct-helix mediated interaction between GDP-bound MglA and MglB is that the two proteins will remain together before and after GTP hydrolysis (Figure 5.2). This creates a conundrum since MglA and MglB exhibits a mutually exclusive localization to the opposite poles in *M. xanthus* during oscillations. However, as demonstrated above, MglB without Ct-helix interacts only with the GTP conformation of MglA, and not with the GDP-bound state. Therefore, in the cell, other factors could act to regulate the interaction of MglB Ct-helix with MglA, allowing GTP-specific interaction as and when required. Such a modulation could also reduce the MglA GTP hydrolysis rate when needed, and thus regulate the reversal frequencies.

5.4 Future prospects

The motility switch has been proposed to be triggered by an oscillator "gate" in which the oscillation frequency is dependent on a trigger activated by an environmental cue, and/or GTP hydrolysis rate (Guzzo *et al.*, 2018). Examples of possible candidates for the trigger include RomR, which interacts with MglB to recruit MglA to the future leading pole (Keilberg *et al.*, 2012; Zhang *et al.*, 2012; Keilberg and Søgaard-Andersen, 2014), and the phosphorylated form of FrzX that triggers oscillation by an as yet unknown mechanism (Guzzo *et al.*, 2018). This sets the stage for future experiments to confirm the role of the Ct-helix in modulating interaction of MglAB with RomR and FrzX at the poles.

Insights gained from the prokaryotic small Ras-like GTPase *Mx*MglA and its interacting partner *Mx*MglB bring out unifying features between prokaryotic and eukaryotic Ras-like GTPases and highlight the dual role of *Mx*MglB functioning both as a GAP and a GEF. The study also opens up a new avenue for design of compounds or factors that can modulate the enzyme activity by targeting the newly discovered allosteric binding pocket of the universal Ras-like fold.

Appendix

Table: Interface residues in structure of *M. xanthus* and *T. thermophilus* MglAB

	Myxococcus xanthus		*Thermous thermophilus*	
	MxMglA	MxMglB1	TtMglA	TtMglB1
Hydrogen bond (main chain)				
	Val 96 (O)	Gly 2 (N)		
	Ser 2 (O)	Leu 5 (N)		
	Ile 4 (O)	Mse 7 (N)		
	Ser 2 (N)	Thr 3 (O)		
	Ile 4 (N)	Leu 5 (O)		
	Tyr 6 (N)	Mse 7 (O)		
Hydrogen bond (side chain)				
	Lys 14 (NZ)	Asn 37 (O)	Glu 43 (OE1)	Thr 58 (OG1)
	His 75 (NE2)	Gln 39 (OE1)	Tyr 77 (OH)	Thr 61 (OG1)
	Arg 68 (NE)	Pro 144 (O)	Tyr 77 (OH)	Lys 38 (O)
	Lys 192 (NZ)	Mse 148 (O)	Arg 73 (NH2)	Asp 57 (OD2)
	Asn 12 (OD1)	Gln 39 (NE2)	Arg 94 (NH1)	Gln 71 (OE1)
	Tyr 77 (OH)	Ser 57 (OG)		
Salt bridge				
	Asp 97 (OD1)	Gly 2 (N)	Arg 73 (NH2)	Asp 57 (OD1)
	Lys 192 (NZ)	Asp 154 (OD1)	Arg 73 (NH2)	Asp 57 (OD2)
Hydrophibic interaction				
	Phe 3	Gln 4	Arg 9	Ser 5
	Asn 5	Val 6	Glu 10	Leu 8
	Ser 7	Tyr 8	Asn 12	Tyr 9
	Ser 8	Glu 9	Phe 13	Gly 10
	Ile 11	Phe 12	Lys 14	Tyr 13
	Gly 42	Thr 13	Gly 42	Arg 37
	Lys 43	Lys 36	Val 45	Gly 39
	Ile 45	Gly 38	Leu 47	Phe 40
	Leu 47	Leu 40	Phe 56	Val 41
	Phe 57	Ile 41	Phe 57	Leu 42
	Phe 59	Asp 51	Phe 59	Pro 55
	Pro 61	Thr 53	Pro 61	Leu 62
	Leu 64	Ser 54	His 75	Ser 65
	Gly 65	Leu 58	Ala 87	Asn 66
	Glu 66	Gly 61	Leu 91	Ala 68
	Ile 67	Asn 62	Ile 92	Ala 69
	Phe 70	Ala 64	Gly 95	Ala 72
	Thr 72	Ala 65	Asp 97	Glu 101
	Phe 74	Gly 68		His 102
	Ala 87	Leu 72		
	Leu 91	Arg 98		
	Ile 92	Ser 143		
	Lys 94	Phe 145		
	Gly 95	Glu 147		
	Tyr 129	Ser 149		
	Ile 134	Asp 150		
	Lys 181	Asp 152		
	Ala 184	Ile 153		
	Leu 188	Leu 156		
	Thr 189	Phe 157		
	Leu 191			
	MxMglA	MxMglB2	TtMglA	TtMglB2
Hydrogen bond				
	Glu 50 (OE2)	Arg 98 (NH1)	Asp 51 (OD2)	Lys 38 (NZ)
	Ser 88 (OG)	Ser 57 (OG)	Phe 84 (O)	Thr 61 (OG1)
	Tyr 85 (OH)	Asn 37 (O)	Ser 88 (OG)	Ser 65 (OG)
	Ser 88 (N)	Ser 57 (OG)	Leu 55 (O)	Ser 65 (OG)
	Ser 88 (OG)	Ser 57 (O)	Tyr 85 (OH)	Lys 38 (O)
Salt bridge				
	Glu 50 (OE2)	Arg 98 (NH1)	Glu 50 (OE1)	Lys 38 (NZ)
			Asp 51 (OD2)	Lys 38 (NZ)
Hydrophobic interaction				
	Ile 45	Lys 36	Glu 43	Arg 37
	Leu 47	Gly 38	Val 45	Thr 58
	Ser 48	Gln 39	Leu 47	Leu 62
	Thr 49	Thr 53	Thr 49	Ala 64
	Leu 55	Ser 54	Phe 56	Asn 66
	Phe 56	Leu 58	Phe 57	Ala 68
	Phe 57		Ala 87	Ala 69
	Phe 84		Lys 90	Ala 72
	Ala 87		Leu 91	Leu 76
	Leu 91			

Table: List of primers

S. No.	Name	Nucleotide sequence
1	**AB-Operon-f**	5'CGACAACCTCTTCAGCGAGTAACCCGGGAAGCCATGTCCTTCA TCAATTACTCATCC3'
2	**MglB3D-r**	5'CTCGGCTGAAGAGGTTGGCGATAGCGGCGTCGGAGATCTCGG C3'
3	**MglB4D-r**	5'CTCGGCTGAAGAGGTTGGCGATAGCGGCGGCGGAGATCTCGG C3'
4	**MglA-F5759H-r**	5'GCGACAGCGGCAGGTGGTCGTGGAAGAGCGTGCGG3'
5	**MglA-R53A-r**	5'GTCGAAGAAGAGCGTGGCGTCCGTCTCCGTGGAG3'
6	**MglB-I148M-r**	5'GTCGATATCGTCGTCGGACATCTCGGCGAAGGGCGACCC3'
7	**MglA-F172A-r**	5' CGCCTTGAGCGTGTCAGCGACGCCACGCCCG 3'
8	**MglA-L64I67A-f**	5'CTGCCGCTGTCGGCCGGTGAGGC3'
9	**RpMglBC139dH6**	5' GGATCCTTAAGGACTGTCAGTCTTCTTCACC 3'
10	**MglA-K181185A-r**	5'GGTGAGGACGAGCGCGGCCACGGCCGCGAGCGTGTCGAAG3'
11	**MglB-I153M-r**	5'CTCGCTGAAGAGGTTGTCCATATCGTCGTCGGAGATCTC3'
12	**MglB-L156M-stop-r**	5'GATGATGATGTTAGGATCCTTACTCGCTGAACATGTTGTCGATA TCGTC3'
13	**MglB139-H6-r**	5'GCTTTTAATGATGATGATGATGATGGGATCCAGGACTGTCAGTC TTCT3'
14	**MglA-G21V-f**	5'GTCTATTACGGGGCCCGTCCTCTGCGGGAAGACGAC 3'
15	**MglB-H6r**	5'GCTTTTAATGATGATGATGATGATGGG 3'
16	**MglA-f**	5'GTTTAACTTTAAGAAGGAGATATACAT3'
17	**MglA-Q82L-r**	5'GGCGTCGTAGAAGACCAGACCGGGCACCGT3'
18	**MglA-H6r**	5'GCTTTTAATGATGATGATGATGATGGG3'
19	**MglB-f**	5'GTTTAACTTTAAGAAGGAGATATACAT3'
20	**MglBC139-His**	5'GGATCCTTAATGATGATGATGATGATGAGGACTGTCAGTCTTCT TCACC3'
21	**MglB-stop-r**	5'GATGATGATGATGTTAGGATCCTTACTCGCTGAAGAGG3'
22	**MxMgB-RSF-BH1-r**	5' CCAATTGGGATCCGGTTACTCGCTGAAGAGGTTG 3'

Table: List of clones

Plasmid construct	Relevant characteristics	Source or reference
pHis17 mglA^{WT}	C terminal-His_6	This work
pHis17 mglA^{Q82L}	C terminal-His_6	This work
pHis17 mglA$^{K181/185A}$	C terminal-His_6	This work
pHis17 mglA$^{L64/I67A}$	C terminal-His_6	This work
pHis17 mglB^{WT}	C terminal-His_6	This work
pHis17 mglB^{WT}dH6	No tag	This work
pHis17 mglB^{3D}	No tag	This work
pHis17 mglB^{Ct}	C terminal-His_6	This work
pHis17 mglB^{L156M}	No Tag	This work
pHis17 mglB^{I148M}	No Tag	This work
pHis17 mglA^{R53A}	C terminal-His_6	This work

Bradford Standard (one representative graph):

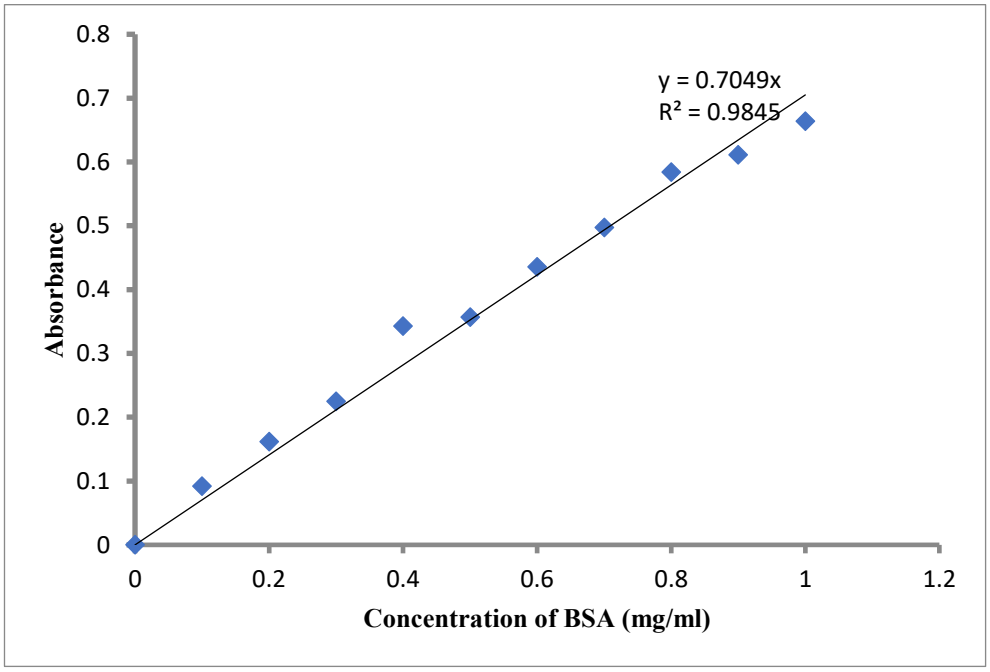

Conc of BSA (mg/ml)	O.D. Values	Blank Subtracted
0	0.361214	0
0.1	0.453181	0.091967
0.2	0.522969	0.161755
0.3	0.585937	0.224723
0.4	0.703794	0.34258
0.5	0.717759	0.356545
0.6	0.796704	0.43549
0.7	0.858111	0.496897
0.8	0.945214	0.584
0.9	0.97229	0.611076
1	1.02467	0.663456

Standard Size-Exclusion Chromatography (SEC):

Standard Protein	Size (KDa)	Elution Volume (Ve) ml
Cytochrome C	13	14.49
Carbonic Anhydrase	29	11.9
Ova Albumin	49	10.39
Albumin	66	9.75
Blue Dextran		8.48 (Void)

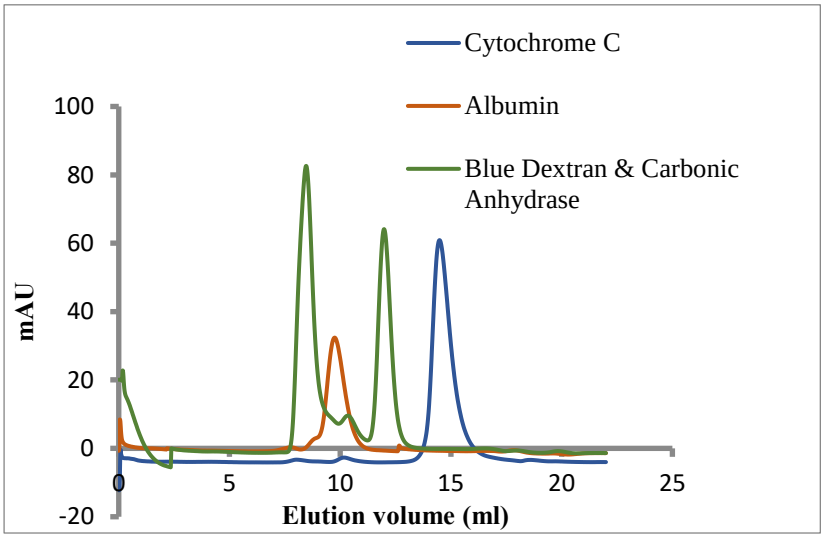

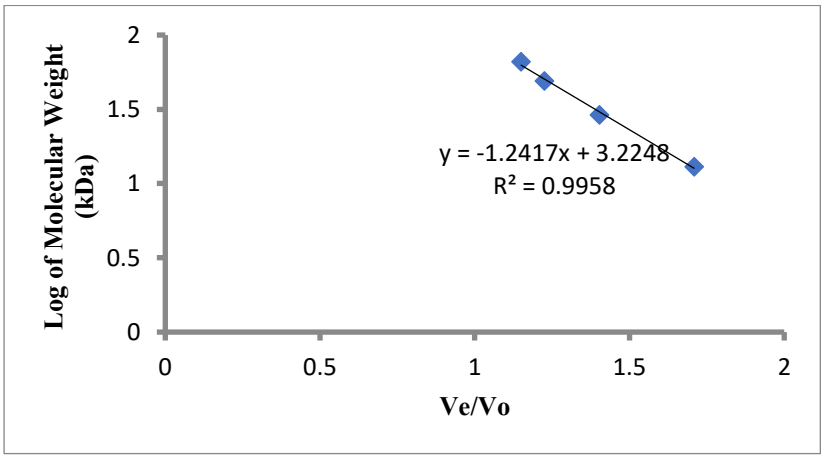

Standard Malachite green (one representative graph):

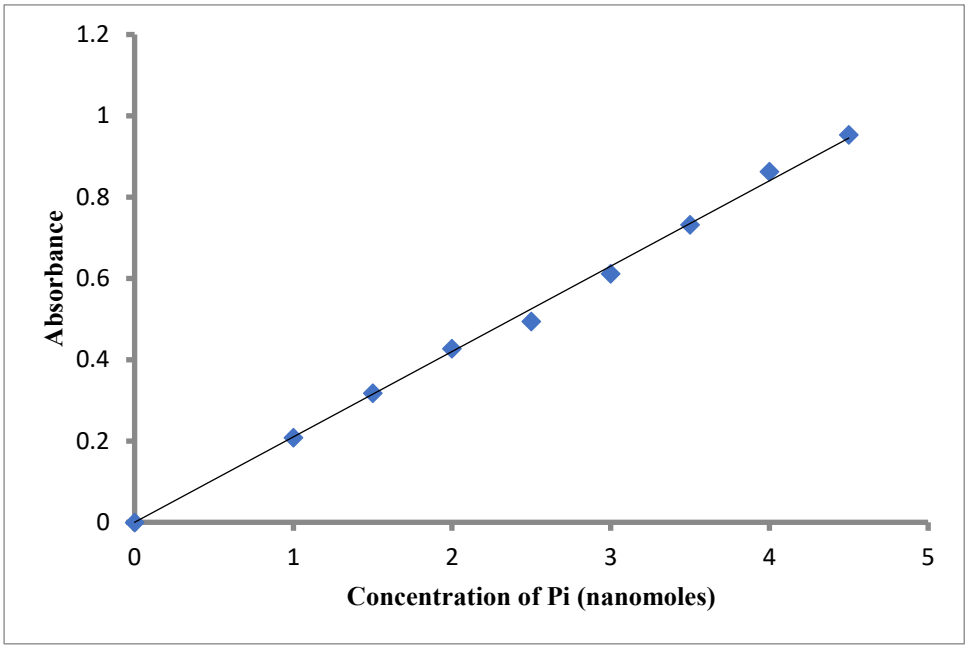

Conc.(nanomoles)	O.D. Values	Blank subtracted
0	0.100409	0
1	0.308503	0.208094
1.5	0.418695	0.318286
2	0.527514	0.427105
2.5	0.594889	0.49448
3	0.711992	0.611583
3.5	0.832804	0.732395
4	0.962967	0.862558
4.5	1.05365	0.953241

MALDI-TOF (Mass-spectrometry) data for all the proteins:

$MglB^{I156M}$ (Expected mass 17.19 kDa, Observed mass 17.2 kDa)

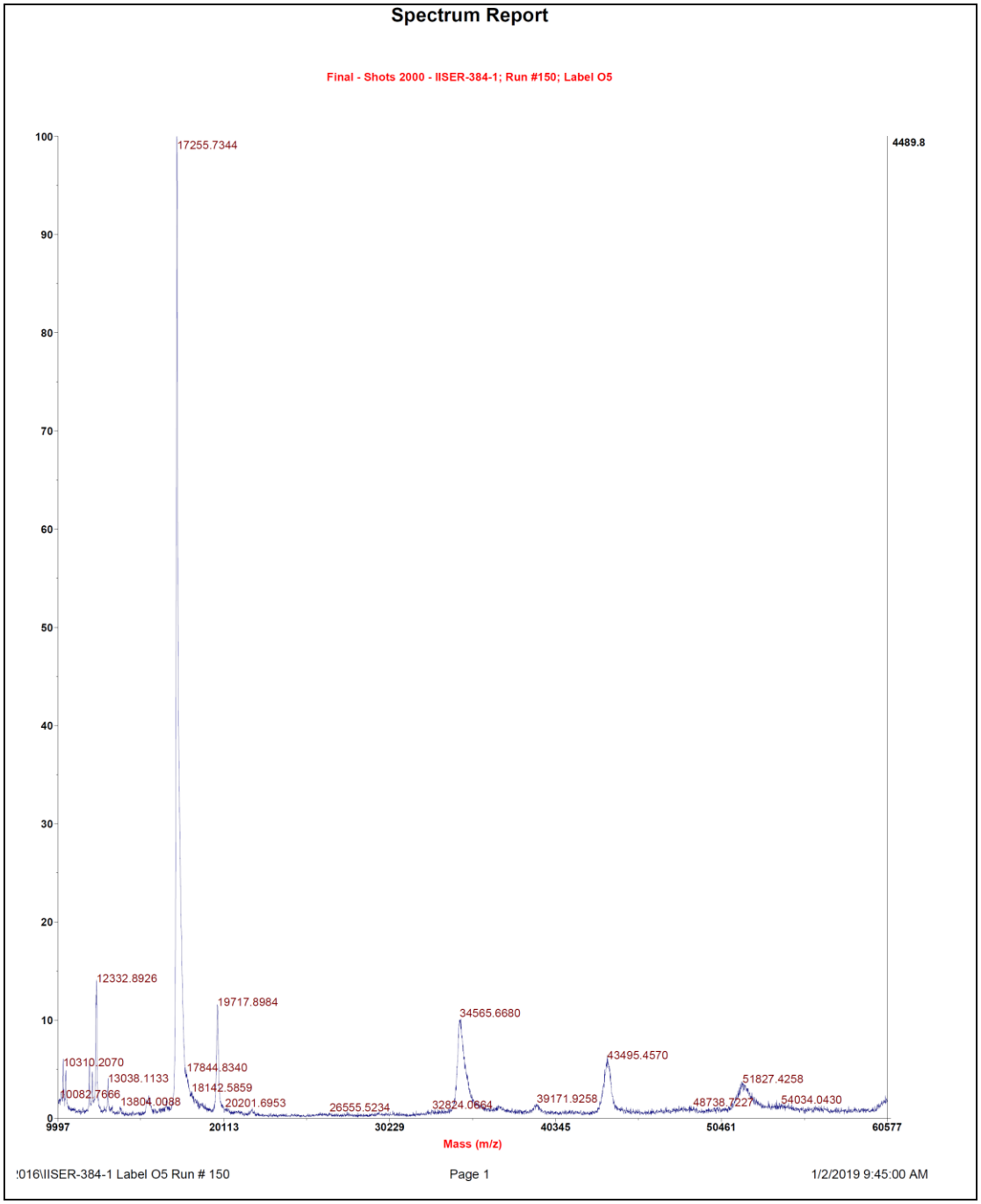

MglB (Expected mass 18 kDa, Observed mass 18 kDa)

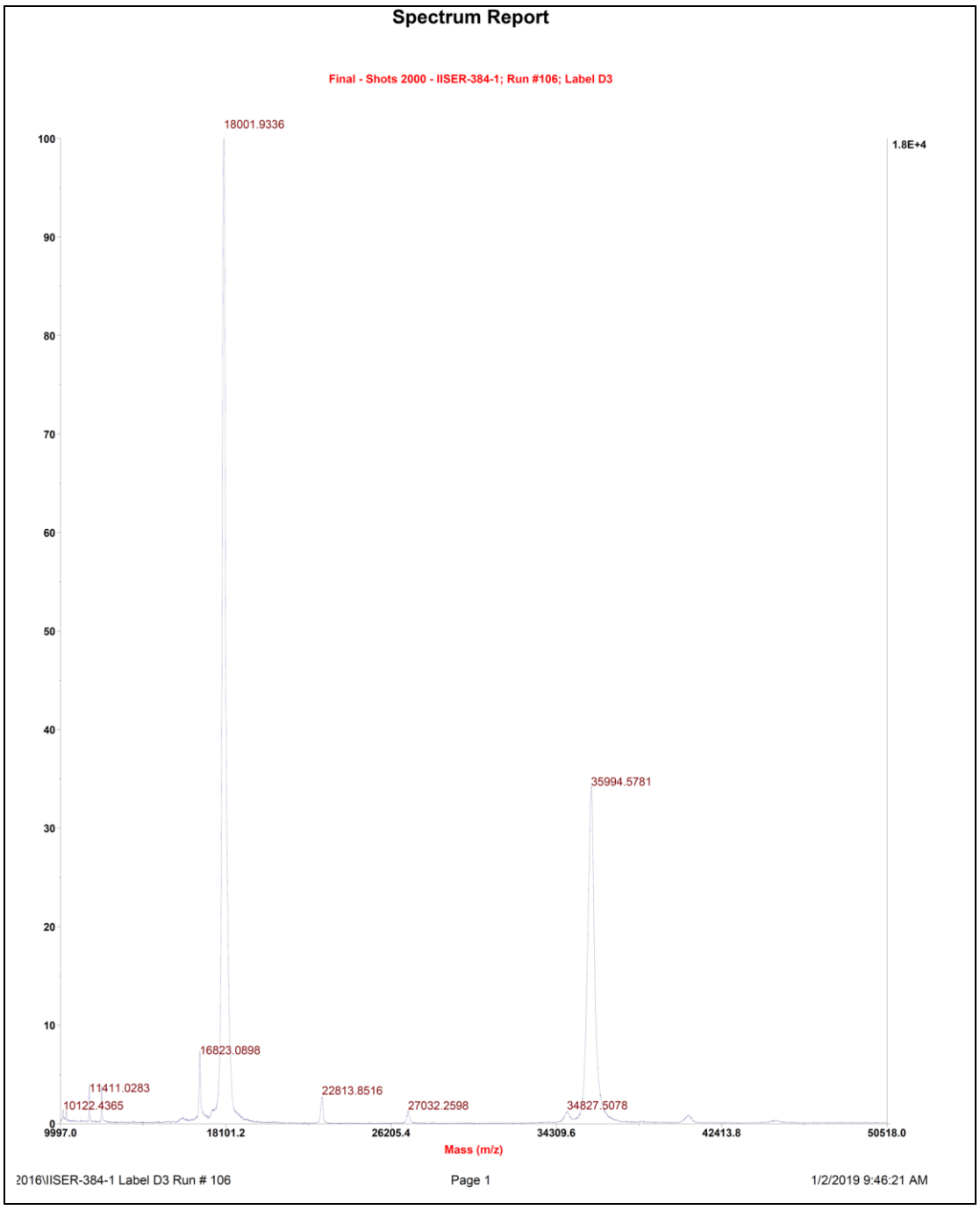

MglB^{3D} (Expected mass 17.19 kDa, Observed mass 17.2 kDa)

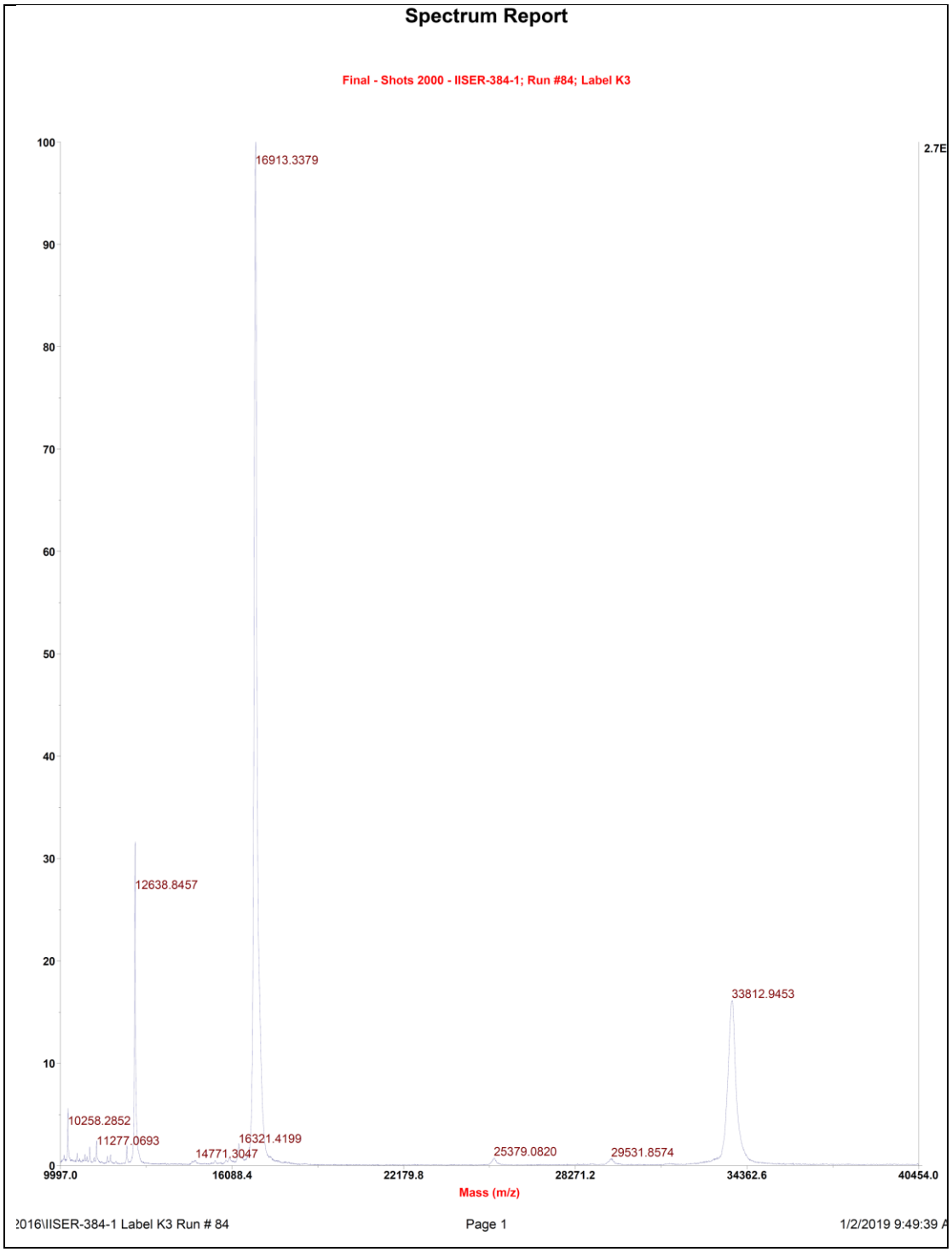

$MglB^{Ct}$ (Expected mass 15.9 kDa, Observed mass 15.9 kDa)

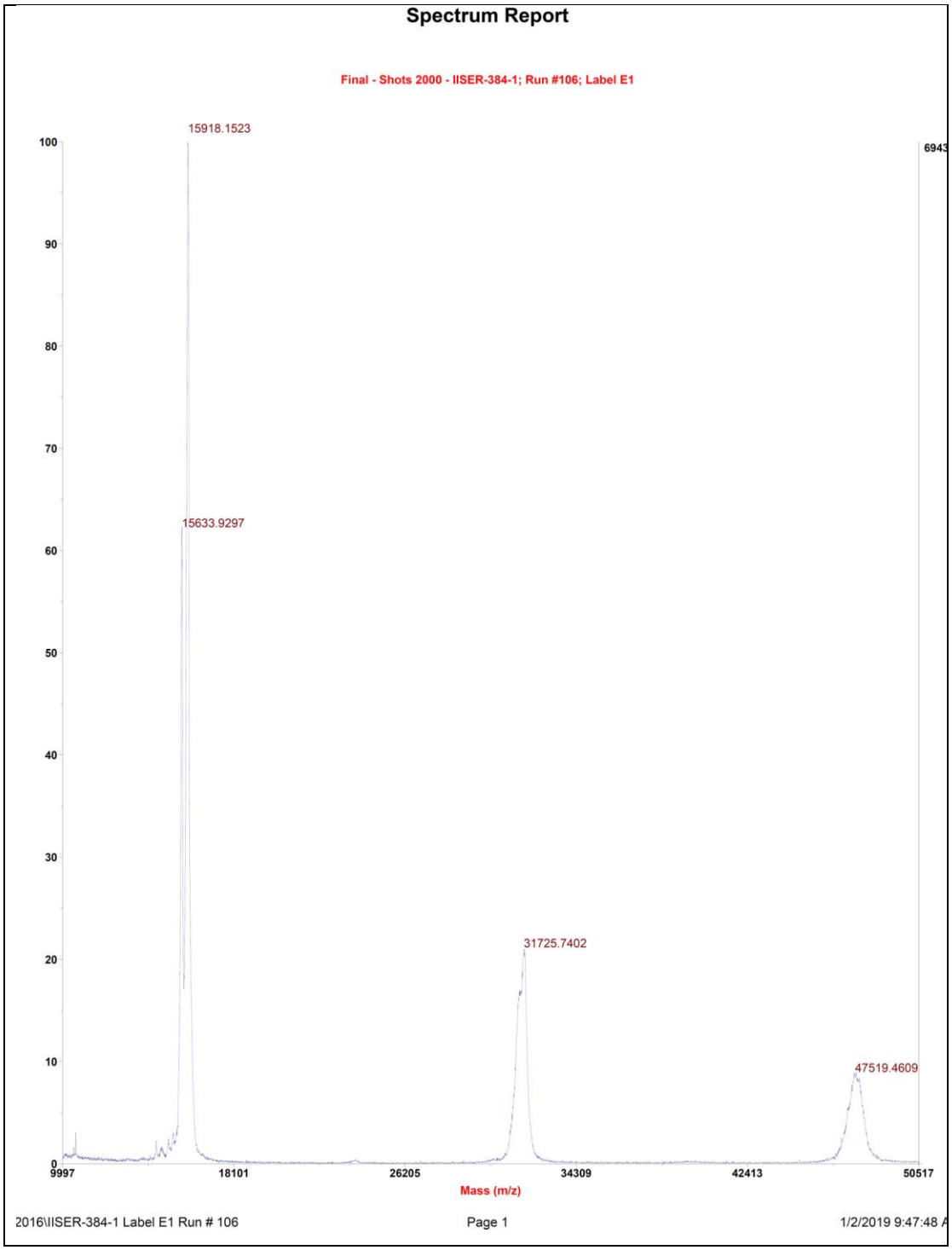

MglA (Expected mass 22.83 kDa, Observed mass 22.8 kDa)

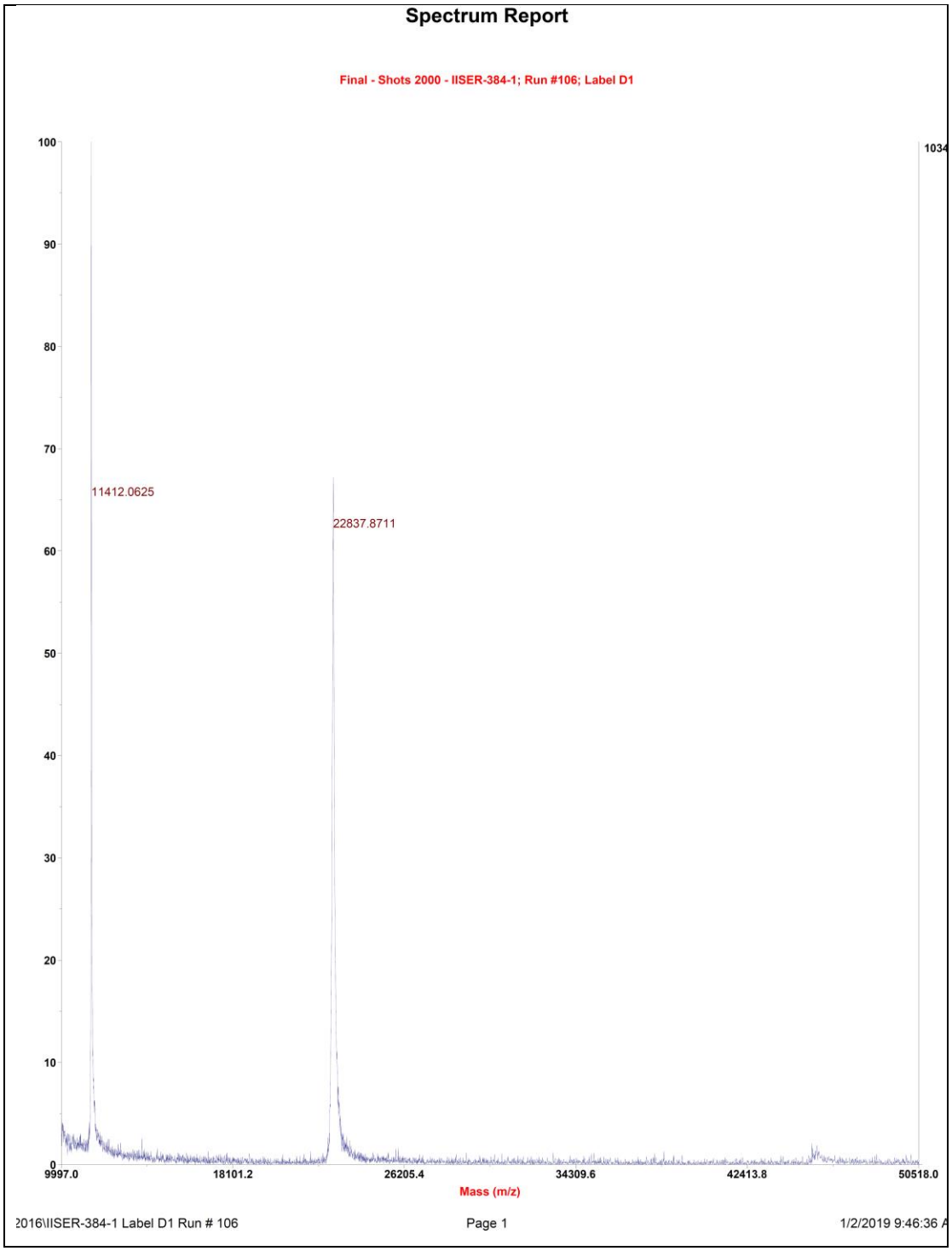

$MglA^{L}$ (Expected mass 22.83 kDa, Observed mass 22.75 kDa)

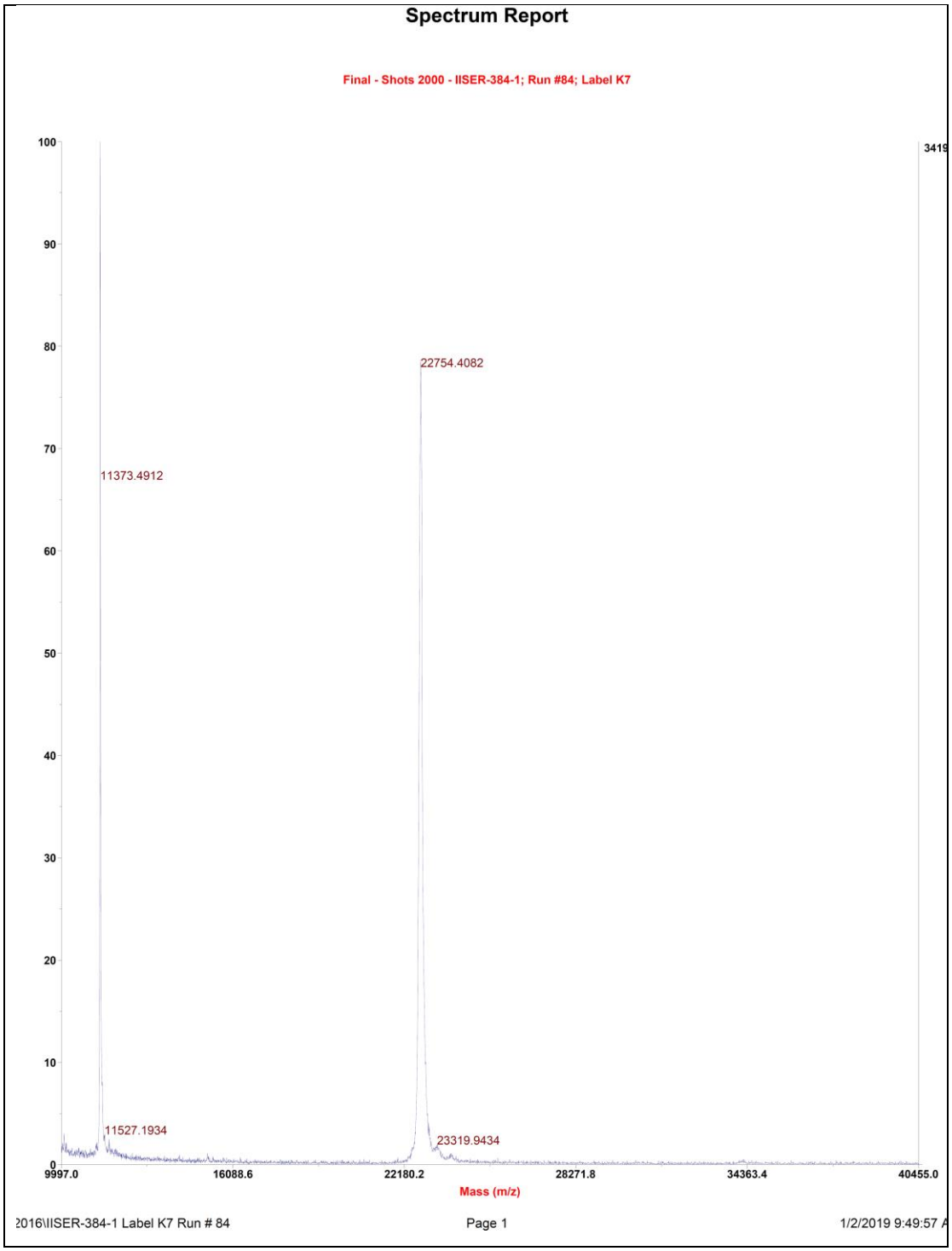

$MglA^{Q}$ (Expected mass 22.83 kDa, Observed mass 23.49 kDa)

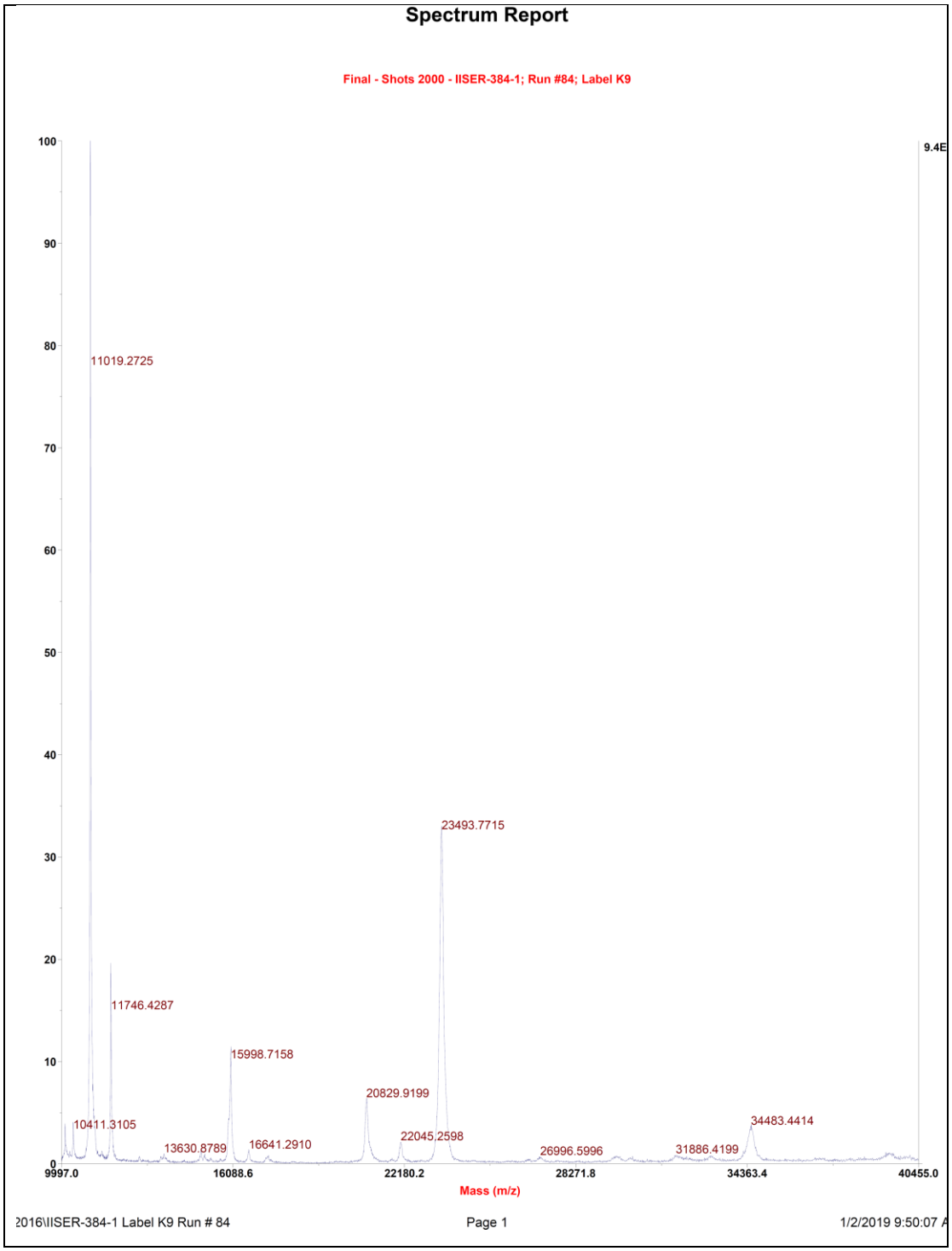

References

- Åkesson, S., Ilieva, M., Karagicheva, J., Rakhimberdiev, E., Tomotani, B., and Helm, B. (2017). Timing avian long-distance migration: from internal clock mechanisms to global flights. Philosophical Transactions of the Royal Society B: Biological Sciences *372*, 20160252.
- Alerstam, T., and Bäckman, J. (2018). Ecology of animal migration, Vol 28.
- Andreeva, A., Howorth, D., Chandonia, J.-M., Brenner, S.E., Hubbard, T.J.P., Chothia, C., and Murzin, A.G. (2008). Data growth and its impact on the SCOP database: new developments. Nucleic Acids Research *36*, D419-D425.
- Bar-Peled, L., Schweitzer, Lawrence D., Zoncu, R., and Sabatini, David M. (2012). Ragulator Is a GEF for the Rag GTPases that Signal Amino Acid Levels to mTORC1. Cell *150*, 1196-1208.
- Battye, T.G.G., Kontogiannis, L., Johnson, O., Powell, H.R., and Leslie, A.G.W. (2011). iMOSFLM: a new graphical interface for diffraction-image processing with MOSFLM. Acta crystallographica Section D, Biological crystallography *67*, 271-281.
- Baykov, A.A., Evtushenko, O.A., and Avaeva, S.M. (1988). A malachite green procedure for orthophosphate determination and its use in alkaline phosphatase-based enzyme immunoassay. Analytical Biochemistry *171*, 266-270.
- Berleman, J.E., Scott, J., Chumley, T., and Kirby, J.R. (2008). Predataxis behavior in <em>Myxococcus xanthus</em&gt. Proceedings of the National Academy of Sciences *105*, 17127.
- Bershadsky, A.D., and Kozlov, M.M. (2011). Crawling cell locomotion revisited. Proceedings of the National Academy of Sciences *108*, 20275.
- Bi, X., Corpina, R.A., and Goldberg, J. (2002). Structure of the Sec23/24–Sar1 pre-budding complex of the COPII vesicle coat. Nature *419*, 271.
- Bischof, L.F., Friedrich, C., Harms, A., Søgaard-Andersen, L., and van der Does, C. (2016). The Type IV Pilus Assembly ATPase PilB of Myxococcus xanthus Interacts with the Inner Membrane Platform Protein PilC and the Nucleotide-binding Protein PilM. Journal of Biological Chemistry *291*, 6946-6957.
- Blackhart, B.D., and Zusman, D.R. (1985). "Frizzy" genes of Myxococcus xanthus are involved in control of frequency of reversal of gliding motility. Proc Natl Acad Sci U S A *82*, 8767-8770.
- Blackhart, B.D., and Zusman, D.R. (1986). Analysis of the products of the Myxococcus xanthus frz genes. Journal of bacteriology *166*, 673-678.
- Bockhorn, M., Jain, R.K., and Munn, L.L. (2007). Active versus passive mechanisms in metastasis: do cancer cells crawl into vessels, or are they pushed? The Lancet Oncology *8*, 444-448.
- Boriack-Sjodin, P.A., Margarit, S.M., Bar-Sagi, D., and Kuriyan, J. (1998). The structural basis of the activation of Ras by Sos. Nature *394*, 337.
- Bos, J.L., Rehmann, H., and Wittinghofer, A. (2007). GEFs and GAPs: Critical Elements in the Control of Small G Proteins. Cell *129*, 865-877.
- Bourne, H.R., Sanders, D.A., and McCormick, F. (1990). The GTPase superfamily: a conserved switch for diverse cell functions. Nature *348*, 125.
- Bourne, H.R., Sanders, D.A., and McCormick, F. (1991). The GTPase superfamily: conserved structure and molecular mechanism. Nature *349*, 117.

- Bradford, M.M. (1976). A rapid and sensitive method for the quantitation of microgram quantities of protein utilizing the principle of protein-dye binding. Analytical Biochemistry *72*, 248-254.
- Brownbridge, G.G., Lowe, P.N., Moore, K.J., Skinner, R.H., and Webb, M.R. (1993). Interaction of GTPase activating proteins (GAPs) with p21ras measured by a novel fluorescence anisotropy method. Essential role of Arg-903 of GAP in activation of GTP hydrolysis on p21ras. Journal of Biological Chemistry *268*, 10914-10919.
- Bulyha, I., Hot, E., Huntley, S., and Søgaard-Andersen, L. (2011). GTPases in bacterial cell polarity and signalling. Current Opinion in Microbiology *14*, 726-733.
- Bulyha, I., Lindow, S., Lin, L., Bolte, K., Wuichet, K., Kahnt, J., van der Does, C., Thanbichler, M., and Søgaard-Andersen, L. (2013). Two Small GTPases Act in Concert with the Bactofilin Cytoskeleton to Regulate Dynamic Bacterial Cell Polarity. Developmental Cell *25*, 119-131.
- Bulyha, I., Schmidt, C., Lenz, P., Jakovljevic, V., Höne, A., Maier, B., Hoppert, M., and Søgaard-Andersen, L. (2009). Regulation of the type IV pili molecular machine by dynamic localization of two motor proteins. Molecular Microbiology *74*, 691-706.
- Bunkóczi, G., Echols, N., McCoy, A.J., Oeffner, R.D., Adams, P.D., and Read, R.J. (2013). Phaser.MRage: automated molecular replacement. Acta crystallographica Section D, Biological crystallography *69*, 2276-2286.
- Burchard, R.P. (1981). Gliding Motility of Prokaryotes: Ultrastructure, Physiology, and Genetics. Annual Review of Microbiology *35*, 497-529.
- Burkinshaw, B.J., Prehna, G., Worrall, L.J., and Strynadka, N.C.J. (2012). Structure of Salmonella Effector Protein SopB N-terminal Domain in Complex with Host Rho GTPase Cdc42. Journal of Biological Chemistry *287*, 13348-13355.
- Carvalho, A.T.P., Szeler, K., Vavitsas, K., Åqvist, J., and Kamerlin, S.C.L. (2015). Modeling the mechanisms of biological GTP hydrolysis. Archives of Biochemistry and Biophysics *582*, 80-90.
- Chen, H., Keseler, I.M., and Shimkets, L.J. (1990). Genome size of Myxococcus xanthus determined by pulsed-field gel electrophoresis. Journal of Bacteriology *172*, 4206.
- Cherfils, J. (2014). GEFs and GAPs: Mechanisms and Structures. In Ras Superfamily Small G Proteins: Biology and Mechanisms 1: General Features, Signaling, A. Wittinghofer, ed. (Vienna: Springer Vienna), pp. 51-63.
- Cherfils, J. (2017). Encoding Allostery in mTOR Signaling: The Structure of the Rag GTPase/Ragulator Complex. Molecular Cell *68*, 823-824.
- Cherfils, J., and Zeghouf, M. (2013). Regulation of Small GTPases by GEFs, GAPs, and GDIs. Physiological Reviews *93*, 269-309.
- Claessen, D., Rozen, D.E., Kuipers, O.P., Søgaard-Andersen, L., and van Wezel, G.P. (2014). Bacterial solutions to multicellularity: a tale of biofilms, filaments and fruiting bodies. Nature Reviews Microbiology *12*, 115.
- Cogan, N.G., and Guy, R.D. (2010). Multiphase flow models of biogels from crawling cells to bacterial biofilms. HFSP Journal *4*, 11-25.
- Copley, R.R., and Barton, G.J. (1994). A Structural Analysis of Phosphate and Sulphate Binding Sites in Proteins: Estimation of Propensities for Binding and

Conservation of Phosphate Binding Sites. Journal of Molecular Biology *242*, 321-329.
- Corbett, K.D., and Alber, T. (2001). The many faces of Ras: recognition of small GTP-binding proteins. Trends in Biochemical Sciences *26*, 710-716.
- Coskun, O. (2016). Separation techniques: Chromatography. Northern clinics of Istanbul *3*, 156-160.
- de Araujo, M.E.G., Naschberger, A., Fürnrohr, B.G., Stasyk, T., Dunzendorfer-Matt, T., Lechner, S., Welti, S., Kremser, L., Shivalingaiah, G., Offterdinger, M.*, et al.* (2017). Crystal structure of the human lysosomal mTORC1 scaffold complex and its impact on signaling. Science *358*, 377.
- DeLucas, L.J., Bray, T.L., Nagy, L., McCombs, D., Chernov, N., Hamrick, D., Cosenza, L., Belgovskiy, A., Stoops, B., and Chait, A. (2003). Efficient protein crystallization. Journal of Structural Biology *142*, 188-206.
- Derewenda, Z.S. (2004). The use of recombinant methods and molecular engineering in protein crystallization. Methods *34*, 354-363.
- Dessau, M.A., and Modis, Y. (2011). Protein crystallization for X-ray crystallography. Journal of visualized experiments : JoVE, 2285.
- Ebersbach, G., and Jacobs-Wagner, C. (2007). Exploration into the spatial and temporal mechanisms of bacterial polarity. Trends in Microbiology *15*, 101-108.
- Eberth, A., and Ahmadian, M.R. (2009). In Vitro GEF and GAP Assays. Current Protocols in Cell Biology *43*, 14.19.11-14.19.25.
- Echols, N., Grosse-Kunstleve, R.W., Afonine, P.V., Bunkóczi, G., Chen, V.B., Headd, J.J., McCoy, A.J., Moriarty, N.W., Read, R.J., Richardson, D.C.*, et al.* (2012). Graphical tools for macromolecular crystallography in PHENIX. Journal of applied crystallography *45*, 581-586.
- Eckhert, E., Rangamani, P., Davis, Annie E., Oster, G., and Berleman, James E. (2014). Dual Biochemical Oscillators May Control Cellular Reversals in Myxococcus xanthus. Biophysical Journal *107*, 2700-2711.
- Emsley, P., Lohkamp, B., Scott, W.G., and Cowtan, K. (2010). Features and development of Coot. Acta crystallographica Section D, Biological crystallography *66*, 486-501.
- Evans, P.R., and Murshudov, G.N. (2013). How good are my data and what is the resolution? Acta crystallographica Section D, Biological crystallography *69*, 1204-1214.
- Faure, L.M., Fiche, J.-B., Espinosa, L., Ducret, A., Anantharaman, V., Luciano, J., Lhospice, S., Islam, S.T., Tréguier, J., Sotes, M.*, et al.* (2016). The mechanism of force transmission at bacterial focal adhesion complexes. Nature *539*, 530.
- Fife, C.M., McCarroll, J.A., and Kavallaris, M. (2014). Movers and shakers: cell cytoskeleton in cancer metastasis. British Journal of Pharmacology *171*, 5507-5523.
- Folta-Stogniew, E., and Williams, K.R. (1999). Determination of molecular masses of proteins in solution: Implementation of an HPLC size exclusion chromatography and laser light scattering service in a core laboratory. Journal of biomolecular techniques : JBT *10*, 51-63.
- Fremgen, S.A., Burke, N.S., and Hartzell, P.L. (2010). Effects of site-directed mutagenesis of mglA on motility and swarming of Myxococcus xanthus. BMC Microbiology *10*, 295.

- Geladopoulos, T.P., Sotiroudis, T.G., and Evangelopoulos, A.E. (1991). A malachite green colorimetric assay for protein phosphatase activity. Analytical Biochemistry *192*, 112-116.
- Goldberg, J. (1999). Structural and Functional Analysis of the ARF1–ARFGAP Complex Reveals a Role for Coatomer in GTP Hydrolysis. Cell *96*, 893-902.
- Gotthardt, K., Lokaj, M., Koerner, C., Falk, N., Gießl, A., and Wittinghofer, A. (2015). A G-protein activation cascade from Arl13B to Arl3 and implications for ciliary targeting of lipidated proteins. eLife *4*, e11859.
- Grizot, S., Fauré, J., Fieschi, F., Vignais, P.V., Dagher, M.C., and Pebay-Peyroula, E. (2001). Crystal Structure of the Rac1−RhoGDI Complex Involved in NADPH Oxidase Activation. Biochemistry *40*, 10007-10013.
- Guillard, S., Kolasinska-Zwierz, P., Debreczeni, J., Breed, J., Zhang, J., Bery, N., Marwood, R., Tart, J., Overman, R., Stocki, P.*, et al.* (2017). Structural and functional characterization of a DARPin which inhibits Ras nucleotide exchange. Nature Communications *8*, 16111.
- Guzzo, M., Agrebi, R., Espinosa, L., Baronian, G., Molle, V., Mauriello, E.M.F., Brochier-Armanet, C., and Mignot, T. (2015). Evolution and Design Governing Signal Precision and Amplification in a Bacterial Chemosensory Pathway. PLOS Genetics *11*, e1005460.
- Guzzo, M., Murray, S.M., Martineau, E., Lhospice, S., Baronian, G., My, L., Zhang, Y., Espinosa, L., Vincentelli, R., Bratton, B.P.*, et al.* (2018). A gated relaxation oscillator mediated by FrzX controls morphogenetic movements in Myxococcus xanthus. Nature Microbiology *3*, 948-959.
- Hartzell, P., and Kaiser, D. (1991a). Function of MglA, a 22-kilodalton protein essential for gliding in Myxococcus xanthus. Journal of bacteriology *173*, 7615-7624.
- Hartzell, P., and Kaiser, D. (1991b). Upstream gene of the mgl operon controls the level of MglA protein in Myxococcus xanthus. Journal of bacteriology *173*, 7625-7635.
- Hartzell, P., and Kaiser, D. (1991c). Upstream gene of the mgl operon controls the level of MglA protein in Myxococcus xanthus. Journal of bacteriology *173*, 7625-7635.
- Henrichsen, J. (1983). TWITCHING MOTILITY. Annual Review of Microbiology *37*, 81-93.
- Hillig, R.C., Hanzal-Bayer, M., Linari, M., Becker, J., Wittinghofer, A., and Renault, L. (2000). Structural and Biochemical Properties Show ARL3-GDP as a Distinct GTP Binding Protein. Structure *8*, 1239-1245.
- Hodgkin, J., and Kaiser, D. (1977). Cell-to-cell stimulation of movement in nonmotile mutants of Myxococcus. Proceedings of the National Academy of Sciences of the United States of America *74*, 2938-2942.
- Hodgkin, J., and Kaiser, D. (1979). Genetics of gliding motility in Myxococcus xanthus (Myxobacterales): Two gene systems control movement. Molecular and General Genetics MGG *171*, 177-191.
- Hui, R., and Edwards, A. (2003). High-throughput protein crystallization. Journal of Structural Biology *142*, 154-161.
- Ingerman, E., and Nunnari, J. (2005). A Continuous, Regenerative Coupled GTPase Assay for Dynamin-Related Proteins. In Methods in Enzymology (Academic Press), pp. 611-619.

- Islam, S.T., and Mignot, T. (2015). The mysterious nature of bacterial surface (gliding) motility: A focal adhesion-based mechanism in Myxococcus xanthus. Seminars in Cell & Developmental Biology *46*, 143-154.
- Jarrell, K.F., and McBride, M.J. (2008). The surprisingly diverse ways that prokaryotes move. Nature Reviews Microbiology *6*, 466.
- Jelsbak, L., and Søgaard-Andersen, L. (1999). The cell surface-associated intercellular C-signal induces behavioral changes in individual Myxococcus xanthus cells during fruiting body morphogenesis. Proceedings of the National Academy of Sciences of the United States of America *96*, 5031-5036.
- Kabsch, W. (2010a). Integration, scaling, space-group assignment and post-refinement. Acta crystallographica Section D, Biological crystallography *66*, 133-144.
- Kabsch, W. (2010b). XDS. Acta crystallographica Section D, Biological crystallography *66*, 125-132.
- Kaimer, C., Berleman, J.E., and Zusman, D.R. (2012). Chemosensory signaling controls motility and subcellular polarity in Myxococcus xanthus. Current Opinion in Microbiology *15*, 751-757.
- Kaiser, D. (2003). Coupling cell movement to multicellular development in myxobacteria. Nature Reviews Microbiology *1*, 45.
- Kaiser, D., and Warrick, H. (2014). Transmission of a signal that synchronizes cell movements in swarms of <em>Myxococcus xanthus</em&gt. Proceedings of the National Academy of Sciences *111*, 13105.
- Kapp, G.T., Liu, S., Stein, A., Wong, D.T., Reményi, A., Yeh, B.J., Fraser, J.S., Taunton, J., Lim, W.A., and Kortemme, T. (2012). Control of protein signaling using a computationally designed GTPase/GEF orthogonal pair. Proceedings of the National Academy of Sciences *109*, 5277.
- Karplus, P.A., and Diederichs, K. (2015). Assessing and maximizing data quality in macromolecular crystallography. Current Opinion in Structural Biology *34*, 60-68.
- Keilberg, D., and Søgaard-Andersen, L. (2014). Regulation of Bacterial Cell Polarity by Small GTPases. Biochemistry *53*, 1899-1907.
- Keilberg, D., Wuichet, K., Drescher, F., and Søgaard-Andersen, L. (2012). A Response Regulator Interfaces between the Frz Chemosensory System and the MglA/MglB GTPase/GAP Module to Regulate Polarity in Myxococcus xanthus. PLOS Genetics *8*, e1002951.
- Kiianitsa, K., Solinger, J.A., and Heyer, W.-D. (2003). NADH-coupled microplate photometric assay for kinetic studies of ATP-hydrolyzing enzymes with low and high specific activities. Analytical Biochemistry *321*, 266-271.
- Kroos, L. (2007). The Bacillus and Myxococcus Developmental Networks and Their Transcriptional Regulators. Annual Review of Genetics *41*, 13-39.
- Kroos, L., Hartzell, P., Stephens, K., and Kaiser, D. (1988). A link between cell movement and gene expression argues that motility is required for cell-cell signaling during fruiting body development. Genes & Development *2*, 1677-1685.
- L DeLano, W. (2002). The PyMOL Molecular Graphics System (2002) DeLano Scientific, Palo Alto, CA, USA. **http://www.pymol.org**.
- Laloux, G., and Jacobs-Wagner, C. (2014). How do bacteria localize proteins to the cell pole? Journal of Cell Science *127*, 11.

- Lennox, R.J., Chapman, J.M., Souliere, C.M., Tudorache, C., Wikelski, M., Metcalfe, J.D., and Cooke, S.J. (2016). Conservation physiology of animal migration. Conservation Physiology *4*, cov072-cov072.
- Leonardy, S., Miertzschke, M., Bulyha, I., Sperling, E., Wittinghofer, A., and Søgaard-Andersen, L. (2010). Regulation of dynamic polarity switching in bacteria by a Ras-like G-protein and its cognate GAP. The EMBO journal *29*, 2276-2289.
- Letunic, I., and Bork, P. (2018). 20 years of the SMART protein domain annotation resource. Nucleic Acids Research *46*, D493-D496.
- Letunic, I., Doerks, T., and Bork, P. (2015). SMART: recent updates, new developments and status in 2015. Nucleic Acids Research *43*, D257-D260.
- Levine, T.P., Daniels, R.D., Wong, L.H., Gatta, A.T., Gerondopoulos, A., and Barr, F.A. (2013). Discovery of new Longin and Roadblock domains that form platforms for small GTPases in Ragulator and TRAPP-II. Small GTPases *4*, 62-69.
- Lybarger, S.R., and Maddock, J.R. (2001). Polarity in Action: Asymmetric Protein Localization in Bacteria. Journal of Bacteriology *183*, 3261.
- Manuel García-Ruiz, J. (2003). Nucleation of protein crystals. Journal of Structural Biology *142*, 22-31.
- Margarit, S.M., Sondermann, H., Hall, B.E., Nagar, B., Hoelz, A., Pirruccello, M., Bar-Sagi, D., and Kuriyan, J. (2003). Structural Evidence for Feedback Activation by Ras·GTP of the Ras-Specific Nucleotide Exchange Factor SOS. Cell *112*, 685-695.
- Mauriello, E.M., Mouhamar, F., Nan, B., Ducret, A., Dai, D., Zusman, D.R., and Mignot, T. (2010a). Bacterial motility complexes require the actin-like protein, MreB and the Ras homologue, MglA. EMBO J *29*, 315-326.
- Mauriello, E.M.F. (2010). Cell polarity/motility in bacteria: closer to eukaryotes than expected? The EMBO Journal *29*, 2258.
- Mauriello, E.M.F., Mouhamar, F., Nan, B., Ducret, A., Dai, D., Zusman, D.R., and Mignot, T. (2010b). Bacterial motility complexes require the actin-like protein, MreB and the Ras homologue, MglA. The EMBO Journal *29*, 315.
- Mauriello, E.M.F., Nan, B., and Zusman, D.R. (2009). AglZ regulates adventurous (A-) motility in Myxococcus xanthus through its interaction with the cytoplasmic receptor, FrzCD. Molecular Microbiology *72*, 964-977.
- Mauriello, E.M.F., and Zusman, D.R. (2007). Polarity of motility systems in Myxococcus xanthus. Current Opinion in Microbiology *10*, 624-629.
- Maziarz, M., and Garcia-Marcos, M. (2017). Chapter 11 - Fluorescence polarization assays to measure interactions between Gα subunits of heterotrimeric G proteins and regulatory motifs. In Methods in Cell Biology, A.K. Shukla, ed. (Academic Press), pp. 133-143.
- McBride, M.J. (2001). Bacterial Gliding Motility: Multiple Mechanisms for Cell Movement over Surfaces. Annual Review of Microbiology *55*, 49-75.
- McBride, M.J., Köhler, T., and Zusman, D.R. (1992). Methylation of FrzCD, a methyl-accepting taxis protein of Myxococcus xanthus, is correlated with factors affecting cell behavior. Journal of bacteriology *174*, 4246-4257.
- McBride, M.J., Weinberg, R.A., and Zusman, D.R. (1989). "Frizzy" aggregation genes of the gliding bacterium Myxococcus xanthus show sequence similarities to the chemotaxis genes of enteric bacteria. Proceedings of the National Academy of Sciences of the United States of America *86*, 424-428.

- McCleary, W.R., and Zusman, D.R. (1990). FrzE of Myxococcus xanthus is homologous to both CheA and CheY of Salmonella typhimurium. Proceedings of the National Academy of Sciences *87*, 5898.
- McPherson, A. (2017). Protein Crystallization. In Protein Crystallography: Methods and Protocols, A. Wlodawer, Z. Dauter, and M. Jaskolski, eds. (New York, NY: Springer New York), pp. 17-50.
- Mercier, R., and Mignot, T. (2016). Regulations governing the multicellular lifestyle of Myxococcus xanthus. Current Opinion in Microbiology *34*, 104-110.
- Miertzschke, M., Koerner, C., Vetter, I.R., Keilberg, D., Hot, E., Leonardy, S., Søgaard-Andersen, L., and Wittinghofer, A. (2011). Structural analysis of the Ras-like G protein MglA and its cognate GAP MglB and implications for bacterial polarity. The EMBO journal *30*, 4185-4197.
- Mignot, T. (2007). The elusive engine in Myxococcus xanthus gliding motility. Cellular and Molecular Life Sciences *64*, 2733-2745.
- Mignot, T., and Kirby, J.R. (2008). Genetic circuitry controlling motility behaviors of Myxococcus xanthus. BioEssays *30*, 733-743.
- Mignot, T., and Nöllmann, M. (2017). New insights into the function of a versatile class of membrane molecular motors from studies of Myxococcus xanthus surface (gliding) motility. Microbial cell (Graz, Austria) *4*, 98-100.
- Mignot, T., Shaevitz, J.W., Hartzell, P.L., and Zusman, D.R. (2007). Evidence That Focal Adhesion Complexes Power Bacterial Gliding Motility. Science *315*, 853.
- Mishra, A.K., and Lambright, D.G. (2016). Invited review: Small GTPases and their GAPs. Biopolymers *105*, 431-448.
- Mitchell, J.G., and Kogure, K. (2006). Bacterial motility: links to the environment and a driving force for microbial physics. FEMS Microbiology Ecology *55*, 3-16.
- Moerke, N.J. (2009). Fluorescence Polarization (FP) Assays for Monitoring Peptide-Protein or Nucleic Acid-Protein Binding. Current Protocols in Chemical Biology *1*, 1-15.
- Monroy, A., I Mackie, D., and Roman, D. (2013). A High Throughput Screen for RGS Proteins Using Steady State Monitoring of Free Phosphate Formation, Vol 8.
- Müller, M.P., and Goody, R.S. (2018). Molecular control of Rab activity by GEFs, GAPs and GDI. Small GTPases *9*, 5-21.
- Mungi, V.C., and Rajamani, S. (2015). Characterization of RNA-Like Oligomers from Lipid-Assisted Nonenzymatic Synthesis: Implications for Origin of Informational Molecules on Early Earth. Life *5*.
- Murshudov, G.N., Vagin, A.A., and Dodson, E.J. (1997). Refinement of Macromolecular Structures by the Maximum-Likelihood Method. Acta Crystallographica Section D *53*, 240-255.
- Nan, B., Bandaria, J.N., Moghtaderi, A., Sun, I.-H., Yildiz, A., and Zusman, D.R. (2013). Flagella stator homologs function as motors for myxobacterial gliding motility by moving in helical trajectories. Proceedings of the National Academy of Sciences of the United States of America *110*, E1508-E1513.
- Nan, B., Chen, J., Neu, J.C., Berry, R.M., Oster, G., and Zusman, D.R. (2011). Myxobacteria gliding motility requires cytoskeleton rotation powered by proton motive force. Proceedings of the National Academy of Sciences *108*, 2498.

- Nan, B., Mauriello, E.M.F., Sun, I.-H., Wong, A., and Zusman, D.R. (2010). A multi-protein complex from Myxococcus xanthus required for bacterial gliding motility. Molecular Microbiology *76*, 1539-1554.
- Nan, B., and Zusman, D.R. (2011). Uncovering the Mystery of Gliding Motility in the Myxobacteria. Annual Review of Genetics *45*, 21-39.
- Nanev, C.N. (2013). Kinetics and intimate mechanism of protein crystal nucleation. Progress in Crystal Growth and Characterization of Materials *59*, 133-169.
- Nudleman, E., Wall, D., and Kaiser, D. (2006). Polar assembly of the type IV pilus secretin in Myxococcus xanthus. Molecular Microbiology *60*, 16-29.
- Pei, J., Kim, B.-H., and Grishin, N.V. (2008). PROMALS3D: a tool for multiple protein sequence and structure alignments. Nucleic Acids Research *36*, 2295-2300.
- Pichoff, S., and Lutkenhaus, J. (2001). Escherichia coli Division Inhibitor MinCD Blocks Septation by Preventing Z-Ring Formation. Journal of Bacteriology *183*, 6630.
- Potterton, L., Agirre, J., Ballard, C., Cowtan, K., Dodson, E., Evans, P.R., Jenkins, H.T., Keegan, R., Krissinel, E., Stevenson, K.*, et al.* (2018). CCP4i2: the new graphical user interface to the CCP4 program suite. Acta crystallographica Section D, Structural biology *74*, 68-84.
- Renault, L., Kuhlmann, J., Henkel, A., and Wittinghofer, A. (2001). Structural Basis for Guanine Nucleotide Exchange on Ran by the Regulator of Chromosome Condensation (RCC1). Cell *105*, 245-255.
- Ridley, A.J., Schwartz, M.A., Burridge, K., Firtel, R.A., Ginsberg, M.H., Borisy, G., Parsons, J.T., and Horwitz, A.R. (2003). Cell Migration: Integrating Signals from Front to Back. Science *302*, 1704.
- Rupp, B. (2010). Biomolecular crystallography : principles, practice, and application to structural biology (New York: Garland Science).
- Salemme, F.R. (1972). A free interface diffusion technique for the crystallization of proteins for X-ray crystallography. Archives of Biochemistry and Biophysics *151*, 533-539.
- Samokhvalov, A.V., Safenkova, I.V., Eremin, S.A., Zherdev, A.V., and Dzantiev, B.B. (2017). Use of anchor protein modules in fluorescence polarisation aptamer assay for ochratoxin A determination. Analytica Chimica Acta *962*, 80-87.
- Saponaro, A. (2018). Isothermal Titration Calorimetry: A Biophysical Method to Characterize the Interaction between Label-free Biomolecules in Solution. Bio-protocol *8*, e2957.
- Sekiguchi, T., Hirose, E., Nakashima, N., Ii, M., and Nishimoto, T. (2001). Novel G Proteins, Rag C and Rag D, Interact with GTP-binding Proteins, Rag A and Rag B. Journal of Biological Chemistry *276*, 7246-7257.
- Shapiro, L., McAdams, H.H., and Losick, R. (2002). Generating and Exploiting Polarity in Bacteria. Science *298*, 1942.
- Shen, K., Huang, R.K., Brignole, E.J., Condon, K.J., Valenstein, M.L., Chantranupong, L., Bomaliyamu, A., Choe, A., Hong, C., Yu, Z.*, et al.* (2018). Architecture of the human GATOR1 and GATOR1–Rag GTPases complexes. Nature *556*, 64.
- Shimizu, H., Toma-Fukai, S., Kontani, K., Katada, T., and Shimizu, T. (2018). GEF mechanism revealed by the structure of SmgGDS-558 and farnesylated

RhoA complex and its implication for a chaperone mechanism. Proceedings of the National Academy of Sciences *115*, 9563.
- Shimkets, L.J. (1990). Social and developmental biology of the myxobacteria. Microbiological Reviews *54*, 473.
- Sliusarenko, O., Zusman, D.R., and Oster, G. (2007). The Motors Powering A-Motility in Myxococcus xanthus Are Distributed along the Cell Body. Journal of Bacteriology *189*, 7920.
- Song, S., Cong, W., Zhou, S., Shi, Y., Dai, W., Zhang, H., Wang, X., He, B., and Zhang, Q. (2018). Small GTPases: Structure, biological function and its interaction with nanoparticles. Asian Journal of Pharmaceutical Sciences.
- Spormann, A.M. (1999). Gliding motility in bacteria: insights from studies of Myxococcus xanthus. Microbiology and molecular biology reviews : MMBR *63*, 621-641.
- Spormann, A.M., and Kaiser, D. (1999). Gliding Mutants of Myxococcus xanthuswith High Reversal Frequencies and Small Displacements. Journal of Bacteriology *181*, 2593.
- Sprang, S.R. (1997). G Protein Mechanisms: Insights from Structural Analysis. Annual Review of Biochemistry *66*, 639-678.
- Su, M.-Y., Morris, K.L., Kim, D.J., Fu, Y., Lawrence, R., Stjepanovic, G., Zoncu, R., and Hurley, J.H. (2017). Hybrid Structure of the RagA/C-Ragulator mTORC1 Activation Complex. Molecular Cell *68*, 835-846.e833.
- Thomas, C., Fricke, I., Weyand, M., and Berken, A. (2009). 3D structure of a binary ROP-PRONE complex: the final intermediate for a complete set of molecular snapshots of the RopGEF reaction. In Biological Chemistry, pp. 427.
- Treuner-Lange, A., Macia, E., Guzzo, M., Hot, E., Faure, L.M., Jakobczak, B., Espinosa, L., Alcor, D., Ducret, A., Keilberg, D.*, et al.* (2015). The small G-protein MglA connects to the MreB actin cytoskeleton at bacterial focal adhesions. The Journal of Cell Biology *210*, 243.
- Treuner-Lange, A., and Sogaard-Andersen, L. (2014). Regulation of cell polarity in bacteria. J Cell Biol *206*, 7-17.
- Treuner-Lange, A., and Søgaard-Andersen, L. (2014). Regulation of cell polarity in bacteria. The Journal of Cell Biology *206*, 7.
- van Dam, T.J.P., Bos, J.L., and Snel, B. (2011). Evolution of the Ras-like small GTPases and their regulators. Small GTPases *2*, 4-16.
- van Teeffelen, S., Wang, S., Furchtgott, L., Huang, K.C., Wingreen, N.S., Shaevitz, J.W., and Gitai, Z. (2011). The bacterial actin MreB rotates, and rotation depends on cell-wall assembly. Proceedings of the National Academy of Sciences *108*, 15822.
- Vetter Ingrid, R. (2017). Interface analysis of small GTP binding protein complexes suggests preferred membrane orientations. In Biological Chemistry, pp. 637.
- Vetter, I.R. (2014). The Structure of the G Domain of the Ras Superfamily. In Ras Superfamily Small G Proteins: Biology and Mechanisms 1: General Features, Signaling, A. Wittinghofer, ed. (Vienna: Springer Vienna), pp. 25-50.
- Vetter, I.R., and Wittinghofer, A. (2001). The Guanine Nucleotide-Binding Switch in Three Dimensions. Science *294*, 1299.
- Vicente-Manzanares, M., and Horwitz, A.R. (2011). Cell Migration: An Overview. In Cell Migration: Developmental Methods and Protocols, C.M. Wells, and M. Parsons, eds. (Totowa, NJ: Humana Press), pp. 1-24.

- Wall, D., and Kaiser, D. (1999). Type IV pili and cell motility. Molecular Microbiology *32*, 01-10.
- Ward, M.J., and Zusman, D.R. (1997). Regulation of directed motility in Myxococcus xanthus. Molecular Microbiology *24*, 885-893.
- Wartel, M., Ducret, A., Thutupalli, S., Czerwinski, F., Le Gall, A.-V., Mauriello, E.M.F., Bergam, P., Brun, Y.V., Shaevitz, J., and Mignot, T. (2013). A Versatile Class of Cell Surface Directional Motors Gives Rise to Gliding Motility and Sporulation in Myxococcus xanthus. PLOS Biology *11*, e1001728.
- Wennerberg, K., Rossman, K.L., and Der, C.J. (2005). The Ras superfamily at a glance. Journal of Cell Science *118*, 843.
- Whitchurch, C.B., Hobbs, M., Livingston, S.P., Krishnapillai, V., and Mattick, J.S. (1991). Characterisation of a Pseudomonas aeruginosa twitching motility gene and evidence for a specialised protein export system widespread in eubacteria. Gene *101*, 33-44.
- Winn, M.D., Ballard, C.C., Cowtan, K.D., Dodson, E.J., Emsley, P., Evans, P.R., Keegan, R.M., Krissinel, E.B., Leslie, A.G.W., McCoy, A.*, et al.* (2011). Overview of the CCP4 suite and current developments. Acta crystallographica Section D, Biological crystallography *67*, 235-242.
- Wittinghofer, A., and Vetter, I.R. (2011). Structure-Function Relationships of the G Domain, a Canonical Switch Motif. Annual Review of Biochemistry *80*, 943-971.
- Wolgemuth, C.W., Igoshin, O., and Oster, G. (2003). The Motility of Mollicutes. Biophysical Journal *85*, 828-842.
- Wuichet, K., and Søgaard-Andersen, L. (2015). Evolution and Diversity of the Ras Superfamily of Small GTPases in Prokaryotes. Genome Biology and Evolution *7*, 57-70.
- Yang, J., Zhang, Z., Roe, S.M., Marshall, C.J., and Barford, D. (2009). Activation of Rho GTPases by DOCK Exchange Factors Is Mediated by a Nucleotide Sensor. Science *325*, 1398.
- Yang, R., Bartle, S., Otto, R., Stassinopoulos, A., Rogers, M., Plamann, L., and Hartzell, P. (2004). AglZ Is a Filament-Forming Coiled-Coil Protein Required for Adventurous Gliding Motility of <em>Myxococcus xanthus</em&gt. Journal of Bacteriology *186*, 6168.
- Zhang, Y., Franco, M., Ducret, A., and Mignot, T. (2010). A Bacterial Ras-Like Small GTP-Binding Protein and Its Cognate GAP Establish a Dynamic Spatial Polarity Axis to Control Directed Motility. PLOS Biology *8*, e1000430.
- Zhang, Y., Guzzo, M., Ducret, A., Li, Y.-Z., and Mignot, T. (2012). A Dynamic Response Regulator Protein Modulates G-Protein–Dependent Polarity in the Bacterium Myxococcus xanthus. PLOS Genetics *8*, e1002872.
- Zusman, D.R. (1982). "Frizzy" mutants: a new class of aggregation-defective developmental mutants of Myxococcus xanthus. Journal of bacteriology *150*, 1430-1437.